IMPROVE

Interagency Monitoring of Protected Visual Environments

Spatial and Seasonal Patterns and Long Term Variability of the Composition of the Haze in the United States:

An Analysis of Data from the IMPROVE Network

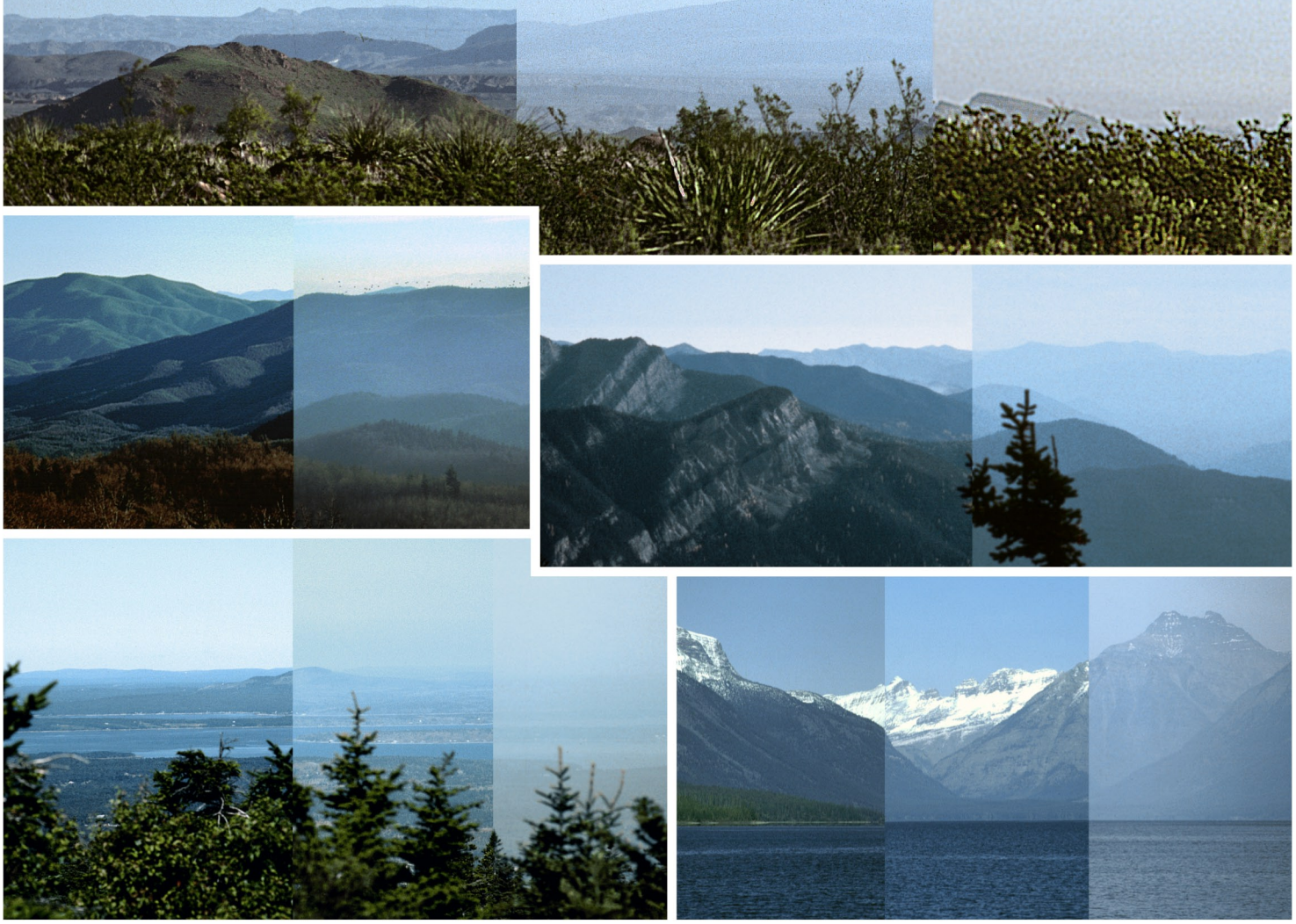

July, 1996
ISSN: 0737-5352-32

CIRA
Cooperative Institute for
Research in the Atmosphere

Colorado
State
University

ISSN: 0737-5352-32

SPATIAL AND SEASONAL PATTERNS AND LONG TERM VARIABILITY OF THE COMPOSITION OF THE HAZE IN THE UNITED STATES:

An Analysis of Data from the IMPROVE Network

James F. Sisler
Cooperative Institute for Research in the Atmosphere
Colorado State University
Fort Collins, CO 80523

Contributions by

William C. Malm
Kristi A. Gebhart
Air Resources Division
National Park Service
Colorado State University
Fort Collins, CO 80523

Principal Investigators

William C. Malm
National Park Service
Air Resources Division
Colorado State University
Fort Collins, CO 80523

Marc L. Pitchford
Applied Sciences Branch
ARL/NOAA
c/o Desert Research Institute
PO Box 10940
Las Vegas, NV 89132-0040

July 1996

DISCLAIMER

The assumptions, findings, conclusions, judgements, and views presented herein are those of the authors and should not be interpreted as necessarily representing official National Park Service policies, and are not necessarily endorsed by the management and sponsors of project MOHAVE.

ACKNOWLEDGEMENTS

This report is the result of a collaborative effort involving the authors and a number of individuals from several institutions. We thank Drs. Thomas Cahill and Robert Eldred of the University of California at Davis for their efforts in developing the IMPROVE aerosol monitoring network, managing the aerosol database, and providing input to the report concerning aerosol sampling and analysis. Also, we thank Dr. Judith Chow and associates at Desert Research Institute, University of Nevada Systems at Reno for their input on the analysis of carbonaceous species. We also wish to acknowledge Mr. John Molenar and Dr. David Dietrich of Air Resource Specialists in Fort Collins, Colorado for developing and managing the IMPROVE visibility monitoring network, supplying the optical and relative humidity data, and for their input to this report.

We would like to recognize Dr. Marc Pitchford, Chief of Applied Sciences Branch, National Oceanic and Atmospheric Administration in Las Vegas, Nevada, for his efforts in establishing, designing, and managing the IMPROVE program. We would also like to recognize Richard Damberg of the U.S. Environmental Protection Agency's Office of Air Quality Planning and Standards in Research Triangle Park, North Carolina, for his review and comments of this report.

ISSN: 0737-5352-32

SPATIAL AND SEASONAL PATTERNS AND LONG TERM VARIABILITY OF THE COMPOSITION OF THE HAZE IN THE UNITED STATES:

An Analysis of Data from the IMPROVE Network

APPENDICES

CIRA Cooperative Institute for Research in the Atmosphere

TABLE OF CONTENTS

LIST OF FIGURES

4 LIGHT EXTINCTION AND ITS RELATIONSHIP TO AEROSOLS

LIST OF TABLES

LIST OF APPENDICES

APPENDIX 1 Long term stacked timelines of fine mass concentrations (FM), sulfur concentrations (S), and concentrations of light-absorbing mass (b_{abs}) by site in ng/m^3.

APPENDIX 2 Long term seasonal statistics of fine mass concentrations, sulfur concentrations, and concentration of light-absorbing mass by site in ng/m^3.

APPENDIX 3 Matrix scatter plots of light-absorbing mass concentrations (b_{abs}), fine mass concentrations (FM), and sulfur concentrations (S) by site in ìg/m^3.

Copies of appendices available upon request to National Park Service office at 970/491-8292.

OVERVIEW AND SUMMARY

This report describes data for the three year period, March 1992 through February 1995, of the Interagency Monitoring of Protected Visual Environments (IMPROVE) measurement program. IMPROVE is a cooperative visibility monitoring effort between the United States Environmental Protection Agency, (EPA) federal land management agencies, and state air agencies.

The objectives of IMPROVE are:

(1) To establish current background visibility in Class I areas;

(2) To identify chemical species and emission sources responsible for existing man-made visibility impairment; and

(3) To document long-term trends.

The design of the IMPROVE monitoring network was resource and funding limited so that it was not practical to place monitoring stations at all 156 mandatory Class I areas where visibility is an important attribute. Instead, the IMPROVE Steering Committee selected a set of sites that were representative of the Class I areas. For the first IMPROVE report, published in the spring of 1993, data for 36 sites was summarized. In the intervening time the IMPROVE network has evolved; two sites were dropped, some sites were downgraded to the measurement of a subset of the variables measured at a fully complemented site, and other sites have been added. There are currently a total of 58 IMPROVE sites with various configurations of optical and aerosol monitoring equipment. For this report, the 43 IMPROVE sites that are fully configured as aerosol monitoring sites with data for the three-year period, March 1992 through February 1995, are utilized. However, only 26 of the sites have optical monitoring equipment (e.g., transmissometers or nephelometers to measure visibility-related parameters). Figure S.1 shows a map of the United States indicating the locations of the 43 monitoring sites analyzed in this report. On the basis of regional similarities, the sites were grouped into 21 regions, listed in Table S.1.

S.1 Optical and Aerosol Data

Aerosol monitoring in the IMPROVE network is accomplished by a combination of particle sampling and sample analysis. The sampler was designed specifically for IMPROVE. It collects four simultaneous samples: one PM_{10} sample (particles less than 10 ìm in diameter) on a Teflon filter and three $PM_{2.5}$ samples on Teflon, nylon, and quartz filters. The IMPROVE sampler is programmed to collect two 24-hour duration samples per week (i.e., 26 per season, 104 per year). The PM_{10} filter is used to determine total PM_{10} mass. The $PM_{2.5}$ Teflon filter is used to measure

Figure S.1 The 42 IMPROVE sites out of 43 included in the report. Denali National Park in Alaska is not shown.

Table S.1 IMPROVE and NPS/IMPROVE protocol sites according to region.

Alaska (AKA)
- Denali NP (DENA)

Appalachian Mountains (APP)
- Great Smoky Mountains NP (GRSM)
- Shenandoah NP (SHEN)
- Dolly Sods WA (DOSO)

Boundary Waters (BWA)
- Boundary Waters Canoe Area (BOWA)

Cascade Mountains (CAS)
- Mount Rainier NP (MORA)

Central Rocky Mountains (CRK)
- Bridger WA (BRID)
- Great Sand Dunes NM (GRSA)
- Rocky Mountain NP (ROMO)
- Weminuche WA (WEMI)
- Yellowstone NP (YELL)

Coastal Mountains (CST)
- Pinnacles NM (PINN)
- Point Reyes NS (PORE)
- Redwood NP (REDW)

Colorado Plateau (CPL)
- Bandelier NM (BAND)
- Bryce Canyon NP (BRCA)
- Canyonlands NP (CANY)
- Grand Canyon NP (GRCA)
- Mesa Verde NP (MEVE)
- Petrified Forest NP (PEFO)

Florida (FLA)
- Chassahowitzka NWR (CHAS)
- Okefenokee NWR (OKEF)

Great Basin (GBA)
- Jarbidge WA (JARB)
- Great Basin NP (GRBA)

Lake Tahoe (LTA)
- D.L. Bliss State Park (BLISS)
- South Lake Tahoe (SOLA)

Mid Atlantic (MAT)
- Edmond B. Forsythe NWR (EBFO)

Mid South (MDS)
- Upper Buffalo WA (UPBU)
- Sipsey WA (SIPS)
- Mammoth Cave NP (MACA)

Northeast (NEA)
- Acadia NP (ACAD)
- Lye Brook WA (LYBR)

Northern Great Plains (NGP)
- Badlands NM (BADL)

Northern Rocky Mountains (NRK)
- Glacier NP (GLAC)

Sierra Nevada (SRA)
- Yosemite NP (YOSE)

Sierra-Humboldt (SRH)
- Crater Lake NP (CRLA)
- Lassen Volcanoes NP (LAVO)

Sonoran Desert (SON)
- Chiricahua NM (CHIR)
- Tonto NM (TONT)

Southern California (SCA)
- San Gorgonio WA (SAGO)

Washington, D.C. (WDC)
- Washington, D.C. (WASH)

West Texas (WTX)
- Big Bend NP (BIBE)
- Guadalupe Mountains NM (GUMO)

NP = National Park NM = National Monument WA = Wilderness Area
NWR = National Wildlife Refuge NS = National Seashore

total fine aerosol mass, individual chemical species using Proton Induced X-ray Emission (PIXE) and Proton Elastic Scattering Analysis (PESA), and light-absorption coefficient using the Laser Integrating Plate Method (LIPM). The nylon filter is used to measure nitrate and sulfate aerosol concentrations with Ion Chromatography (IC). Finally, the quartz filters are analyzed for organic and elemental carbon using the Thermal Optical Reflectance (TOR) method.

Transmissometers are employed to measure the light-extinction coefficient at 15 of the IMPROVE sites, and 11 sites have integrating nephelometers, which measure the scattering coefficient. Transmissometers measure the light transmitted through the atmosphere over a distance of one to fifteen kilometers. The light transmitted between the light source (transmitter) and the light monitoring component (receiver) is converted to the path-averaged light extinction coefficient (b_{ext}), which is the sum of scattering (b_{scat}) and absorption (b_{abs}). Integrating nephelometers measure the scattering of light over a defined band of visible wavelengths from an enclosed volume of air and represents a point measurement of scattering. By combining the absorption coefficient from the particle sampler with the scattering coefficient from the nephelometer the extinction coefficient can be reconstructed at the 11 nephelometer sites. Relative humidity was measured continuously at the transmissometer and nephelometer sites.

S.2 Spatial and Seasonal Distribution of Aerosol Concentration and Chemical Composition

Fine aerosol concentrations are highest in the eastern United States (in the Appalachian Mountains, Mid South, Mid Atlantic and in Washington, D.C.). Concentrations are also relatively high in southern California. The lowest concentrations occur in the Great Basin in Nevada, the Colorado Plateau in the four corners states, Wyoming, and in Alaska.

The largest single component of the fine aerosol in the East is sulfate, while in the Pacific Northwest it is organics, and in southern California it is nitrate. In general, the largest mass fractions of the fine aerosol are sulfate and organics. Of the 21 regions in the IMPROVE network, organic carbon is the largest single component in 10 regions (Alaska, Cascades, Colorado Plateau, Central Rockies, Pacific Coastal Mountains, Great Basin, Northern Rockies, Sierra Nevada, Sierra-Humboldt, and Lake Tahoe). Sulfate is the largest single component of fine aerosol in seven regions, primarily in the East (Appalachian Mountains, Florida, Northeast, Mid South, Mid Atlantic, Washington D.C., and West Texas). The contributions of organic carbon and sulfate are approximately equal in three regions (Boundary Waters, Sonoran Desert, and Northern Great Plains). Soil is the next largest contributor, followed by nitrate and light-absorbing carbon. Nitrate is the largest component of fine aerosol in southern California only.

With few exceptions, average fine mass concentrations, as well as the sulfate, organic carbon, and light-absorbing carbon components of fine mass, are highest in summer. Soil concentrations are highest in spring or summer. Nitrate concentrations are generally highest in winter or spring.

S.3 Light Extinction and its Relationship to Aerosols

Two unique data sets were used to explore the relationship between optical extinction, absorption, scattering, and various aerosol species. The Measurement of Haze and Visual Effects (MOHAVE) special study provided, at one monitoring site, independent optical measurements of b_{ext}, b_{scat}, and b_{abs}, and the various aerosol species. This data set provided for a variety of ways for exploring absorption and scattering efficiencies. The second data set, IMPROVE, provides for the first time, an opportunity to explore the relationship between measured extinction (as opposed to scattering) and aerosol species over the whole western United States. These are the first data sets where extinction was directly measured as opposed to estimated by summing b_{scat} and absorption as derived from "elemental" carbon measurements.

The most surprising outcome of the analysis relates to estimates of absorption. It has been known for some time that, at remote nonurban locations, b_{abs} as derived from the LIPM, was about twice the absorption as estimated from elemental carbon derived from thermal optical reflectance techniques (b_{lac}). Although there may be alternative interpretations, the most straightforward explanation of the relationships between b_{ext}, b_{scat}, b_{abs}, and b_{lac} is that b_{abs} is a more accurate predictor of absorption than b_{lac}. If this is the case, then absorption is on average at about 30% of the non-Rayleigh extinction budget, as opposed to about 10% as conventional wisdom would have dictated.

An examination of the hygroscopic nature of organics lead to the conclusion that organics are not hygroscopic to weakly hygroscopic. However, it is estimated that they have about a 4.0 m^2/g rather than a 3.0 m^2/g mass scattering efficiency.

Another result of the b_{abs} analysis is that a significant amount of b_{abs} is linked to light absorption by soil. Of fine mass absorption, 15-20% is soil related, while elemental and organic carbon contribute about equal amounts of absorption.

S.4 Spatial and Seasonal Distribution of Reconstructed Light Extinction and Species Contributions

The light-extinction coefficient (b_{ext}) is calculated from the measured aerosol species' concentrations by multiplying the concentration of a given species by its light-extinction efficiency, and summing over all species. Since sulfates and nitrates were assumed to be hygroscopic, their light-extinction efficiencies increase with relative humidity; therefore, extinction efficiencies for soluble species must be adjusted according to the seasonal and annual average relative humidity at each site.

Figures S.2a through S.2f summarize the spatial distribution of reconstructed light extinction (in Mm^{-1}), as well as the contributions to the total extinction from coarse particles and fine soil, sulfate, organics, nitrate, and light-absorbing carbon, averaged over three years of IMPROVE (March 1992 through February 1995).

Reconstructed light extinction varies throughout the United States in a way analogous to fine aerosol concentrations. The greatest light extinction occurs in the eastern United States and in

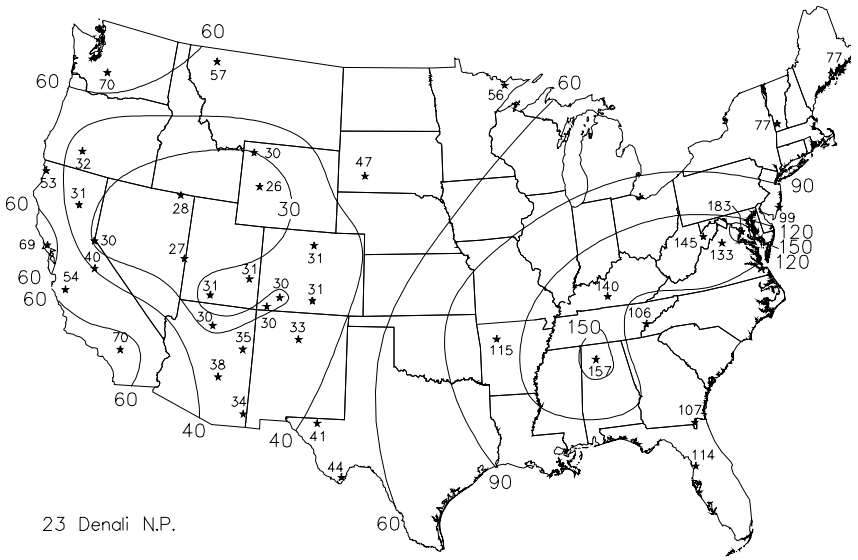

S.2(a) Total light extinction b_{ext} (Mm^{-1})

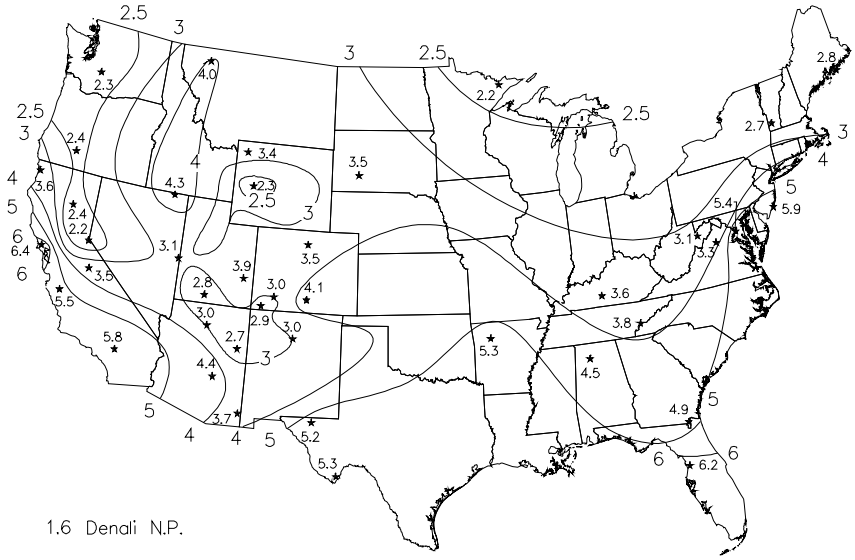

S.2(b) Extinction due to coarse particles and fine soil (Mm^{-1})

Figure S.2 Average reconstructed light extinction coefficient (Mm^{-1}) calculated from the aerosol concentrations measured during three years of IMPROVE, March 1992 through February 1995. The various panels of this figure show total extinction (including Rayleigh scattering due to air) and the contributions due to the various aerosol components: coarse particles and fine soil, sulfate, organic carbon, nitrate, and absorption.

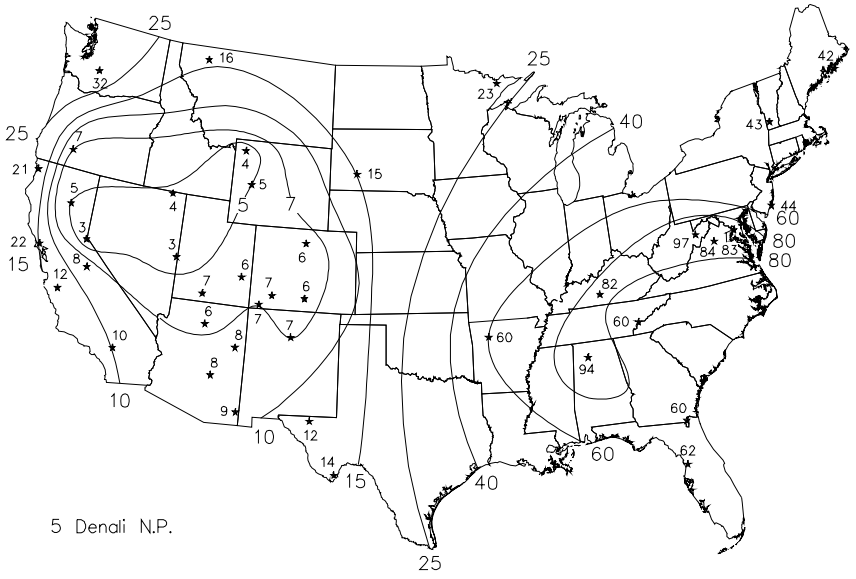

S.2(c) Extinction due to sulfate (Mm^{-1})

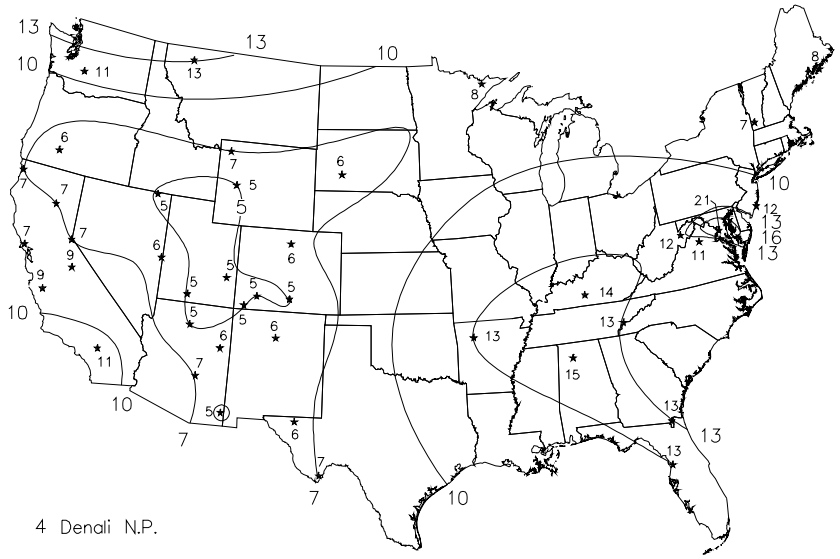

S.2(d) Extinction due to organic carbon (Mm^{-1})

Figure S.2 Continued.

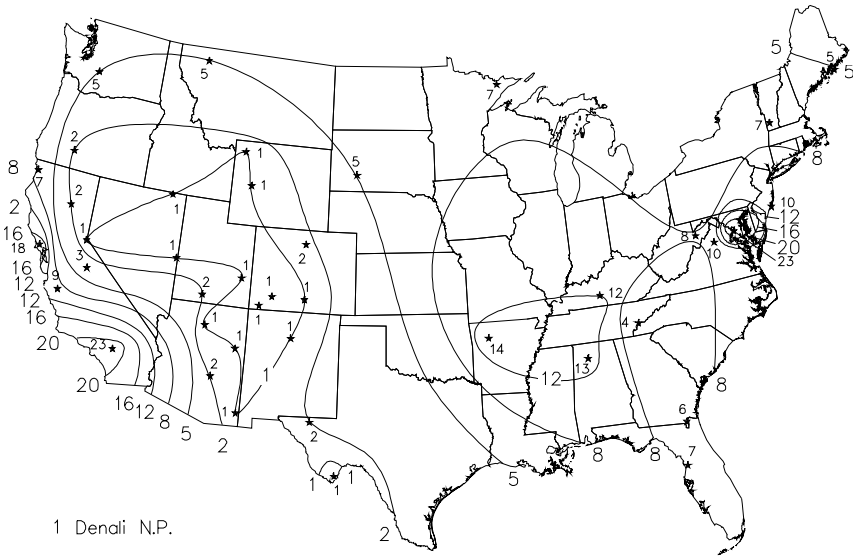

S.2(e) Extinction due to nitrate (Mm^{-1})

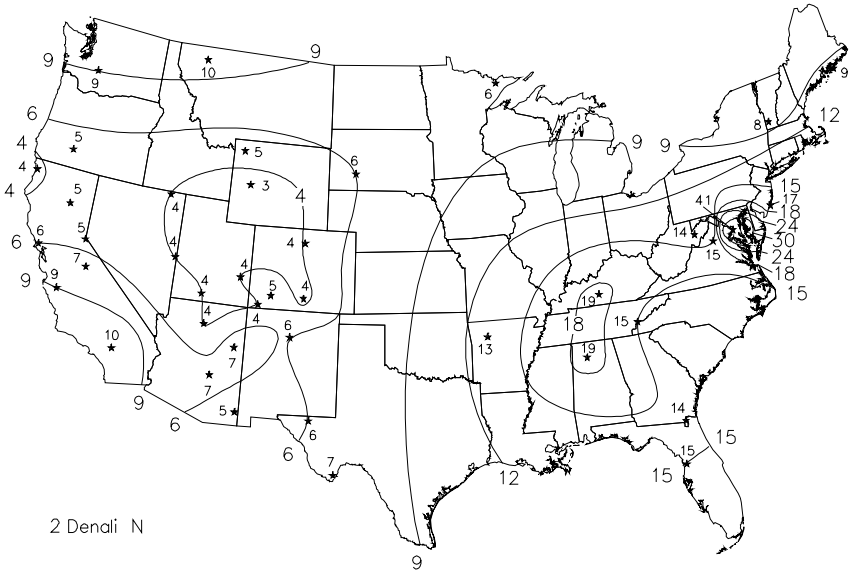

S.2(f) Extinction due to light absorption (Mm^{-1})

Figure S.2 Continued.

southern California, while the least light extinction occurs in the nonurban west (e.g., the Great Basin of Nevada and the Colorado Plateau) and in Alaska. However, since relative humidity (and hence the light-scattering efficiency of sulfate and nitrate) is higher in the East than in the West, the difference between eastern and western light extinction is even more pronounced than the difference in aerosol concentrations.

Fine aerosols are the most effective in scattered light and are the major contributors to light extinction. In most cases, the sulfate component of fine aerosol is the largest single contributor to light extinction. This is because sulfate, being hygroscopic, generally has a higher light extinction efficiency than other species due to associated liquid water. This is especially true in the eastern United States, where relative humidity is high. In the Appalachian Mountains (Shenandoah and Great Smoky Mountains), sulfate accounts for 2/3 of the total aerosol light extinction throughout the year, and 3/4 of the total in summer. Sulfate is the largest single contributor to light extinction in 14 of the 21 regions, and is comparable with organics as the most significant contributor in three additional regions (Northern Rockies, Central Rockies, and Sierra-Humboldt). Organic carbon is the largest single contributor to light extinction in three of the 21 regions (Great Basin, Sierra Nevada, and Lake Tahoe) and is a major contributor in the two previously mentioned regions. Smaller contributions come from wind-blown dust (coarse particles and fine soil) and nitrate. Nitrate is the single largest contributor to light extinction only in southern California.

Generally, reconstructed light extinction is highest in summer and lowest in winter; however, there are many exceptions to this general rule. Higher extinction occurs in summer generally because of elevated sulfate and carbonaceous aerosol concentrations. Also, higher average RH's occur in the East during the summer, which increases extinction.

S.5 Spatial and Seasonal Trends in Visibility in the United States

To show the effect on visibility of aerosol extinction, the deciview (*dv*) scale is applied to the total (Rayleigh included) reconstructed aerosol extinction (see Chapter 1). By utilizing the *dv* scale, the effect of light extinction on visibility is portrayed in a way that is approximately linear with respect to perceived visual air quality.

Because higher extinction coefficients lead to higher *dv* numbers, the geographic trends in visibility follow the trends in reconstructed extinction. Pristine or Rayleigh conditions correspond to a *dv* of zero.

Figure S.3 shows isopleths of deciviews averaged over three years of IMPROVE, March 1992 through February 1995. The smallest *dv* or best visibility is reported at Denali NP with 8 *dv*. A broad region, which includes the Great Basin, most of the Colorado Plateau, and portions of the Central Rockies, has visibility impairment of less than 11 *dv*. Moving in any direction from this region generally results in increasing *dv*. West of the Sierra Range and including southern California one finds *dv* values in excess of 15, with a maximum value of 19 *dv* at Point Reyes and San Gorgonio. The northwest United States and all of the eastern half of the United States have an excess of 15 *dv* of impaired visibility. The region east of the Mississippi and south of the Great Lakes has impairment in excess of 20 *dv*, with the Appalachian, Mid South

and Florida regions exceeding 24 *dv*. The highest annual *dv* is reported in Washington D.C. at 29 *dv*, followed by Sipsey Wilderness at 28 *dv*.

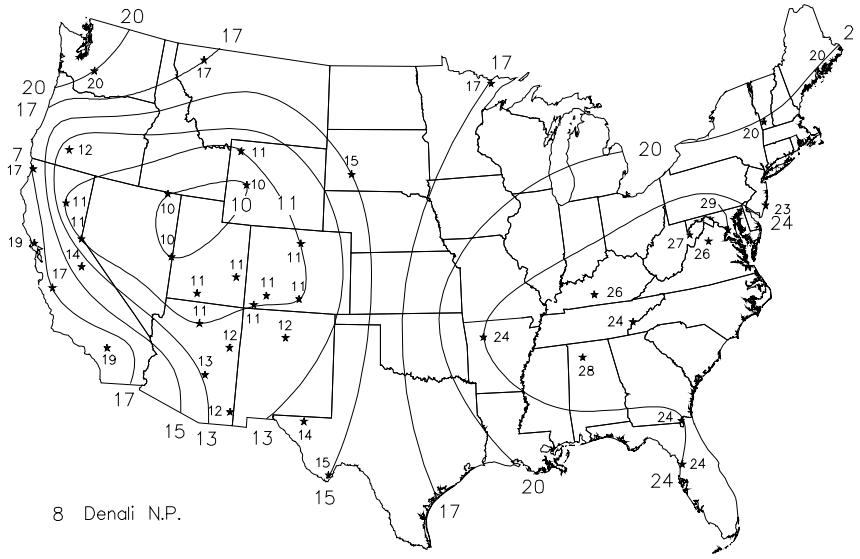

Figure S.3 Average visibility impairment in deciviews calculated from total (Rayleigh included) reconstructed light extinction for three years of IMPROVE, March 1992 through February 1995.

The general spatial trend noted above for the annual average *dv* generally holds true for each season's average *dv* as well. Specifically, the least impairment occurs in all or part of the Great Basin, Colorado Plateau, and Central Rockies, with gradients of increasing *dv* in any direction. The best visibility occurs during the winter and the worst in the summer. Visibility impairment in the spring and autumn are comparable.

S.6 Temporal Trends and Interrelationships of Aerosol Concentrations

The IMPROVE aerosol monitoring network, established in March 1988, initially consisted of 36 sites instrumented with aerosol sampling modules A through D. Many of the IMPROVE sites are successors to sites where aerosol monitoring with stacked filter units (SFU) was carried out as early as 1979. The IMPROVE sites that can be paired with antecedent SFU sites have an almost unbroken record of fine mass and sulfur from as early as 1979, and b_{abs} from 1983. Table S.2 lists the sites and time periods that IMPROVE or SFU samplers were operated. These data provide an excellent opportunity to look for evidence of temporal trends in aerosol concentrations. Two

distinct temporal trends are considered here: seasonal, and long-term trends of statistical measures such as maxima, minima, percentiles, and standard deviations.

Table S.2 Sites and time periods for IMPROVE and SFU.

Acronym	Full Name	SFU Start	SFU End	IMPROVE Start	IMPROVE End
ACAD	Acadia NP	9/21/85	11/28/87	3/01/88	Present
ARCH	Arches NP	9/28/79	11/28/87	3/01/88	5/92
BAND	Bandelier NM	10/02/82	2/09/85	3/01/88	Present
BIBE	Big Bend NP	7/27/82	11/28/87	3/01/88	Present
BRCA	Bryce Canyon NP	9/21/79	12/02/87	3/01/88	Present
BRLA	Brooklyn Lake	3/01/91	7/31/93	7/31/93	Present
CANY	Canyonlands NP	9/21/79	11/28/87	3/01/88	Present
CHIR	Chiricahua NM	6/8/82	5/31/86	3/01/88	Present
CRLA	Crater Lake NP	10/12/82	11/28/87	3/01/88	Present
CRMO	Craters of the Moon	7/17/82	3/29/86	5/12/92	Present
DENA	Denali NP &	9/10/86	11/25/87	3/01/88	Present
DEVA	Death Valley NP	6/01/82	3/29/86	10/18/93	Present
GLAC	Glacier NP	9/28/82	12/5/87	3/01/88	Present
GICL	Gila NF	10/1/79	8/31/81	3/28/94	Present
GRBA	Great Basin NP	10/12/82	3/29/86	5/00/88	Present
GRCA	Grand Canyon NP	8/03/79	11/28/87	3/01/88	Present
GRSA	Great Sand Dunes	9/15/80	8/31/81	5/04/88	Present
GRSM	Great Smoky Mtns	1/31/84	11/28/87	3/01/88	Present
GUMO	Guadalupe Mtns NP	2/19/83	12/02/87	3/01/88	Present
LAVO	Lassen Volcanic NP	6/29/82	5/29/84	3/01/88	Present
MEVE	Mesa Verde NP	10/30/82	12/05/87	3/01/88	Present
MORA	Mount Rainier NP	7/23/83	12/16/87	3/01/88	Present
PEFO	Petrified Forest NP	7/30/79	11/25/87	3/01/88	Present
ROMO	Rocky Mountain NP	9/21/79	12/02/87	9/15/90	Present
SAGU	Saguaro NM	7/2/85	8/31/88	3/1/88	Present
SALM	Salmon NF	9/01/90	11/13/93	11/09/93	Present
SHEN	Shenandoah NP	7/13/82	11/28/87	3/01/88	Present
TONT	Tonto NM	8/3/79	11/29/83	3/01/88	Present
VOYA	Voyageurs NP	7/13/85	Present	3/01/88	Present
YELL	Yellowstone NP	9/29/79	12/05/87	3/01/88	Present
YOSE	Yosemite NP	9/25/82	10/28/87	3/01/88	Present

NP = National Park NM = National Monument NF = National Forest

A hallmark of sites impacted by sulfate pollution is a distinct seasonal trend of sulfate concentrations manifested by high concentrations during the summer and lowest during the winter. Sulfate seasonality is attributed to many factors with seasonal changes in meteorology and photochemistry being the most influential. Sites that demonstrate the most sulfate seasonality are in the East and southern California, while sites in the intermountain west have little or no seasonality. Absorption also demonstrates a clear seasonal trend at many sites and tends to be highest during the summer and early autumn. The seasonality of absorption, unlike sulfate seasonality, is driven by seasonal changes of emissions. In the West, where the absorption seasonality is strongest, controlled burning and wildfires have a strong influence, while in the East the seasonality is less pronounced.

Demonstrated long-term trends fall into three categories: increases, decreases, and variable. Sites that demonstrate decreases are at Crater Lake and Rocky Mountain National Parks, where absorption dropped dramatically, and at Guadalupe Mountains National Park where sulfur is decreasing in the autumn. A clear demonstration of decreased sulfur concentrations as a result of emission reductions is in the desert southwest at Chiricahua National Monument. Two sites where increases have been observed are at Grand Canyon National Park in the autumn, where the 25th percentile of sulfur concentrations have increased steadily since 1980, and at Great Smoky Mountains National Park, where autumn concentrations of sulfur and absorption have increased. Other sites that demonstrate little or variable changes in sulfur concentrations are at Bryce Canyon, Rocky Mountain, and Crater Lake National Parks. Variable or little change in absorption was noted at Grand Canyon in the winter and Chiricahua in the summer.

The most notable observation from a national perspective is the lack of a clear uniform trend of sulfur concentration or absorption. There are local success stories related to emission controls, and there are failures most likely associated with increased local emissions or long-range transport. The bulk of the sites show little or variable trends in the long run.

The matrix scatter plots demonstrate correlations ranging between slight to strong between gravimetric fine mass, b_{abs}, and sulfur. Some of the strongest correlations are between fine mass and b_{abs}, even though light-absorbing material is a small fraction of fine mass suggesting an internal mixture of carbon with the primary constituents of the fine mass. The exceptions to this are sites in the eastern United States where sulfur is a large fraction of the fine mass; here sulfur shows strong correlations with fine mass indicative of strong sources. Weak correlations are usually manifested by 'fan shaped' scatters, some with hard edges, which suggest multiple sources with variable ratios of b_{abs} or sulfur.

S.7 Recommended Future Research

There are a number of uncertainties raised by the work described in this report that deserve additional study.

Organic Aerosol Measurement. The measurement of organic mass is still responsible for the most uncertainty in estimates of how various aerosol species affect visibility. Adjustments are made to the organic carbon mass to correct for the adsorption of organic aerosols on the filter. However, this adjustment often results in negative concentrations. This area needs to be considered in future studies. Also, the mass fractions of hydrogen and carbon in organics are based on an assumption of the hydrocarbon type. Future research should evaluate these fractions on the basis of the most common organic molecules in the samples.

Light-Absorbing Carbon Measurement. The work reported here suggests that b_{abs} estimated from LIPM is a more accurate measure of absorption than that derived from elemental carbon measurements. The difference between the estimates is significant at about a factor of two.

Hygroscopicity of Aerosols. The relative humidity correction terms applied to sulfate and nitrate need to be reevaluated. The sulfate and nitrate RH factors are based on ammonium sulfate. Specific curves should be developed for ammonium nitrate, which has a different deliquescence point than sulfate. Also, acidic sulfates (e.g., sulfuric acid and ammonium bisulfate) have higher water contents and higher light scattering efficiencies than ammonium sulfate. Furthermore, the hygroscopicity of organics is not currently well understood. Basic research is required in this area. Until such research is available, alternative assumptions regarding organic hygroscopicity should be tested.

Long-Term Trends. The analysis of long-term trends of fine mass concentrations, sulfur concentrations, and absorption as presented here is based on descriptive statistics and inspection. A major point of contention is the fact that two protocol changes occurred in the middle of the data record (SFU vs IMPROVE samplers; and, 72 hour vs 24 hour duration samples). No IMPROVE and SFU samplers were operated concurrently side by side, nor were any 72-hour duration samples collected concurrently with 24-hour duration samples. Therefore, any bias in the data due to protocol changes should be revealed in the data; moreover, since the protocol changes were system wide any bias should be systematic. If there is a bias in the data then long- term trends, if any, could be masked or exaggerated. A detailed statistical analysis across all sites needs to be carried out to look for and quantify systematic changes in the data behavior that can be attributed to protocol changes. This understanding is required for correct interpretation of long-term trends.

In addition to the above refinements in the analyses conducted in this report, additional data analysis is recommended. For example, back trajectory analysis and spatial/temporal pattern analysis of episodes is recommended to determine the source region contributions to elevated concentrations. Also, the cleanest days should be studied to determine the source areas and meteorological causes of clean air.

CHAPTER 1

INTRODUCTION

This report is the second in a series of periodic reports that describe the data collected by the Interagency Monitoring of Protected Visual Environments (IMPROVE) monitoring network. The objectives of this report are threefold:

(1) To describe the spatial and temporal variation of visibility, as measured by the light-extinction coefficient, and the chemical composition of the visibility-degrading aerosol[1] for three years of operation of the network: March 1992 through February 1995.

(2) To provide a first estimate of the apportionment of visibility impairment to the fundamental chemical species, such as sulfates, nitrates, organics and elemental carbon, and soil dust.

(3) To document the long-term trends (or lack of trends) of aerosol mass and its principal aerosol species.

1.1 Objectives of Visibility Monitoring

The primary objectives of IMPROVE are the following:

(1) To establish current background visibility levels in Class I areas;

(2) To identify chemical species and emission sources responsible for existing man-made visibility impairment.

(3) To document long-term trends for assessing progress toward the national visibility goal.

By measuring visibility routinely over a network and over a sufficiently long period of time, the first and third objectives of IMPROVE can be met. The monitoring also meets a portion of the second objective: the identification of the chemical composition of the visibility-degrading aerosol.

[1]An aerosol is a suspension of fine and coarse solid and liquid particles in air. Particles, especially fine particles less than 2.5 ìm, scatter light and degrade the visual information content of a scene (e.g., contrast, color, line, and texture). Fine particles consist of different chemical species either within the same particle (internally mixed) or in different particles (externally mixed). Significant chemical species found in particles include sulfates, nitrates, organics and elemental carbon, and soil dust. The sulfates, nitrates, and some hygroscopic organics absorb water from the atmosphere, thereby increasing significantly the light-scattering particle size and mass.

Each of these IMPROVE objectives are discussed in greater detail below.

Establish Current Visibility. This is necessary for two reasons. First, visibility levels monitored at a Class I area, when compared to surrounding area visibility or area estimates for natural levels, may be sufficient to indicate man-made impairment. Second, knowledge of existing visibility levels is required to model the anticipated visibility effects of proposed emission sources, because increments of pollution are more noticeable in clear conditions.

Establishment of present visibility levels requires monitoring that is appropriate for both surface and elevated layer impairment distributions. Optical monitoring systems, such as the transmissometer, are appropriate for surface haze monitoring, while scene monitoring with photography is the only practical way to routinely monitor elevated layers.

Visibility changes with time: diurnal, seasonal, and yearly variations all exist. Though five to eight years of data would be considered ideal for establishing present seasonal and annual averaged conditions, a minimum of one year is a reasonable compromise if that year is typical from a meteorological and source activity point of view.

Source Identification. Identification of chemical species and emission sources responsible for man-made visibility impairment is necessary to protect Class I areas, as called for by Congress. Monitoring is the principal means of gathering information needed to identify the contribution to impairment by emission sources. Even to distinguish man-made from natural impairment, which is fundamental to the national visibility goals, requires information derived from monitoring data.

Aerosol and scene monitoring are the primary sources of emission source identification information. Photography of a plume emanating from its source and impacting a Class I area is sufficient to indicate impairment. Furthermore, photographs can be evaluated to indicate the density or intensity of the visible plume. Unfortunately, most visibility impairment does not lend itself to this simple type of source attribution. Often sources are not visible from any line of sight that includes the Class I area, or their plumes disperse to a haze layer before reaching it.

Visibility impacts are often caused by aerosols formed over time from gaseous pollutants that are emitted without visibly noticeable plumes. Characteristics of the aerosol that are responsible for the haze provide valuable information that can be used in conjunction with other information to help identify the responsible emission sources. It is possible to statistically relate measured optical data to corresponding aerosol composition data to estimate the relative importance of the various major components of the aerosol. The result, known as an extinction budget, should narrow the list of possible sources responsible for large impacts. For example, if organic carbon is shown to be responsible for 75% of the extinction coefficient, the major sources responsible must emit organic carbon or precursor gases that form organic aerosols.

Another related approach for source identification using aerosol data is known as receptor modeling. Instead of using only the major aerosol components that are directly responsible for the impairment, receptor models use relative concentrations of trace components that can more specifically identify the influence of individual sources (or source types).

Long-Term Trends. With the establishment of a long-term goal of no man-made visibility impairment in protected areas, Congress imposed the responsibility to show progress towards meeting that goal. Trends monitoring is an ideal approach for tracking the visibility conditions of Class I areas.

Optical and scene monitoring conducted to establish present visibility levels (described above), if conducted in perpetuity, can provide the data required to determine long-term visibility trends. Alternatively, tracking levels of ambient aerosols and the key aerosol species will reveal the effectiveness of emission control programs. In either case, in order to determine the effectiveness of individual concurrent emission reduction programs, it is necessary to conduct aerosol monitoring to support extinction budget analysis as described above.

1.2 Overview of the IMPROVE Monitoring Network

The design of the IMPROVE monitoring network was resource and funding limited so that it was not practical to place monitoring stations at all 156 mandatory Class I areas where visibility is an important attribute. Instead, the IMPROVE Steering Committee selected a set of sites that were representative of the Class I areas. For the first IMPROVE report, published in the spring of 1993, data for 36 sites was summarized. In the intervening time the IMPROVE network has evolved; two sites were dropped, some sites were downgraded to the measurement of a subset of the variables measured at a fully complemented site, and other sites have been added. There are currently a total of 58 IMPROVE sites with various configurations of optical and aerosol monitoring equipment. For this report, only the 43 IMPROVE sites that are fully configured as aerosol monitoring sites with data for the three-year period, March 1992 through February 1995, are utilized. However, only 26 of the sites have optical monitoring equipment (e.g., transmissometers or nephelometers to measure visibility-related parameters).

View monitoring at all aerosol monitoring sites was routinely done for the first five years of the IMPROVE program. View monitoring is used to document the range of visibility conditions for a particular scene. Due to resource considerations, five years of scene monitoring was judged to adequately document the range of visibility. Now, view monitoring is only carried out at selected sites with less than five years of data. View monitoring is accomplished by automated 35-mm camera systems. These systems provide three color slides per day to document the appearance of a selected scene at each of the IMPROVE sites. The slides are used to interpret measurements, to communicate perceived visual conditions, and, if needed, to derive quantitative estimates of light extinction by microdensitometry.

Figure 1.1 shows a map of the United States indicating the locations of the 43 monitoring sites analyzed in this report. On the basis of regional similarities, the sites were grouped into 21 regions, listed in Table 1.1.

Figure 1.1 The 42 IMPROVE sites out of 43 included in the report. Denali National Park in Alaska is not shown.

Table 1.1 IMPROVE and NPS/IMPROVE protocol sites according to region.

Alaska (AKA) •Denali NP (DENA) **Appalachian Mountains (APP)** •Great Smoky Mountains NP (GRSM) •Shenandoah NP (SHEN) •Dolly Sods WA (DOSO) **Boundary Waters (BWA)** •Boundary Waters Canoe Area (BOWA) **Cascade Mountains (CAS)** •Mount Rainier NP (MORA) **Central Rocky Mountains (CRK)** •Bridger WA (BRID) •Great Sand Dunes NM (GRSA) •Rocky Mountain NP (ROMO) •Weminuche WA (WEMI) •Yellowstone NP (YELL) **Coastal Mountains (CST)** •Pinnacles NM (PINN) •Point Reyes NS (PORE) •Redwood NP (REDW) **Colorado Plateau (CPL)** •Bandelier NM (BAND) •Bryce Canyon NP (BRCA) •Canyonlands NP (CANY) •Grand Canyon NP (GRCA) •Mesa Verde NP (MEVE) •Petrified Forest NP (PEFO) **Florida (FLA)** •Chassahowitzka NWR (CHAS) •Okefenokee NWR (OKEF) **Great Basin (GBA)** •Jarbidge WA (JARB) •Great Basin NP (GRBA)	**Lake Tahoe (LTA)** •D.L. Bliss State Park (BLISS) •South Lake Tahoe (SOLA) **Mid Atlantic (MAT)** •Edmond B. Forsythe NWR (EBFO) **Mid South (MDS)** •Upper Buffalo WA (UPBU) •Sipsey WA (SIPS) •Mammoth Cave NP (MACA) **Northeast (NEA)** •Acadia NP (ACAD) •Lye Brook WA (LYBR) **Northern Great Plains (NGP)** •Badlands NM (BADL) **Northern Rocky Mountains (NRK)** •Glacier NP (GLAC) **Sierra Nevada (SRA)** •Yosemite NP (YOSE) **Sierra-Humboldt (SRH)** •Crater Lake NP (CRLA) •Lassen Volcanoes NP (LAVO) **Sonoran Desert (SON)** •Chiricahua NM (CHIR) •Tonto NM (TONT) **Southern California (SCA)** •San Gorgonio WA (SAGO) **Washington, D.C. (WDC)** •Washington, D.C. (WASH) **West Texas (WTX)** •Big Bend NP (BIBE) •Guadalupe Mountains NM (GUMO)

NP = National Park
NM = National Monument
WA = Wilderness Area
NWR = National Wildlife Refuge
NS = National Seashore

The routine IMPROVE monitoring approach now involves aerosol, and optical monitoring. Aerosol monitoring measures the mass concentration (in micrograms per cubic meter, $\mu g/m^3$) and the chemical composition of the particles. Optical monitoring measures the light-extinction coefficient (b_{ext}) using a transmissometer or the light-scattering coefficient (b_{scat}) using a nephelometer.

Aerosol monitoring in the IMPROVE network is accomplished by a combination of particle sampling and sample analysis. The sampler employed was designed specifically for the program. It collects four simultaneous samples: one PM_{10} sample (particles less than 10 micrometers, μm, in diameter) on a Teflon filter and three $PM_{2.5}$ samples (particles less than 2.5 μm in diameter) on Teflon, nylon, and quartz filters. Each of the four samples is collected by a separate subsystem (or module) including everything from the inlet to the pump with only the support structure and controller/timer in common. The particle size segregation for the PM_{10} module is accomplished by a wind insensitive inlet with a 10 μm cutoff, while the $PM_{2.5}$ segregation is produced by passing the sampled air through a cyclone separator. Constant sample flow is maintained by a critical orifice in each module. The IMPROVE sampler is programmed to automatically collect two 24-hour duration samples per week.

Only mass analyses are conducted on the PM_{10} samples. The $PM_{2.5}$ samples are analyzed for mass, elements, ions (including particulate nitrate sampled through a denuder), organics and elemental carbon, and optical absorption.

At many sites in the IMPROVE network, long-path transmissometers are employed for optical measurements. These instruments measure the amount of light transmitted through the atmosphere over a known distance, usually 0.5 to 10 kilometers, between the light source (transmitter) and the light-monitoring component (receiver). Transmission measurements are converted electronically to the path-averaged, light-extinction coefficient (b_{ext}). At other sites nephelometers are used that measure the light-scattering coefficient (b_{scat}) from an enclosed volume of air.

In addition to the aerosol and optical monitoring, those sites that have optical monitoring have temperature and relative humidity instruments. Liquid water is a component of the hygroscopic sulfate, nitrate, and possibly organic carbon fractions, but it is not quantified by any of the filter sampling techniques. Relative humidity measurements are used to estimate the amount of liquid water associated with these particles.

1.3 Background Regarding Visibility Impairment and Aerosols

Visibility is usually characterized either by visual range (the greatest distance that a large dark object can be seen) or by the light-extinction coefficient (the attenuation of light per unit distance due to scattering and absorption by gases and particles in the atmosphere). Under certain assumed conditions these two measures of visibility can be shown to be inversely related to each other. Visual range functions well as an aid in military operations and transportation safety. Issues of

concern for such use include: the minimum distance required to land an aircraft, the distance to the first appearance of a military target or an enemy aircraft or ship, and safe maneuvering distances under impaired visibility conditions. Because of the use of familiar distance units, the simple definition, and the ability of any sighted person to characterize visual conditions with this parameter without instruments, visual range is likely to remain the most popular measure of atmospheric visibility.

Extinction coefficient is used most by scientists concerned with the causes of reduced visibility. There are direct relationships between the concentrations of the atmospheric constituents and their contribution to the extinction coefficient. Apportioning the extinction coefficient to atmospheric constituents provides a method to estimate the change in visibility caused by a change in constituent concentrations. This methodology, known as extinction budget analysis, is important for assessing the visibility consequences of proposed pollutant emission sources, or for determining the extent of pollution control required to meet a desired visibility condition. Interest in the causes of visibility impairment is expected to continue and the extinction coefficient will remain important in visibility research and assessment.

Neither visual range nor extinction coefficient is linear with humanly perceived changes caused by uniform haze (i.e., as opposed to elevated haze layers and plumes). For example, a given change in visual range or extinction coefficient can result in a scene change that is either unnoticeably small or very apparent depending on the baseline visibility conditions. Presentation of visibility measurement data or model results in terms of visual range or extinction coefficient can lead to misinterpretation by those who are not aware of the nonlinear relationship.

To rigorously determine the perceived visual effect of a change in extinction coefficient requires the use of radiative transfer modeling to determine the changes in light from the field of view arriving at the observer location, followed by the use of psychophysical modeling to determine the response to the light by the eye-brain system. Results are dependent not only on the baseline and changes to atmospheric optical conditions, but also on the characteristics of the scene and its lighting. The complexity of employing such a procedure and the dependence of the results on non-atmospheric factors prevent its widespread use to characterize perceived visibility changes resulting from changes in air quality.

Parametric analysis methods have been used to suggest that a constant fractional change in extinction coefficient or visual range produces a similar perceptual change for a scene regardless of baseline conditions. Simplifying assumptions eliminate the need to consider the visibility effects of scene and lighting conditions. Using the relationship of a constant fractional change in extinction coefficient to perceived visual change, a new visibility index called deciview (dv) is defined as:

$$dv = 10 \ln(b_{ext}/0.01 \text{ km}^{-1}) \tag{1.1}$$

where extinction coefficient is expressed in km^{-1} [Pitchford and Malm, 1994]. A one *dv* change is about a 10% change in extinction coefficient, which is a small but perceptible scenic change under many circumstances. The deciview scale is near zero for pristine atmosphere (*dv* = 0 for Rayleigh condition at about 1.8 km elevation) and increases as visibility is degraded. Like the decibel scale for sound, equal changes in deciview are equally perceptible.

1.3.1 Relationship Between Visibility and Aerosol Concentrations

Visibility is degraded by light scattered into and out of the line of sight and by light absorbed along the line of sight. Light extinction (the sum of light scattering and absorption) is usually quantified using the light-extinction coefficient (b_{ext}), which may be thought of as the atmospheric concentration of light-extinction, cross-sectional area. Light extinction has units of 1/length.

The light-extinction coefficient (b_{ext}) is the sum of the light-scattering coefficient (b_{scat}) and the light-absorption coefficient (b_{abs}). Light scattering results from the natural Rayleigh scatter (b_{Ray}) from air molecules (which causes the blue sky) and the scattering caused by suspended particles in the atmosphere (aerosols). Particle scatter (b_{sp}) can be caused by natural aerosol (e.g., wind-blown dust and fog) or by man-made aerosols (e.g., sulfates, nitrates, carbonaceous aerosols, and other fine and coarse particles). Light absorption results from gases (b_{ag}) and particles (b_{ap}). Nitrogen dioxide (NO_2) is the only major light-absorbing gas in the lower atmosphere. Its strong wavelength-dependent scatter causes yellow-brown discoloration if present in sufficient quantities. Soot (elemental carbon) is thought to be the dominant light-absorbing particle in the atmosphere. Thus, the total light extinction is the sum of its components:

$$b_{ext} = b_{scat} + b_{abs} = b_{Ray} + b_{sp} + b_{ag} + b_{ap} \qquad (1.2)$$

The particle light-scattering coefficient (b_{sp}), in turn, is composed of the contributions from individual species. Fine particles are much more efficient at light scattering (per unit mass) than larger particles. Thus, it makes sense to divide the contributions to b_{sp} into the contributions from various species of fine and coarse particles. In this study, we specifically evaluated the following components of fine particles (those with diameters less than 2.5 ìm): sulfate (SO), nitrate (NO), organic carbon, elemental carbon (soot), and soil. In addition to these chemical species, the effect of water associated with sulfates, nitrates, and some organics need to be considered in the overall assessment of light extinction. Finally, the coarse fraction of PM_{10} (those with diameters between 2.5 and 10 ìm) are separately considered.

The light-extinction coefficient can be written with a number of assumptions, as the sum of the products of the concentrations of individual species and their respective light-extinction efficiencies:

$$b_{ext} = b_{Ray} + \sum \beta_i C_i \qquad (1.3)$$

where $\hat{a}_i$ is the light-extinction efficiency (m^2/g) of species *i*, C_i is the atmospheric concentration of

species *i* (ìg/m^3), and the summation is over all light-interacting species (i.e., sulfates, nitrates, organic carbon, elemental carbon, other fine particles, coarse particles, and NO_2). The above units, when multiplied, yield units for b_{ext} of 10^{-6} m^{-1} or $(10^6 \text{ m})^{-1}$, or as we prefer to label it here, inverse megameters (Mm^{-1}).

1.3.2 Effect of Relative Humidity on Light Scattering

Sulfates, nitrates, and some organics can combine with water in the vapor phase to form solutions. Thus, at some humidity conditions, considerable water may be associated with these species. Although the overall light-scattering efficiency is on the order of 3 m^2/g for these solutions, if the light-scattering efficiency is stated in terms of the mass of dry sulfate ($SO_4^=$), the efficiency must be larger than 3 m^2/g to account for the additional mass (and volume) of the associated water. In addition, the associated cations (H^+ and NH_4^+) must also be included. As a result, light-scattering efficiency per unit of dry sulfate can be much larger than 3 m^2/g. This hygroscopic effect can be described by the following equation:

$$\beta_{wet} = k f_{RH} \beta_{dry} \tag{1.4}$$

where $\hat{a}_{wet}$ is the light extinction efficiency of the wet sulfate, nitrate, and/or organic solution, *k* is the ratio in molecular weight of the neutralized species (e.g., ammonium sulfate or ammonium nitrate) to the anion (sulfate, nitrate), f_{RH} is a factor that accounts for the liquid water associated with the aerosol at the given relative humidity (*RH*), and $\hat{a}_{dry}$ is the light-extinction efficiency of the dry particle.

1.4 Organization of the Report

This report is divided into six chapters. Chapter 2 summarizes the optical and aerosol measurement techniques and details the assumptions for determining the chemical composition of the aerosol species. The spatial and seasonal patterns of aerosol mass and chemical composition are summarized in Chapter 3. Chapter 4 discusses the theory of light extinction in detail and specifies the assumptions used to reconstruct light extinction from aerosol measurements. Using reconstructed light extinction, Chapter 5 discusses the spatial and seasonal patterns of reconstructed light extinction. Chapter 6 discusses the long-term temporal trends of two key aerosol species, sulfur and light-absorbing carbon.

1.5 References

Pitchford, M.L., and Malm, W.C. Development and applications of a standard visual index, *Atmospheric Environment*, **28**(5):1049-1054, 1994.

CHAPTER 2

OPTICAL AND AEROSOL DATA

Monitoring of protected visibility areas is conducted on two complementary fronts: 1) optical monitoring of visibility in these areas; and 2) monitoring the concentration and composition of the aerosols in these areas. For optical monitoring, two measurements are possible, extinction (b_{ext}) measured by transmissometers and scattering (b_{scat}) measured by nephelometers. The IMPROVE particulate monitors provide measurements of PM_{10} mass and $PM_{2.5}$ mass. Chemical and elemental analysis of the $PM_{2.5}$ fraction is carried out to identify the fine aerosol species. What follows is a brief description of the IMPROVE monitoring instruments, their operating characteristics, and the data derived from them.

2.1 Transmissometers

Transmissometers are calibrated to measure the irradiance, at a wavelength of 550 nm, of a light source after the light has traveled over a finite atmospheric path. The transmittance of the path is calculated by dividing the measured irradiance at the end of the path by the calibrated initial intensity of the light source. Bouger's law is applied to calculate the extinction. Because of the relatively clean atmospheres found in the western United States, path lengths of a few kilometers are required to achieve the necessary sensitivity to resolve extinctions near the Rayleigh limit.

The transmissometers used in this study are the OPTEC, Inc., LPV-2 instruments, which have been in use since 1986. Their use in remote locations such as national parks is discussed by Molenar *et a1*. [1989], while their use in urban settings is presented by Dietrich *et al.* [1989]. Data processing algorithms that incorporate corrections for interferences are thoroughly discussed by Molenar and Malm [1992]. Basically, there are five checks the data must pass to be incorporated into a validated data set. They are:

1) relative humidity must be less than 90%;
2) maximum extinction cannot exceed a threshold value based on photometer sensitivity and path length;
3) variability in extinction readings taken over a period of one hour cannot exceed a threshold value;
4) rate of change of hourly average extinction measurements cannot exceed a threshold value; and
5) isolated data points. (By definition any hourly average data point passing the above four criteria but falling in between two hourly average data points that have failed the criteria is referred to as "isolated." It is conservatively assumed that it has also been affected by

interferences.)

Molenar *et al.* [1989] discuss the inherent uncertainties associated with the measurement. The accuracy of the transmission measurement, as determined by field and laboratory calibrations, is better than 1%. However, the accuracy of the derived extinction is dependent on the accuracy of the transmission measurement in field conditions. The transmission calculation is determined from an absolute (as opposed to relative) measurement of irradiance of a light source of known intensity that is located some known distance from the receiver. The measurement is made through optics that are exposed to the ambient atmosphere but are assumed to be free of dust or other films, which tend to build up on the optical surfaces. The uncertainties associated with these parameters contribute to the overall uncertainty of the measurement. For a typical 5 km path length the estimated uncertainty is about 4 Mm^{-1}.

2.2 Integrating Nephelometers

Integrating nephelometers measure the scattering of light over a defined band of visible wavelengths from an enclosed volume of air. Historically, integrating nephelometers used in most major field studies have underestimated scattering because of:

1) modification of the ambient aerosol by heating when a large fraction of the sampled aerosol is hygroscopic;
2) inlet, sampling train, and optical chamber design that limits the size of particles that make it into the sampling chamber;
3) optical geometry that causes a truncation of the true scattering volume; and
4) electronics that display large nonlinear drifts in zero and span values.

The OPTEC NGN-2 ambient integrating nephelometer was developed to minimize these limitations of integrating nephelometry. The instrument, which measures light scattering at an effective wavelength of 550 nm, is described in some detail by Molenar *et al.* [1989]. It is an "open air" design that has minimal heating characteristics, and because it is open air it tends to allow a wider spectrum of particles to pass through the instrument. However, the cutpoint of the instrument has not been characterized. It is also designed with solid-state electronics that are very stable over wide temperature and humidity shifts. It still has an inherent limitation of an abbreviated acceptance angle in that it only samples light scattered between 5 and 175^{o}. Calibration of the instrument and data validation and processing algorithms are also discussed in detail in Molenar and Malm [1992].

Unlike transmissometers, where an uncertainty in transmittance leads to an additive error in extinction, uncertainties in nephelometer calibration lead to a multiplicative error in measured scattering. Typical uncertainties for the OPTEC instrument are on the order of 5-10% [Molenar and Malm, 1992].

2.3 Particle Sampling System

The standard IMPROVE sampling module consists of: 1) a size selective inlet; 2) a cyclone to provide a particle size cutoff based on the flow rate; 3) collection substrates; 4) a critical orifice that provides the proper flow rate for the desired particle size cutoff; and 5) a vacuum pump that produces the flow. The system is described in some detail by Malm *et al.* [1994] and Eldred *et al.* [1988] and is only briefly described here.

The sampling system consists of four independent sampling modules. Three modules (denoted A, B, and C) employ a cyclone with a flow rate of 22.7 l/min that allows for collection of fine particles less than 2.5 ìm in diameter [John *et al.*, 1988]. The fourth module (D) is a PM_{10} sampler with a wind insensitive size selective inlet that collects particles less than 10 ìm in diameter. Table 2.1 summarizes the substrates used and aerosol species measured on each filter.

Table 2.1 Filter media and analysis techniques used to determine concentrations of particulate matter species from IMPROVE sampler modules.

Module	Filter Media	Analyses
A	Teflon	gravimetric analysis for mass < 2.5 ìm dia. [1]LIPM for optical absorption [2]PIXE for elements Na to Pb [3]PESA for H
B	nylon (denuded)	ion chromatography for NO_3 and SO_4
C	quartz	[4]TOR for organic and light-absorbing C
D	Teflon	gravimetric analysis for mass < 10 ìm dia.

[1]LIPM - Laser Integrating Plate Method
[2]PIXE - Particle Induced X-ray Emission
[3]PESA - Proton Elastic Scattering
[4]TOR - Thermal Optical Reflectance

Gravimetric mass (channel A fine mass, channel D PM_{10} mass) is measured as the difference between the weight of the substrates before and after sampling, using an electromicrobalance. The channel A Teflon substrates are analyzed for sulfur and other elements by Particle Induced X-ray Emission (PIXE), and simultaneously for hydrogen by Proton Elastic Scattering Analysis (PESA) [Cahill *et al.*, 1986].

The coefficient of light absorption for fine particles, b_{abs}, is also determined from the channel A Teflon substrates using a Laser Integrating Plate Method (LIPM) [Cahill *et al.*, 1986]. This involves direct measurement of the absorption of a laser beam by a sample over the area of the sample.

Extract from the channel B nylon substrates are analyzed by Ion Chromatography (IC) for sulfate and nitrate ions from which the sulfate and nitrate compounds can be estimated [Cahill *et al.*, 1986; Malm *et al.*, 1994].

The channel C quartz substrates are analyzed by Thermal Optical Reflectance (TOR) combustion for organic and elemental carbon [Chow *et al.*, 1993]. Because carbon derived from TOR analysis will be explored in some detail in Chapter 4, a more complete description of the analysis scheme is presented than for the other analytic procedures.

TOR involves: 1) heating a sample through a series of temperature increases or steps (in a pure helium atmosphere to which oxygen is added in the later stages to enable the volatilization of elemental carbon); 2) converting the carbon evolved at each step into CO_2, using an oxidizer (MnO_2 at 912^oC); and 3) reducing the CO_2 to methane, which is then quantified by passage through a flame ionization detector. Over the mid range of the TOR heating (between about 130^oC and 550^oC), charring of the sample occurs, due to pyrolysis of organic particles; this is monitored as a decrease in the reflectance from the sample surface. When the reflectance reaches a minimum, 2% oxygen is added to the atmosphere. This allows the elemental carbon in the sample, including the char produced by pyrolysis of organic matter, to oxidize and the reflectance of the sample increases as the char is removed. All carbon measured up to the point where the reflectance reattains its initial value is traditionally interpreted as organic carbon. Carbon evolved beyond this point is reported as elemental carbon. Overall, the peaks in the carbon evolution from the sample are operationally defined as O1 (25^oC-140^oC), O2 (140^oC-230^oC), O3 (230^oC-450^oC), and O4 (450^oC-550^oC). At 1100 seconds and at 550^oC, 2% oxygen is introduced. The carbon evolved between 1100 seconds and when the sample reflectance returns to its initial value is referred to as pyrolized carbon (OP). The remainder of the carbon evolved at 550^oC and 2% oxygen is labeled as E1. Temperatures are then ramped up to 800^oC in two steps. The evolved carbon is labeled as E2 (550^oC-700^oC) and E3 (700^oC-800^oC). Traditionally, O1, O2+O3+O4+OP, E1, and E2+E3 are referred to as OCLT, OCHT, ECLT, and ECHT, respectively. Organic carbon (OC) is assumed to be the sum of OCLT and OCHT. High temperature carbon, often referred to as elemental carbon or light-absorbing carbon (LAC), is the sum of ECLT and ECHT.

2.4 Determination of Aerosol Types

The fine aerosol species at most continental sites are classified into five major types: sulfates, nitrates, organics, light-absorbing carbon, and soil. Methods for apportionment of measured mass to the various aerosol species are detailed in Malm *et al.* [1994] and only a summary will be presented here. The major aerosol types are composites of the elements and ions measured in IMPROVE samplers, and their concentrations or masses are calculated from the masses of the

measured elements and ions according to their presumed or probable composition and are summarized by Table 2.2. The convention used here to denote the mass concentration of a measured element, ion, or species is to enclose its symbol in brackets ([ ]).

In the West, most sulfur is in the form of ammonium sulfate. In the East, or other environments where ammonia can be limited, it is recognized that acidic species such as ammonium bisulfate and sulfuric acid are not uncommon. However, for a first approximation, all elemental sulfur is interpreted as being in the form of ammonium sulfate, and ammonium sulfate concentrations are estimated by multiplying elemental sulfur concentrations by 4.125. For simplicity, ammonium sulfate is referred to as sulfate.

Table 2.2. The formulae and assumptions applied to IMPROVE sampler measurements to derive the principal fine aerosol species, reconstructed fine mass, and coarse mass. The brackets indicate the mass concentration of the aerosol species or element.

SPECIES	FORMULA	ASSUMPTIONS
SULFATE	4.125[S]	All elemental S is from sulfate. All sulfate is from ammonium sulfate.
NITRATE	1.29[NO_3]	Denuder efficiency is close to 100%. All nitrate is from ammonium nitrate.
EC (elemental carbon)	[ECLT] + [ECHT]	All high temperature carbon is elemental.
OMC (organic mass from carbon)	1.4{[OCLT]+[OCHT]}	Average organic molecule is 70% carbon.
SOIL (fine soil)	2.2[Al]+2.19[Si] +1.63[Ca]+2.42[Fe] +1.94[Ti]	[Soil K]=0.6[Fe]. FeO and Fe_2O_3 are equally abundant. A factor of 1.16 is used for MgO, Na_2O, H_2O, CO_2.
RCFM (reconstructed fine mass)	[SULFATE]+[NITRATE] +[LAC]+[OMC]+[SOIL]	Represents dry ambient fine aerosol mass for continental sites.
CM (coarse mass)	[PM_{10}] - [$PM_{2.5}$]	Consists only of insoluble soil particles.

Assuming, as is the case for sulfate, that the collected nitrate ion is associated with fully neutralized ammonium nitrate aerosol (NH_4NO_3). The mass of ammonium nitrate is estimated by using a multiplication factor of 1.29 and is referred to as simply nitrate.

Organic mass (organics) concentration is estimated by:

$$[OMC] = 1.4([OCLT] + [OCHT]\ ) \qquad (2.1)$$

The factor of 1.4 assumes that organic mass contains a constant fraction of carbon by weight [Watson *et al.,* 1988].

Light-absorbing carbon concentration, usually thought of as elemental carbon, is defined as the sum of E1+E2+E3 or more conventionally as:

$$[LAC] = [ECLT + ECHT] \qquad (2.2)$$

where ECLT and ECHT are the low and high temperature elemental carbon concentrations.

Soil mass concentration is estimated by summing the elements predominantly associated with soil, plus oxygen for the normal oxides (Al_2O_3, SiO_2, CaO, K_2O, FeO, Fe_2O_3, TiO_2), plus a correction for other compounds such as MgO, Na_2O, water, and carbonate. The final equation for fine soil is:

$$[SOIL] = 2.20[Al] + 2.49[Si] + 1.63[Ca] + 2.42[Fe] + 1.94[Ti] \qquad (2.3)$$

Components of these factors were confirmed in comparisons of local resuspended soils and ambient aerosols in the western United States [Cahill *et al.,* 1981; Pitchford *et al.,* 1981].

The sum of the above five composites should provide a reasonable estimate of the ambient fine mass concentration measured in the atmosphere (RCFM). The equation for RCFM concentration is therefore:

$$[RCFM] = [SULFATE] + [NITRATE] + [LAC] + [OMC] + [SOIL] \qquad (2.4)$$

Coarse mass (CM) is estimated gravimetrically by subtracting fine mass ($PM_{2.5}$) concentration from total aerosol mass (PM_{10}) concentration:

$$[CM] = [PM_{10}] - [PM_{2.5}] \qquad (2.5)$$

In the IMPROVE program additional chemical analysis is not carried out on the coarse fraction. However, it is known that in rural or remote areas of the country the primary constituent of coarse mass is naturally occurring wind-blown dust along with some vegetative material [Noll *et al.,* 1985; Noll, 1991].

The self consistency and overall quality of the aerosol measurements are assured by redundancy and intercomparisons between independently measured species. A detailed description of

validation and quality assurance procedures is available in Malm *et al.* [1994], Sisler *et al.* [1993], and Eldred *et al.* [1988]. In the most general sense, validation is a matter of comparing chemically-related species that have been measured in different channels. Fortunately, the design of the IMPROVE sampler allows for redundancy between certain channel A measurements and channel B and C measurements of the ions and carbons enabling quality control checks. For example, in the IMPROVE network, it was found that elemental sulfur mass times three agrees well with the sulfate ion measured in channel B; validating the assumption that concentrations of sulfate aerosols can be estimated by channel A PIXE analysis [Sisler et al., 1993]. However, when comparing measured fine mass to RCFM, two complicating factors must be dealt with. First, a large portion of the nitrates (≥50%) are presumed to volatilize from the channel A teflon filter; and second, it is presumed that there is residual water on the filters due to the soluble species.

2.5 References

Cahill, T.A., R.A. Eldred, and P.J. Feeney, Particulate monitoring and data analysis for theNational Park Service 1982-1985, University of California, Davis, 1986.

Cahill, T.A., L.L. Ashbaugh, R.A. Eldred, P.J. Feeney, B.H. Kusko, and R.G. Flocchini, Comparisons between size-segregated resuspended soil samples and ambient aerosols in the western united States, In *Atmospheric Aerosol: Source/Air Quality Relationships, Am. Chem. Soc. Symp. Ser.*, **167**, edited by E. Macias, Washington, D.C., 1981.

Chow, J.C., J.G. Watson, L.C. Pritchett, W.R. Pierson, C.A. Frazier, and R.G. Purcell, The DRI thermal/optical reflectance carbon analysis system: description, evaluation, and applications in U.S. air quality studies, *Atmospheric Environment*, **27(A)**, (8), 1185-1201, 1993.

Dietrich, D.L., J.D. Molenar, J.F. Faust, Transmissometer extinction measurements in an urban environment, In Visibility and Fine Particles, C.V. Mathai, Ed., AWMA, Pittsburgh, pages 374-383, 1989.

Eldred, R.A., T.A. Cahill, M. Pitchford, and W.C. Malm, IMPROVE-a new remote areaparticulate monitoring system for visibility studies, *Proc. APCA (Air Pollution Control Assoc.) Ann. Mtg.*, **81**, 1-16, 1988.

John, W., S.M. Wall, and J.L. Ondo, A new method for nitric acid and nitrate aerosol measurement using the dichotomous, *Atmospheric Environment*, **22**, 1627-1635, 1988.

Malm, W.C., J.F. Sisler, D. Huffman, R.A. Eldred, and T.A. Cahill, Spatial and seasonal trends in particle concentration and optical extinction in the United States, *J. Geo. Res.*, **99(D1)**, 1347-1370, 1994.

Molenar, J.F. and W.C. Malm, Ambient optical monitoring techniques, presented at the Conference

on Visibility and Fine Particles, Vienna, Austria, September, 1992.

Molenar, J.F, D.L. Dietrich, and R.M. Tree, Application of a long range transmissometer to measure the ambient atmospheric extinction coefficient in remote pristine environments, In Visibility and Fine Particles, C.V. Mathai, Ed., 374-383. AWMA, Pittsburgh, 1989.

Noll, K.E., Collection and characteristics of atmospheric coarse particles, Final Report, Dept. of Environmental Engineering, Illinois Institute of Technology, Chicago, 1991.

Noll, K.E., A. Pontius, R. Frey, and M. Gould, Comparison of atmospheric coarse particles at an urban and non-urban site, *Atmospheric Environment*, **19(11)**: 1931-1943, 1985.

Pitchford, M., R.G. Flocchini, R.G. Draftz, T.A. Cahill, L.L. Ashbaugh, and R.A. Eldred, Silicon in submicron particles in the southwest, *Atmospheric Environment*, **15**, 321-333, 1981.

Sisler, J.F., D. Huffman, D.A. Latimer, W.C. Malm, and M.L. Pitchford, Spatial and temporal patterns and the chemical composition of the haze in the United States: An analysis of data from the IMPROVE network, 1988-1991, 1993.

Watson, J.G., J.C Chow, L.C. Pritchett, W.R. Pierson, C.A. Frazier, Purcell, R.G., I. Olmez, The 1987-88 Metro Denver brown cloud study, Desert Reserch Institute, Doc 8810 1F2, Desert Resert Institute, Reno, NV, 1988.

CHAPTER 3

AEROSOL MASS BUDGETS AND SPATIAL DISTRIBUTIONS

This chapter discusses the observed spatial and temporal variations in aerosol concentration and chemical composition throughout the United States on the basis of the IMPROVE measurements [Sisler *et al*., 1993] for the three-year period, March 1992 through February 1995.

Aerosol concentrations and chemical composition vary because of a number of factors, including the spatial distribution of natural and anthropogenic emission sources and meteorological conditions. The highest aerosol concentrations tend to occur in significant urban or industrialized areas where emission densities are high. Also, concentrations are highest when atmospheric dilution is minimal such as what occurs in stagnation periods or periods of limited mixing. In addition, since sulfate and nitrate aerosols are formed from SO_2 and NO_x emissions and chemical reactions in the atmosphere, these aerosols are highest when photochemistry is strongest.

For example, concentrations of sulfates tend to be highest in areas of significant sulfur dioxide (SO_2) emissions such as the eastern United States where SO_2 is emitted from coal-fired stationary sources, and in the Southwest due to copper smelters, power plants, and SO_2 emissions from Mexico. Organic carbon concentrations tend to be highest in regions such as the Pacific Northwest and Southeast due in part to forests and forest-product industries, which cause organics to dominate fine aerosol mass in the Pacific Northwest. Nitrates tend to be most prevalent in California where both NO_x emissions from motor vehicles and industry are high.

Spatial and temporal variations in aerosol composition and concentrations can be qualitatively examined through the use of annual and seasonal mass budgets. Mass budgets are the contribution of individual aerosol species to the reconstructed fine particle mass [Sisler *et al*., 1993]. Mass budgets are calculated by dividing the average concentration of each species by the average reconstructed fine particle mass for each region and time period of interest.

In this chapter, the observed spatial and seasonal trends in aerosol concentrations and chemical composition from the three-year period, March 1992 through February 1995, of the IMPROVE network are presented. There are 58 sites in the IMPROVE network that are fully instrumented for aerosol monitoring (channels A-D). Only 43 sites with data for this three-year period are summarized in this report. Since the last IMPROVE report [Sisler *et al*., 1993] five sites have been downgraded to channel A only or were discontinued and are not summarized here. The downgraded sites are at Everglades and Voyageurs National Parks. The discontinued sites are Arches, Isle Royale, and Hawaii Volcanoes National Parks.

The 43 IMPROVE sites are grouped into 21 regions according to their relative location, climatology, similarities in concentrations, and seasonal trends. Since the last IMPROVE report, three new regions have been introduced, the Mid-South, Mid-Atlantic, and Lake Tahoe region, while one region was dropped, Hawaii. Average concentrations and chemical composition are calculated on the basis of measurements for each region. Tables 3.1 and 3.2 show the mass concentrations of fine and coarse aerosol and the chemical composition (mass budgets) of the fine aerosol for each of the 21 regions in the United States. These concentrations and mass budgets are averaged over the entire three-year period to provide the annual average and over the three years for each of the four seasonal averages.

First, the characteristics of each of the regions (in alphabetic order) are discussed, followed by the spatial and temporal trends of the fine and coarse mass concentrations and the constituents of the fine-particle mass.

3.1 Characteristics of the Regions

Alaska. The Alaska region has only one monitoring site, Denali National Park. The average concentrations of fine and coarse aerosols over the three-year period were 1.8 and 3.3 $\mu g/m^3$, respectively. The fine aerosol concentration was the lowest measured anywhere in the United States during this period. Both fine and coarse aerosol concentrations are largest in summer and smallest in autumn. Organics are the largest contributor of fine particle mass (52%), followed by sulfate (28.6%), soil (10.2%), light-absorbing carbon (4.6%), and nitrate (3.3%). The concentrations of organics and light-absorbing carbon are largest in summer, perhaps due to the prescribed burning and forest fires that usually occur during that season.

Appalachian Mountains. This region has five sites of which three are reported here: Great Smoky Mountains and Shenandoah National Parks, both initiated in March 1988, and Dolly Sods Wilderness Area in West Virginia, initiated in September 1991. The other two sites, Shinning Rock in North Carolina and James River Face in Virginia have less than one year of data.

The average concentrations of fine and coarse aerosol for this region were 11.3 $\mu g/m^3$ and 4.8 $\mu g/m^3$, respectively. Both fine and coarse aerosol concentrations are maximum in summer and minimum in winter. Sulfate is by far the largest component of the fine particle mass. At 59.9%, it is more than twice that of the next largest contributor, organics (26%). Other contributors include nitrate (5.5%), soil (4.7%), and light-absorbing carbon (3.7%). Except for nitrate and light-absorbing carbon, which have their maximum concentrations in the winter and autumn, respectively, all other species have maximum concentrations in summer. The seasonal variation in sulfate concentrations is particularly strong with summer concentrations more than three times the winter concentrations at 11.2 $\mu g/m^3$.

Table 3.1. Measured fine and coarse aerosol concentration (in micro-g/m^3) for the 21 regions in the IMPROVE network.

Season	Fine Mass	Sulfate	Nitrate	Organics	Elemental Carbon	Soil	Coarse Mass
Alaska							
Spring	2.0	0.8	0.1	0.8	0.1	0.3	2.8
Summer	2.4	0.5	0.0	1.6	0.1	0.2	2.9
Autumn	1.4	0.4	0.0	0.7	0.1	0.1	1.9
Winter	1.5	0.5	0.1	0.7	0.1	0.1	1.7
ANNUAL	1.8	0.5	0.1	1.0	0.1	0.2	2.3
Appalachian Mountains							
Spring	10.3	6.0	0.8	2.7	0.4	0.5	5.5
Summer	16.8	11.2	0.3	3.7	0.4	1.2	6.3
Autumn	10.6	6.3	0.5	3.0	0.5	0.3	4.3
Winter	7.1	3.2	0.9	2.3	0.4	0.2	3.3
ANNUAL	11.3	6.7	0.6	2.9	0.4	0.6	4.8
Boundary Waters							
Spring	5.4	2.8	0.5	1.5	0.2	0.4	3.4
Summer	5.2	1.9	0.1	2.8	0.2	0.2	3.8
Autumn	4.3	1.7	0.5	1.7	0.2	0.2	3.0
Winter	5.5	2.1	1.4	1.5	0.2	0.2	2.6
ANNUAL	5.1	2.1	0.6	1.9	0.2	0.3	3.2
Cascade Mountains							
Spring	5.6	1.6	0.3	3.0	0.4	0.3	4.0
Summer	6.3	2.4	0.4	2.9	0.4	0.3	3.7
Autumn	5.3	1.3	0.2	3.2	0.5	0.2	3.9
Winter	3.5	0.5	0.1	2.3	0.4	0.1	2.5
ANNUAL	5.2	1.5	0.2	2.8	0.4	0.2	3.5
Central Rocky Mountains							
Spring	3.3	0.9	0.2	1.1	0.1	0.9	5.0
Summer	4.0	1.0	0.2	1.8	0.2	0.8	5.7
Autumn	3.1	0.8	0.2	1.4	0.2	0.5	3.9
Winter	2.1	0.6	0.2	1.0	0.1	0.2	2.8
ANNUAL	3.1	0.8	0.2	1.3	0.2	0.6	4.4

Table 3.1 Continued

Season	Fine Mass	Sulfate	Nitrate	Organics	Elemental Carbon	Soil	Coarse Mass
Colorado Plateau							
Spring	3.5	1.1	0.2	1.2	0.1	0.9	4.2
Summer	3.9	1.3	0.2	1.5	0.2	0.7	5.3
Autumn	3.4	1.1	0.2	1.5	0.2	0.4	4.0
Winter	2.6	0.8	0.2	1.1	0.2	0.2	3.0
ANNUAL	3.3	1.1	0.2	1.3	0.2	0.6	4.1
Florida							
Spring	11.0	6.0	0.6	3.3	0.6	0.6	6.8
Summer	11.8	4.9	0.5	3.0	0.4	3.1	10.1
Autumn	8.8	4.5	0.4	2.9	0.6	0.4	6.4
Winter	8.9	3.9	0.6	3.3	0.8	0.2	6.3
ANNUAL	10.1	4.8	0.5	3.1	0.6	1.1	7.4
Great Basin							
Spring	3.2	0.7	0.2	1.2	0.1	1.0	5.4
Summer	4.2	0.8	0.2	1.7	0.2	1.4	7.1
Autumn	3.0	0.6	0.1	1.5	0.2	0.6	4.6
Winter	2.1	0.4	0.2	1.1	0.2	0.2	2.6
ANNUAL	3.1	0.7	0.2	1.4	0.2	0.8	4.9
Lake Tahoe							
Spring	5.7	0.9	0.4	2.6	0.6	1.1	6.8
Summer	5.4	1.1	0.3	2.6	0.6	0.8	5.4
Autumn	6.8	0.8	0.4	3.9	1.1	0.6	5.2
Winter	8.0	0.4	0.5	5.0	1.5	0.6	9.2
ANNUAL	6.4	0.8	0.4	3.5	0.9	0.8	6.6
Mid Atlantic							
Spring	10.1	5.6	1.2	2.4	0.5	0.4	10.1
Summer	13.9	8.3	0.7	3.5	0.6	0.9	11.4
Autumn	10.5	5.3	1.1	3.1	0.7	0.4	8.6
Winter	11.1	4.5	2.2	3.3	0.8	0.3	7.2
ANNUAL	11.4	5.9	1.3	3.1	0.6	0.5	9.1

Table 3.1 Continued

Season	Fine Mass	Sulfate	Nitrate	Organics	Elemental Carbon	Soil	Coarse Mass
Mid South							
Spring	11.8	6.3	1.2	3.3	0.5	0.6	5.3
Summer	15.3	8.3	0.4	3.9	0.5	2.2	8.9
Autumn	11.0	5.8	0.7	3.6	0.6	0.4	5.6
Winter	10.3	4.5	1.8	3.1	0.6	0.3	4.5
ANNUAL	12.1	6.2	1.0	3.5	0.5	0.9	6.0
Northeast							
Spring	5.7	3.0	0.4	1.6	0.3	0.3	4.4
Summer	8.4	4.8	0.3	2.6	0.3	0.3	4.5
Autumn	5.7	3.0	0.4	1.8	0.3	0.2	4.0
Winter	5.6	2.5	0.7	1.9	0.4	0.2	4.0
ANNUAL	6.4	3.4	0.5	2.0	0.3	0.2	4.2
Northern Great Plains							
Spring	4.7	1.9	0.6	1.3	0.2	0.7	5.6
Summer	4.5	1.7	0.2	2.0	0.2	0.5	5.6
Autumn	4.2	1.3	0.5	1.7	0.2	0.5	5.5
Winter	4.7	1.7	1.2	1.3	0.2	0.2	3.1
ANNUAL	4.5	1.7	0.6	1.6	0.2	0.5	5.0
Northern Rocky Mountains							
Spring	4.7	1.0	0.2	2.6	0.3	0.6	5.0
Summer	5.2	1.0	0.1	3.0	0.3	0.8	8.2
Autumn	7.4	1.0	0.3	4.7	0.6	0.7	6.9
Winter	5.3	1.1	0.6	2.9	0.5	0.3	2.8
ANNUAL	5.7	1.0	0.3	3.3	0.4	0.6	5.8
Pacific Coast							
Spring	4.2	1.4	0.7	1.5	0.2	0.3	9.3
Summer	4.2	1.8	0.7	1.4	0.2	0.3	8.9
Autumn	5.4	1.4	0.8	2.5	0.4	0.4	8.2
Winter	4.7	0.8	1.6	1.9	0.3	0.1	6.0
ANNUAL	4.6	1.3	0.9	1.8	0.2	0.3	8.2

Table 3.1 Continued

Season	Fine Mass	Sulfate	Nitrate	Organics	Elemental Carbon	Soil	Coarse Mass
Sierra-Humboldt							
Spring	3.1	0.7	0.3	1.4	0.2	0.7	3.7
Summer	3.8	0.8	0.2	2.1	0.3	0.6	4.1
Autumn	3.3	0.6	0.2	1.8	0.2	0.4	3.0
Winter	1.9	0.3	0.2	1.0	0.3	0.1	1.8
ANNUAL	3.1	0.6	0.2	1.6	0.2	0.5	3.2
Sierra Nevada							
Spring	4.6	1.2	0.6	1.9	0.2	0.7	5.3
Summer	6.8	1.6	0.5	3.7	0.4	0.7	6.2
Autumn	4.9	1.0	0.5	2.5	0.3	0.6	5.1
Winter	1.9	0.3	0.2	1.1	0.1	0.1	3.3
ANNUAL	4.5	1.0	0.4	2.3	0.2	0.5	5.0
Sonoran Desert							
Spring	4.6	1.5	0.3	1.5	0.2	1.1	6.4
Summer	5.0	1.9	0.2	1.7	0.2	1.0	6.6
Autumn	4.3	1.6	0.2	1.7	0.3	0.5	4.9
Winter	3.1	1.1	0.2	1.3	0.2	0.3	4.0
ANNUAL	4.3	1.5	0.2	1.6	0.2	0.7	5.5
Southern California							
Spring	12.5	1.8	6.1	3.2	0.5	0.9	8.9
Summer	12.0	2.4	4.2	4.0	0.6	0.7	11.1
Autumn	7.5	1.3	2.5	2.2	0.4	1.1	11.8
Winter	3.4	0.6	1.3	1.1	0.2	0.2	2.9
ANNUAL	9.0	1.5	3.7	2.6	0.4	0.7	8.4
Washington D.C.							
Spring	17.1	8.0	2.6	4.2	1.4	0.9	7.6
Summer	23.0	13.9	1.3	5.1	1.4	1.3	6.9
Autumn	18.6	7.9	2.4	5.4	2.0	0.9	7.4
Winter	18.4	5.9	3.9	5.9	1.9	0.8	7.8
ANNUAL	19.2	9.0	2.5	5.2	1.7	1.0	7.4
West Texas							
Spring	5.3	2.1	0.2	1.7	0.2	1.1	7.6
Summer	7.0	2.7	0.3	1.8	0.2	2.0	7.8
Autumn	4.6	2.0	0.2	1.4	0.2	0.7	6.8
Winter	3.8	1.6	0.3	1.3	0.2	0.4	5.4
ANNUAL	5.2	2.1	0.2	1.5	0.2	1.1	6.9

Table 3.2 Measured fine aerosol mass budgets (in percent) for the 21 regions in the IMPROVE network.

Season	Sulfate	Nitrate	Organics	Elemental Carbon	Soil
Alaska					
Spring	38.1	3.7	38.0	4.7	15.5
Summer	19.4	1.8	65.8	4.9	8.1
Autumn	26.5	3.1	51.9	7.9	10.7
Winter	34.0	5.6	46.7	7.2	6.5
ANNUAL	28.6	3.3	52.0	5.9	10.2
Appalachian Mountains					
Spring	58.4	7.4	25.9	3.8	4.6
Summer	66.8	1.9	22.0	2.3	7.0
Autumn	58.9	5.0	28.5	4.3	3.2
Winter	46.0	12.6	32.6	5.9	2.9
ANNUAL	59.9	5.5	26.0	3.7	4.9
Boundary Waters					
Spring	51.8	9.1	28.1	3.6	7.5
Summer	36.2	2.2	53.2	3.8	4.6
Autumn	40.2	11.3	38.4	4.7	5.4
Winter	38.9	26.0	27.1	3.9	4.0
ANNUAL	41.8	11.9	37.0	4.0	5.4
Cascade Mountains					
Spring	27.8	5.4	53.1	7.5	6.2
Summer	38.4	5.6	45.6	6.4	4.0
Autumn	24.1	3.6	59.4	9.4	3.6
Winter	15.4	3.8	66.6	10.9	3.3
ANNUAL	28.1	4.7	54.6	8.2	4.4
Central Rocky Mountains					
Spring	27.8	7.3	33.4	3.8	27.7
Summer	24.2	4.1	46.3	4.9	20.5
Autumn	27.1	5.4	45.5	5.8	16.2
Winter	27.6	8.2	47.8	6.3	10.0
ANNUAL	26.5	5.9	42.9	5.1	19.6

Table 3.2 Continued

Season	Sulfate	Nitrate	Organics	Elemental Carbon	Soil
Colorado Plateau					
Spring	30.0	6.2	33.6	4.2	26.0
Summer	34.5	4.8	37.7	4.8	18.1
Autumn	33.1	5.2	43.1	6.0	12.6
Winter	33.1	9.2	42.9	7.2	7.6
ANNUAL	32.6	6.1	39.1	5.4	16.7
Florida					
Spring	54.0	5.5	30.1	5.3	5.1
Summer	41.9	3.9	25.0	3.2	25.9
Autumn	51.0	4.9	33.3	6.5	4.4
Winter	43.8	7.3	37.5	8.8	2.8
ANNUAL	47.4	5.3	30.9	5.7	10.7
Great Basin					
Spring	22.2	5.6	37.3	4.2	30.7
Summer	19.8	3.7	41.1	3.6	31.9
Autumn	20.9	4.0	48.8	5.9	20.4
Winter	20.9	8.1	53.7	8.1	9.2
ANNUAL	21.1	5.0	44.3	5.1	24.5
Lake Tahoe					
Spring	16.3	7.6	46.4	10.1	19.6
Summer	20.6	5.8	48.3	10.2	15.0
Autumn	11.9	6.1	57.3	15.5	9.2
Winter	5.3	6.5	62.6	18.3	7.2
ANNUAL	13.0	6.5	54.3	13.9	12.3
Mid Atlantic					
Spring	55.6	11.8	23.7	4.8	4.1
Summer	59.5	5.3	25.0	4.0	6.2
Autumn	50.0	10.0	29.1	6.8	4.0
Winter	40.5	19.8	29.8	7.1	2.9
ANNUAL	51.8	11.3	26.8	5.6	4.4

Table 3.2 Continued

Season	Sulfate	Nitrate	Organics	Elemental Carbon	Soil
Mid South					
Spring	53.3	9.8	27.6	4.5	4.8
Summer	54.2	2.7	25.2	3.3	14.5
Autumn	52.4	6.1	32.6	5.2	3.7
Winter	43.1	17.9	30.3	5.7	3.0
ANNUAL	51.3	8.4	28.6	4.5	7.2
Northeast					
Spring	53.5	7.8	28.7	4.8	5.3
Summer	57.7	3.6	30.8	4.1	3.8
Autumn	52.1	7.4	31.2	6.1	3.2
Winter	45.0	12.4	33.1	6.4	3.0
ANNUAL	52.9	7.2	30.9	5.2	3.8
Northern Great Plains					
Spring	41.1	12.9	28.4	3.3	14.3
Summer	37.6	3.4	45.0	3.6	10.4
Autumn	31.8	11.3	39.7	4.3	12.8
Winter	37.5	25.2	27.9	4.0	5.4
ANNUAL	37.2	13.3	35.1	3.8	10.7
Northern Rocky Mountains					
Spring	20.9	4.4	55.0	6.7	13.1
Summer	18.7	2.5	58.5	5.8	14.6
Autumn	14.0	4.3	63.7	8.4	9.6
Winter	20.0	11.6	53.9	9.5	5.0
ANNUAL	17.9	5.6	58.4	7.7	10.4
Pacific Coast					
Spring	33.2	17.8	36.3	4.5	8.2
Summer	41.5	15.3	33.5	3.6	6.0
Autumn	25.2	15.3	46.3	6.5	6.7
Winter	17.2	33.8	40.3	6.3	2.5
ANNUAL	29.0	20.2	39.6	5.3	5.9

Table 3.2 Continued

Season	Sulfate	Nitrate	Organics	Elemental	Soil
Sierra-Humboldt					
Spring	20.7	8.0	43.8	5.5	21.9
Summer	19.7	4.1	54.8	6.6	14.8
Autumn	18.4	6.8	54.2	6.9	13.7
Winter	16.5	9.1	53.6	13.1	7.7
ANNUAL	19.1	6.5	51.7	7.4	15.2
Sierra Nevada					
Spring	25.3	13.2	41.1	4.3	16.0
Summer	23.6	7.0	54.0	5.8	9.7
Autumn	21.4	10.1	51.4	5.7	11.4
Winter	17.8	10.5	57.8	7.0	7.0
ANNUAL	22.8	9.8	50.3	5.5	11.6
Sonoran Desert					
Spring	31.5	6.8	32.5	4.3	24.9
Summer	38.0	4.3	33.7	4.4	19.6
Autumn	37.9	4.4	39.6	6.1	12.0
Winter	34.0	7.8	42.8	7.3	8.2
ANNUAL	35.4	5.7	36.6	5.3	17.1
Southern California					
Spring	14.3	49.2	25.3	3.8	7.4
Summer	19.9	35.3	33.5	5.0	6.2
Autumn	17.2	33.5	28.8	5.3	15.3
Winter	16.5	38.9	33.1	6.5	5.0
ANNUAL	17.0	40.8	29.3	4.7	8.2
Washington D.C.					
Spring	46.6	15.1	24.9	8.0	5.5
Summer	60.4	5.6	22.1	6.1	5.7
Autumn	42.7	12.8	29.0	10.8	4.8
Winter	32.0	21.5	32.1	10.2	4.3
ANNUAL	46.6	12.9	26.8	8.6	5.1
West Texas					
Spring	40.2	4.3	31.5	3.6	20.4
Summer	38.6	4.4	25.6	2.4	29.1
Autumn	44.1	4.2	31.6	3.9	16.2
Winter	42.2	7.1	34.1	5.0	11.5
ANNUAL	40.8	4.8	30.0	3.5	20.9

Boundary Waters. This region in northern Minnesota is monitored at Boundary Waters Canoe Area in the Superior National Forest, which began monitoring in August 1991. Previously, this region was represented by two sites, Isle Royale National Park, which was discontinued in July 1991, and Voyageurs National Park, which has been downgraded to channel-A only.

The average fine and coarse aerosol concentrations were 5.1 and 3.7 $\mu g/m^3$, respectively. The highest fine and coarse aerosol concentrations occurred during summer, but there was not as strong a seasonal variation as in Alaska and the Appalachian Mountains. In this region, sulfate was the largest fraction of fine particle mass (41.8%), followed closely by organics (37%), and more distantly by nitrate (11.9%), soil (5.4%), and light-absorbing carbon (4%).

Cascade Mountains. This region in the states of Washington and Oregon has two monitoring sites out of the four reported here. Mount Rainier National Park, initiated in March 1988, is southeast of Seattle, and the Columbia River Gorge on the Hood River National Forest, east of Portland, began monitoring in June 1993. The other two sites, Three Sisters Wilderness Area on the Willamette National Forest and Snoqualamie Pass on the Snoqualamie National Forest, were implemented in July 1993 but were not fully operational until September 1994.

Here the average fine and coarse aerosol concentrations are 5.2 and 3.5 $\mu g/m^3$, respectively. Fine and coarse aerosol concentrations reach their maxima in summer and minima in winter. Sulfate and nitrate concentrations have strong seasonal variations, with maxima for sulfate in summer and nitrate in winter. This seasonal variation could be, in part, the result of seasonal variations in mixing and in photochemistry. In this region, organics are the single most significant contributor (54.6%) to fine particle mass. Sulfate (28.1%) is about half the contribution of organics. Nitrate contributes 4.7%, followed by light-absorbing carbon (8.2%) then soil (5.4%).

Central Rocky Mountains. The measurements in this region were made at five locations in the mountainous Class I areas of Colorado and Wyoming, including the Bridger and Weminuche Wilderness Areas, Rocky Mountain and Yellowstone National Parks, and Great Sand Dunes National Monument. Fine and coarse aerosol concentrations in this region averaged 3.1 and 4.4 $\mu g/m^3$ over the three-year period. Like many of the other regions, concentrations, especially of sulfate, organics, light-absorbing carbon, and coarse aerosol, were highest in summer and lowest in winter. The largest contributor to fine particle mass in this region was organics (42.9%), followed by sulfate (26.5%), soil (19.6%), nitrate (5.9%), and light-absorbing carbon (5.1%).

Colorado Plateau. This region in the Four Corners' states of the Southwest is the most intensively monitored in the IMPROVE network. There are six sites, most of them within the so-called Golden Circle of National Parks: Bandelier, Bryce Canyon, Canyonlands, Grand Canyon, Mesa Verde, and Petrified Forest National Parks. A seventh site, Arches National Park, was discontinued in May 1992. This region is of particular concern to the Grand Canyon Visibility Transport Commission as required by Congress in the 1990 amendments to the Clean Air Act [Stensvaag, 1991].

In this region, fine and coarse aerosol concentrations averaged 3.3 and 4.1 $\mu g/m^3$, respectively. Fine and coarse aerosol concentrations here were greatest in summer and minimum in winter. Concentrations of sulfate and organics were also greatest in summer and smallest in winter. However, nitrate and light-absorbing carbon were both largest in winter. Here organics (39.1%) and sulfate (32.6%), contribute the most followed by soil (16.7%), nitrate (6.1%), and light-absorbing carbon

(5.4%).

Florida. Previously, this region had its monitoring site at Everglades National Park, which has now been downgraded to a channel-A only site. This region is now represented by two sites at Chassahowitzka Wildlife Refuge on the Gulf Coast north of Tampa, and Okefenokee Wilderness Area on the Georgia-Florida border. Monitoring at these two sites began in April 1993 and September 1991, respectively. Only Chassahowitzka is reported here for the three-year averages.

The fine and coarse aerosol concentrations averaged 10.1 and 7.4 $\mu g/m^3$, their concentrations were highest in summer. Fine and coarse aerosol concentrations were smallest in winter. Sulfate was found to be the largest contributor to fine particle mass (47.4%), followed by organics (30.9%), soil (10.7%), light-absorbing carbon (5.7%), and nitrate (5.3%).

Great Basin. The Great Basin of Nevada has two sets of measurements at Jarbidge Wilderness Area in northeastern Nevada and Great Basin National Park, which began monitoring in March 1988 and May 1992, respectively. Here the fine and coarse aerosol concentrations averaged 3.1 and 4.9 $\mu g/m^3$. The fine mass concentration was the lowest of any of the regions in the lower 48 states. Perhaps this is due to the fact that this site is relatively remote from high emission density areas and is generally well ventilated. Both fine and coarse aerosol concentrations, as well as all of the fine aerosol components, except nitrate and light-absorbing carbon, experienced largest concentrations in the summer and lowest concentrations in the winter. The largest single contributors to fine particle mass at this region were organics (44.3%) and soil (24.6%). Sulfate was a smaller contributor (21.1%), followed by light-absorbing carbon (5.1%) and nitrate (5%).

Lake Tahoe. Two sites are monitored for this region: one site is in Bliss State Park in southern California and a bit east of the lake and began sampling in March 1989. The other is close to the urban area of Lake Tahoe and sampling started in November 1990. Fine and coarse aerosol concentrations averaged 6.4 and 6.6 $\mu g/m^3$, respectively; there is a modest seasonality with highest concentrations occurring in the winter, and the least for fine aerosols in the summer and for coarse aerosol in the autumn. Sulfate, nitrate, organics, and light-absorbing carbon have strong seasonal trends with sulfate concentrations being more than twice as high in the summer than in the winter; however, nitrates, organics, and light-absorbing carbon have winter maxima at least twice their summer concentrations. The largest contributor to fine aerosol is organics (54.3%), followed by light-absorbing carbon (13.9%), sulfate (13%), soil (12.3%), and nitrate (6.5%).

Mid Atlantic. This new region is represented by the Edmond D. Forsyth Wildlife Refuge west of Atlantic City, New Jersey and began monitoring in September 1991. Fine and coarse aerosol concentrations averaged 11.4 and 9.1 $\mu g/m^3$, respectively. A moderate seasonality is evident with the highest fine and coarse aerosol concentrations occurring in the summer, and the least in the spring and winter, respectively. Sulfate, organics, and fine soil are the fine aerosol constituents that follow the seasonal trend for fine aerosol mass. Nitrate peaks in the winter at three times its summer concentration, and light-absorbing carbon peaks in the winter as well but only shows a small seasonality. Sulfate comprises the bulk of the fine aerosol mass (51.8%) followed by organics (26.8%), nitrate (11.3%), light-absorbing carbon (5.8%), and soil (4.4%).

Mid South. Three sites are monitored for this new region: Upper Buffalo Wilderness Area in north central Arkansas initiated in December 1991, Mammoth Cave National Park in Kentucky initiated in September 1991, and Sipsey Wilderness Area in northern Alabama initiated in March 1992. The

average concentration of fine and coarse aerosol was 12.1 and 6.0 $\mu g/m^3$, respectively. Outside of Washington D.C., which is an urban site, this region has the highest average concentration of fine aerosol. A modest seasonality is evident for fine and coarse aerosols with the minima occurring in the winter and the maxima the summer. All fine aerosol constituents except nitrate and light-absorbing carbon follow the seasonality of fine aerosol. Nitrate has its maximum concentrations in the winter, while light-absorbing carbon is fairly constant between seasons. Sulfate (51.3%) composes the bulk of fine aerosol followed by organics (28.6%), nitrate (8.4%), soil (7.2%), and light-absorbing carbon (4.5%).

Northeast. The northeastern United States is represented by measurements at two sites: Acadia National Park on the coast of Maine, which began monitoring in March 1988, and Lye Brook Wilderness Area in southern Vermont, which began in September 1991. Here fine and coarse aerosol concentrations averaged 6.4 and 4.2 $\mu g/m^3$. Although fine and coarse aerosol concentrations were both largest in summer, there was not a strong seasonal variation. Sulfate, organics, and soil concentrations were also largest in summer. Nitrate concentrations reached their maximum in winter. The contributors to fine particle mass included sulfate (52.9%), organics (30.9%), nitrate (7.2%), light-absorbing carbon (5.2%), and soil (3.8%).

Northern Great Plains. Only one set of measurements was made in this region, at Badlands National Monument in South Dakota. Here fine and coarse aerosol concentrations averaged 4.5 and 5.0 $\mu g/m^3$, respectively. The maximum concentrations for fine mass occurred in the winter and spring and was least in the autumn. The maximum for coarse mass occurred in the spring and summer and was least during the winter. Sulfate (37.2%) and organics (35.1%) each contributed to fine mass about equally, followed by nitrate (13.3%), soil (10.7%), and light-absorbing carbon (3.8%).

Northern Rocky Mountains. This region has measurements made at Glacier National Park in Montana, close to the Canada border. Fine aerosol and coarse aerosol concentrations averaged 5.5 $\mu g/m^3$ each. There were no strong seasonal variations except for nitrate, which showed a strong winter peak, and coarse mass, which peaked in the winter. Organics are by far the largest contributor to fine particle mass (58.4%) followed by sulfate (17.9%), soil (10.4%), light-absorbing carbon (7.7%), and nitrate (5.6%).

Pacific Coast. This region includes three Class I areas along and near the coast of northern California: Pinnacles National Monument, Point Reyes National Seashore, and Redwoods National Park. In this region, the fine and coarse aerosol concentrations over the three-year period averaged 4.6 and 8.2 $\mu g/m^3$. There was no strong seasonal variation in concentration, except for sulfate that had maxima and minima in summer and winter, and nitrate that showed the opposite trend, with maxima and minima in winter and summer, respectively. One would expect sulfate to reach its maximum concentration in summer because of photochemistry. Nitrate would be expected to reach its peak during the colder months of winter because of the extreme thermal volatility of ammonium nitrate. Organics in this region are the largest single component of fine aerosol (39.6%), followed by sulfate (29%), nitrate (20.2%), soil (5.9%), and light-absorbing carbon (5.3%).

Sierra-Humboldt. The region further north in the Sierra Nevada and Humboldt Mountain Ranges was measured with sites at Crater Lake National Park in Oregon and Lassen Volcanoes National Park in northern California. This region is relatively remote from high emission density areas. Its fine and coarse aerosol concentrations were relatively low, at 3.1 and 3.2 $\mu g/m^3$, respectively. Summer concentrations were generally about twice those during the winter. Organics contributed most of the

fine particle mass (51.7%), followed by sulfate (19.1%), soil, (15.2%), light-absorbing carbon (7.4%), and nitrate (6.5%).

Sierra Nevada. The Sierra Nevada Mountains in California was monitored at two sites: Yosemite and Sequoia National Parks. Yosemite National Park has been monitored since March 1988. Sequoia National Park had channel A and D since March 1992 but was not fully instrumented until July 1993.

Average fine and coarse aerosol concentrations were 4.5 and 5.0 $\mu g/m^3$. There was a strong moderate variation, with maximum concentrations in summer and minimum concentrations in winter. The only exception was nitrate, which was relatively constant throughout the year. Organics contributed more than twice what sulfate contributed (50.3% and 22.8%, respectively). Soil was the next largest contributor (11.6%), followed by nitrate (9.8%), and light-absorbing carbon (5.5%).

Sonoran Desert. This region in southeastern Arizona was monitored at two sites: Chiracahua and Tonto National Monuments and were initiated in March 1988. The three-year average of fine and coarse mass concentrations in this region were 4.3 and 5.5 $\mu g/m^3$, respectively. These concentrations were highest in summer and lowest in winter. The sulfate, organics, and soil components of fine particle mass also had maxima and minima in these seasons. The contributions to fine particle mass were distributed nearly equally between sulfate (35.4%) and organics (36.6%), followed by soil (17.1%), nitrate (5.7%), and light-absorbing carbon (5.3%).

Southern California. Measurements in this region were made in San Gorgonio National Monument, east of the Los Angeles metropolitan area. Fine and coarse aerosol concentrations were highest of any western United States site (9.0 and 8.4 $\mu g/m^3$); concentrations were only higher in the eastern United States. Like many sites in the IMPROVE network, concentrations were highest in summer and lowest in winter. This trend was also observed for nitrate: actually nitrate was highest in spring and lowest in winter, but concentrations in summer were twice those in winter. This site was the only site in the IMPROVE network in which nitrate was a larger contributor to fine particle mass than either sulfate or organic carbon. The contributions were nitrate (40.8%), organics (29.3%), sulfate (17%), soil (8.2%), and light-absorbing carbon (4.7%).

Washington, D.C. This is a single monitoring site in the nation's capital. Fine and coarse aerosol concentrations were higher here than anywhere in the IMPROVE network. They averaged 19.2 and 7.4 $\mu g/m^3$ over the three-year period. There was a moderate seasonal variation in fine aerosol concentrations; in spring they ranged from 17.1 to 23 $\mu g/m^3$ in summer. However, the sulfate and nitrate components varied significantly by season: sulfate concentrations were largest in summer and smallest in winter, while nitrate concentrations were largest in winter and smallest in summer. The sulfate behavior could be caused by the seasonal variation in photochemistry. The nitrate behavior may be due to the extreme volatility of nitrate in warm weather. Over the entire three-year period, fine particle mass was constituted of sulfate (46.6%), organics (26.8%), nitrate (12.9%), light-absorbing carbon (8.6%), and soil (45.1%).

West Texas. Two measurement sites in west Texas were included: Big Bend and Guadalupe Mountains National Parks. Both sites are near the Mexico border in southwestern Texas and have operated since March 1988. The fine and coarse aerosol concentrations averaged 5.2 and 6.9 $\mu g/m^3$ over the last three years. Minimum concentrations generally occurred during winter, while maximum concentrations occurred in summer. The only exception was light-absorbing carbon, which remained constant. The contributions to fine particle mass averaged 40.8% for sulfate, 30% for organics, 20.9% for soil, 4.8% for nitrate, and 3.5% for light-absorbing carbon.

In general, the following observations can be made. With few exceptions, aerosol concentrations are highest in summer and lowest in winter. This is consistent with the fact that sulfate formation rates, natural organic carbon emissions, and mixing into mountainous regions are all maximum in summer and minimum in winter. With the notable exception of southern California where nitrate is dominant, sulfate and organics are the two principal components of the fine particle mass throughout the United States. Sulfate's contribution is much higher in the eastern United States than in the western United States and in Alaska.

3.2 Spatial Trends in Aerosol Concentrations in the United States

Because of the relatively large number of IMPROVE aerosol monitoring sites in the western United States, isopleth maps of the average aerosol concentrations measured over the three-year period from March 1992 through February 1995 could be drawn. Figures 3.1 through 3.8 show isopleth maps of the three-year average aerosol concentrations (PM_{10}, fine mass, coarse mass, sulfate, nitrate, organics, light-absorbing carbon, and soil). These figures provide us with information on how aerosol concentrations and mass budgets vary over the United States.

3.2.1 PM_{10} Aerosol

Figure 3.1 shows isopleths of the PM_{10} aerosol mass concentration measured during this three-year period. The highest concentrations occur in the eastern United States. With the exceptions of the Northern Great Plains states, almost all the area east of Colorado and New Mexico has concentrations in excess of 10 $\mu g/m^3$. The highest concentrations are in Washington D.C. at 22 $\mu g/m^3$, followed by Florida and the Mid South, which experienced concentrations in excess of 18 $\mu g/m^3$. Outside of California and the Northern Rockies the least amount of PM_{10} concentrations occur in the western United States, where there is a large swath extending from Oregon, northern California, Nevada, Utah, Wyoming, into northern Arizona and northern New Mexico and western Colorado, where the concentration of PM_{10} is less than 8.5 $\mu g/m^3$. The lowest concentration in the lower 48 states occurs at Bridger Wilderness Area in Wyoming with only 5.7 $\mu g/m^3$ on average, the least was recorded at Denali National Park in Alaska at 4.2 $\mu g/m^3$. The strongest gradient is between northern California and Utah and the coastal regions of California, where concentrations vary form 6.4 $\mu g/m^3$ to an excess of 15 $\mu g/m^3$.

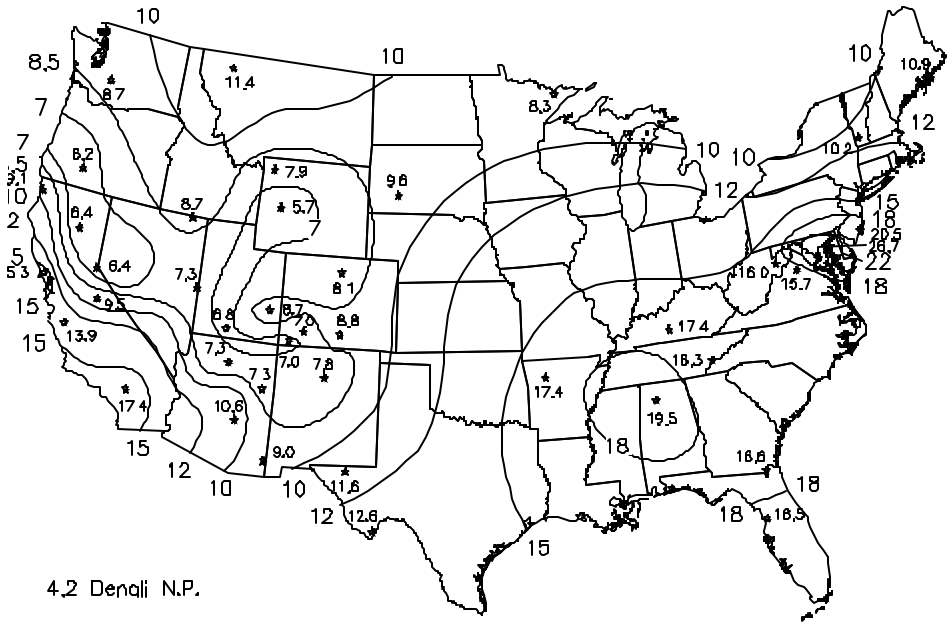

Figure 3.1 Average PM_{10} mass concentration (in micro-g/m^3) for each site in the IMPROVE network.

3.2.2 Fine Aerosol

Figure 3.2 shows isopleths of the average fine aerosol concentrations measured during the three-year period. Note the strong gradient in fine particle concentrations from southern California, a local maximum of 9 ìg/m^3 to minima of 2.7 to 3.1 ìg/m^3 observed in southern Oregon, Nevada, southern Utah, western Colorado, and Wyoming. This is a factor of three variations in average fine aerosol concentration. Also, note that fine aerosol concentrations increase again as one moves to the eastern United States with maxima of about 13.5 ìg/m^3 in Shenandoah and Great Smoky Mountains National Parks and over 19 ìg/m^3 in Washington D.C. Thus, from the minima in the western United States to the maxima in the East, there is a factor of six variations in average concentration. Average fine aerosol concentrations in Denali National Park of 1.8 ìg/m^3 are lower than any measured in the lower 48 states. There is a factor of 10 variations between the average measured in Alaska and that measured in Washington D.C.

The lower map in Figure 3.2 shows isopleths that depict the fraction of PM_{10} that is fine aerosol ($PM_{2.5}$). Almost all of the country outside of the intermountain west has a fine mass fraction of PM_{10} that exceeds 50%. East of the Mississippi and south of the Great Lakes there is a broad region that exceeds 65%. The highest values encompass a region that covers the Ohio Valley, parts of the Mid South, West Virginia, Shenandoah, and Washington D.C., where fine mass fraction is greater than 70%. The smallest fine mass fraction occurs in the Great Basin Region, central Utah, and portions of Colorado, where less than 40% of PM_{10} is fine mass.

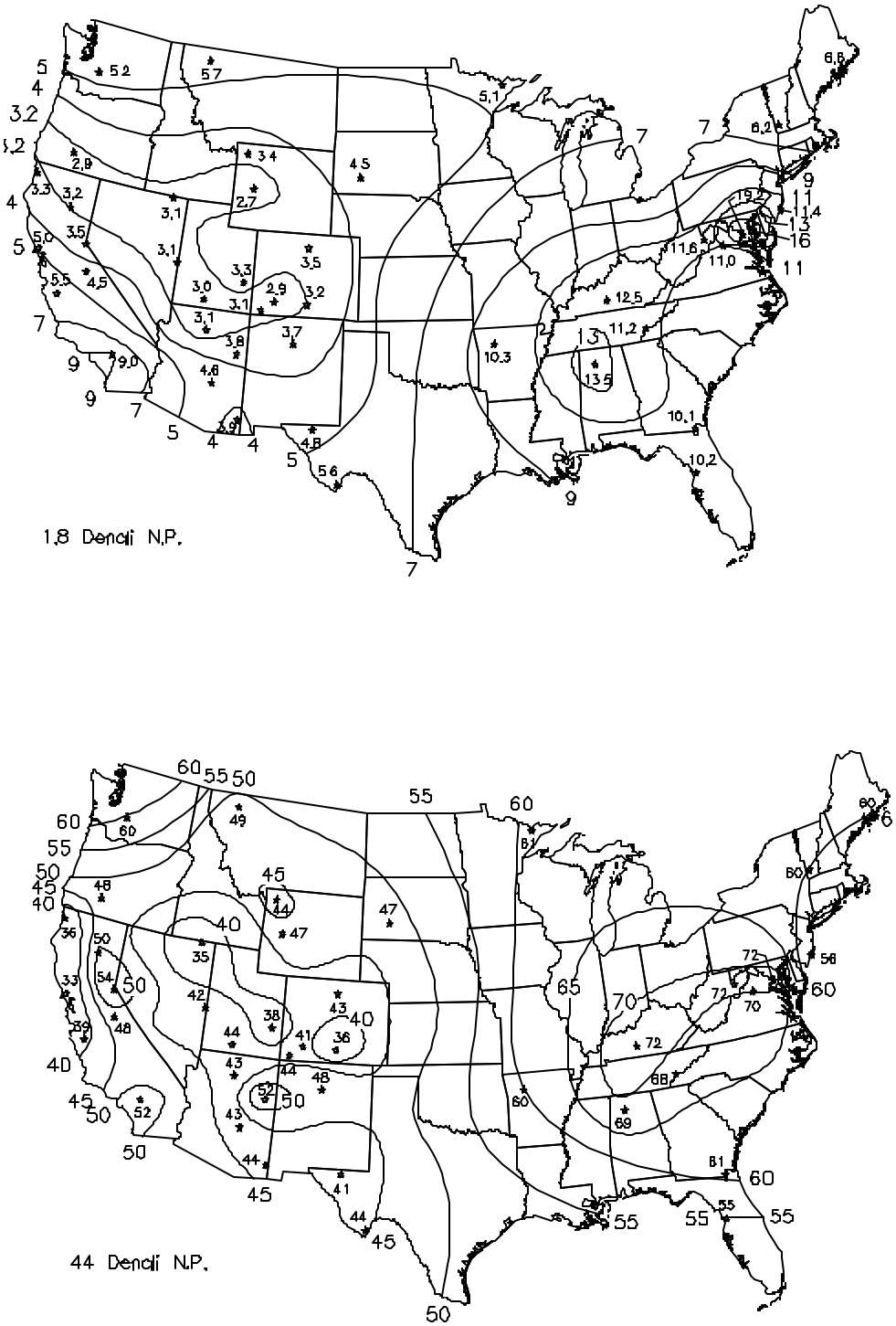

Figure 3.2 Average fine mass aerosol concentrations (in micro-g/m^3) (top) and fine mass fraction of PM_{10} (bottom) for each site in the IMPROVE network.

3.2.3 Coarse Aerosol

Figure 3.3 shows isopleths of the three-year average coarse aerosol concentrations. There are a few local maxima from 7.4 to 10.3 $\mu g/m^3$ that are noticeable near Los Angeles, San Francisco, and Washington D.C. The lowest coarse aerosol concentrations occur in the swath from the Pacific Northwest through Nevada to southern Utah. Concentrations in this region average around 4 $\mu g/m^3$. Throughout the United States coarse aerosol concentrations are generally in the factor-of-two range from 4 to 8 $\mu g/m^3$. The patterns in the eastern United States, with the exception of Washington D.C., shows a steady north-south trend of increasing coarse aerosol concentrations. Coarse aerosol concentrations in Alaska are not significantly lower than in the lower 48 states. There is approximately a factor-of-three range from the lowest average concentrations measured in Oregon and Utah and the highest measured in Washington D.C.

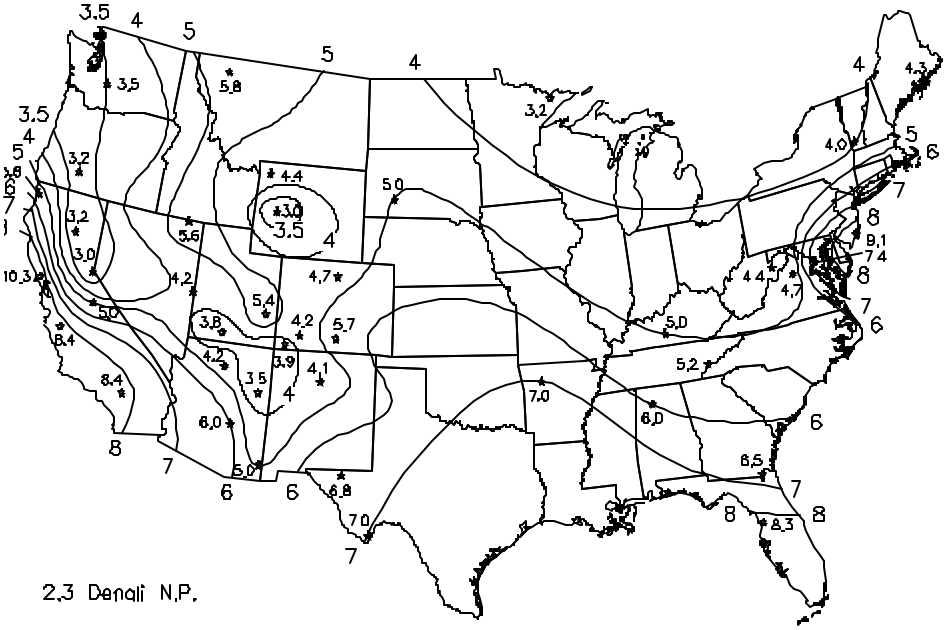

Figure 3.3 Average coarse particle mass concentration (in micro-g/m^3) for each site in the IMPROVE network.

3.2.4 Fine Sulfate Aerosol

The average sulfate component of the fine aerosol measured over the three-year period is shown in Figure 3.4. Since sulfate is one of the two major components of fine particle mass, it is not surprising to observe similar gradients across the United States to what was observed for total fine particle mass. There is a strong gradient from high concentrations in California urban areas to low concentrations in southern Oregon and Nevada. There is also a strong gradient from the relatively low concentrations in the West to those in the East. There is a factor of 15 variations from the lowest concentration measured in Nevada to the highest concentration measured in Washington, D.C. This gradient is most likely indicative of the strong regional gradient in SO_2 emission density. The eastern United States has a concentration of power plants that burn high sulfur coal, while the western United States has relatively

low SO_2 emission densities. A relative maximum in sulfate concentration is observed in southern Arizona, which is near copper smelters that emit large quantities of SO_2. The lower map in Figure 3.4 shows that sulfate constitutes as little as 17% of fine particle mass in southern California to as much as 61% of total fine mass in Shenandoah National Park. In the Golden Circle of parks in the Four Corners' states, sulfate is 31 to 35% of the fine particle mass.

In the eastern United States sulfate is the largest single component of fine particle mass. In the Boundary Waters, Sonoran Desert, and West Texas regions, sulfate is tied with organic carbon as the largest component of fine particle mass. Sulfate is the second largest component of fine mass in all other regions studied except southern California and the Great Basin (where sulfate is the third largest component).

3.2.5 Fine Nitrate Aerosol

Figure 3.5 shows isopleth maps of the nitrate concentration and nitrate mass fraction of fine aerosol, averaged over the three-year period. Note that the highest concentration of 3.7 $\mu g/m^3$ was measured in San Gorgonio Wilderness, just east of the Los Angeles metropolitan area. Other high concentrations occur in Washington, D.C. (2.5 $\mu g/m^3$), and near the San Francisco area (1.3 $\mu g/m^3$). There is a strong gradient from the high concentrations in the California urban areas to the minima of 0.1 $\mu g/m^3$ measured in Oregon, Nevada, Wyoming, and Colorado. There is a long swath of low nitrate concentrations extending from Oregon, Nevada, and Idaho into Utah, Wyoming, Colorado and into southern Arizona and southern New Mexico (<0.2 $\mu g/m^3$). Nitrate mass fractions are typically 4 to 12% except in California where they are 30% and higher. In the north central part of the United States and the mid-Atlantic region nitrates constitute over 12% of the fine aerosol mass. Nitrates generally reach their maxima in the winter when colder temperatures favor the formation of ammonium nitrate aerosol from nitric acid vapor. Nitrate is the largest single component of fine aerosol mass in southern California at San Gorgonio Wilderness Area.

3.2.6 Fine Organic Aerosol

Figure 3.6 shows isopleth maps of the organic carbon mass fraction of the fine aerosol concentration, averaged over the three-year period. There is a significant spatial gradient from the Pacific Northwest, with average concentrations of 2.0 to 3.0 $\mu g/m^3$ to the intermountain region of Wyoming, Colorado, Utah, and Arizona of 1.2 $\mu g/m^3$ or less. In the eastern United States, organics range generally from 2.0 to 4 $\mu g/m^3$. In Alaska, organic aerosol concentrations are the lowest at 1 $\mu g/m^3$.

Except in the northwestern United States, where organics are over half of the fine particle mass, organics generally constitute between 25 to 40% of the fine particle mass. Moreover, organics are the largest single component of fine particle mass in most of the regions in the United States. Exceptions include the Mid South and eastern United States where sulfate is the dominant component and southern California, where nitrate is the dominant component.

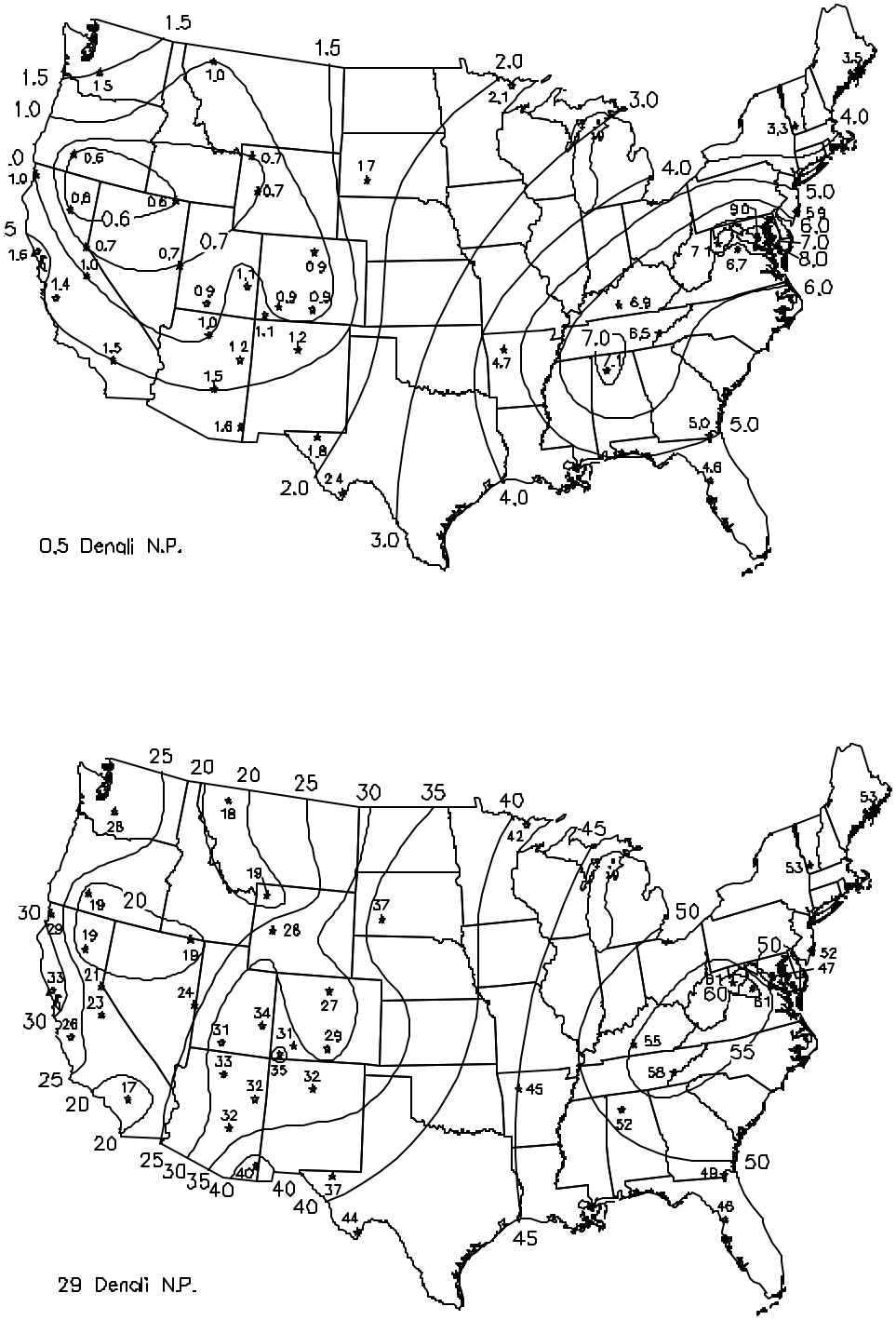

Figure 3.4 Average fine sulfate aerosol concentrations (in micro-g/m^3) (top) and sulfate fine mass fractions (bottom) for each site in the IMPROVE network.

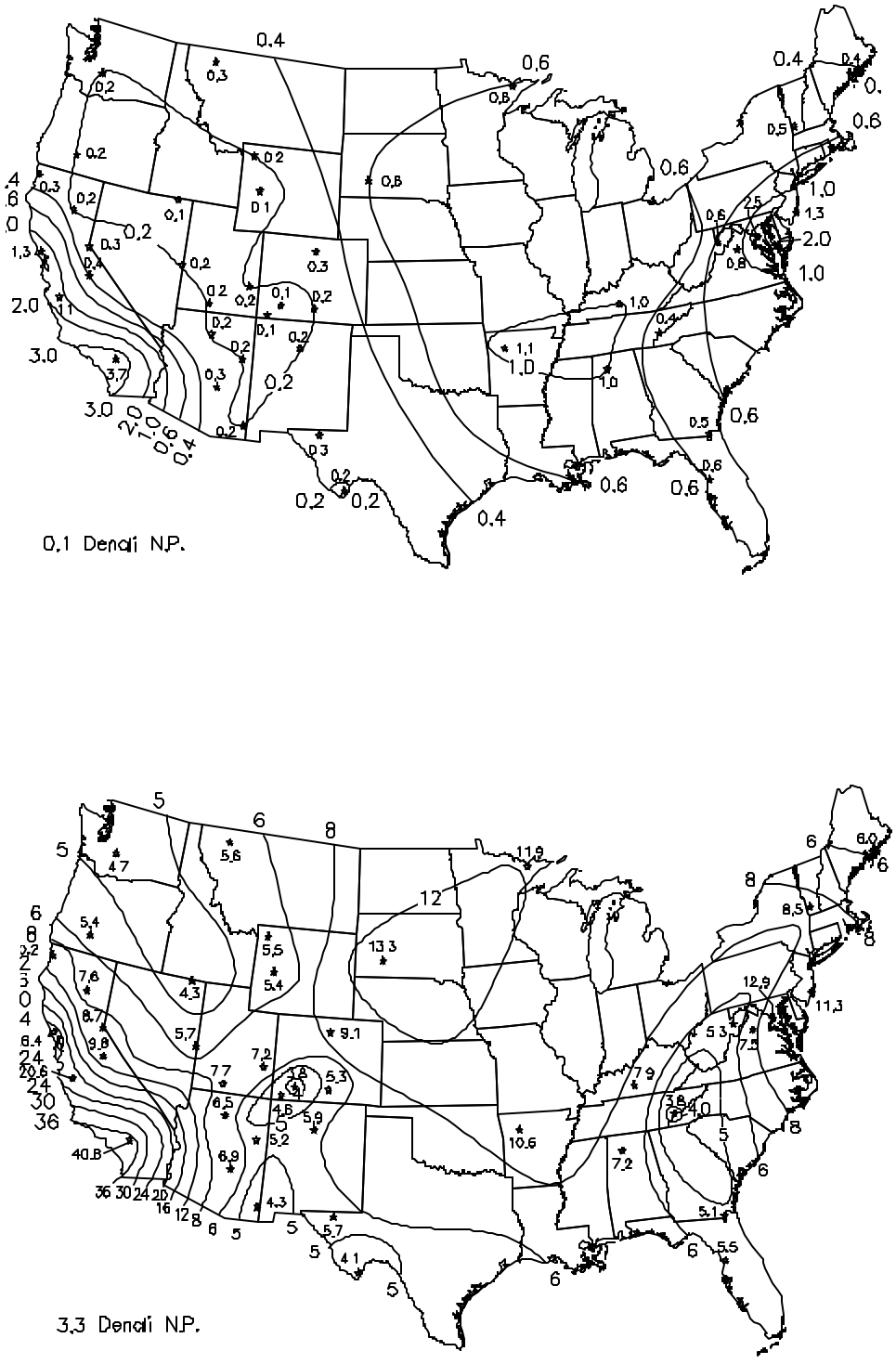

Figure 3.5 Average fine nitrate aerosol concentrations (in micro-g/m^3) (top) and nitrate fine mass fractions (bottom) for each site in the IMPROVE network.

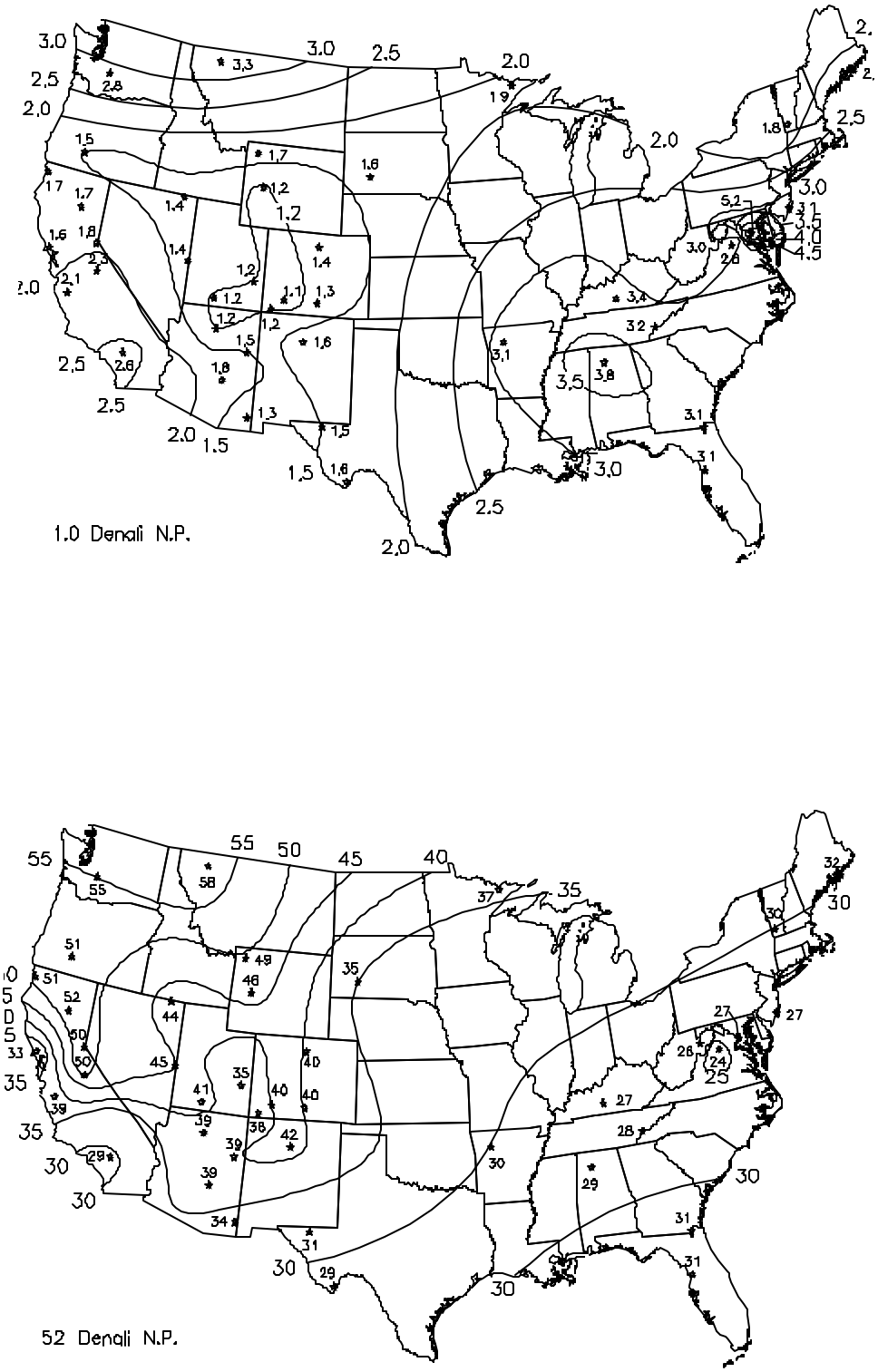

Figure 3.6 Average fine organic aerosol concentrations (in micro-g/m^3) (top) and organic fine mass fractions (bottom) for each site in the IMPROVE network.

3.2.7 Fine Light-Absorbing Carbon Aerosol

Figure 3.7 shows isopleth maps of the light-absorbing carbon concentration and mass fraction of the fine aerosol, averaged over the three-year period. Note that light-absorbing carbon concentrations are highest in the Pacific Northwest, the area east of the Mississippi and south of the Great Lakes, and southern California, while concentrations are much lower in much of the West (Wyoming, Utah, and Nevada). Light-absorbing carbon is the smallest contributor to fine particle mass, constituting generally 3 to 5% of the fine particle mass. Exceptions to this are the Pacific Northwest and Washington, D.C. areas where light-absorbing carbon contributes as much as 8% of the fine particle mass.

3.2.8 Fine Soil Aerosol

Figure 3.8 shows isopleth maps for fine soil. The contribution of soil to the fine aerosol in the United States is generally small, except for the elevated concentrations (<1 $\mu g/m^3$) in the southern tier of the United States. There is a quite noticeable north-south trend of increasing soil concentrations with the Northeast being the lowest. Soil contributes approximately 5 to 10% of the fine aerosol mass in the East. Except for Florida, all of the area east of the Mississippi, the Pacific Northwest, and parts of California, soil contributes less than 10% to fine aerosol mass with much of the intermountain west in excess of 20%.

3.3 Summary

The following are the major patterns observed in the three-year period of IMPROVE from March 1992 through February 1995:

1. Spatial Patterns. Concentrations of fine particles (those most important in determining visibility) are highest in the eastern United States and in southern California and lowest in the relatively unpopulated areas of the West.

2. Major Contributions to Fine Aerosol. The largest single component of the fine aerosol in the East is sulfate, while in the Pacific Northwest it is organics, and in southern California it is nitrate. In general, the largest mass fractions of the fine aerosol are sulfates and organics. Of the 21 regions in the IMPROVE network, organic carbon is the largest single component in ten regions (Alaska, Cascades, Colorado Plateau, Central Rockies, Pacific Coastal Mountains, Great Basin, Northern Rockies, Sierra Nevada, Sierra-Humboldt, and Lake Tahoe). Sulfate is the largest single component of fine aerosol in seven regions, primarily in the East (Appalachian Mountains, Florida, Northeast, Mid South, Mid Atlantic, Washington D.C., and West Texas). The contributions of organic carbon and sulfate are approximately equal in three regions (Boundary Waters, Sonoran Desert, and Northern Great Plains). Soil is the next largest contributor, followed by nitrate and light-absorbing carbon. Nitrate is the largest component of fine aerosol in southern California only.

3. Smaller Contributors. After the contributions of organics and sulfate, soil is the next largest, followed by nitrate and light-absorbing carbon.

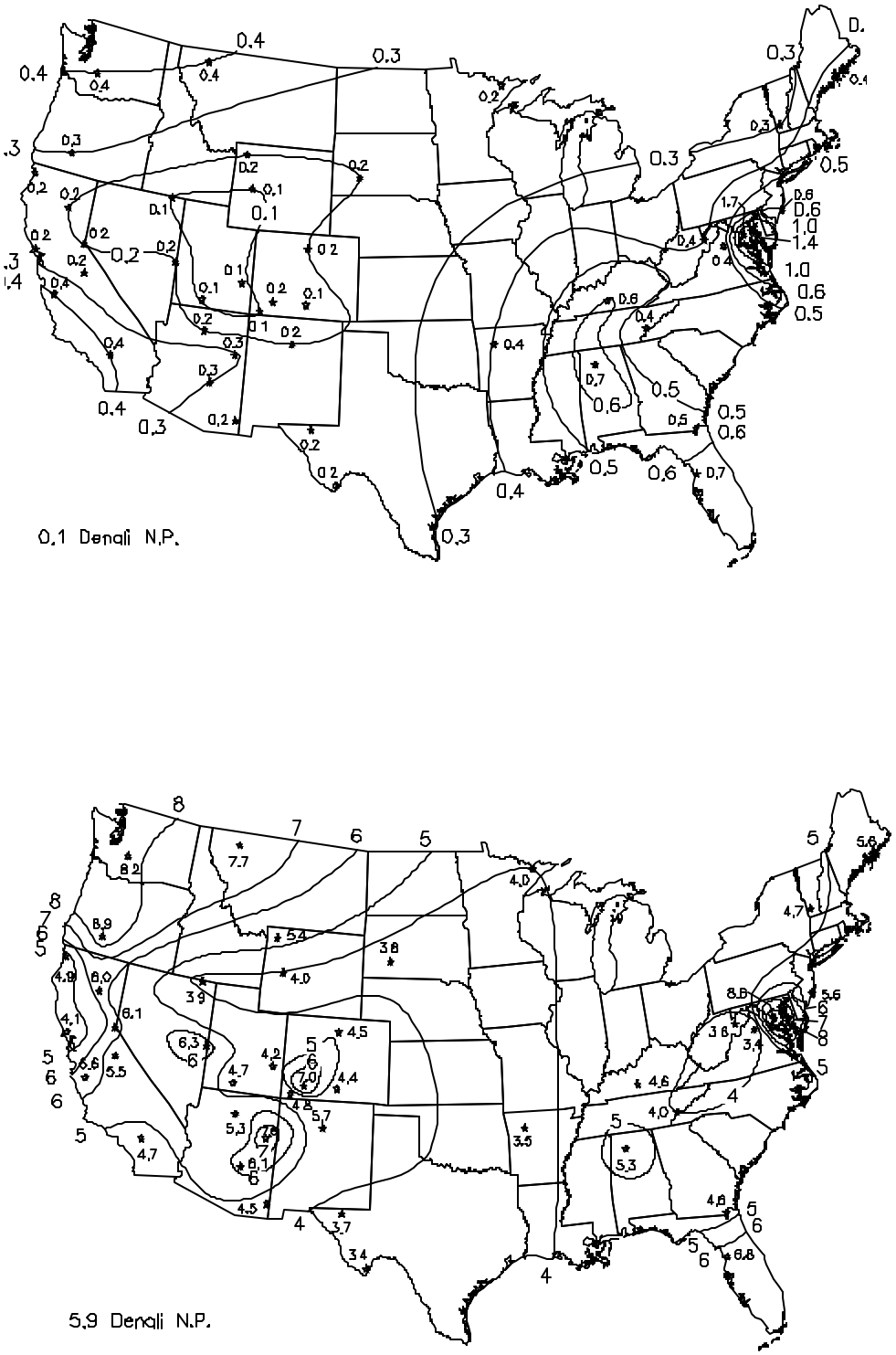

Figure 3.7 Average fine elemental carbon aerosol concentrations (in micro-g/m^3) (top) and elemental carbon fine mass fractions (bottom) for each site in the IMPROVE network.

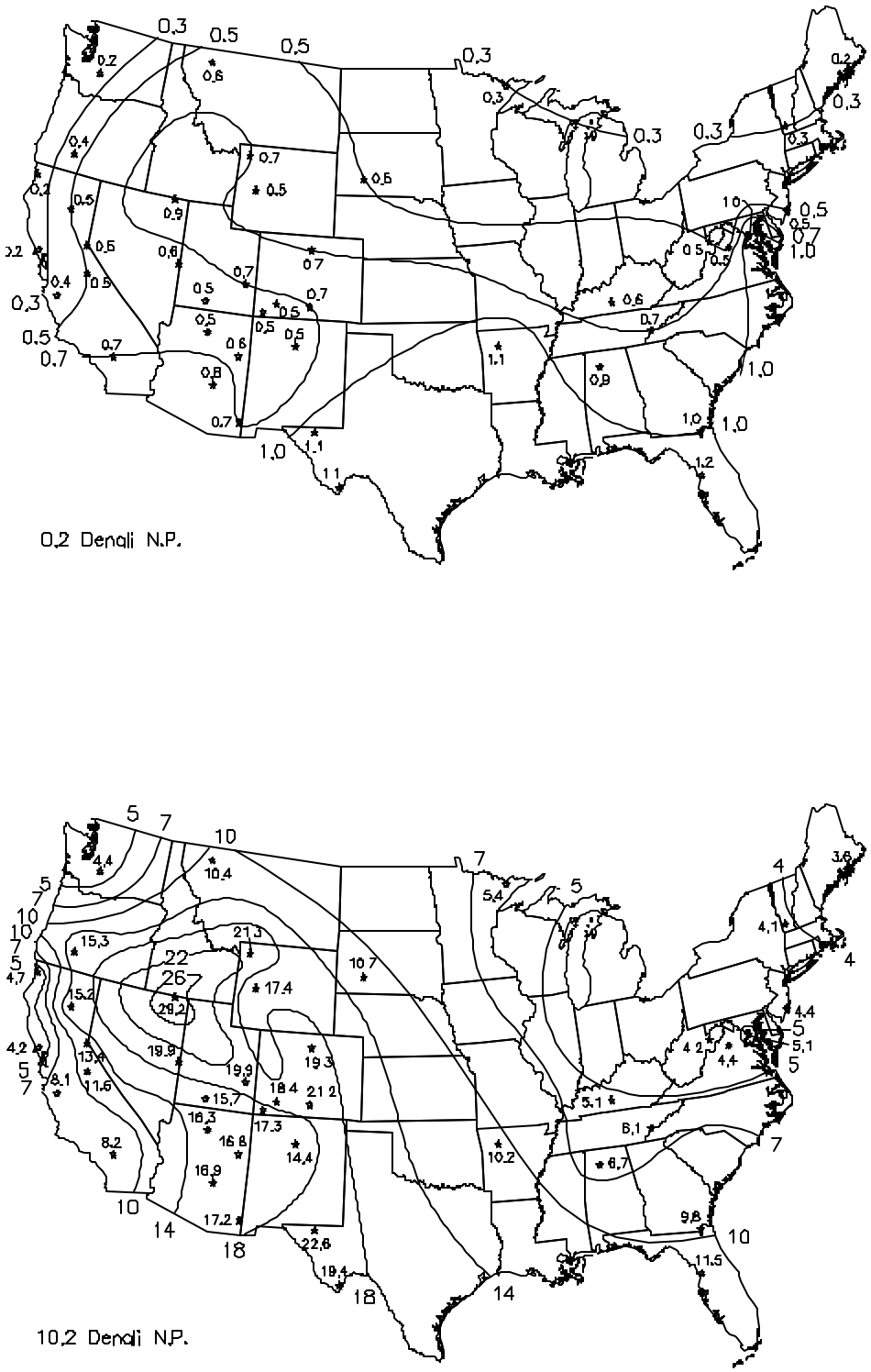

Figure 3.8 Average fine soil aerosol concentrations (in micro-g/m^3) (top) and soil fine mass fractions (bottom) for each site in the IMPROVE network.

4. Seasonality. With a few exceptions, average fine mass concentrations, organics and sulfate components of fine mass are highest in summer. Soil concentrations are highest in spring or summer. On the other hand, nitrate concentrations are generally highest in winter or spring. Light-absorbing carbon exhibits relatively little seasonal variation.

5. PM_{10}. The highest concentrations of PM_{10} occur in a region east of the Mississippi and south of the Great Lakes, followed by coastal and southern California. In the East, the high concentrations are driven by high fine mass, which contributes as much as 70% of PM_{10}.

3.4 References

Sisler, J.F., Huffman, D., Latimer, D.A., Malm, W.C., Pitchford, M.L. "Spatial and temporal patterns and the chemical composition of the haze in the United States: an analysis of data from the IMPROVE network, 1988-1991," Report by Cooperative Institute for Research in the Atmosphere (CIRA), Colorado State University, Ft. Collins, Co 80523, ISSN: 0737-5352-26, 1993.

Stensvaag, J-M., Clean Air Act 1990 Amendments: Law and Practice, John Wiley & Sons, New York, NY., 1991.

CHAPTER 4

LIGHT EXTINCTION AND ITS RELATIONSHIP TO AEROSOLS

In this chapter the relationship between aerosol concentration and measured extinction will be explored. Transmissometers are operated at a number of sites, in part, as a quality assurance check on apportionment of extinction to aerosol species. It is anticipated that the estimated scattering and absorption associated with the various aerosol species should sum to equal the measured extinction. However, White [1990] and Trijonis [1990] have shown that under some conditions this assumption may not be true. One difficulty in reconstructing extinction is the accurate estimation of absorption. The IMPROVE data set, along with the Measurements of Haze and Visual Effects (MOHAVE) special study data set, allow for a unique opportunity to explore the interrelationships between aerosol mass and absorption. From these intercomparisons a "best estimate" of scattering and absorption efficiencies will be developed for purposes of calculating the contribution of each aerosol species to extinction and therefore visibility impairment.

In 1991, Congress mandated a regional haze study whose goal was to assess the contribution of the Mohave Power Project (MPP), other nearby point sources, and regional emissions to visibility impairment in Grand Canyon National Park. The location of monitoring sites, selected national parks and wilderness areas, and major urban areas, are shown in Figure 4.1. The MOHAVE study was carried out over a period of one year (1992) with two major field intensives during the summer and winter months. An objective of MOHAVE was to apportion (or attribute) the haze observed in the Grand Canyon region to the various measured aerosol species. One set of measurements made during the summer intensive at Meadview, Lake Mead National Recreation Area, employed independent measurements of b_{ext}, b_{scat}, and b_{abs} using optical techniques as well as a full suite of aerosol mass concentrations including carbonaceous material. Independent measurements of these three variables allow for internal consistency checks on the optical measurements in that absorption and scattering should sum to extinction. Furthermore, the sum of aerosol scattering should equal measured scattering, and absorption estimated from measured aerosol species should equal measured absorption.

A second data set consists of measured extinction using transmissometers and aerosol mass concentration measurements, including b_{abs}, by optical techniques in 18 monitoring sites in western national parks.

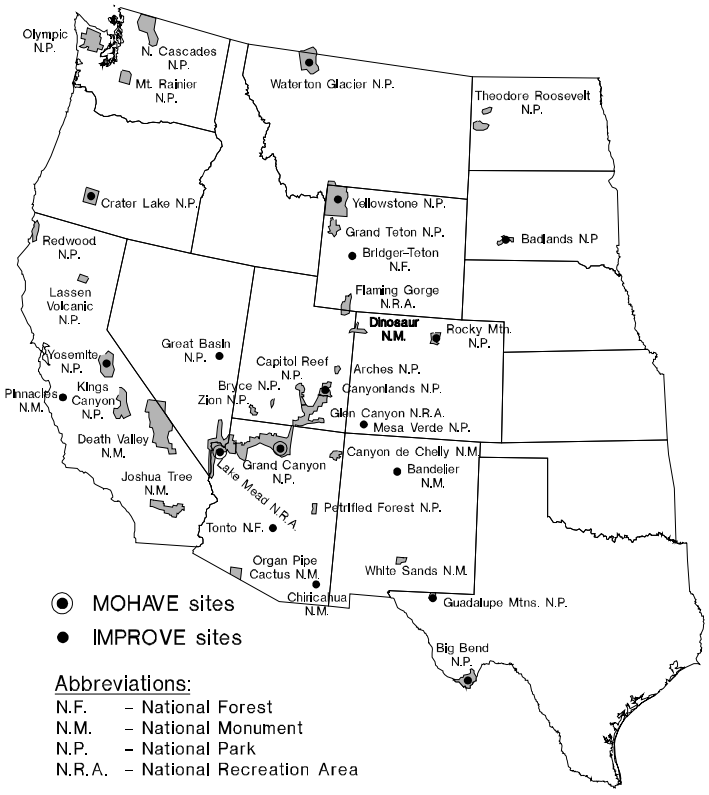

Figure 4.1 Map showing the location of monitoring sites and some of the larger national park units.

In many early visibility studies, comparisons were made between b_{scat}, as measured by nephelometry, and the various aerosol species to derive or validate scattering budgets, while extinction was estimated by summing absorption and scattering [Appel *et al.,* 1985; Ouimette *et al.,* 1981; Groblicki *et al.,* 1981; Macias *et al.,* 1981]. In many of these early studies the nephelometer sampling chamber was warmer than ambient temperatures and therefore underestimated scattering due to absorbed water at higher relative humidities. Furthermore, the absorption coefficient was not directly validated by independent methods.

More recent studies carried out in urban environments included estimates of extinction from teleradiometer techniques but utilized nephelometers, which heated the aerosol by about 4^oC [Dzubay and Clubb, 1981; Dzubay *et al.,* 1982; Lewis and Dzubay, 1986]. At 90% relative humidity (RH) a 1^oC difference between ambient and sampling chamber temperature will cause the sampling chamber relative humidity to reduce to about 84% RH. A 4^oC temperature difference translates into a chamber RH of 70%, which in turn results in a substantial underestimation of scattering from hygroscopic particles.

The most recent urban studies at Denver, Phoenix/Tucson, and Tucson [Watson *et al.,* 1988, 1989; Heisler *et al.,* 1980a,b; Watson *et al.,* 1990a,b; Heisler *et al.,* 1994] employed transmissometers to measure extinction [Dietrich *et al.,* 1989] ambient nephelometers to measure

scattering [Malm *et al.,* 1994] and integrating plate transmission measurements for absorption [Watson *et al.,* 1988, 1989]. These studies also included a full suite of aerosol measurements. For the most part, the sum of absorption and scattering equaled measured extinction within measurement uncertainty and measured absorption, and scattering could be predicted from aerosol measurements.

Only one study has explored the relationship between ambient measurements of b_{ext}, $b_{scat,}$ and b_{abs} in nonurban settings [White *et al.,* 1994]. They were able to show that the scattering and absorption as measured by optical techniques and the fraction of coarse mass scattering not captured by the nephelometer summed to extinction and were consistent with measurements of fine and coarse mass. They did not explore the relationship between measured absorption and estimates of absorption from aerosol concentrations.

4.1 Comparison of Reconstructed to Measured Fine Mass

Table 4.1 contains statistical summaries of the aerosol mass concentrations for the Meadview, AZ data set, along with the fraction that each aerosol species contributes to reconstructed fine mass, while Figure 4.2 is a scatter plot of reconstructed and measured fine mass. The error bars are calculated from reported measurement uncertainties. O1, O2, O3, O4, and OP have been multiplied by 1.4 to account for the assumed mass of oxygen and other elements in organic carbon.

Although water associated with hygroscopic aerosols was not explicitly measured, it is expected that a significant amount of water was retained on the filter when the filters were weighed. The filters were equilibrated in the laboratory at approximately 50% relative humidity, a value which is well above the relative humidity at which ammonium sulfate or other hygroscopic particles dry out [Tang *et al.,* 1981]. Therefore, retained water will cause scatter in the data points below, but not above, the 1:1 line because measured gravimetric mass includes some water, while reconstructed mass does not. Figure 4.2 clearly shows this trend.

Measured and reconstructed fine mass accounts for 33% and 31% of measured PM_{10} mass. Sulfates are the largest fraction of reconstructed fine mass at 56%. Soil and organic carbon are virtually tied for second at 19% and 16%, respectively, while light-absorbing carbon (LAC) is 3% and nitrates are 6%. It is worth noting that the sulfate mass fraction of fine mass is somewhat greater than reported by others for studies carried out in the same region: 42% at Zilnez Mesa by Macias *et al.* [1981], 40% at Glen Canyon by Sutherland and Bhardwaja [1990], and 40% at Meadview by Vasconcelos *et al.* [1994].

Table 4.2 is a similar summary of aerosol mass species concentrations for 14 western IMPROVE sites, while Figure 4.3 shows a scatter plot of reconstructed and measured fine mass. As with the Meadview data set there is more scatter below the 1:1 line suggesting that hygroscopic aerosols may have retained water during the weighing procedures. In the case of

Table 4.1 Summary statistics for aerosol mass concentrations for the summer Meadview data set. The number of valid data points is 97.

Variable	Mean (ìg/m^3)	Std Dev	Minimum (ìg/m^3)	Maximum (ìg/m^3)	Fraction of reconstructed fine mass
CM	9.60	3.84	3.29	18.14	--
FM	4.80	1.66	1.72	10.40	--
FM_{recon}	4.14	1.50	1.26	9.98	--
$(NH_4)_2SO_4$	2.31	0.95	0.93	6.68	0.56
NH_4NO_3	0.24	0.19	0.04	0.95	0.06
O1	0.02	0.11	-0.12	0.51	_0.01
O2	0.14	0.23	-0.26	1.27	0.03
O3	0.13	0.17	-0.19	0.59	0.03
O4	0.16	0.10	-0.03	0.62	0.04
OP	0.23	0.12	0.00	0.60	0.06
E1	0.04	0.05	0.00	0.26	0.01
E2	0.08	0.04	0.00	0.22	0.02
E3	0.01	0.02	-0.02	0.14	_0.01
SOIL	0.78	0.33	0.35	2.20	0.19
OMC	0.67	0.49	-0.25	2.59	0.16
LAC	0.13	0.08	0.00	0.42	0.03

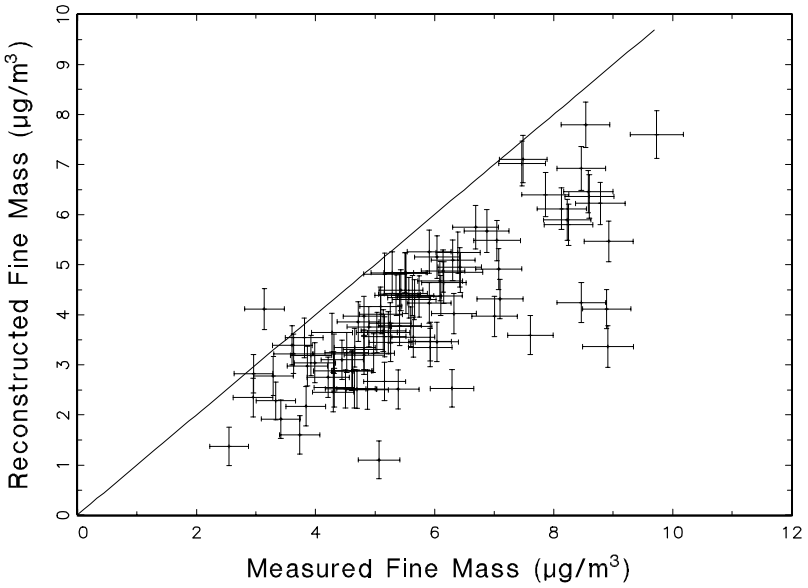

Figure 4.2 Scatter plot of measured and reconstructed fine mass for the summer Meadview data set. The error bars show the measurement uncertainty.

the IMPROVE sites, organic carbon is the largest fraction of fine mass at 41% with sulfate being second at 33%. Nitrates and LAC each contribute about 7% of the fine mass.

Table 4.2. Summary statistics for aerosol mass concentrations for the IMPROVE data set. The number of valid data points is 5108.

Variable	Mean (ìg/m^3)	Std Dev	Minimum (ìg/m^3)	Maximum (ìg/m^3)	Fraction of reconstructed fine mass
CM	4.81	4.48	0.00	72.43	--
FM	4.06	2.36	0.00	23.05	--
FM_{recon}	3.86	2.00	0.00	26.14	--
$(NH_4)_2SO_4$	1.26	0.87	0.00	9.45	0.33
NH_4NO_3	0.26	0.43	-0.06	10.15	0.07
O1	0.22	0.22	0.00	5.12	0.06
O2	0.32	0.22	0.00	4.11	0.08
O3	0.45	0.40	0.00	4.64	0.12
O4	0.28	0.23	0.00	3.06	0.07
OP	0.30	0.24	0.00	5.09	0.08
E1	0.11	0.15	0.00	2.42	0.03
E2	0.14	0.07	0.00	0.56	0.04
E3	0.03	0.03	0.00	1.37	0.01
SOIL	0.49	0.44	0.00	7.03	0.13
OMC	1.57	1.11	0.00	19.95	0.41
LAC	0.28	0.19	0.00	3.12	0.07

4.2 Extinction Components

The total extinction coefficient, $b_{ext,t}$, is the sum:

$$b_{ext,t} = b_{ext} + b_{ext,g}, where$$
$$b_{ext} = b_{scat} + b_{abs}, and \qquad (4.1)$$
$$b_{ext,g} = b_{scat,g} + b_{abs,g}.$$

b_{ext} and $b_{ext,g}$ are the extinctions due to particles and gases, respectively. b_{ext} is the sum of scattering, b_{scat}, and absorption, b_{abs}, by particles, while $b_{ext,g}$ is the sum of scattering, $b_{scat,g}$, and absorption, $b_{abs,g}$, by gases. All terms are wavelength dependent. Light scattering by gases in the atmosphere is described by the Rayleigh scattering theory [vandeHulst, 1981] and will be referred to as Rayleigh scattering. The only gas that is normally found in the atmosphere and absorbs light is nitrogen dioxide. In most instances, particle scattering and absorption are primarily responsible for visibility reduction [Trijonis and Pitchford, 1987].

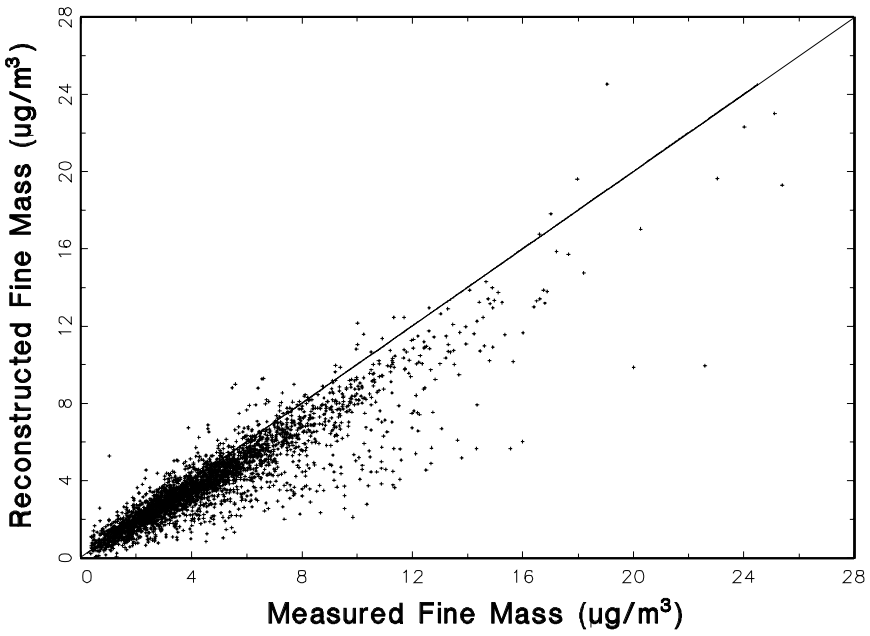

Figure 4.3 Scatter plot of measured and reconstructed fine mass for the IMPROVE data set.

Any particle in the atmosphere, whether it is externally or internally mixed, scatters and/or absorbs a specific amount of radiant energy and as such has a quantifiable mass extinction efficiency. White [1986] refers to this quantity as the specific extinction efficiency. Summing the extinction associated with each particle along some path must equal the total atmospheric extinction in that path. Therefore, a fraction of total extinction can be assigned to each particle type, and an extinction or scattering "budget" can be calculated.

Historically, researchers have invoked a number of assumptions concerning measured aerosol distributions. They have calculated or estimated specific mass scattering and absorption efficiencies, and used these to form estimates of extinction budgets. Because specific bulk aerosol species' concentrations are measured, the implicit assumption is one of externally mixed particles. However, under realistic assumptions concerning the microphysical properties of the particles the postulation of an external or internal mixture is not important to the estimation of specific mass extinction efficiencies. Ouimette and Flagan [1982] have shown that if an aerosol is mixed externally or if in an internally mixed aerosol the index of refraction is not a function of composition or size, and the aerosol density is independent of volume, then:

$$b_{ext} = \sum_i \alpha_i m_i \qquad (4.2)$$

where $\acute{a}_i$ is the specific mass scattering or absorption efficiency and m_i is the mass of the individual species. It should be pointed out, however, that as water is absorbed by hygroscopic particles the

index of refraction will change and that change will be dependent on the growth and mixture models that are assumed.

All routine aerosol monitoring programs and most special study visibility characterization programs were designed to measure aerosol species such as sulfates, nitrates, elements, and carbonaceous material [Heisler *et al*., 1980a; Malm *et al*., 1994; Tombach and Thurston, 1994; Watson *et al*., 1990a; and Macias *et al*., 1981]. They were not designed to determine whether these species were internally or externally mixed. Therefore, b_{ext} is usually apportioned by assigning specific mass extinction efficiencies to each species and calculating the total extinction using Equation (4.2).

A number of investigators have taken advantage of the form of Equation (4.2) to construct a multilinear regression model with b_{ext} as the dependent variable and the measured aerosol mass concentrations of species *I* as the independent variables. The regression coefficients are then interpreted as specific extinction to mass efficiencies [White and Roberts, 1977; Cass 1979; Groblicki *et al.,* 1981]. The use of multivariate regression models to apportion mass concentrations to scattering and absorption requires that the model meet a number of limiting assumptions, and should be used with caution. White [1986] discusses some of the issues associated with this problem.

Any apportionment of aerosol mass to extinction is only approximate. The assumptions required for extinction-mass relationships implied by Equation (4.2) probably are never exactly met. The appropriateness of any apportionment scheme can only be judged within the context of whether the model is physically "reasonable," and whether independent apportionment of mass to extinction is consistent with measurements of scattering and absorption.

The strategy used to examine extinction apportionment is to use Equation (4.2) to examine various relationships between measured scattering, extinction, and absorption, and between these variables and nominal dry particle extinction efficiencies that have been synthesized from a variety of estimates. Scattering associated with absorbed water is prorated among hygroscopic aerosol species. Regression analysis will be used to investigate the validity of assumptions utilized in the apportionment scheme.

4.2.1 Estimating Light Scattering

Because certain aerosols, such as sulfates and nitrates, have an affinity for water, their scattering characteristics change as a function of relative humidity (RH). Therefore, aerosol scattering of the so-called hygroscopic species as a function of relative humidity must be considered.

In general, the higher the RH the greater the scattering of soluble aerosols. The relationship between RH and scattering efficiency for ammonium sulfate aerosols with a mass mean diameter of 0.3 ìm and a geometric size distribution of 1.5 is shown in Figure 4.4. This function, referred to as *f*(RH), is:

$$f(RH) = b_{scat}(RH)/b_{scat}(0\%) \qquad (4.3)$$

where b_{scat}(0%) and b_{scat}(RH) are the dry and wet scattering, respectively. The aerosol growth was calculated following the scheme proposed by Tang [1981]. Ammonium sulfate and ammonium

nitrate mass are associated with this function.

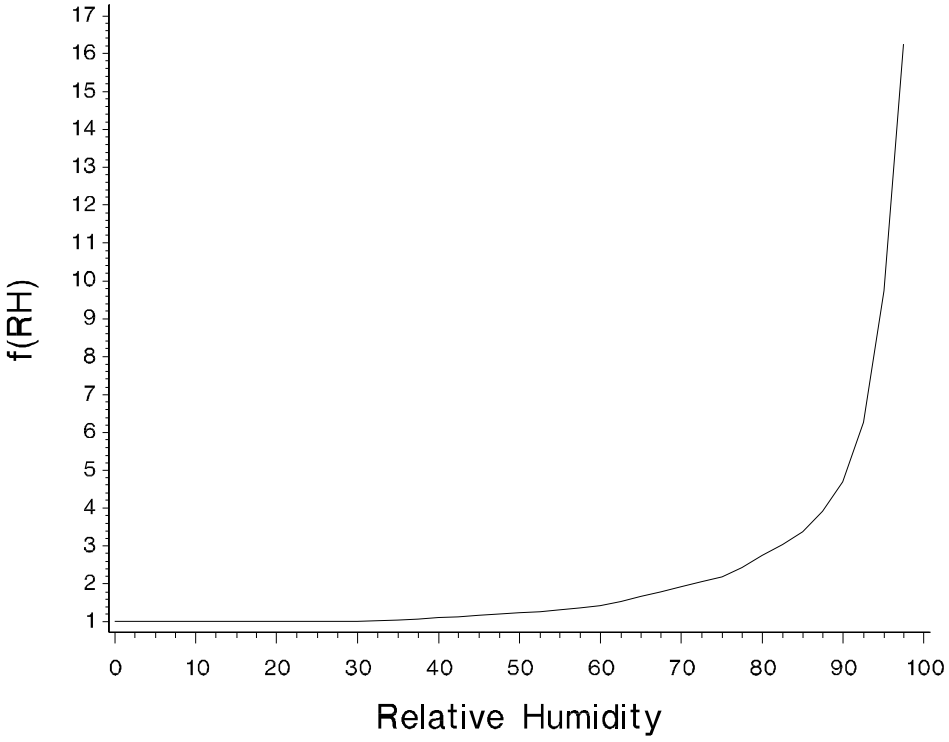

Figure 4.4 *f*(RH) for ammonium sulfate is plotted as a function of relative humidity.

Various functions for the hygroscopicity of organics have been proposed. Assumptions must not only be made about the solubility of organics but also on the fraction of organics that are soluble. White [1990] discusses this issue. Given the variety of organic species, it is possible that a geographic variation in organic species exists with large fractions of soluble species occurring in certain parts of the continent and much smaller fractions in other areas.

The following equation is used to estimate reconstructed particle scattering:

$$\begin{aligned} b_{scat} &= (3) f(RH)[SULFATE] \\ &+ (3) f(RH)[NITRATE] \\ &+ (3) f_{org}(RH)[OMC] \\ &+ (1)[SOIL] \\ &+ (0.6)[CM] \end{aligned} \qquad (4.4)$$

The brackets indicate the species concentration, 3 m^2/g is the dry scattering efficiency of sulfates, nitrates, and organic carbon, while 1 m^2/g and 0.6 m^2/g are the respective scattering efficiencies for soil and coarse mass. The efficiencies for fine soil and coarse mass are taken from a literature review by Trijonis and Pitchford [1987].

A dry scattering efficiency of 3 m^2/g is a nominal scattering efficiency based on a literature review by Trijonis *et al.* [1988, 1990] and a review by White [1990]. Trijonis' best estimate for sulfates and nitrates is 2.5 m^2/g with an error factor of 2, while for organics it is 3.75 m^2/g again with an error factor of 2. White [1990] took a somewhat different approach in that he reviewed 30 studies in which particle scattering and mass were measured. He then estimated a high and low scattering efficiency by using mass measurements to prorate the measured extinction. For sulfate the low estimate was arrived at by assuming that sulfate, nitrates, and organics scatter twice as efficiently as all other species, and for the high estimate he assumed that only sulfate was twice as efficient. His low and high sulfate mass scattering efficiencies for the rural west were 3.0 and 3.7 m^2/g, respectively. For organics, his low estimate assumes that organics and other nonsulfate species scatter half as efficiently as sulfates, and for the high estimate he assumes organics are three, and sulfates two times as efficient at scattering light as other species. His low and high estimates for organic mass scattering coefficients are 1.8 and 4.1 m^2/g. It is worth noting that an ammonium sulfate scattering efficiency of 3 m^2/g is also consistent with sulfur particle mass size distributions measured at Grand Canyon [Malm *et al.,* 1986].

The validity of using Equation (4.4) and the use of associated specific mass scattering efficiencies to estimate particle scattering from bulk measurements of aerosol species are explored in the next sections.

4.2.2 Estimating Aerosol Absorption

On channel A, b_{abs} is quantified directly by the LIPM analysis and is stated in units of 10^{-8} m^{-1}. It can also be estimated using Equation (4.2) in the form of:

$$b_{lac} = \alpha_{abs}[LAC] \qquad (4.5)$$

where á$_{abs}$ is the absorption efficiency of light-absorbing carbon. b_{lac} is used to represent particle absorption estimates derived from LAC mass concentrations. Horvath [1993] reviewed a number of studies where á$_{abs}$ for soot and black carbon were measured. He also reviewed a number of theoretical calculations of á$_{abs}$ where a variety of refractive indices and densities were assumed. Measured values of á$_{abs}$ range from a low of 3.8 to a high of 17 m^2/g, while theoretical calculations of á$_{abs}$ suggest a value of 8-12 m^2/g. The relationship between LAC and b_{abs} will be further explored in the following analysis.

4.3 Aerosol Scattering and Absorption

Table 4.3 presents the statistical summaries of the scattering or absorption associated with each variable for the summer Meadview data. The scattering associated with each species was calculated using the efficiencies presented in Equation (4.4) and an absorption efficiency for LAC of 10 m^2/g. Rb_{ext1} and Rb_{ext2} are reconstructed extinctions using b_{abs} and b_{lac}, respectively and Rb_{scat} is reconstructed scattering. Also presented in the table are summary statistics for measured b_{scat}, b_{ext}, ambient relative humidity (RH), and f(RH).

Table 4.3. Summary statistics for optical variables for the summer Meadview data set. The numbers reported are associated with the scattering, absorption, or extinction associated with each variable. Units on scattering, absorption, and extinction are in Mm^{-1}, while relative humidity is in percent and *f*(RH) factors have no units. Rb_{ext1} and Rb_{ext2} refer to reconstructed extinction using b_{lac} and b_{abs}, respectively and Rb_{scat} is reconstructed scattering. Units on scattering, absorption, and extinction are in Mm^{-1}, while relative humidity is in percent and *f*(RH) factors have no units. The number of valid data points is 82.

Variable	Mean (Mm^{-1})	Std Dev	Minimum (Mm^{-1})	Maximum (Mm^{-1})
b_{ext}	23.65	5.67	14.08	41.36
Rb_{ext1}	17.70	5.45	7.69	36.05
Rb_{ext2}	23.27	6.88	10.62	48.94
b_{scat}	12.44	5.22	4.33	36.83
Rb_{scat}	16.48	5.02	7.51	35.05
b_{abs}	6.80	2.07	3.11	14.93
b_{lac}	1.23	0.75	0.00	3.08
$(NH_4)_2SO_4$	7.23	3.15	3.01	20.03
NH_4NO_3	0.80	0.58	0.12	2.84
OC	1.88	1.24	-0.53	6.51
SOIL	0.80	0.34	0.35	2.20
CM	5.76	2.28	1.98	10.89
RH	25.79	13.25	6.08	61.92
f(RH)	1.06	0.12	1.00	1.63
$f(RH_c)$	1.05	0.11	1.00	1.60

The nephelometer chamber relative humidity is estimated from chamber temperature using:

$$RH_c = RH_a e^{\frac{5210.5(T_a - T_c)}{T_a T_c}} \qquad (4.6)$$

where RH_a, RH_c, T_a, and T_c are the ambient and chamber relative humidities and temperatures, respectively. From RH_c the $f(\mathrm{RH}_c)$ function inside the nephelometer can be estimated. It is also summarized in Table 4.3.

Because of the low relative humidities during the MOHAVE summer intensive, and because the "ambient" nephelometer exhibited minimal heating of the aerosol while in the sampling chamber, the $f(\mathrm{RH}_c)$ within the nephelometer was close to the ambient f(RH). The average f(RH) values for ambient and within the nephelometer were 1.06 and 1.05, while the maximum f(RH) values were 1.63 and 1.60, respectively. Because the f(RH) values were nearly the same, adjustments were not made to measured b_{scat} to account for chamber heating.

Figure 4.5 is a temporal plot of measured b_{ext}, b_{scat}, b_{abs}, ambient RH, and f(RH), while Figure 4.6 is a temporal plot of scattering associated with each aerosol species. Error bars were not included because of the unknown uncertainty in the prescribed efficiencies. The reported error on the b_{ext} and b_{scat} measurements are about 10%.

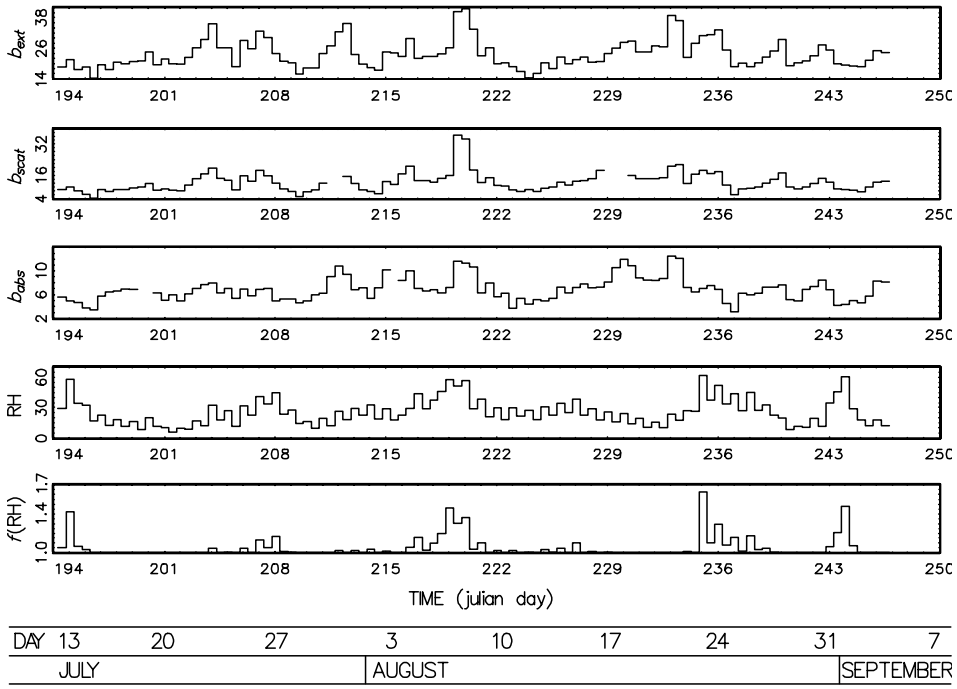

Figure 4.5 Temporal plot of measured b_{ext}, b_{scat}, b_{abs}, relative humidity, and f(RH) for the summer Meadview data set. Units on extinction, scattering, and absorption are Mm^{-1}, while relative humidity is in percent and f(RH) is unitless. Time is in Julian day, and for reference the month and day axis is also included.

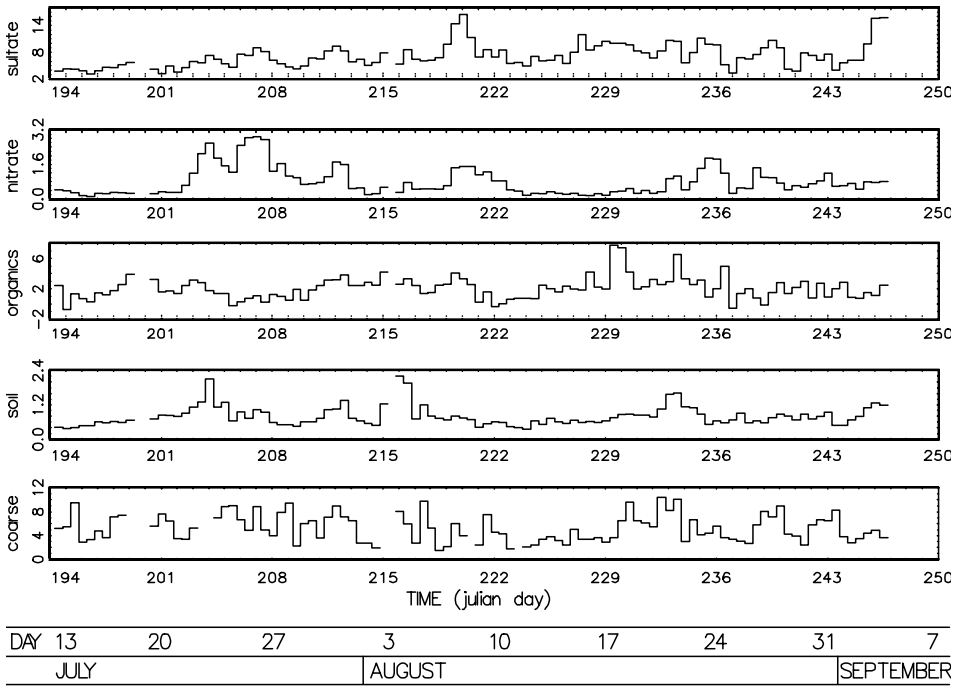

Figure 4.6 Temporal plot of estimated scattering associated with ammonium sulfate, ammonium nitrate, organics, fine soil, and coarse mass. Units are in Mm^{-1}.

Table 4.4 presents similar information for the IMPROVE data set. The scattering associated with each species was calculated using the efficiencies presented in Equation (4.4) and an absorption efficiency for LAC of 10 m^2/g. Of the 18 IMPROVE sites that have a transmissometer, nine sites were chosen to intercompare aerosol and b_{ext} measurements. They are Grand Canyon, Petrified Forest, Guadalupe Mountains, Yellowstone, Rocky Mountain, Glacier, Pinnacles, and Bandelier National Parks and Bridger Wilderness Area. At the other nine sites the transmissometer site path is directed over a slanted site path or over a canyon. Thus, the aerosol sampler and transmissometer are not sampling the same air masses.

The IMPROVE particle sampler collects samples for 24 hours, while the transmissometer and RH data is gathered on an hourly basis. Therefore, the transmissometer and RH data is averaged to 24 hours. There are about 5000 total data points consisting of 24-hr average transmissometer extinction, however, because of cloudy or foggy conditions not all 24-hr averages contain 24 data points. The analysis is restricted to those data points where there are at least 18 hourly readings for the transmissometer. With this restriction there remains 1642 valid readings.

Table 4.4 Summary statistics for optical variables for the IMPROVE data set. The numbers reported are associated with the scattering, absorption, or extinction associated with each variable. Units on scattering, absorption, and extinction are in Mm^{-1}, while relative humidity is in percent and *f*(RH) factors have no units. Rb_{ext1} and Rb_{ext2} refer to reconstructed extinction using b_{lac} and b_{abs}, respectively. The number of valid data points is 1642.

Variable	Mean (Mm^{-1})	Std Dev	Minimum (Mm^{-1})	Maximum (Mm^{-1})
b_{ext}	22.68	10.47	0.00	56.10
Rb_{ext1}	15.91	8.20	-0.32	59.70
Rb_{ext2}	20.41	10.02	0.92	67.97
b_{abs}	6.29	3.47	0.00	24.19
b_{lac}	1.79	1.71	-1.35	15.60
$(NH_4)_2SO_4$	4.76	3.39	0.18	28.52
NH_4NO_3	1.23	1.77	-0.24	23.09
OMC	3.87	2.33	-0.95	19.51
SOIL	0.71	0.62	0.02	4.35
CM	3.55	3.05	0.00	26.08
RH	46.67	15.30	7.79	87.17
f(RH)	1.45	0.44	1.00	3.91

4.4 Comparison of Reconstructed Extinction and Scattering

The Meadview data set offers a unique opportunity to examine the relationship among extinction, scattering and absorption directly without having to unduly rely on estimates of aerosol scattering from various species. Extinction, scattering, and absorption are all measured optically and thus allow for an independent assessment of the accuracy of these measurements. If the validity of these measurements can be established then scattering and absorption, as estimated from aerosol measurements, can be independently compared to each of these measures.

4.4.1 Extinction, Scattering, and Absorption Characteristics at Meadview

Extinction and scattering measurements are directly compared by using the following equation:

$$b_{ext} = b_{scat} + b_{abs} + CMS/2 \qquad (4.7)$$

where *CMS/2* is half the estimated total coarse mass scattering. Hasan and Lewis [1983] have carried out theoretical calculations to show that because of the forward angle truncation error in the nephelometer, it underestimates coarse mass scattering by about a factor of two. Furthermore, White *et al.*, [1994] were able to show from transmissometer derived total scattering and nephelometer measurements of fine and coarse particle scattering that the nephelometer underestimates scattering by particles greater than 2.5 ìm by about a factor of two.

Equation (4.7) consists of all measured optical variables except for CMS. Figure 4.7 is a scatter plot of the left and right side of Equation (4.7) along with the one-to-one line. Considering the uncertainty in estimated coarse mass scattering and the nephelometer response to coarse particles, the agreement is quite good. On the average, b_{ext} is only about 1 Mm^{-1} greater than $b_{scat}+b_{abs}+$ CMS/2. However, Figure 4.7 shows that for the main body of data points, b_{ext} is underestimated by about 2 Mm^{-1}, while the two largest extinctions are clearly overestimated.

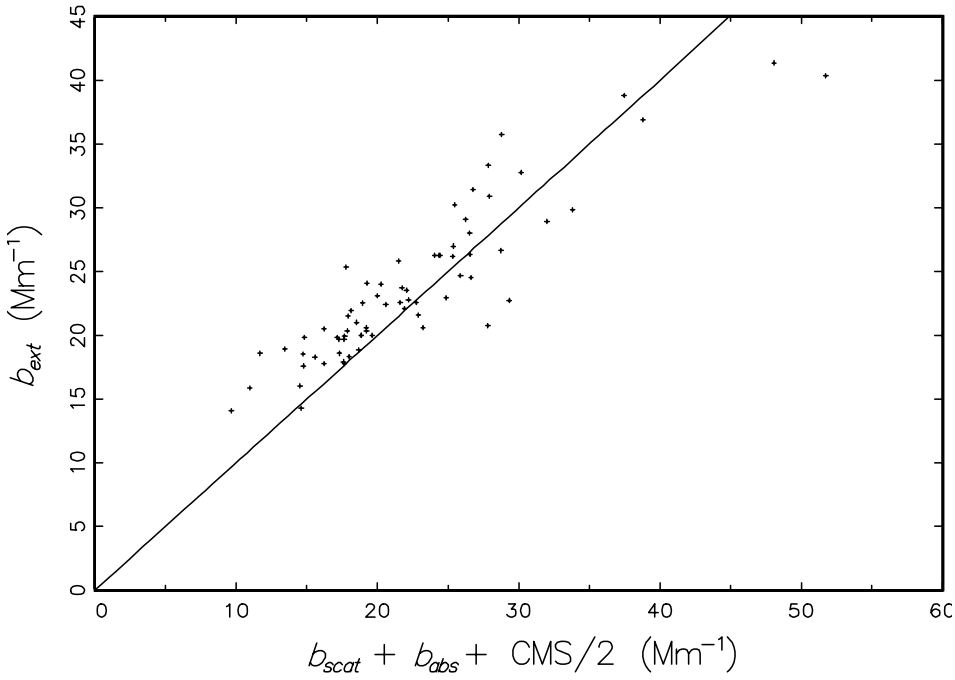

Figure 4.7 Reconstructed extinction using b_{scat}, b_{abs}, and coarse mass divided by 2 is plotted against measured extinction. Units are in Mm^{-1}.

In the above analysis b_{ext} was compared to reconstructed b_{ext} using the direct measurement of absorption, b_{abs}, by the laser integrated plate technique (LIPM) as opposed to using absorption estimates derived from LAC mass concentrations (b_{lac}). Figure 4.8 shows a scatter plot of reconstructed and measured extinction when b_{lac} is used as an estimate of absorption instead of b_{abs}. Using b_{lac}, which has been the traditional method of estimating b_{abs}, apparently yields an underestimation of extinction by about 7-8 Mm^{-1}. Examination of Table 4.4 shows that b_{abs} is 5.6 times larger than b_{lac}.

Using b_{abs} without any adjustments for reconstituting extinction gives a reasonable fit to measured extinction suggesting that b_{ext}, b_{scat}, and b_{abs} are accurate representations of ambient extinction, scattering, and absorption, while b_{lac} is not.

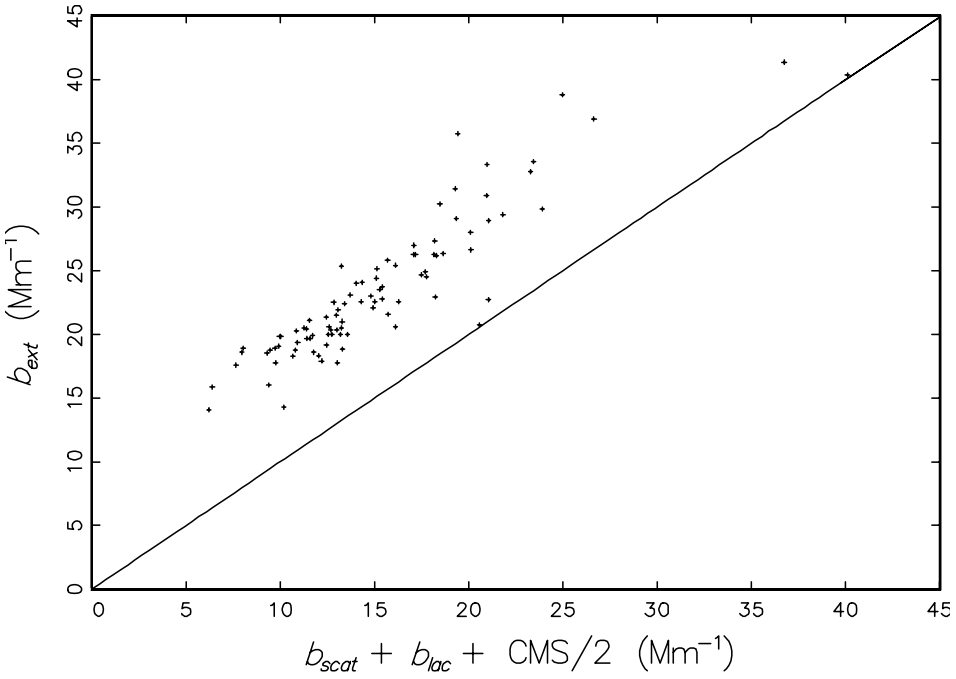

Figure 4.8 Reconstructed extinction using b_{scat}, b_{lac}, and coarse mass divided by 2 is plotted against measured extinction. Units are in Mm^{-1}.

4.4.2 Comparison of Estimated and Measured Scattering at Meadview

Figure 4.9 is a scatter plot of reconstructed and measured b_{scat} along with the 1:1 line for the summer Meadview data using CMS/2. Reconstructed scattering was calculated using Equation (4.4). The agreement is quite good. Most data points fall about the 1:1 line with the two highest measured values being about 7 Mm^{-1} greater than the 1:1 line. The close agreement between measured and reconstructed scattering gives some confidence that the aerosol species mass concentrations have been accurately measured and their associated scattering fairly represented.

4.4.3 Comparison of Estimated and Measured Extinction at Meadview and IMPROVE Sites

Figure 4.10 is a scatter plot of reconstructed and measured extinction using b_{abs}. Again, reconstructed b_{scat} was calculated using Equation (4.4). The agreement between reconstructed and measured extinction is quite good with reconstructed extinction being about 1 Mm^{-1} lower than measured extinction.

These results are consistent with the direct comparison between b_{ext}, b_{scat}, and b_{abs}. The real difference between the direct comparison of the optical variables is that the nephelometer scattering was corrected for underestimation of large particle scattering. In the reconstructions

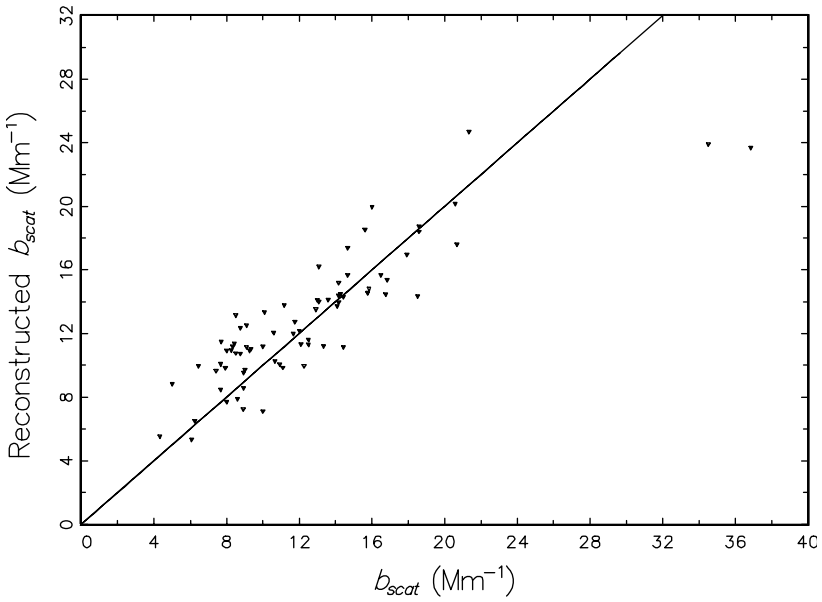

Figure 4.9 Reconstructed b_{scat} using the sum of estimated aerosol species scattering is plotted against measured b_{scat}. Units are in Mm^{-1}.

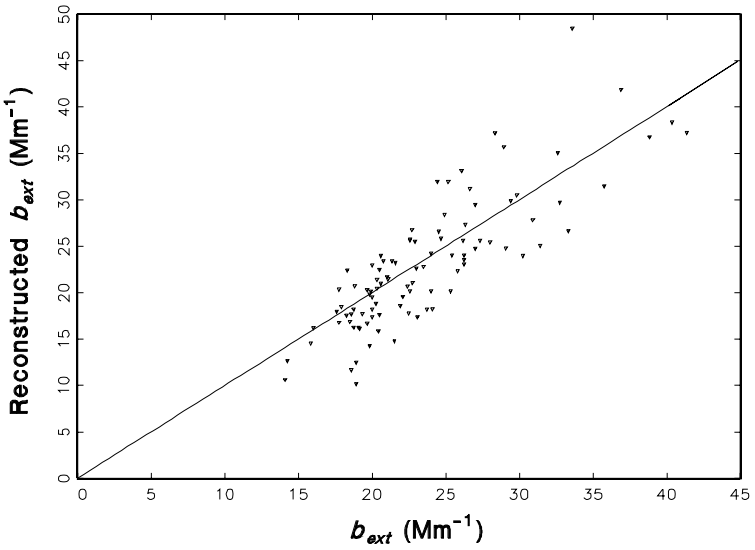

Figure 4.10 Reconstructed b_{ext} using the sum of estimated aerosol species scattering but with coarse mass scattering divided by 2 is plotted against measured b_{scat}. Units are in Mm^{-1}.

of extinction, this correction was not made because the transmissometer does not have a built-in underestimation of large particle scattering. In fact, the 0.6 m^2/g estimate of coarse particle scattering was derived from nephelometer measurements and it may be an underestimate of ambient coarse particle scattering and is certainly an underestimate of coarse particle absorption. Figure 4.10 suggests that the extinction in the 20-25 Mm^{-1} is somewhat underestimated, which may in part be due to an underestimation of coarse particle scattering and/or absorption.

The overriding issue, however, is the difference between b_{abs} and b_{lac}. The Meadview data set suggests that b_{abs} for the LIPM is a more accurate representation of absorption than b_{lac} as derived from LAC and that atmospheric absorption calculated using LAC may be a severe underestimate. The Meadview data set is small in that it covers about one month of time and is at only one location. The IMPROVE data set allows reconstructions of extinction using b_{abs} and b_{lac} to be compared with measured extinction over wide geographic regions and over a period of about four years.

Figures 4.11 and 4.12 are comparisons between reconstructed and measured extinctions using b_{lac} and b_{abs}, respectively, for the previously identified nine sites. As in the Meadview data set, reconstructed extinction is significantly lower than measured extinction when using b_{lac} and nearly the same when using b_{abs}. When using b_{lac}, reconstructed extinction is about 30% lower than measured extinction and about 10% lower when using b_{abs}.

For the reconstructed extinctions used in Figures 4.11 and 4.12 organics were not considered to be hygroscopic, and they were assumed to have the same dry mass scattering efficiency as sulfates. The hygroscopicity of organics was examined by assuming various fractions of organics being hygroscopic and assigning a variety of f(RH) curves to those fractions. Nonlinear growth curves caused the relationship between reconstructed and measured extinction to degrade as judged by the r^2 value associated with an ordinary least square (OLS) regression between the two variables.

The best fit between reconstructed and measured extinction, as judged by r^2 values, is achieved by increasing the dry mass scattering efficiency from 3 m^2/g to about 4 m^2/g. A 4 m^2/g dry mass scattering efficiency is consistent with the density of organics being lower than for sulfates. The resulting scatter plot between measured and reconstructed extinction is shown in Figure 4.13. The r^2= 0.63 with data points being nearly equally distributed above and below the 1:1 line. On the average, measured extinction is about 1 Mm^{-1} or 4% greater than reconstructed extinction. This difference is well within the uncertainties of the measurements.

The choice of scattering efficiencies used to match measured and reconstructed extinction are well within the constraints of known physical principles, however, they are by no means unique. The one outstanding feature is the need to use b_{abs} as derived from LIPM as opposed to b_{lac} to bring measured and reconstructed extinction into agreement. If b_{lac} is assumed to be the true atmospheric absorption any choice of growth functions, f(RH), and dry scattering efficiencies that force measured and reconstructed extinction to be equal are outside constraints imposed by known physical and chemical principles. Furthermore, the overall relationship between measured and reconstructed extinction is degraded as judged by r^2 values between the two quantities.

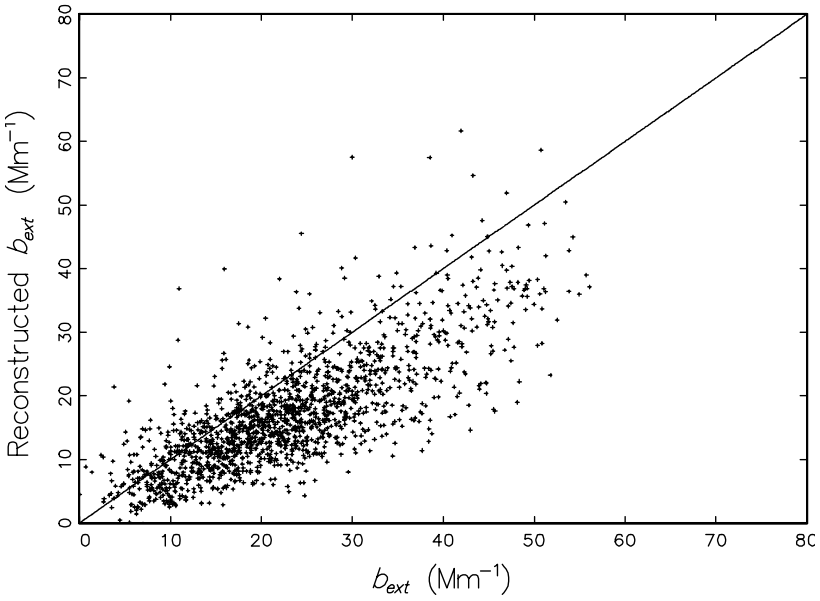

Figure 4.11 Reconstructed b_{ext} using b_{lac} and the sum of estimated aerosol scattering from the various aerosol species is plotted against measured b_{ext}. Units are in Mm^{-1}.

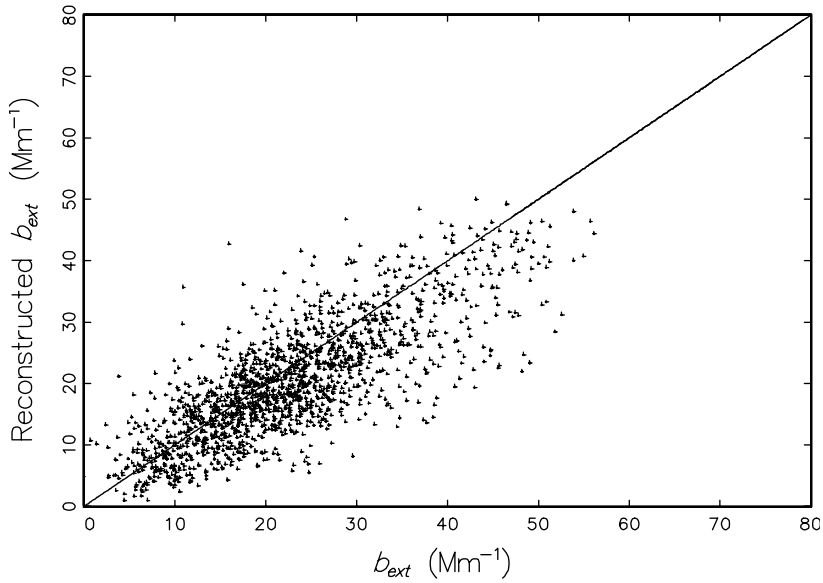

Figure 4.12 Reconstructed b_{ext} using b_{abs} and the sum of estimated aerosol scattering from the various aerosol species is plotted against measured b_{ext}. Units are in Mm^{-1}.

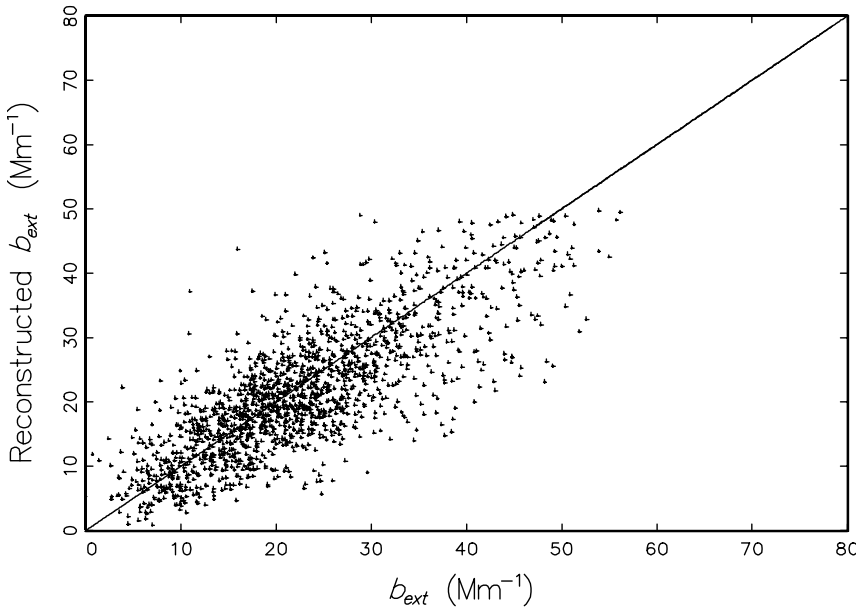

Figure 4.13 Reconstructed b_{ext} using b_{lac} and the sum of estimated aerosol scattering from the various aerosol species is plotted against measured b_{ext} for the IMPROVE data set. Units are in Mm^{-1}.

4.4.4 Regression Analysis

One can further examine the appropriateness of best estimates of scattering and absorption efficiencies using regressional techniques. Typically, the regression equation takes on the form of Equation (4.2) with either the extinction or scattering coefficient being the dependent variable and the aerosol species the independent variables. The regression coefficients are then interpreted as the scattering or absorption to mass efficiencies.

One problem with using regressional techniques is collinearity. One way to investigate the independence of variables is factor analysis. Table 4.5 presents a factor analysis using varimax rotation of the optical and aerosol scattering variables. b_{ext}, b_{abs}, b_{scat}, $SO_{4,scat}$, and $NO_{3,scat}$ are all loaded into the same factor, while organics (b_{lac}) and b_{abs} load into a second factor, and fine soil scattering ($soil_{scat}$) and scattering due to the sum of coarse mass and soil (CM_{scat}+$soil_{scat}$) load into a third factor. Therefore, for purposes of regression analysis sulfates and nitrates were combined into one variable, coarse mass and soil in a second, b_{abs} in a third, and organics in a fourth.

Table 4.5. Results of a factor analysis on various extinction, scattering, and absorption variables for the summer Meadview data set.

VARIABLE	FACTOR 1	FACTOR 2	FACTOR 3
b_{ext}	0.84663	0.25915	0.36179
b_{scat}	0.84947	0.33622	0.19281
$SO_{4,scat}$	0.84729	0.28517	-0.12735
$NO_{3,scat}$	0.67126	-0.42681	0.43896
OMC_{scat}	0.15304	0.84407	0.13199
$soil_{scat}$	0.24992	0.41696	0.62812
CM_{scat} + $soil_{scat}$	0.06930	0.09632	0.90461
LAC	0.25854	0.79690	0.14658
b_{abs}	0.63729	0.62277	0.24615
Variance explained by each factor			
	FACTOR 1	FACTOR 2	FACTOR 3
	3.170547	2.362169	1.689319

A three-step linear least squares regression was carried out on the following equations:

$$\begin{aligned} b_{ext} &= a_1(b_{scat}) + a_2(b_{abs}) + a_3(soilcms), \\ b_{ext} &= a_4(S4N3) + a_5(OMS) + a_6(b_{abs}) + a_7(soilcms), \text{and} \\ b_{scat} &= a_8(S4N3) + a_9(OMS) + a_{10}(soilcms). \end{aligned} \tag{4.8}$$

b_{scat}, b_{abs}, and b_{ext} are the measured variables, while *soilcms* is estimated soil plus coarse mass scattering. *S4N3* is estimated sulfate plus nitrate scattering, and *OMS* is estimated scattering attributed to organics. A three-step regression optimizes the coefficients for a best fit to all three equations simultaneously [Judge *et al.*, 1988, 1985].

Results of the regression is presented in Table 4.6. If the estimates of efficiencies are representative, the regression coefficients should equal one except for a_{10}, the *soilcms* coefficient associated with the nephelometer scattering, which should be closer to 0.5. (The nephelometer measures about ½ of the coarse mass scattering.) The coefficients are all surprisingly near one except for a_{10}, which is closer to the expected 0.5. The regression coefficients suggest that the estimates used for calculating scattering are correct, and more importantly b_{abs}, as opposed to b_{lac}, is the more accurate measure of absorption.

Table 4.6 Results of a three-step ordinary least square (OLS) regression with various optical variables as dependent and independent variables.

Dependent Variable	Independent Variable	Estimate	Std Error	t-value	r^2
b_{ext}	b_{scat}	0.93	0.21	4.4	0.65
	b_{abs}	1.06	0.42	2.5	
	soilcms	0.65	0.15	4.3	
b_{ext}	S4N3	0.94	0.16	5.9	0.56
	OMS	1.10	0.28	3.9	
	soilcms	1.01	0.16	6.3	
	b_{abs}	0.98	0.29	3.3	
b_{scat}	S4N3	0.96	0.09	11.3	0.66
	OMS	1.14	0.21	5.3	
	soilcms	0.36	0.10	3.6	

4.5 Attribution of Extinction to Aerosol Species

4.5.1 The Attribution Equation

Two unique data sets were used to explore the relationship between optical extinction, absorption, and scattering, and various aerosol species. The MOHAVE special study provided, at one monitoring site, independent optical measurements of b_{ext}, b_{scat}, and b_{abs}, and the various aerosol species. This data set provided for a variety of ways for exploring absorption and scattering efficiencies. A second data set, IMPROVE, provides for the first time, an opportunity to explore the relationship between measured extinction (as opposed to scattering) and aerosol species over the whole western United States. These are the first data sets where extinction was directly measured as opposed to estimated by summing b_{scat} and absorption as derived from "elemental" carbon measurements.

The most surprising outcome of the analysis relates to estimates of absorption. It has been known for some time that, at remote nonurban locations, b_{abs} as derived from the LIPM, was about twice the absorption as estimated from elemental carbon derived from thermal optical reflectance techniques (b_{lac}). Although there may be alternative interpretations, the most straightforward explanation of the relationships between b_{ext}, b_{scat}, b_{abs}, and b_{lac} is that b_{abs} is a more accurate predictor of absorption than b_{lac}.

Therefore, absorption estimates will be based on b_{abs}, while scattering apportionment will be based on Equation (4.4), but with the scattering efficiency for organic mass set equal to 4 m^2/g, and f_{org}(RH) set equal to one. The equation used for reconstructing extinction then becomes:

$$
\begin{aligned}
b_{ext} &= (3) f(RH)[SULFATE] \\
&+ (3) f(RH)[NITRATE] \\
&+ (4)[OMC] \\
&+ (1)[SOIL] \\
&+ (0.6)[CM] \\
&+ b_{abs}
\end{aligned}
\qquad (4.9)
$$

4.5.2 Estimating *f*(RH) from Average Relative Humidity

One remaining issue for the apportionment of scattering to hygroscopic aerosol species is the disparity between the instantaneous effects of relative humidity on scattering and the fact that aerosol samples are gathered on a 24-hour period. Light extinction and mass budgets involve averaging samples collected over a time interval. The extinction and mass budget represents the average contribution of each aerosol species to the average extinction or mass for the time interval. When soluble aerosols dominate the mass concentration, the distribution of RH over the interval becomes an issue. Failure to consider the distribution of RH can have significant effects on the average extinction attributed to the soluble aerosol.

Mass budgets, for a particular time interval, are calculated by finding the average concentrations of the individual species of fine mass, then dividing each by the sum of the averages. If the aerosol data can be time matched with RH data, then light extinction budgets can be calculated in a parallel fashion. Specifically, a light extinction for each species and each sample can be calculated. Thus, the average light extinction due to each species over the time interval can be estimated.

If collocated and time-matched RH data are not available, but reliable estimates of the average RH over the time interval are, then a first approximation of an average light extinction for a given species can be made. One initial approach would be to apply the RH correction factor associated with the average RH to estimate the average extinction due to a soluble species. However, it can be demonstrated that for sites where the average RH is high, this approach will seriously underestimate the average extinction of a soluble aerosol when the soluble aerosol concentration is independent of RH. This is due to the convex and highly nonlinear nature of the aerosol growth curves and the subsequent functions, f_T(RH). In the case of the *f*(RH) associated with Tang's growth curve, shown in Figure 4.4, Equation (4.9) holds

$$f_T\left(\overline{RH}\right) \leq \overline{f_T(RH)}. \qquad (4.10)$$

Moreover, if the distribution of soluble species concentrations are independent of RH, then

$$\overline{f_T(RH)c} \approx \overline{f_T(RH)}\,\overline{(c)} \qquad (4.11)$$

Equality would occur as a limiting value when the sample size increases without bound.

In this report, light extinction due to a soluble species at site *s* is derived using hourly RH values less than or equal to 98% and the equation is

$$b_{ext} = \beta F_{T,s} \bar{c}, \qquad (4.12)$$

where

$$F_{T,s} = \overline{f_T(RH_s)}. \qquad (4.13)$$

Using Equation (4.9), extinction budgets for a time interval may be calculated by replacing $f_T(RH_s)$ with $F_{T,s}$ and by using the average concentration of each species over the time interval as the mass concentration.

Using the data for the collocated sites, Figure 4.14 has the plot of Tang's RH dependent factor, as defined by Equation (4.12), versus annual average RH for the 39 IMPROVE sites with RH and light extinction measurements. A polynomial curve was fitted to the annual and seasonal data as defined by,

$$F = b_0 + b_2\left(100/\left(100 - \overline{RH}\right)\right)^2 + b_3\left(100/\left(100 - \overline{RH}\right)\right)^3 + b_4\left(100/\left(100 - \overline{RH}\right)\right)^4 \qquad (4.14)$$

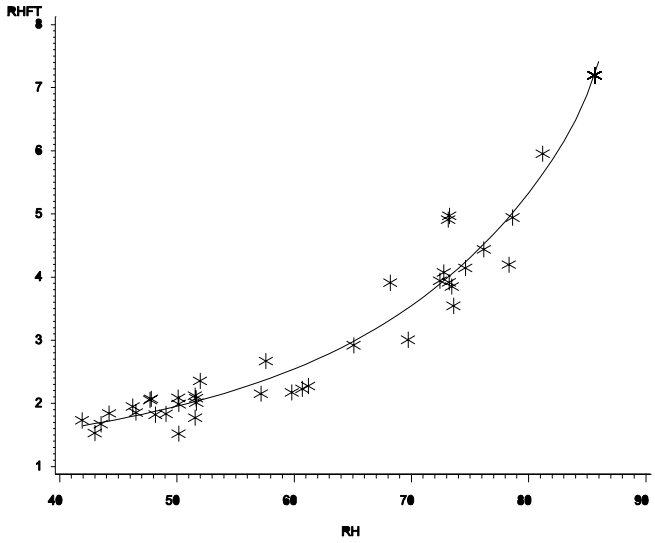

Figure 4.14Dependence on average site relative humidity of the relative humidity correction factor for sulfate ($F_{T,s}$) for the 39 IMPROVE sites with relative humidity measurements.

Table 4.7 shows the results of the regressions for Tang's weighted correction factors. The high r^2 values arise from the fact that the noise in the relationship is due primarily to differences in the RH distributions between sites. More explicitly, if two sites had the same average RH, their weighted factors would be the same if their RH distributions were identical.

Table 4.7 Parameters of the best-fit quadratic equation relating the relative humidity light extinction correction factors (F_T) to average site relative humidity ($F = b_0 + b_2(1/(1-rh))^2 + b_3(1/(1-rh))^3 + b_4(1/(1-rh))^4$).

Season	Intercept	T2	T3	T4	r^2
Spring	0.76	0.31	-0.004	-0.004	0.95
Summer	0.51	0.47	-0.081	0.004	0.95
Autumn	-0.03	0.83	-0.196	0.014	0.93
Winter	1.19	0.29	-0.033	0.001	0.87
ANNUAL	0.52	0.53	-0.095	0.006	0.94

In the IMPROVE monitoring network there are currently 55 sites operating that have fully complemented aerosol samplers (channels A-D); however, only those sites with a year or more of aerosol data are reported here. Of these sites, 39 have optical monitoring and hence RH data. Using the results of the regressions, annual and seasonal weighted factors were calculated for the additional sites by estimating their annual and seasonal average RH from weather service RH contour maps [NOAA, 1978] (Figure 4.15) or from alternate sources.

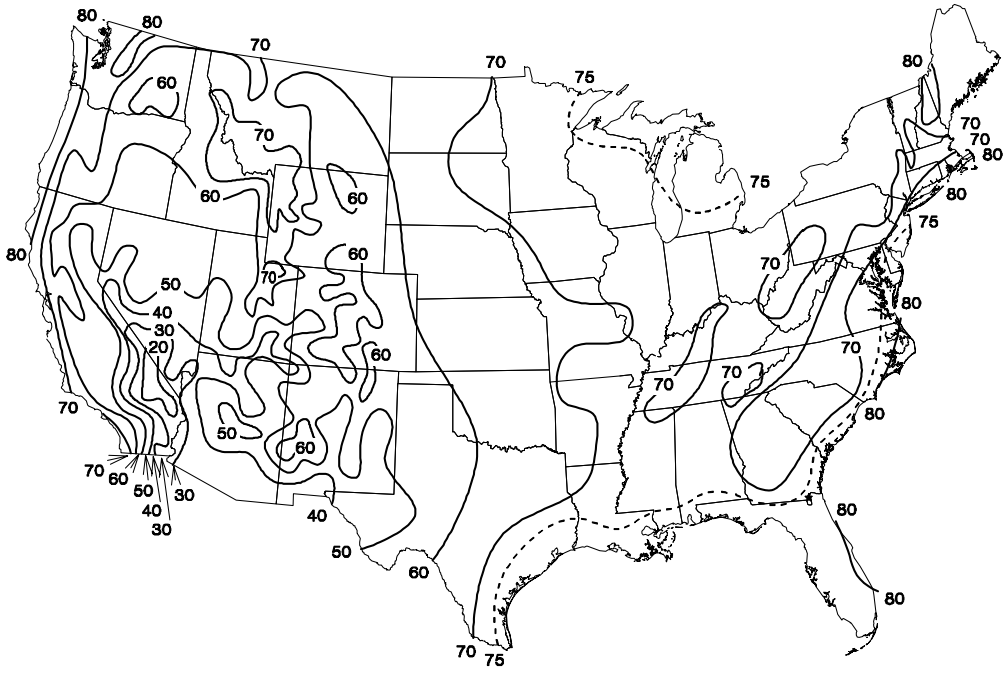

Figure 4.15 Spatial variation in annual average relative humidity [NOAA, 1978].

4.6 References

Appel, B.R., Y. Tokiwa, J. Hsu, L.E. Kothny, E. Hahn, and J.J. Wesolowski, Visibility as related to atmospheric aerosol constituents, *Atmos. Environ.*, **19**, 1525-1534, 1985.

Cass, G.R., On the relationship between sulfate air quality and visibility with examples in Los Angeles, *Atmos. Environ.*, **13**, 1069-1084, 1979.

Dietrich, D.L., J.D. Molenar, J.F. Faust, Transmissometer extinction measurements in an urban environment, In Visibility and Fine Particles, C.V. Mathai, Ed., AWMA, Pittsburgh, 1989.

Dzubay, T.G., and K.W. Clubb, Comparison of telephotometer measurements of extinction coefficients with scattering and absorption coefficients, *Atmos. Environ.*, **15**, 2617-2624, 1981.

Dzubay, T.G., R.K. Stevens, C.W. Lewis, D.H. Hern, W.J. Courtney, J.W. Tesch, and M.A. Mason, Visibility and aerosol composition in Houston, TX, *Environ. Sci. and Tech.*, **16**, 514-525, 1982.

Groblicki, P.J., G.T. Wolff, and R.J. Countess. Visibility-reducing species in the Denver "brown cloud"-I. Relationships between extinction and chemical composition, *Atmos. Environ.*, **15**, 2473-2484, 1981.

Hasan, H. and C.W. Lewis, Integrating nephelometer response corrections for bimodal size distributions, *Aerosol Sci. & Technol.*, **2**, 443-453, 1983.

Heisler, S.L., R.C. Henry, J.G. Watson, and G.M. Hidy, The 1978 Denver winter haze study volume II. ERT document #P-5417-1. Environmental Research and Technology, Inc., West Lake Village, CA, 1980a.

Heisler, S.L., R.C. Henry, and J.G. Watson, The source of the Denver haze in November and December 1978, Paper 80-58.6, presented at the 73rd Annual Meeting of the Air Pollution Control Association, Pittsburgh, PA, 1980b.

Heisler, S.L., I. Tombach, D. Fitz, J. Watson, and J. Chow, Tucson urban haze study, Final Report, Arizona Dept. Of Environmental Quality, Phoenix, AZ, Doc. #0493-005-804, 1994.

Horvath, H., Atmospheric light absorption - A review, *Atmos. Environ.*, **27**(A), 3, 293-317, 1993.

Judge, G.G., W.E. Griffiths, R.C. Hill, H. Lutkepohl, and T.C. Lee, "The theory and practice of econometrics", 2nd Edition, New York, John Wiley & Sons, 1985.

Judge, G.G., R.C. Hill, W.E. Griffiths, H. Lutkepohl, and T.C. Lee, "Introduction to the theory and practice of econometrics", 2nd Edition, New York, John Wiley & Sons, 1988.

Lewis, C.W., and T.G. Dzubay, Measurement of light absorption extinction in Denver, *Aerosol Sci.Tech.*, **5**, 325-336, 1986.

Macias, E.S., J.O. Zwicker, and W.H. White, Regional haze case studies in the southwestern United States II: source contributions, *Atmos. Environ.*, **15**, 1987-1997, 1981.

Malm, W.C., T.A. Cahill, K.A. Gebhart, and A. Waggoner, Optical characteristics of atmospheric sulfur at Grand Canyon, Arizona, In Visibility Protection, Research and Polisy Aspects, edited by P.S. Bhardwaja, pp. 418-433, 1986.

Malm, W.C., K.A. Gebhart, J.V. Molenar, T.A. Cahill, R.A. Eldred, and D. Huffman, Examining the relationship between atmospheric aerosols and light extinction at Mount Rainier and North Cascades National Parks, *Atmos. Environ.*, **28**, 347-360, 1994.

National Oceanic and Atmosperic Administration, Climatic Atlas of the United States, ESSA, Department of Commerce - 1968, Reprinted by NOAA, October, 1978.

Ouimette, J.R., and R.C. Flagan, The extinction coefficient of multicomponent aerosols, *Atmos. Environ.*, **16**, 2405-2419, 1982.

Ouimette, J.R., R.C. Flagan, and A.R. Kelso, Chemical species contributions to light scattering by aerosols at a remote arid site, In: E.S. Macias and P.K. Hopke, eds. Amer. Chem. Soc. Symposium, Series 167: Atmospheric Aerosol, 1981.

Sutherland, J.L. and P.S. Bhardwaja, Seasonal fine mass budgets through regression-application to the Glen Canyon SCENES data, In: Transactions of Visibility and Fine Particles, C.V. Mathai (ed), Air & Waste Management/EPA International Conference, Pittsburgh, PA, 207-212, 1990.

Tang, I.N., W.T. Wong, and H.R. Munkelwitz, The relative importance of atmospheric sulfates and nitrates in visibility reduction, *Atmos. Environ.*, **15**, 2463, 1981.

Tombach, I. and S.A. Thurston, The quality of the SCENES measurements: the roles of data quality goals and evolving technology, In *Proc. Aerosols and Atmospheric Optics: Radiative Balance and Visual Air Quality*, Air & Waste Management Association, Pittsburgh, PA, 1994.

Trijonis, J.C., and M. Pitchford, *Preliminary extinction budget results from the RESOLVE program*, edited by P.S. Bhardwaja, Visibility Protection Research and Policy Aspects, Air Pollution Control Association, Pittsburgh, Pa., 1987.

Trijonis, J.C. M. McGown, M. Pitchford, D. Blumenthal, P. Roberts, W. White, E. Macias, R. Weiss, A. Waggoner, J. Watson, J. Chow, and R. Flocchini, RESOLVE Project Final Report: Visibility Conditions and Causes of Visibility Degradation in the Mojave Desert of California, NWC TP #6869, Naval Weapons Center, China Lake, CA, 1988.

Trijonis, J.C., R. Charlson, R.B. Husar, W.C. Malm, M. Pitchford, and W. White, Visisbility: Existing and Historical Conditions-Causes and Effects. State of Science and State of Technology, Report No. 24. National Acid Precipitation Assessment Program, 1990.

vandeHulst, H.C., *Light scattering by small particles*, Dover Publications, New York, 1981.

Vasconcelos, L.A., E.S. Macias, and W. White, Aerosol composition as a function of haze and humidity levels in the southwestern U.S., *Atmos Environ* **28***(22)*, 3679-3691, 1994.

Watson, J.G., J.C. Chow, L.C. Pritchett, L.W. Richards, D.L. Dietrich, J. Molenar, J. Faust, S.R. Andersen, and C.S. Sloane, Comparison of three measures of extinction in Denver, CO, Paper #89-151.4, Presented at the Air Pollution Control Association Annual Meeting, 1989.

Watson, J.G., J.C. Chow, L.W. Richards, S.R. Anderson, J.E. Houck, and D.L. Dietrich, The 1987-88 metro Denver brown cloud air pollution study, Volume I: program plan. DRI document 8810.1F1, prepared for the Greater Denver Chamber of Commerce, Denver, CO, by Desert Research Institute, Reno, NV, 1988.

Watson, J.G., J.C. Chow, L.W. Richards, D.L. Haase, C. McDade, L.D. Dietrich, D. Moon, L. Chinkin, and C. Sloane, The 1989-90 Phoenix urban haze study. Volume I: program plan. DRI document 8931.1F, prepared for Arizona Department of Environmental Quality, Phoenix, AZ, by Desert Research Institute, Reno, NV, 1990a.

Watson, J.G., J.C. Chow, L.W. Richards, D.L. Haase, C. McDade, D.L. Dietrich, D. Moon, L. Chinkin, and C. Sloane, The 1989-90 pilot Tucson urban haze study. Volume I: program plan. DRI document 8931.3F, prepared for Arizona Department of Environmental Quality, Phoenix, AZ, by Desert Research Institute, Reno, NV, 1990b.

White, W.H., On the theoretical and empirical basis for apportioning extinction by aerosols: a critical review, *Atmos. Environ.*, **20**, 1659, 1986.

White, W.H., Contributions to light scattering, In: Acidic Deposition: State of Science and Technology Report 24, J. Trijonis (lead author), National Acid Precipitation Assessment Program, Washington, DC, pp85-102, 1990.

White, W.H. and P.T. Roberts, On the nature and origins of visibility-reducing aerosols in the Los Angeles air basin, *Atmos. Environ.* **11**, 803-812, 1977.

White, W.H., E.S. Macias, R.C. Ninger, and S. Schorran, Size-resolved measurement of light scattering by ambient particles in the southwestern U.S.A., *Atmos. Environ.*, **28***(50*), 909-921, 1994.

CHAPTER 5

SPATIAL DISTRIBUTIONS OF RECONSTRUCTED LIGHT EXTINCTION AND LIGHT EXTINCTION BUDGETS

In the previous chapter, a model for reconstructing light extinction was presented. In this chapter, this model is used to derive the reconstructed light extinction coefficient for the 43 sites examined here. In addition, the relative contribution of various aerosol components to total light extinction are combined into a light extinction budget.

5.1 Reconstructing Light Extinction from Aerosol Measurements

To review the discussion presented in Chapter 4, the light extinction coefficient is the sum of several components:

$$b_{ext} = b_{scat} + b_{abs} = b_{Ray} + b_{sp} + b_{ag} + b_{ap} \qquad (5.1)$$

where b_{ext} = light extinction coefficient,
b_{scat} = light scattering coefficient,
b_{abs} = light absorption coefficient,
b_{Ray} = Rayleigh light scattering coefficient,
b_{sp} = light scattering coefficient due to particles,
b_{ag} = light absorption coefficient due to gases, and
b_{ap} = light absorption coefficient due to particles.

The Rayleigh scattering coefficient (b_{Ray}) is the light scattered by molecules of gas in the natural atmosphere (i.e., oxygen and nitrogen, primarily). The Rayleigh scattering coefficient will vary with atmospheric pressure. For this report, we assume the Rayleigh scattering coefficient is 10 Mm^{-1} (inverse megameters) at all sites.

In most instances, b_{sp} and b_{ap} are primarily responsible for visibility reduction. The light absorption coefficient due to gases (b_{ag}) is dominated in the atmosphere by the effect of nitrogen dioxide (NO_2) gas. For this report, we assume this component is negligible, however, this assumption may not be correct at locations close to significant NO_x emission sources (e.g., urban areas or power plants).

The approach used here to estimate scattering assumes externally mixed aerosols. The light scattering coefficient can then be calculated (or reconstructed) from aerosol concentrations by taking Equation (5.1) and describing the light scattering contributed by aerosol component (i) as the product of the aerosol component's concentration (C_i) and its light scattering efficiency (b_i). Thus, the total light scattering coefficient is simply the sum of the light extinctions of each aerosol component:

$$b_{ext} = b_{Ray} + \sum \beta_i C_i \qquad (5.2)$$

Equation (5.2) can be cast into the following form for the aerosol components measured as part of the IMPROVE program:

$$b_{ext} = b_{Ray} + \beta_{sulfate}[SULFATE] + \beta_{NITRATE}[NITRATE] + \beta_{OC}[OCM] + \beta_{SOIL}[SOIL] + \beta_{CM}[CM] + b_{abs} \qquad (5.3)$$

where b_{ext} is the total light extinction coefficient (in Mm^{-1}), b_{Ray} is the Rayleigh scattering coefficient (10 Mm^{-1}), the $\hat{a}$'s are the light extinction coefficients for each component (in m^2/g), and the parameters in brackets ([ ]) are the concentrations of the aerosol components (in $ìg/m^3$). To complete the equation for estimating extinction the channel A determination of absorption, b_{abs}, is used.

The values of light scattering efficiency (in m^2/g) used in this report are as follows:

Sulfates and Nitrates	3 $f_T(RH)$
Organic Carbon	4
Fine Soil	1
Coarse Particles	0.6

In this report, we assume that coarse particles and fine soil particles are from a single natural source, wind-blown dust. Thus, the scattering calculated for these two components is combined into a single category and is reported as coarse scattering.

The function $f_T(RH)$ is a correction factor to account for the liquid water that may be part of the hygroscopic aerosol components. These functions are dependent on the relative humidity (RH) at the given site. In this report, light extinction, due to a soluble species at site s, is derived using hourly RH values less than or equal to 98% and the equation is

$$b_{ext,s} = \beta F_{T,s} \bar{c} \qquad (5.4)$$

where

$$F_{T,s} = \overline{f_T(RH_s)} \qquad (5.5)$$

Using Equation (5.3), extinction budgets for a time interval may be calculated by replacing $f_T(RH_s)$ with $F_{T,s}$ and by using the average concentration of each species over the same time interval as the mass concentration.

Using the data for the collocated sites, a polynomial curve was fitted to the annual and seasonal data as defined by

$$F = b_0 + b_2\left(100/\left(100-\overline{RH}\right)\right)^2 + b_3\left(100/\left(100-\overline{RH}\right)\right)^3 + b_4\left(100/\left(100-\overline{RH}\right)\right)^4 \qquad (5.6)$$

Table 5.1 shows the results of the regressions for Tang's weighted correction factors. For those sites without collocated optical and RH data the annual and seasonal factors can be calculated. In this fashion, all 43 sites are treated the same enabling the same spatial coverage used for aerosol mass concentrations.

Table 5.1 Parameters of the best-fit quadratic equation relating the relative humidity light extinction correction factors (F_T) to average site relative humidity ($F = b_o + b_2(1/(1\text{-}rh))^2 + b_3(1/(1\text{-}rh))^3 + b_4(1/(1\text{-}rh))^4$).

Season	Intercept	T2	T3	T4	r^2
Spring	0.76	0.31	-0.004	-0.004	0.95
Summer	0.51	0.47	-0.081	0.004	0.95
Autumn	-0.03	0.83	-0.196	0.014	0.93
Winter	1.19	0.29	-0.033	0.001	0.87
ANNUAL	0.52	0.53	-0.095	0.006	0.94

5.2 Reconstructed Light Extinction and Light Extinction Budgets

Spatial patterns in the reconstructed light extinction are similar to those observed for aerosols since reconstructed light extinction is calculated from aerosol concentrations. However, since light scattering efficiencies of sulfates and nitrates are larger than other fine aerosols because of associated water, and since light-absorbing carbon has a relatively high extinction efficiency, the extinction budgets are somewhat different from fine aerosol budgets.

Figure 5.1 shows isopleths of the total reconstructed light extinction coefficient (including Rayleigh) for the entire three-year period, March 1992 through February 1995. The highest light extinction (>100 Mm^{-1}) occurs in the eastern United States; the highest extinction for a rural site occurs at Sipsey Wilderness Area in northern Alabama at 157 Mm^{-1} followed by Mammoth Cave National Park at 148 Mm^{-1} then Dolly Sods Wilderness Area at 145 Mm^{-1}. The highest extinction of 183 Mm^{-1} is reported at Washington D.C., an urban site. The lowest extinction (<30 Mm^{-1}) generally occurs in the intermountain west in the Great Basin and Colorado Plateau regions. The lowest extinction for the lower 48 states is at Bridger Wilderness Area at 26 Mm^{-1}. The lowest extinction for the entire United States is at Denali National Park in Alaska with an annual extinction of 23 Mm^{-1}. Jarbidge Wilderness Area and Great Basin National Park have an annual extinction of 28 Mm^{-1} and 27 Mm^{-1}, respectively.

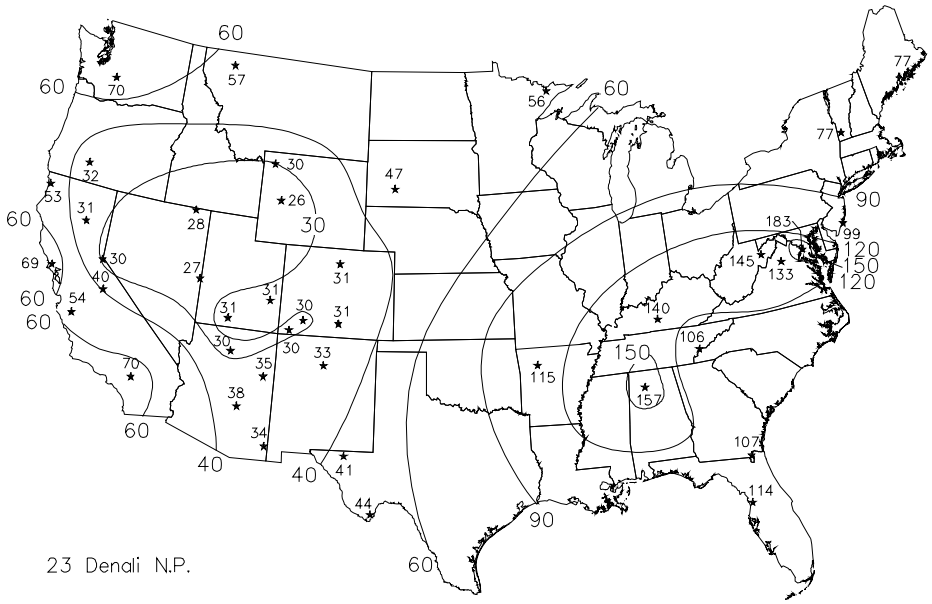

Figure 5.1 Three-year averages of total reconstructed light extinction coefficient (Mm^{-1}) for each of the reported sites in the IMPROVE network in the United States.

5.2.1 Characteristics of the Regions

Tables 5.2, 5.3, and 5.4 summarize the seasonal and annual averages of the reconstructed light extinction coefficients for each of the 21 regions in the United States, averaged over three years of the IMPROVE monitoring program, March 1992 through February 1995.

Table 5.2 shows the breakdown of extinction among fine and coarse particle scattering and light absorption. In addition, this table shows the percentage of total light extinction (including Rayleigh) that is caused by aerosol light extinction (both scattering and absorption). Also, the average relative humidity for each region is reported. Table 5.3 shows the aerosol light extinction

as well as the contributions of sulfate, nitrate, organic carbon, light absorption, and coarse particles (including fine soil). Table 5.4 shows the aerosol light extinction budgets: the fractions (percent) of total aerosol (non-Rayleigh) light extinction contributed by sulfate, nitrate, organic carbon, light absorption, and coarse particles (including fine soil).

The characteristics of each region, in alphabetic order, are briefly discussed.

Alaska. The Alaska region consists only of the measurements at Denali National Park. The three-year annual average extinction is 23.2 Mm^{-1}, of which aerosol extinction constituted 57%. The seasonal variation is small and varies from a low of 20.9 Mm^{-1} in the autumn to a high of 26 Mm^{-1} in the summer. However, the extinction attributable to nitrate and organics show significant seasonal variation. Nitrate extinction ranges from a low of 0.4 Mm^{-1} in the summer to a high of 0.8 Mm^{-1} in the winter. Organics extinction, on the other hand, is highest in the summer at 6.4 Mm^{-1} and lowest in the winter at 2.8 Mm^{-1}. Sulfate is the largest contributor to aerosol extinction at an annual average of 37% and ranges from a seasonal high in the winter of 42.8% to a summer low of 24%. The next largest contributor is organics at a seasonal average of 29% ranges from a summer high of 40.1% to a winter low of 23%. The remaining contributors on an annual basis in order of importance are absorption at 17.8%, soil and coarse particles at 12%, and nitrate at 4.3%.

Appalachian Mountains. This region consists of three sites, Dolly Sods Wilderness Area in the Monongahela National Forest, Shenandoah National Park, and Great Smoky Mountains National Park. With an annual extinction of 128 Mm^{-1} this region is typical of many eastern rural venues. The seasonal variation of extinction is about a factor of 2, ranging from 88 Mm^{-1} in the winter to 181 Mm^{-1} during summer. The seasonal variation is almost entirely due to sulfate extinction, which varies by a factor of 3 from 44 Mm^{-1} in the winter to 129 Mm^{-1} in the summer. Similarly, extinction due to organics, which averages 11.7 Mm^{-1} annually, varies from a winter low of 9.2 Mm^{-1} to 14.7 Mm^{-1} during the summer. Nitrates show a significant variation that is opposed to the variation displayed by sulfates and organics. Nitrate extinction is lowest in the summer at 3.8 Mm^{-1} and in the winter it is 12.1 Mm^{-1}. The seasonal variation of sulfates, organics, and nitrates are driven by seasonal changes in meteorology and photochemistry. For sulfates and organics this leads to higher concentrations during the summer. This coupled with the fact that RH is highest in the summer leads to high extinction efficiencies for sulfate aerosols. Nitrates, on the other hand, are quite volatile. The lower temperatures during the winter lead to higher concentrations of nitrates. Sulfate extinction comprises the largest fraction of aerosol extinction accounting for 68% annually and varies from a high during the summer of 75.7% down to 56.2% in the winter. The next highest contributor on an annual basis is absorption (12.4%), followed by organics (9.9%), nitrates (6.4%), and soil and coarse particles (3.1%).

Boundary Waters. This region, in northern Minnesota, is represented by the Boundary Waters Canoe Area in the Superior National Forest. Annual average extinction here is about 56 Mm^{-1} of which 82% is due to the ambient aerosol. The seasonal variation is slight, and ranges from a high in the winter of 61.3 Mm^{-1} to as low as 52.7 Mm^{-1} in the spring. Sulfate contributes the most to extinction at 50.9% annually and ranges between 44.1% for the winter and up to 54.8% in the spring. Annually, the next largest contributor is organics (16.4%) followed by nitrate (14.5%), absorption (13.4%), and soil and coarse particles (4.8%).

Table 5.2 Seasonal and annual averages of reconstructed total light extinction coefficient (Mm^{-1}) for the 21 regions in the IMPROVE network. Also shown are the light scattering coefficients resulting from fine and coarse aerosols, light absorptions for carbonaceous aerosol, percentage of total extinction resulting from aerosols, and the average region relative humidity.

Season	Total Extinction	Fine Scattering	Coarse Scattering	Absorption	Percent Aerosol	Relative Humidity
Alaska						
Spring	23.4	8.9	2.0	2.5	57	56
Summer	26.0	10.6	1.9	3.5	62	64
Autumn	20.9	7.9	1.3	1.7	52	72
Winter	21.2	8.3	1.1	1.7	53	68
ANNUAL	23.2	9.3	1.6	2.4	57	65
Appalachian						
Spring	107.8	79.2	3.8	14.8	91	67
Summer	180.7	147.6	4.9	18.1	94	76
Autumn	124.9	97.6	2.9	14.5	92	74
Winter	88.3	65.4	2.2	10.8	89	74
ANNUAL	128.0	100.0	3.4	14.6	92	73
Boundary Waters						
Spring	52.7	33.6	2.5	6.7	81	62
Summer	54.0	34.9	2.5	6.6	81	76
Autumn	53.3	35.7	2.0	5.5	81	79
Winter	61.3	43.7	1.8	5.9	84	77
ANNUAL	56.0	37.6	2.2	6.2	82	74
Cascade Mountains						
Spring	70.4	48.1	2.8	9.6	86	82
Summer	87.4	65.0	2.5	10.0	89	83
Autumn	69.6	47.0	2.5	10.1	86	86
Winter	45.3	27.1	1.6	6.5	78	91
ANNUAL	70.5	49.1	2.3	9.0	86	86
Central Rocky Mountains						
Spring	33.9	15.8	3.9	4.3	71	65
Summer	34.0	13.7	4.3	6.1	71	49
Autumn	29.5	12.3	2.9	4.4	66	55
Winter	22.9	8.6	1.9	2.4	56	58
ANNUAL	29.8	12.2	3.2	4.3	66	57

Table 5.2 Continued

Season	Total Extinction	Fine Scattering	Coarse Scattering	Absorption	Percent Aerosol	Relative Humidity
Colorado Plateau						
Spring	30.9	12.7	3.4	4.8	68	48
Summer	33.6	13.8	3.9	5.9	70	44
Autumn	31.6	13.5	2.8	5.3	68	48
Winter	29.3	13.5	2.0	3.8	66	61
ANNUAL	31.4	13.4	3.0	4.9	68	50
Florida						
Spring	115.3	85.5	4.7	15.2	91	70
Summer	112.1	78.8	9.1	14.1	91	75
Autumn	104.5	77.5	4.2	12.7	90	77
Winter	102.0	72.0	4.0	16.0	90	75
ANNUAL	110.6	80.5	5.5	14.6	91	74
Great Basin						
Spring	28.3	9.8	4.2	4.2	65	50
Summer	32.1	10.9	5.6	5.5	69	34
Autumn	27.9	10.3	3.4	4.2	64	49
Winter	23.7	9.3	1.8	2.7	58	64
ANNUAL	27.9	10.1	3.7	4.1	64	49
Lake Tahoe						
Spring	45.1	17.2	5.2	12.8	78	53
Summer	42.6	15.9	4.1	12.6	77	42
Autumn	52.6	21.1	3.8	17.7	81	48
Winter	62.0	25.2	6.1	20.7	84	57
ANNUAL	50.3	19.7	4.7	15.8	80	50
Mid Atlantic						
Spring	92.5	61.6	6.5	14.3	89	72
Summer	128.2	93.0	7.7	17.6	92	76
Autumn	88.5	55.8	5.6	17.1	89	68
Winter	90.2	57.0	4.6	18.6	89	66
ANNUAL	98.8	66.0	5.9	16.9	90	71
Mid South						
Spring	123.8	92.2	3.7	17.9	92	68
Summer	163.9	128.1	7.5	18.2	94	78
Autumn	126.5	97.1	3.8	15.7	92	74
Winter	127.0	98.0	3.0	16.0	92	77
ANNUAL	137.0	105.6	4.5	17.0	93	74

Table 5.2 Continued

Season	Total Extinction	Fine Scattering	Coarse Scattering	Absorption	Percent Aerosol	Relative Humidity
Northeast						
Spring	61.7	41.3	2.9	7.4	84	69
Summer	102.7	80.0	3.0	9.7	90	79
Autumn	79.7	58.9	2.6	8.2	87	79
Winter	65.8	45.0	2.6	8.2	85	74
ANNUAL	77.3	56.1	2.7	8.4	87	75
Northern Great Plains						
Spring	49.9	29.3	4.1	6.6	80	64
Summer	44.2	24.0	3.8	6.3	77	63
Autumn	41.5	21.8	3.9	5.8	76	62
Winter	52.1	34.5	2.1	5.5	81	72
ANNUAL	46.6	27.1	3.5	6.1	79	65
Northern Rocky Mountains						
Spring	48.2	26.4	3.6	8.2	79	77
Summer	49.0	25.1	5.7	8.2	80	71
Autumn	67.6	39.7	4.9	13.1	85	80
Winter	67.0	46.1	1.9	8.9	85	86
ANNUAL	57.2	33.6	4.0	9.6	83	79
Pacific Coast						
Spring	55.4	33.6	5.9	5.8	82	73
Summer	55.5	34.5	5.6	5.4	82	72
Autumn	62.8	39.3	5.3	8.2	84	71
Winter	56.5	36.4	3.7	6.5	82	75
ANNUAL	58.4	36.8	5.2	6.4	83	73
Sierra-Humboldt						
Spring	32.9	15.3	2.9	4.6	70	67
Summer	37.6	18.1	3.0	6.4	73	71
Autumn	31.0	13.5	2.3	5.2	68	55
Winter	24.2	9.6	1.2	3.5	59	66
ANNUAL	31.6	14.2	2.4	5.0	68	65
Sierra Nevada						
Spring	44.8	23.8	3.9	7.0	78	63
Summer	48.9	23.9	4.4	10.6	80	44
Autumn	39.7	18.6	3.6	7.4	75	45
Winter	23.7	9.6	2.1	2.1	58	56
ANNUAL	40.0	19.8	3.5	6.7	75	52

Table 5.2 Continued

Season	Total Extinction	Fine Scattering	Coarse Scattering	Absorption	Percent Aerosol	Relative Humidity
Sonoran Desert						
Spring	35.9	14.0	5.0	6.9	72	37
Summer	39.8	17.6	4.9	7.2	75	43
Autumn	35.5	15.7	3.4	6.4	72	45
Winter	32.5	14.9	2.7	4.9	69	56
ANNUAL	36.2	15.8	4.0	6.4	72	45
Southern California						
Spring	102.3	73.6	6.2	12.5	90	55
Summer	80.3	47.9	7.4	15.0	88	45
Autumn	54.6	27.5	8.2	8.9	82	41
Winter	35.6	19.8	1.9	3.9	72	51
ANNUAL	69.7	43.8	5.8	10.2	86	48
Washington D.C.						
Spring	155.1	102.8	5.5	36.8	94	62
Summer	216.6	160.7	5.4	40.4	95	68
Autumn	188.8	131.6	5.3	41.8	95	68
Winter	161.1	101.9	5.5	43.7	94	62
ANNUAL	182.5	126.5	5.4	40.6	95	65
West Texas						
Spring	41.0	18.1	5.6	7.3	76	41
Summer	51.2	26.3	6.7	8.2	80	54
Autumn	39.7	19.2	4.8	5.7	75	53
Winter	37.1	18.3	3.7	5.1	73	53
ANNUAL	42.3	20.5	5.2	6.6	76	50

Table 5.3 Seasonal and annual averages of reconstructed aerosol light extinction coefficient (Mm^{-1}) for the 21 regions in the IMPROVE network. Also shown are the light extinction coefficients (Mm^{-1}) resulting from sulfate, nitrate, organic carbon, light absorption, and coarse particles/fine soil.

Season	Aerosol Extinction	Sulfate	Nitrate	Organics	Absorption	Soil and Coarse
Alaska						
Spring	13.4	5.3	0.5	3.1	2.5	2.0
Summer	16.0	3.8	0.4	6.4	3.5	1.9
Autumn	10.9	4.5	0.5	2.9	1.7	1.3
Winter	11.2	4.8	0.8	2.8	1.7	1.1
ANNUAL	13.2	4.9	0.6	3.8	2.4	1.6
Appalachian						
Spring	97.8	60.6	7.9	10.7	14.8	3.8
Summer	170.7	129.1	3.8	14.7	18.1	4.9
Autumn	114.9	78.5	6.9	12.1	14.5	2.9
Winter	78.3	44.0	12.1	9.2	10.8	2.2
ANNUAL	118.0	80.7	7.6	11.7	14.6	3.4
Boundary Waters						
Spring	42.7	23.4	4.1	6.1	6.7	2.5
Summer	44.0	22.5	1.4	11.1	6.6	2.5
Autumn	43.3	22.7	6.4	6.7	5.5	2.0
Winter	51.3	22.6	15.1	5.9	5.9	1.8
ANNUAL	46.0	23.4	6.7	7.5	6.2	2.2
Cascade Mountains						
Spring	60.4	30.3	5.9	11.9	9.6	2.8
Summer	77.4	46.7	6.8	11.5	10.0	2.5
Autumn	59.6	29.9	4.5	12.6	10.1	2.5
Winter	35.3	14.4	3.6	9.2	6.5	1.6
ANNUAL	60.5	32.4	5.4	11.3	9.0	2.3
Central Rocky Mountains						
Spring	23.9	9.1	2.2	4.4	4.3	3.9
Summer	24.0	5.4	0.9	7.4	6.1	4.3
Autumn	19.5	5.6	1.1	5.6	4.4	2.9
Winter	12.9	3.6	1.0	4.0	2.4	1.9
ANNUAL	19.8	5.6	1.2	5.4	4.3	3.2

Table 5.3 Continued

Season	Aerosol Extinction	Sulfate	Nitrate	Organics	Absorption	Soil and Coarse
Colorado Plateau						
Spring	20.9	6.5	1.4	4.7	4.8	3.4
Summer	23.6	6.9	1.0	5.9	5.9	3.9
Autumn	21.6	6.6	1.0	5.9	5.3	2.8
Winter	19.3	7.1	2.0	4.4	3.8	2.0
ANNUAL	21.4	6.9	1.3	5.2	4.9	3.0
Florida						
Spring	105.3	65.5	6.7	13.3	15.2	4.7
Summer	102.1	61.2	5.8	11.8	14.1	9.1
Autumn	94.5	60.1	5.8	11.6	12.7	4.2
Winter	92.0	50.3	8.3	13.4	16.0	4.0
ANNUAL	100.6	61.1	6.8	12.5	14.6	5.5
Great Basin						
Spring	18.3	4.0	1.0	4.8	4.2	4.2
Summer	22.1	3.4	0.6	7.0	5.5	5.6
Autumn	17.9	3.7	0.7	5.9	4.2	3.4
Winter	13.7	3.5	1.4	4.4	2.7	1.8
ANNUAL	17.9	3.7	0.9	5.5	4.1	3.7
Lake Tahoe						
Spring	35.1	4.5	2.1	10.5	12.8	5.2
Summer	32.6	4.3	1.2	10.4	12.6	4.1
Autumn	42.6	3.7	1.9	15.5	17.7	3.8
Winter	52.0	2.3	2.9	20.0	20.7	6.1
ANNUAL	40.3	3.9	2.0	13.9	15.8	4.7
Mid Atlantic						
Spring	82.5	42.9	9.2	9.5	14.3	6.5
Summer	118.2	72.5	6.5	13.9	17.6	7.7
Autumn	78.5	36.2	7.3	12.3	17.1	5.6
Winter	80.2	29.4	14.4	13.2	18.6	4.6
ANNUAL	88.8	44.1	9.7	12.2	16.9	5.9
Mid South						
Spring	113.8	66.7	12.6	13.0	17.9	3.7
Summer	153.9	107.1	5.6	15.5	18.2	7.5
Autumn	116.5	74.2	8.5	14.4	15.7	3.8
Winter	117.0	60.8	24.7	12.5	16.0	3.0

ANNUAL	127.0	78.8	12.9	13.8	17.0	4.5

Table 5.3 Continued

Season	Aerosol Extinction	Sulfate	Nitrate	Organics	Absorption	Soil and Coarse
Northeast						
Spring	51.7	30.4	4.4	6.5	7.4	2.9
Summer	92.7	65.6	4.1	10.3	9.7	3.0
Autumn	69.7	45.2	6.5	7.1	8.2	2.6
Winter	55.8	29.5	8.1	7.5	8.2	2.6
ANNUAL	67.3	42.4	5.8	7.9	8.4	2.7
Northern Great Plains						
Spring	39.9	18.2	5.7	5.4	6.6	4.1
Summer	34.2	14.5	1.3	8.2	6.3	3.8
Autumn	31.5	11.1	4.0	6.7	5.8	3.9
Winter	42.1	17.5	11.8	5.2	5.5	2.1
ANNUAL	36.6	15.3	5.4	6.4	6.1	3.5
Northern Rocky Mountains						
Spring	38.2	13.3	2.8	10.3	8.2	3.6
Summer	39.0	11.4	1.5	12.2	8.2	5.7
Autumn	57.6	16.0	4.9	18.8	13.1	4.9
Winter	57.0	21.9	12.7	11.5	8.9	1.9
ANNUAL	47.2	15.5	4.8	13.2	9.6	4.0
Pacific Coast						
Spring	45.4	18.6	8.9	6.1	5.8	5.9
Summer	45.5	21.8	7.0	5.7	5.4	5.6
Autumn	52.8	19.0	10.3	10.0	8.2	5.3
Winter	46.5	10.4	18.4	7.6	6.5	3.7
ANNUAL	48.4	18.1	11.4	7.3	6.4	5.2
Sierra-Humboldt						
Spring	22.9	7.1	2.7	5.5	4.6	2.9
Summer	27.6	8.0	1.7	8.4	6.4	3.0
Autumn	21.0	4.7	1.6	7.1	5.2	2.3
Winter	14.2	3.6	1.8	4.1	3.5	1.2
ANNUAL	21.6	5.9	1.9	6.4	5.0	2.4
Sierra Nevada						
Spring	34.8	10.7	5.6	7.6	7.0	3.9
Summer	38.9	7.1	2.1	14.7	10.6	4.4
Autumn	29.7	5.9	2.8	10.0	7.4	3.6

Winter	13.7	3.3	2.0	4.3	2.1	2.1
ANNUAL	30.0	7.5	3.2	9.0	6.7	3.5

Table 5.3 Continued

Season	Aerosol Extinction	Sulfate	Nitrate	Organics	Absorption	Soil and Coarse
Sonoran Desert						
Spring	25.9	6.5	1.4	6.0	6.9	5.0
Summer	29.8	9.7	1.1	6.8	7.2	4.9
Autumn	25.5	8.0	0.9	6.8	6.4	3.4
Winter	22.5	7.8	1.8	5.4	4.9	2.7
ANNUAL	26.2	8.3	1.3	6.2	6.4	4.0
Southern California						
Spring	92.3	13.7	47.2	12.6	12.5	6.2
Summer	70.3	11.5	20.3	16.1	15.0	7.4
Autumn	44.6	6.4	12.5	8.6	8.9	8.2
Winter	25.6	4.6	10.8	4.5	3.9	1.9
ANNUAL	59.7	9.8	23.5	10.5	10.2	5.8
Washington D.C.						
Spring	145.1	64.8	21.0	17.0	36.8	5.5
Summer	206.6	128.4	11.9	20.4	40.4	5.4
Autumn	178.8	84.7	25.3	21.6	41.8	5.3
Winter	151.1	46.8	31.5	23.6	43.7	5.5
ANNUAL	172.5	83.0	22.9	20.6	40.6	5.4
West Texas						
Spring	31.0	10.3	1.1	6.6	7.3	5.6
Summer	41.2	17.2	1.9	7.2	8.2	6.7
Autumn	29.7	12.2	1.2	5.8	5.7	4.8
Winter	27.1	11.1	2.0	5.2	5.1	3.7
ANNUAL	32.3	12.8	1.5	6.2	6.6	5.2

Table 5.4 Seasonal and annual averages of percentage contributions to the reconstructed aerosol light extinction coefficient (light extinction budget) for the 21 regions in the IMPROVE network for sulfate, nitrate, organic carbon, absorption, and coarse particle/fine soil.

Season	Sulfate	Nitrate	Organics	Absorption	Soil and Coarse
Alaska					
Spring	39.5	3.8	23.2	18.9	14.7
Summer	24.0	2.2	40.1	21.6	12.1
Autumn	41.3	4.8	26.6	15.5	11.8
Winter	42.8	7.0	24.8	15.4	9.9
ANNUAL	37.0	4.3	29.0	17.8	12.0
Appalachian					
Spring	62.0	8.1	10.9	15.2	3.9
Summer	75.7	2.2	8.6	10.6	2.9
Autumn	68.3	6.0	10.5	12.6	2.5
Winter	56.2	15.5	11.8	13.8	2.8
ANNUAL	68.4	6.4	9.9	12.4	2.9
Boundary Waters					
Spring	54.8	9.6	14.2	15.6	5.7
Summer	51.1	3.1	25.2	14.9	5.7
Autumn	52.5	14.7	15.4	12.8	4.7
Winter	44.1	29.4	11.6	11.4	3.5
ANNUAL	50.9	14.5	16.4	13.4	4.8
Cascade Mountains					
Spring	50.2	9.7	19.6	15.8	4.6
Summer	60.3	8.8	14.8	12.9	3.2
Autumn	50.1	7.6	21.2	16.9	4.2
Winter	40.7	10.1	26.1	18.5	4.5
ANNUAL	53.5	9.0	18.7	14.9	3.9
Central Rocky Mountains					
Spring	38.1	9.2	18.6	17.9	16.3
Summer	22.3	3.9	30.7	25.2	17.8
Autumn	28.7	5.7	28.6	22.4	14.7
Winter	28.2	8.0	30.8	18.5	14.5
ANNUAL	28.6	6.3	27.1	21.7	16.4

Table 5.4 Continued

Season	Sulfate	Nitrate	Organics	Absorption	Soil and Coarse
Colorado Plateau					
Spring	31.2	6.8	22.4	23.1	16.4
Summer	29.3	4.1	24.9	25.1	16.5
Autumn	30.3	4.8	27.2	24.5	13.2
Winter	37.0	10.1	22.8	19.7	10.3
ANNUAL	32.3	6.1	24.3	23.1	14.2
Florida					
Spring	62.2	6.3	12.6	14.4	4.4
Summer	60.0	5.7	11.6	13.9	8.9
Autumn	63.6	6.1	12.3	13.5	4.5
Winter	54.6	9.0	14.5	17.4	4.4
ANNUAL	60.8	6.8	12.5	14.5	5.5
Great Basin					
Spring	21.9	5.5	26.3	23.2	23.0
Summer	15.2	2.8	31.5	25.1	25.4
Autumn	20.5	3.9	33.1	23.4	19.1
Winter	25.6	9.9	32.1	19.6	12.7
ANNUAL	20.7	4.9	30.7	23.0	20.8
Lake Tahoe					
Spring	12.9	6.0	30.0	36.4	14.7
Summer	13.1	3.7	32.0	38.6	12.5
Autumn	8.6	4.4	36.5	41.6	8.8
Winter	4.5	5.6	38.4	39.9	11.7
ANNUAL	9.7	4.9	34.5	39.2	11.8
Mid Atlantic					
Spring	52.1	11.1	11.6	17.4	7.9
Summer	61.4	5.5	11.8	14.8	6.5
Autumn	46.2	9.3	15.6	21.8	7.1
Winter	36.7	17.9	16.5	23.2	5.8
ANNUAL	49.7	10.9	13.8	19.0	6.7
Mid South					
Spring	58.6	11.0	11.4	15.7	3.3
Summer	69.6	3.6	10.0	11.8	4.9
Autumn	63.6	7.3	12.3	13.5	3.2

ANNUAL	62.0	10.2	10.9	13.4	3.5

Table 5.4 Continued

Season	Sulfate	Nitrate	Organics	Absorption	Soil/Coarse
Northeast					
Spring	58.9	8.5	12.6	14.3	5.7
Summer	70.7	4.4	11.1	10.5	3.3
Autumn	64.9	9.4	10.2	11.8	3.7
Winter	52.8	14.5	13.4	14.7	4.6
ANNUAL	63.1	8.7	11.7	12.5	4.1
Northern Great Plains					
Spring	45.6	14.3	13.5	16.5	10.2
Summer	42.5	3.9	23.9	18.5	11.2
Autumn	35.4	12.6	21.2	18.6	12.3
Winter	41.6	28.0	12.3	13.0	5.1
ANNUAL	41.7	14.9	17.4	16.6	9.5
Northern Rocky Mountains					
Spring	34.8	7.3	27.0	21.4	9.4
Summer	29.3	3.9	31.2	21.0	14.6
Autumn	27.7	8.5	32.6	22.7	8.4
Winter	38.4	22.3	20.2	15.7	3.4
ANNUAL	32.9	10.3	28.0	20.3	8.6
Pacific Coast					
Spring	41.0	19.7	13.4	12.9	13.1
Summer	47.9	15.4	12.5	11.8	12.3
Autumn	36.0	19.5	19.0	15.5	10.0
Winter	22.4	39.4	16.3	13.9	8.0
ANNUAL	37.3	23.6	15.1	13.3	10.7
Sierra-Humboldt					
Spring	31.2	11.7	24.1	20.3	12.8
Summer	29.1	6.2	30.5	23.4	10.9
Autumn	22.6	7.8	33.8	25.0	10.7
Winter	25.5	12.7	28.9	24.4	8.4
ANNUAL	27.3	9.0	29.4	23.2	11.1
Sierra Nevada					
Spring	30.7	16.0	21.7	20.2	11.3
Summer	18.2	5.4	37.9	27.3	11.3
Autumn	19.7	9.3	33.8	25.1	12.1

Winter	24.1	14.2	31.2	15.1	15.4
ANNUAL	25.0	10.8	30.1	22.4	11.7

Table 5.4 Continued

Season	Sulfate	Nitrate	Organics	Absorption	Soil and Coarse
Sonoran Desert					
Spring	25.2	5.5	23.2	26.7	19.4
Summer	32.7	3.6	22.8	24.3	16.6
Autumn	31.3	3.6	26.5	25.2	13.4
Winter	34.8	7.8	23.8	21.7	11.9
ANNUAL	31.5	5.0	23.8	24.3	15.4
Southern California					
Spring	14.9	51.2	13.7	13.5	6.8
Summer	16.3	28.9	22.9	21.3	10.6
Autumn	14.4	27.9	19.3	20.0	18.4
Winter	17.8	42.1	17.4	15.3	7.4
ANNUAL	16.4	39.3	17.6	17.1	9.7
Washington D.C.					
Spring	44.7	14.5	11.7	25.4	3.8
Summer	62.2	5.8	9.9	19.6	2.6
Autumn	47.4	14.2	12.1	23.4	3.0
Winter	31.0	20.8	15.7	28.9	3.6
ANNUAL	48.1	13.3	11.9	23.6	3.1
West Texas					
Spring	33.3	3.6	21.5	23.5	18.2
Summer	41.7	4.7	17.4	19.9	16.3
Autumn	41.3	4.0	19.4	19.1	16.2
Winter	41.0	7.3	19.2	18.9	13.6
ANNUAL	39.6	4.7	19.2	20.3	16.2

Cascade Mountains. This region is represented by two sites, Mount Rainier National Park southeast of Seattle, and Columbia River Gorge on the Hood River National Forest. The site at Columbia River Gorge has operated for one year out of the last six and only Mount Rainier is reported here. The average annual extinction for this region is 70.5 Mm^{-1}, of which 86% is due to aerosols. The seasonality is significant and ranges from a high in the summer of 87.4 Mm^{-1} then drops to a low in the spring of 45.3 Mm^{-1}. The seasonality is driven primarily by sulfate. Sulfate extinction ranges from a summer high of 46.7 Mm^{-1} then drops to 14.4 Mm^{-1} in the summer. Organics show very little variance between seasons and has an annual average value of 11.3 Mm^{-1}. The largest contributor to aerosol extinction is sulfate (53.5%), followed by organics (18.7%), and absorption (14.9%). Nitrates account for 9% of aerosol extinction and coarse extinction accounts for 3.9%.

Central Rocky Mountains. The measurements in this region are made at five locations in the mountainous Class I areas of Colorado and Wyoming, including the Bridger and Weminuche Wilderness Areas, Rocky Mountain and Yellowstone National Parks, and Great Sand Dunes National Monument. All five sites have been operated for six years and show an annual average total extinction for the three-year period of 29.8 Mm^{-1}, of which 66% is due to aerosol extinction. The seasonal variation is significant and has a maximum in the summer of 34 Mm^{-1} and decreases to 22.9 Mm^{-1} during the winter. The seasonal variance is driven primarily by organic extinction and absorption. Organic extinction peaks at 7.4 Mm^{-1} in the summer and drops in the winter to 4 Mm^{-1}, absorption ranges for 6.1 Mm^{-1} in the summer and drops to 2.4 Mm^{-1} in the winter. Sulfates (28.6%) contribute the most to extinction annually followed by organics (27.1%), absorption (21.7%), coarse mass (16.4%), and nitrate is the smallest contributor (6.4%). During the summer sulfate is the third largest contributor at 22.8% with organics contributing the most at 30.7% followed by absorption at 25.2%.

Coastal Mountains. This region includes three Class I areas along and near the coast of northern California: Pinnacles National Monument, Point Reyes National Seashore, and Redwoods National Park. The average annual extinction during the three-year period for this area is 58.4 Mm^{-1} with 83% due to aerosol extinction. The annual variance is very slight and only ranges between 55.4 Mm^{-1} during the spring and 62.8 Mm^{-1} in the autumn. However, extinction due to sulfate and nitrate show large seasonal variances that are opposed to each other. Sulfate extinction obtains its maximum in the summer at 21.8 Mm^{-1} when nitrate extinction is at its minimum of 7 Mm^{-1}. When nitrate extinction obtains its maximum of 18.4 Mm^{-1} during the winter sulfate extinction is at its minimum of 10.4 Mm^{-1}. Organic extinction and absorption obtain their maxima in the autumn of 10 Mm^{-1} and 8.2 Mm^{-1}, respectively. On an annual basis, the largest contributor to aerosol extinction is sulfate (37.3%), followed by nitrate (23.6%), organics (15.1%), absorption (13.3%), and coarse particles (10.7%). The contribution from sulfate shows considerable variation ranging from a high in the summer of 47.9% to 22.4% in the winter when its contribution is eclipsed by nitrate, which contributes 39.4%.

Colorado Plateau. This region in the Four Corners' states of the Southwest is the most intensively monitored in the IMPROVE network. There are six sites, most of them within the so-called Golden Circle of national parks: Bandelier, Bryce Canyon, Canyonlands, Grand Canyon, Mesa Verde, and Petrified Forest National Parks. The three-year annual average for total extinction

is relatively low at 31.4 Mm^{-1}, 68% of which is aerosol extinction. There is a very slight variance between seasons of total extinction ranging from 29.3 Mm^{-1} in the winter to as high as 33.6 Mm^{-1} during the winter. The peaking of extinction in the winter is unlike most other regions. Here sulfate extinction obtains its maximum of 7.1 Mm^{-1} and is lowest in the spring at 6.5 Mm^{-1}, and is at its next lowest in the autumn at 6.6 Mm^{-1}. However, the seasonality of nitrate extinction is typically high during the winter at 2.0 Mm^{-1} and lowest during the summer at 1.0 Mm^{-1}. The largest contribution to annual aerosol extinction is sulfate (32.3%) followed by organics (24.3%), absorption (23.1%), coarse particles (14.2%), and nitrate (6.1%). However, during the summer, extinction contributions from sulfate (29.3%), organics (24.9%), and absorption (25.1%) are about on par with each other.

Florida. This region now consists of two sites, Chassahowitzka National Wildlife Refuge north of Tampa and Okefenokee National Wildlife Refuge on the Georgia-Florida border. Previously, this site was represented by Everglades National Park, which has been downgraded to a channel A only monitoring site. The annual total extinction for this region is 111 Mm^{-1}, 91% is due to aerosol extinction. Very little seasonal variance exists here, with spring having the most extinction of 115 Mm^{-1} and winter the least at 102 Mm^{-1}. The largest contributor to aerosol extinction is from sulfates (60.8%) followed by absorption (14.5%), organics (12.5%), nitrate (6.8%), and coarse particles (5.5%).

Great Basin. The Great Basin of Nevada is represented by two sites. The site at Jarbidge Wilderness Area in northeastern Nevada was implemented in March of 1988, and the other site at Great Basin National Park began operating in May of 1992. The annual average extinction during the three-year period for this region is quite low at 27.9 Mm^{-1}, with 64% from aerosol extinction, the only region with less extinction is Alaska. A slight seasonal variation exists between 32.1 Mm^{-1} during the summer and 23.7 Mm^{-1} during the winter. On an annual basis the largest contributor to extinction is organics (30.7%) followed by absorption (23%), soil and coarse particles (20.8%), and sulfate (20.7%). This region is unique in that sulfate is the fourth largest contributor to extinction. This holds for two out of the four seasons (spring and summer). During the other seasons, sulfate extinction is larger than extinction from soil and coarse making sulfate the third largest contributor.

Lake Tahoe. Two sites represent the Lake Tahoe region: one is located in Bliss State Park, the other is close to the south end of the lake. The average extinction for this area is 50.3 Mm^{-1} with a modest seasonality with winter being the maximum season at 62 Mm^{-1}, and summer being the clearest at 42.6 Mm^{-1}. The seasonality is driven by organics and absorption, whose winter values of 20.6 Mm^{-1} and 20.7 Mm^{-1}, respectively, are about twice their summer levels. The dominant contributors to aerosol extinction are absorption (39.2%) and organics (34.5%), followed by soil and coarse particles (11.8%), sulfate (9.7%), and nitrate (4.9%).

Mid Atlantic. This region, represented by the Edmond B. Forsythe Wildlife Refuge, just west of Atlantic City, New Jersey, has an average annual reconstructed extinction of 98.8 Mm^{-1}. There is a significant seasonality, with extinction moving from a high during the summer of 128 Mm^{-1}, to 88.5 Mm^{-1} in the autumn. Sulfates move between 72.5 Mm^{-1} in the summer and decreases to 29.4 Mm^{-1} during winter and are responsible for the seasonality. Nitrate has an average winter value of 14.4 Mm^{-1}, about twice of all other seasons. Sulfates contribute about half (47.5%) of the aerosol

extinction, followed by absorption (19.0%), organics (13.8%), nitrate (10.9%), and soil and coarse particles the least (6.7%).

Mid South. Three sites represent this region: Sipsey Wilderness Area in northern Mississippi, Upper Buffalo Wilderness Area in northern Arkansas, and Mammoth Cave National Park in Kentucky. This region has the highest levels of reconstructed extinction for a rural area. The only exception is Washington, D.C., which is an urban area. The average annual reconstructed extinction is 137 Mm^{-1} with a significant seasonal variation of 164 Mm^{-1} between the summer high and the spring low of 124 Mm^{-1}. Sulfate dominates the aerosol extinction and is responsible for much of the seasonality observed. Sulfate extinction is highest in the summer at 107 Mm^{-1} and lowest in the spring at 60.8 Mm^{-1}. Organics, and elemental carbon all have seasonal trends that peak in the summer but are lowest in the winter for organics and autumn for absorption. On an annual average, sulfate contributes 62% of the aerosol extinction peaking in the summer (69.6%) and is least in the winter (52%). The next largest contributor annually is absorption (13.4%) followed by organics (10.9%), and nitrate (10.2%).

Northeast. The northeastern United States is represented by measurements at two sites: Acadia National Park on the coast of Maine, which began operating in March of 1988; and, Lye Brook Wilderness Area in Vermont, which began operations in September of 1991. The average annual extinction during the three-year period for the Northeast is 77.3 Mm^{-1} of which aerosol extinction accounts for 87%. There is a significant seasonal variation of 61.7 Mm^{-1} with the spring being the least and the highest occurs during the summer at 102.7 Mm^{-1}. Sulfates and organics are responsible for most of the seasonal variation with sulfates varying from 29.5 Mm^{-1} to 65.6 Mm^{-1} between winter and summer, and similarly organics vary between 6.5 Mm^{-1} in the spring to 10 Mm^{-1} in the summer. Nitrate extinction obtains its maximum during the winter at 8.1 Mm^{-1} and its minimum at 4.1 Mm^{-1} during the summer. The largest contributor to extinction is from sulfates at 63.1% annually. The next highest contributor is absorption (12.5%), followed by organics (11.7%), nitrate (8.7%), and soil and coarse particles (4.1%).

Northern Great Plains. Only one set of aerosol measurements was made in this region, at Badlands National Monument in South Dakota, where reconstructed light extinction averaged 46.6 Mm^{-1}. Unlike most other regions extinction was highest in spring and lowest in autumn. This seasonality is driven primarily by sulfate and nitrate extinction. Sulfate extinction obtains a maximum of 18.2 Mm^{-1} in the spring and has its seasonal minimum of 11.1 Mm^{-1} in the autumn. Nitrate extinction in the spring, at 5.7 Mm^{-1}, is more than four times its summer extinction of 1.3 Mm^{-1}. The maximum nitrate extinction of 11.8 Mm^{-1} occurs in the winter. The main contributor to annual extinction is sulfate, which accounts for 41.7% of the extinction. The next highest contributor is absorption at 16.6% followed by organics at 17.4%, nitrate (14.9%), and coarse mass (9.5%).

Northern Rocky Mountains. This region is represented by one site at Glacier National Park close to the Canada border. Here, the reconstructed light extinction coefficient is 57.2 Mm^{-1} for an annual average of 83% due to aerosols. There is a modest seasonality ranging between 67.6 Mm^{-1} in the autumn down to 48.2 Mm^{-1} during the spring. The seasonality is driven by sulfate and nitrate extinction. Sulfate and nitrate extinctions peak during the winter at 22.9 Mm^{-1} and 12.7 Mm^{-1},

respectively. The largest contributor to aerosol extinction is sulfate (32.9%) followed by organics (28%), and absorption (20.3%).

Sierra-Humboldt. The region further north in the Sierra Nevada and Humboldt Mountain Ranges was measured at Crater Lake National Park in Oregon and Lassen Volcanoes National Park in northern California. For this region, total reconstructed light extinction averaged 31.6 Mm^{-1} with maximum extinction in summer (37.6 Mm^{-1}) and minimum extinction in winter (23.2 Mm^{-1}). The seasonality is primarily variations from sulfate and organic extinctions and absorption. Organic carbon, sulfate, and elemental carbon contribute almost equally to annual extinction at 29.4%, 27.3%, and 23.2%, respectively.

Sierra Nevada. The aerosol in the Sierra Nevada region is monitored at two sites: Yosemite National Park has been monitored since March 1988, monitoring at Sequoia-Kings Canyon began in March of 1992. The average reconstructed light extinction is 40 Mm^{-1} with a strong seasonal component that has a winter minimum of 23.7 Mm^{-1} and a summer maximum of 48.9 Mm^{-1}. The seasonality is driven primarily by organics and absorption with both species peaking during the summer at 14.7 Mm^{-1} and 10.3 Mm^{-1}, then dropping to 4.3 Mm^{-1} and 2.1 Mm^{-1} their minimum during the winter. Sulfate, to a lesser extent, is responsible for the seasonality, while its maximum occurs in the spring at 10 Mm^{-1}. Its summer extinction drops off to 7.1 Mm^{-1} and obtains its seasonal low in the winter of 3.3 Mm^{-1}.

Sonoran Desert. This region in southeastern Arizona was measured at two sites: Chiracahua and Tonto National Monuments. The three-year average reconstructed extinction is 36.2 Mm^{-1} and varies from a summer high of 39.8 Mm^{-1} to a winter low of 32.5 Mm^{-1}. The seasonality is due to changes in extinction from sulfate, organics, and absorption. Sulfate and absorption obtain their seasonal maxima of 9.7 Mm^{-1} and 7.2 Mm^{-1} during the summer. The largest contributor to extinction is sulfate (31.5%) followed by absorption (24.3%), and organics (23.8%).

Southern California. Measurements in this region were made in San Gorgonio National Monument, east of the Los Angeles metropolitan area. Total reconstructed light extinction averaged over the three-year period was 69.7 Mm^{-1} and varied from a seasonal high of 102 Mm^{-1} in the spring to as little as 35.6 Mm^{-1} in the winter. The seasonality is driven primarily by nitrates and to a lesser extent sulfate, organics, and absorption, all of which obtain their maximum in the spring and their minimum in the winter. This region is unique in that nitrates are by far the largest contributor to annual extinction (39.3%) followed by absorption (17.1%), and organics (17.6%), sulfate (16.4%), and soil and coarse particles (9.7%).

Washington D.C. The highest light extinction coefficient, reconstructed from aerosol concentration, was found in Washington. It averaged 182 Mm^{-1} over the three-year period. Extinction was highest in the summer (216 Mm^{-1}) and lowest in the spring (155 Mm^{-1}). Most of the seasonality is due to sulfate. In the summer, sulfate extinction averaged 128 Mm^{-1}, much higher than other seasons. Except for nitrate, the other species were fairly constant between seasons. Sulfate is the dominate contributor to light extinction, contributing nearly half (48.1%), followed by absorption (23.6%), nitrate (13.3%), organics (11.5%), and soil and coarse particles (3.1%).

West Texas. Total light extinction reconstructed from the aerosol measurements at Big Bend and Guadalupe Mountains National Parks averaged 42.3% over the three-year period. A modest seasonality is evident with the highest extinction in the summer (51.2 Mm^{-1}) and the least during the winter (37.1 Mm^{-1}). The seasonality is primarily due to sulfate, which is the largest contributor to aerosol extinction (39.6%) followed distantly by absorption (20.3%), organics (19.2%), soil and coarse particles (16.2%), and nitrate (4.7%).

5.2.2 Spatial Trends in Reconstructed Light Extinction in the United States

Figure 5.2 shows the sulfate light extinction coefficient averaged over the three-year period of IMPROVE (March 1992 - February 1995). Note that the highest sulfate extinction occurs in the eastern United States, and the lowest sulfate extinction occurs in Oregon, Nevada, Idaho, and Wyoming. The major gradient in sulfate light extinction is from the eastern United States to the nonurban West. However, there is also a gradient from the San Francisco Bay Area and from the Pacific Northwest to the nonurban west. Sulfate extinction is more than half of the total aerosol light extinction in the eastern and north central United States. In the Appalachians, Middle Atlantic states, and the Northeast, sulfate contributes about two thirds of aerosol light extinction. In the worst season for sulfate (summer), sulfate's share is even higher, reaching three quarters in the eastern United States.

Figure 5.3 shows the nitrate light extinction. There is a gradient from east to west, with relatively high nitrate contributions in the Washington D.C. area. However, the strongest gradient is from the urban areas of California, especially the Los Angeles metropolitan area, to the California desert. Nitrate contributions to aerosol light extinction are generally less than 10%, except in California, where nitrate can contribute as much as 40% and the upper midwest where nitrate extinction contributes in excess of 15%.

Figure 5.4 shows isopleths of the light extinction due to organics throughout the United States, averaged over the three-year period. Note that extinction caused by organic carbon is largest in the eastern United States and in the Pacific Northwest, and lowest in the Golden Circle of parks in southern Utah and northern Arizona. The fraction of aerosol light extinction contributed by organic carbon ranges from a high of more than 30% in the Great Basin Region to less than 20% in the urban areas of California and in much of the eastern United States. The reason that organic carbon is a smaller share of aerosol extinction in the East is the much larger contribution of sulfate extinction there.

Figure 5.5 shows isopleths of the extinction caused by absorption. Absorption is highest in the Pacific Northwest and in the eastern United States and lowest in the nonurban west. However, the greatest contribution by absorption is in the nonurban west, Great Basin region, and the Sonoran Desert, with more than 20% of extinction from absorption being routine. Except for the coastal regions of northern California, Oregon, and Washington, most of the western United States has a contribution from absorption in excess of 18%.

Figure 5.6 shows isopleths of light extinction due to coarse material throughout the United States, averaged over the three-year period. Extinction caused by coarse material is highest in the

Coastal Mountains, West Texas, Mid South, Florida, Appalachian, and Mid Atlantic regions. The least contribution occurs in the Northeast, Colorado Plateau, and portions of the Central Rockies. The fraction of aerosol extinction contributed by coarse material shows an east-west dichotomy with the eastern United States having the lowest percentages with the Mid South and Appalachian regions at about 3%. In the West, there is a large region that encompasses the Central Rockies, Sonoran Desert, West Texas, and the Great Basin that routinely exceeds 15%.

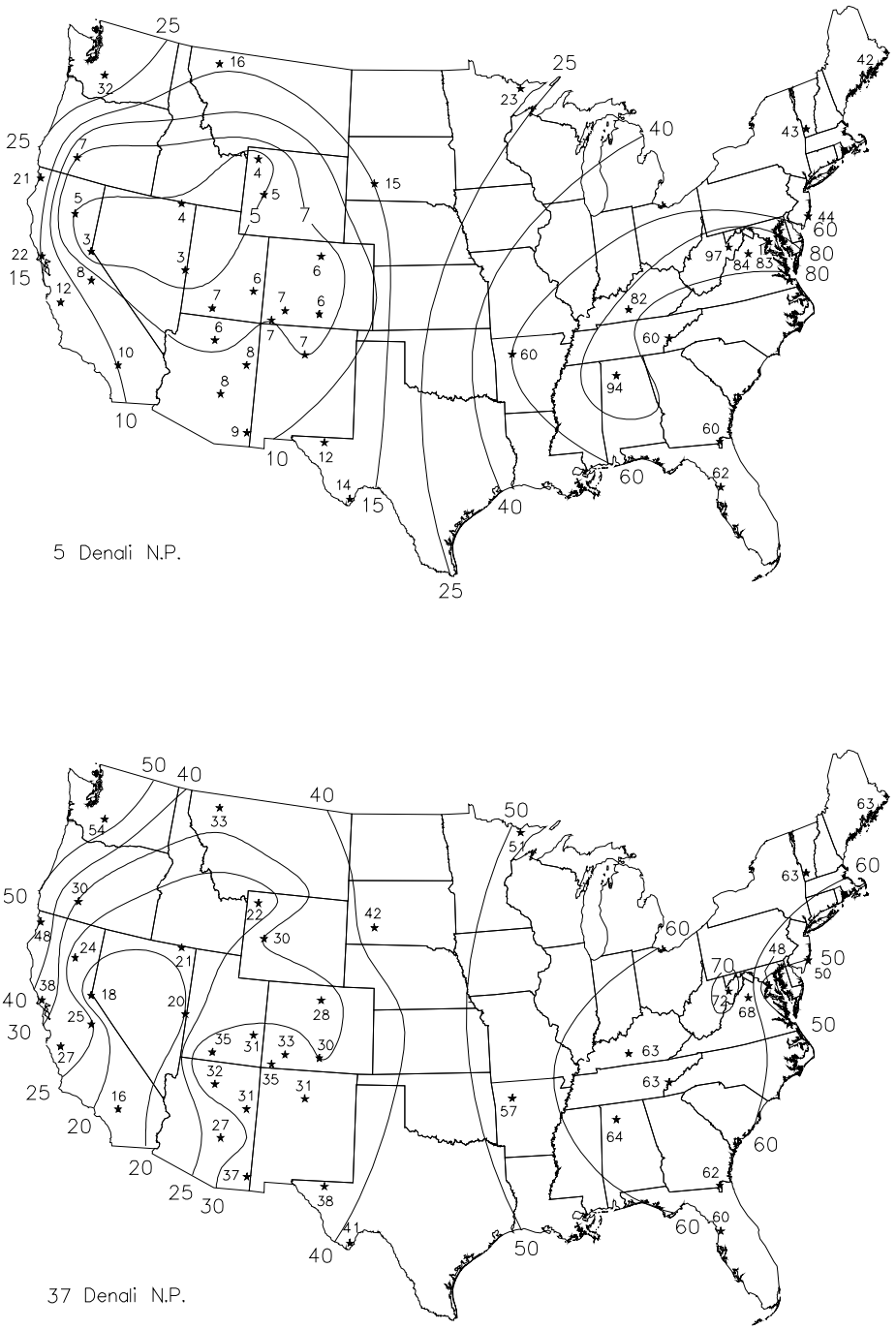

Figure 5.2 Three-year averages of reconstructed sulfate light extinction coefficient in Mm^{-1} (top) and sulfate fraction in percent of aerosol light extinction (bottom), for each of the sites in the IMPROVE network reported for the United States.

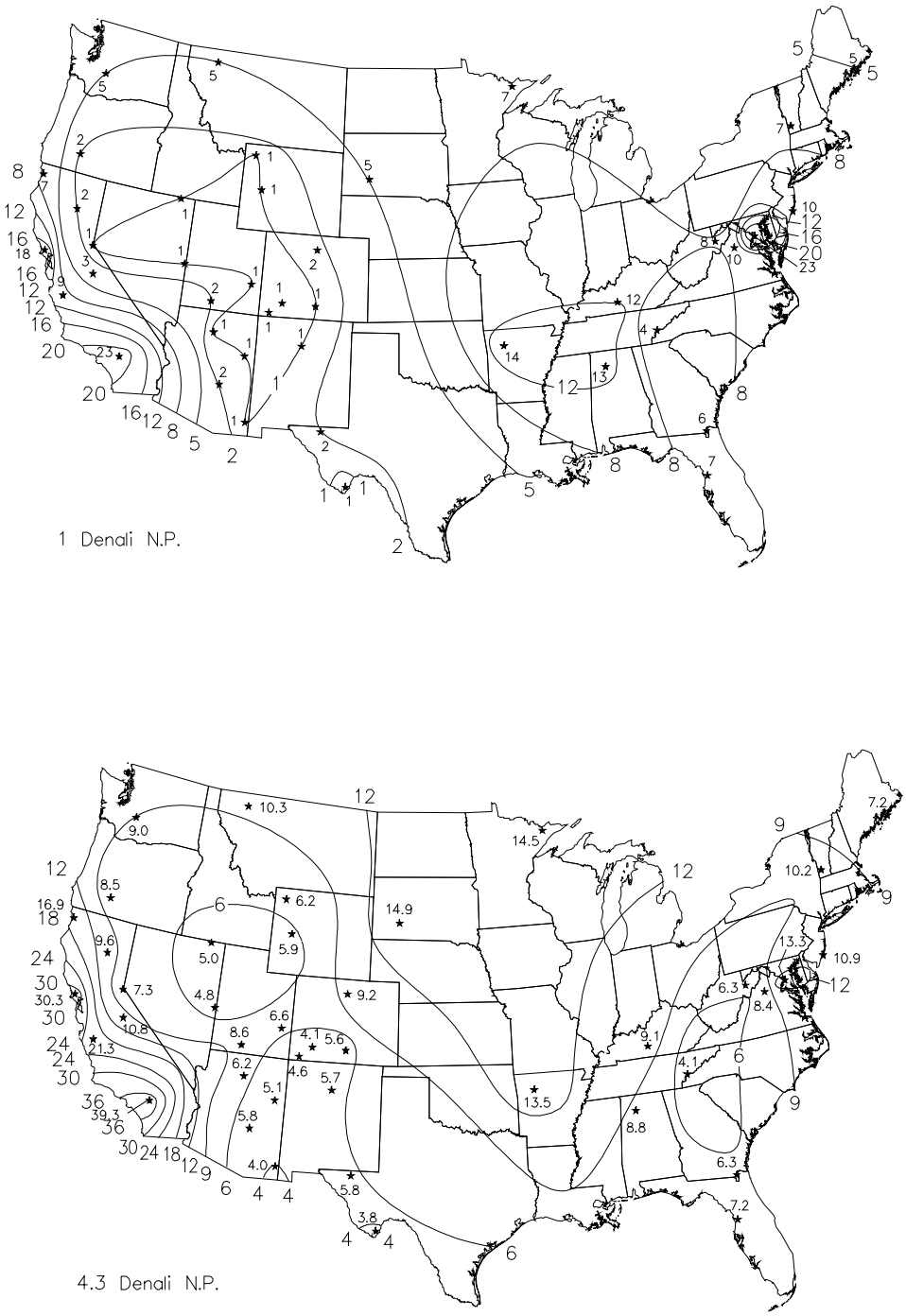

Figure 5.3 Three-year averages of reconstructed nitrate light extinction coefficient in Mm^{-1} (top) and nitrate fraction in percent of aerosol light extinction (bottom), for each of the sites in the IMPROVE network reported for the United States.

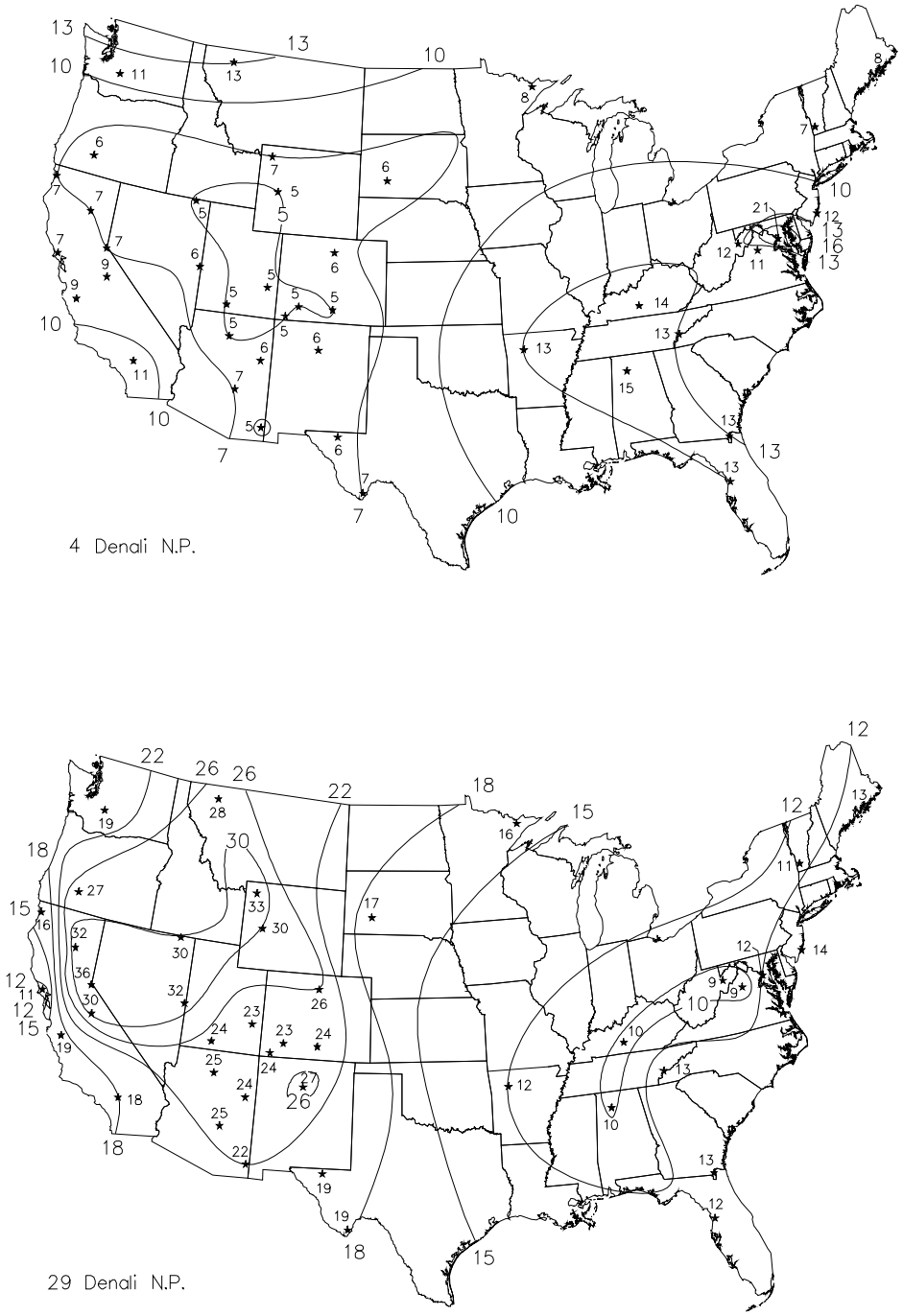

Figure 5.4 Three-year averages of reconstructed organic carbon light extinction coefficient in Mm^{-1} (top) and organic carbon fraction in percent of aerosol light extinction (bottom), for each of the sites in the IMPROVE network reported for the United States.

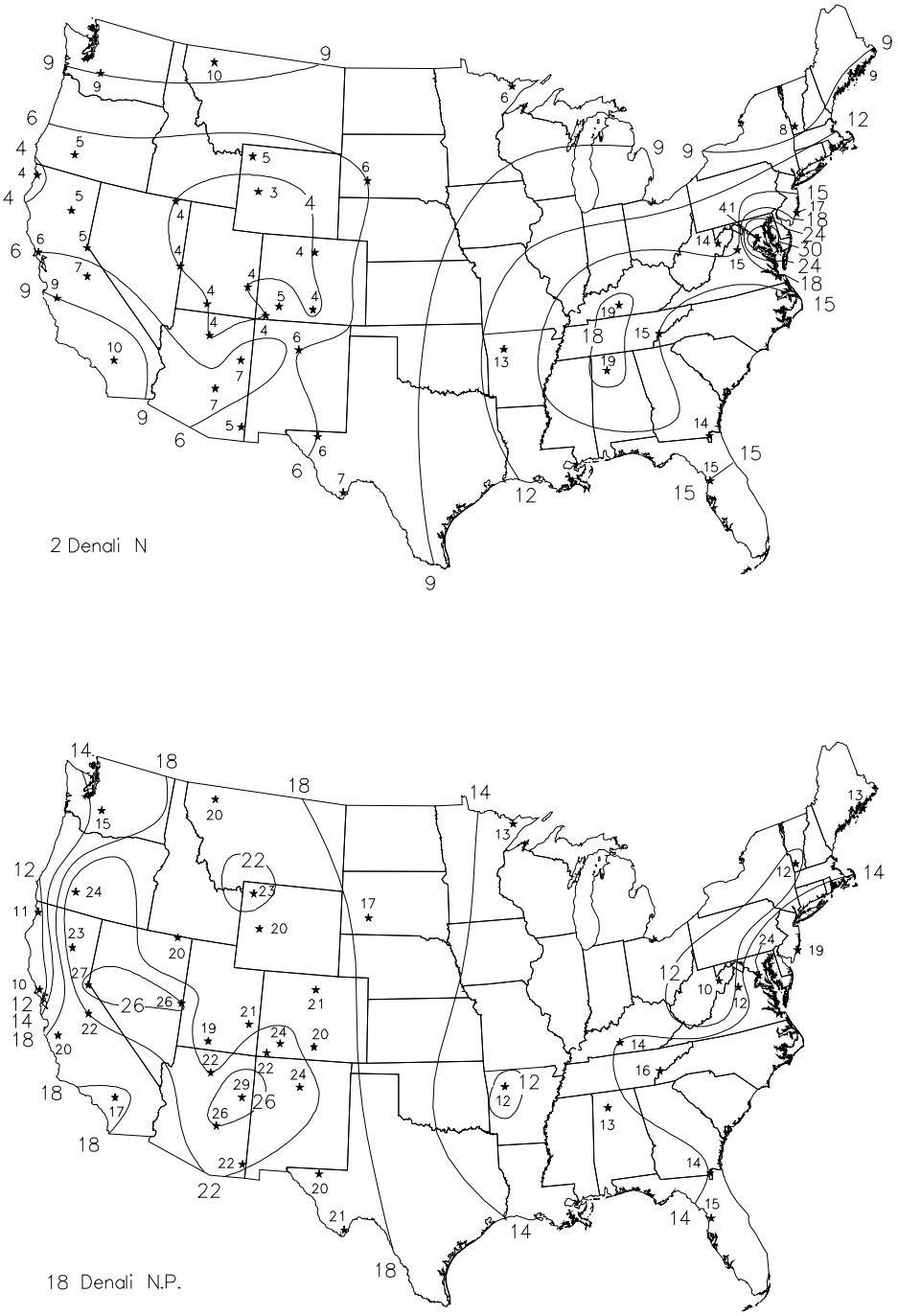

Figure 5.5 Three-year averages of reconstructed absorption coefficient in Mm^{-1} (top) and absorption fraction in percent of aerosol light extinction (bottom), for each of the sites in the IMPROVE network reported for the United States.

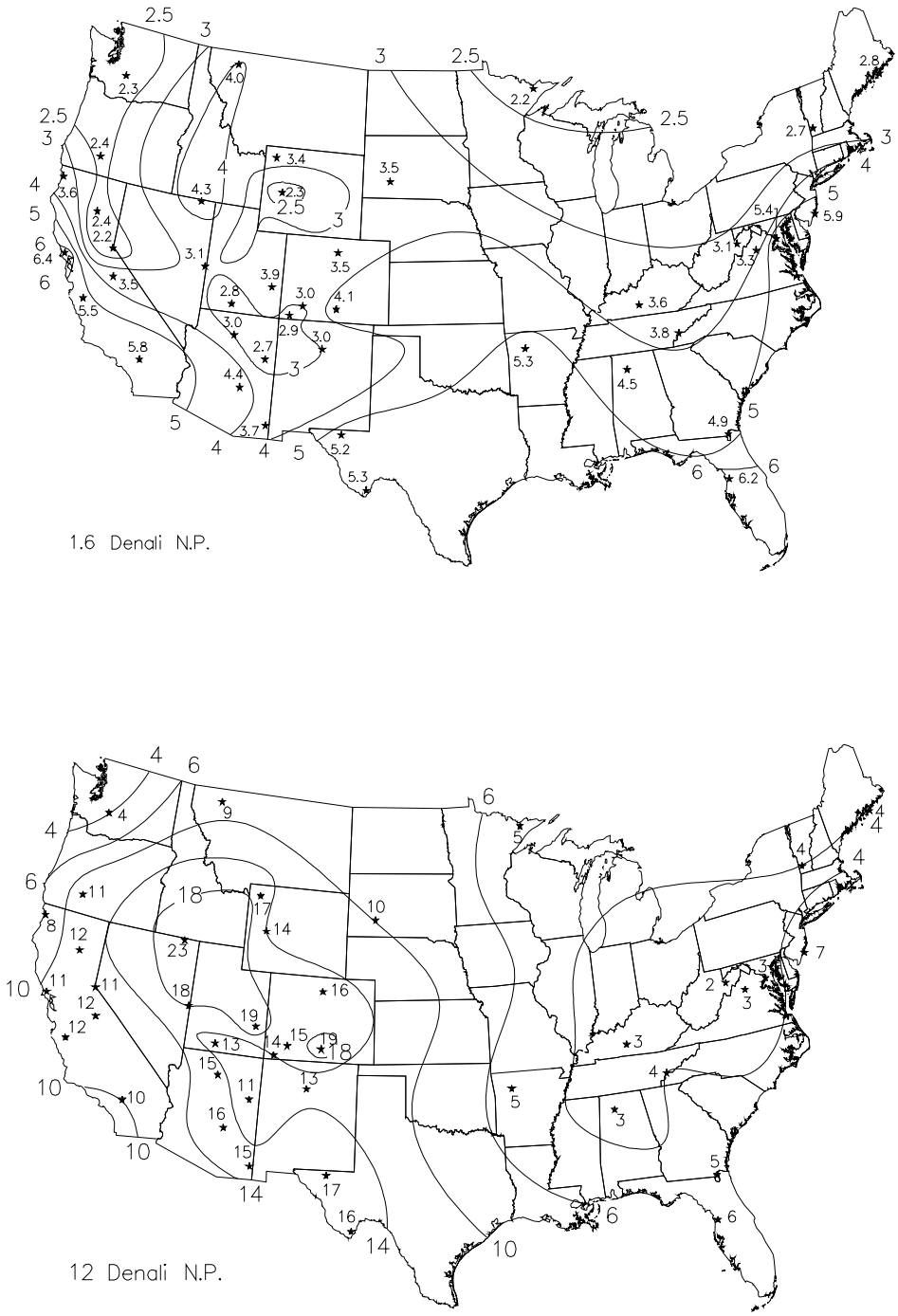

Figure 5.6 Three-year averages of reconstructed light extinction due to coarse material in Mm^{-1} (top) and percent of aerosol extinction (bottom), for each of the sites in the IMPROVE network reported for the United States.

5.2.3 Spatial Trends in Visibility in the United States

To show the effect on visibility of aerosol extinction the deciview (*dv*) scale is applied to the total (Rayleigh included) aerosol extinction (see Chapter 1). By utilizing the *dv* scale the effect of aerosol extinction on the human visual system is portrayed as a linear scale of visibility degradation. Pristine or Rayleigh conditions have a *dv* of zero. A one or two *dv* change is usually associated with the minimal or just noticeable change (JNC) in visibility perceived by the average individual.

Figure 5.7 shows isopleths of deciviews averaged over the three-year period. There is a broad region that includes the Great Basin, most of the Colorado Plateau and portions of the Central Rockies that has visibility impairment of less than 10 *dv* or better visibility. Moving in any direction from this region generally results in a gradient of increasing *dv*. West of the Sierra Range and including southern California have *dv* values in excess of 15. To the north a maximal value of 20 *dv* occurs at Mount Rainier. The northwest United States and all of the eastern half of the United States have in excess of 15 *dv* of impaired visibility and the region east of the Mississippi, and south of the Great Lakes have impairment in excess of 24 *dv* with the Appalachian region exceeding 26 *dv*. The highest annual *dv* is reported at Washington D.C. with an impairment of 29 *dv* followed by Sipsey at 28 *dv*.

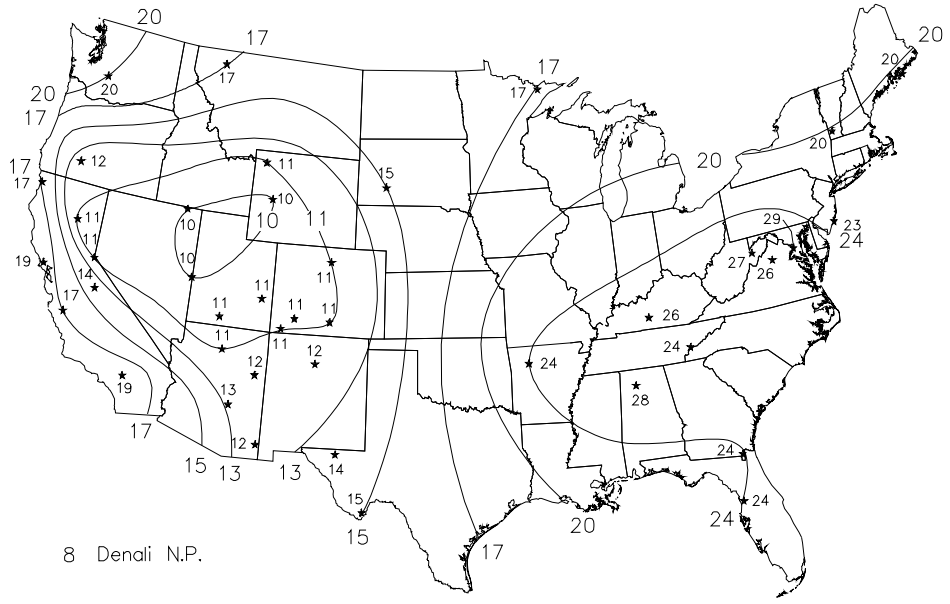

Figure 5.7 Average visibility impairment in deciviews calculated from total (Rayleigh included) reconstructed light extinction for the three-year period, March 1992 through February 1995, of IMPROVE.

Isopleths of *dv* for the winter, spring, summer, and autumn are shown in Figure 5.8 through Figure 5.11, respectively. The general spatial trend noted above for the annual average generally holds true for each season's average *dv* trend. Specifically, the least impairment or lowest *dv*'s generally occur in all or part of the Great Basin, Colorado Plateau, and Central Rockies with gradients of increasing *dv* in any direction. One interesting exception to this occurs in the winter (Figure 5.8), which shows an "island" of impaired visibility in the middle of the Colorado Plateau region at Canyonlands with a *dv* of 12. It is also of interest to note that the eastern United States is almost uniformly above 20 *dv* of impairment for all four seasons.

The best visibility in the West occurs during the winter (Figure 5.8) with a minimum *dv* of 7 being reported at Bridger Wilderness followed by 8 *dv* at Jarbidge. The region of 10 or less *dv*'s encompasses a broad expanse that covers the Sierra-Humboldt, Sierra Nevada, Great Basin, Central Rockies, and the northwestern half of the Colorado Plateau. In the eastern half of the United States the season of best visibility is split between winter and spring. In the Northeast and Florida, the winter is best for visibility, while the Appalachian and Mid-West are variable between sites. However, all sites east of the Mississippi and south of the Great Lakes site have impairment in excess of 20 *dv*'s for both the spring and winter.

Summertime visibilities (Figure 5.10), except for the Coastal Range, are generally the worst. Only small portions of the Great Basin, Central Rockies, and Colorado Plateau regions have impaired visibilities slightly below 12 *dv*. In the East, including the Ozark Plateau, there is a broad region east of the Mississippi with more than 26 *dv* of impairment in visibility. Moreover, Washington, Shenandoah, and Sipsey exceed 30 *dv*'s in impairment.

Visibility impairment in the spring (Figure 5.9) and autumn (Figure 5.11) are quite comparable. The exceptions to this are in the East where extinction is higher in the autumn, while in the intermountain west, autumn is generally less impaired, particularly in the Central Rockies and the Sierra-Humboldt regions. Southern California has better visibility in the autumn.

5.3 Summary

The following are the major patterns in light extinction reconstructed from aerosol measurements and relative humidity during the three-year period of IMPROVE (March 1992-February 1995):

1. Spatial Patterns. Following the patterns observed in fine aerosol concentrations, reconstructed light extinction is highest in the eastern United States and in urban California and lowest in the nonurban west.

2. Major Contributors to Light Extinction. Fine aerosols are the most effective in scattered light and are the major contributors to light extinction. In most cases, the sulfate component of fine aerosol is the largest single contributor to light extinction. This is because sulfate, being hygroscopic, generally has a higher light extinction efficiency than other species due to associated liquid water. This is especially true in the eastern United States, where relative humidity is high. In the Appalachian Mountains (Shenandoah and Great Smoky Mountains),

sulfate accounts for 2/3 of the total aerosol light extinction throughout the year, and 3/4 of the total in summer. Sulfate is the largest single contributor to light extinction in 14 of the 21 regions, and is comparable with organics as the most significant contributor in three additional regions (Northern Rockies, Central Rockies, and Sierra-Humboldt). Organic carbon is the largest single contributor to light extinction in three of the 21 regions (Great Basin, Sierra Nevada, and Lake Tahoe) and is a major contributor in the two previously mentioned regions. Smaller contributions come from wind-blown dust (coarse particles and fine soil) and nitrate. Nitrate is the single largest contributor to light extinction only in southern California.

3. Smaller Contributors. After sulfate and organic carbon, nitrate, and wind-blown dust (coarse particles and fine soil) generally contribute equal amounts. Light-absorbing carbon is generally the smallest contributor.

4. Seasonality. Generally, reconstructed light extinction is highest in summer and lowest in winter; however, there are many exceptions to this general rule. Higher extinction occurs in summer generally because of relatively elevated sulfate and carbonaceous aerosol concentrations.

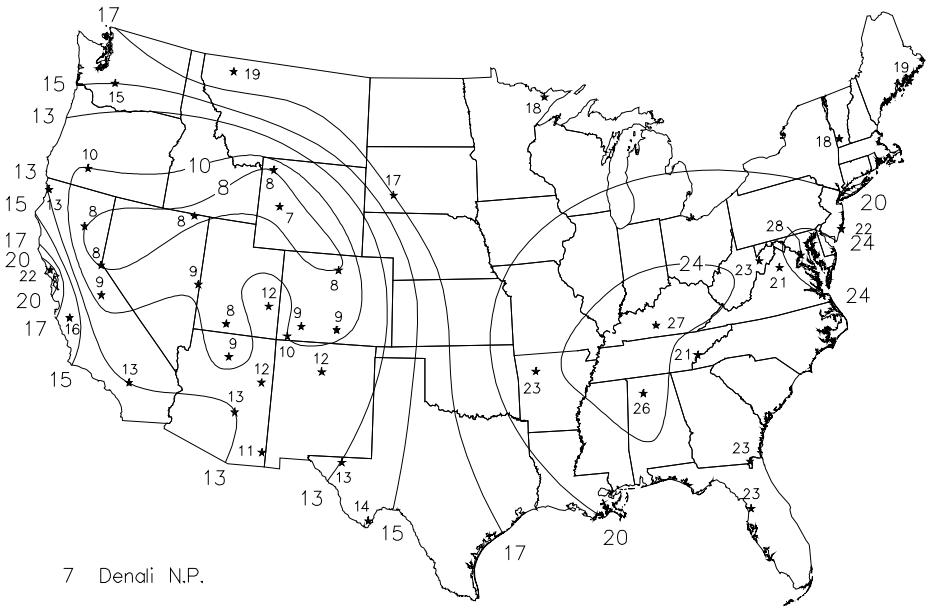

Figure 5.8 Average winter visibility impairment in deciviews calculated from total (Rayleigh included) reconstructed light extinction for the three-year period, March 1992 through February 1995, of IMPROVE.

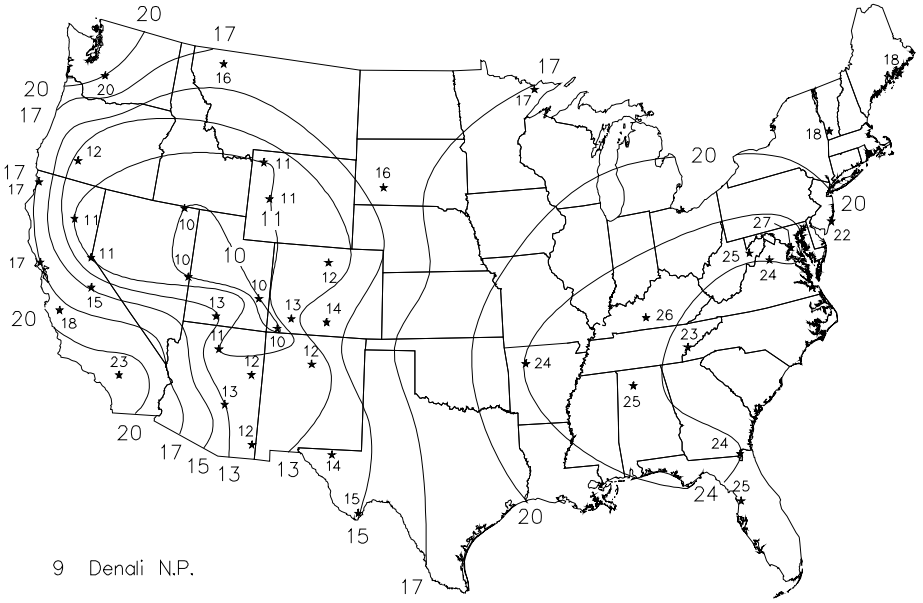

Figure 5.9 Average spring visibility impairment in deciviews calculated from total (Rayleigh included) reconstructed light extinction for the three-year period, March 1992 through February 1995, of IMPROVE.

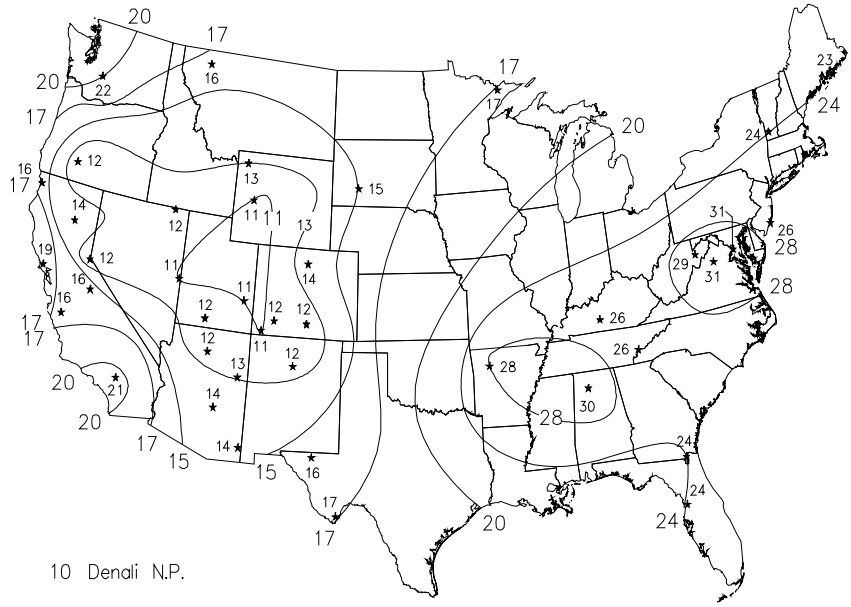

Figure 5.10 Average summer visibility impairment in deciviews calculated from total (Rayleigh included) reconstructed light extinction for the three-year period, March 1992 through February 1995, of IMPROVE.

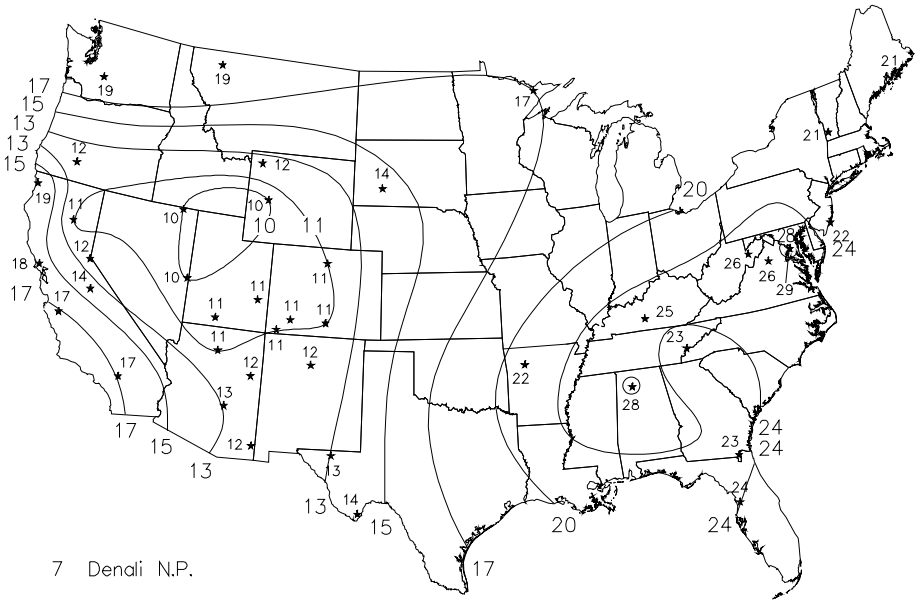

Figure 5.11 Average autumn visibility impairment in deciviews calculated from total (Rayleigh included) reconstructed light extinction for the three-year period, March 1992 through February 1995, of IMPROVE.

CHAPTER 6

TEMPORAL TRENDS AND INTERRELATIONSHIPS OF AEROSOL CONCENTRATIONS

The IMPROVE aerosol monitoring network, established in March 1988, initially consisted of 36 sites instrumented with aerosol sampling modules A through D [Sisler *et al*., 1993]. Many of the IMPROVE sites are successors to sites where aerosol monitoring with stacked filter units (SFU) was carried out as early as 1979 [Sisler and Malm, 1989]. The IMPROVE module A is identical in many aspects to the second stage of the SFU sampler. Both methods measured $PM_{2.5}$ samples of ambient aerosol on Teflon filters and were subjected to the same assay techniques (see Table 2.1). In this discussion, three measured values will be examined in some detail: gravimetric fine mass (FM), sulfur as measured by Proton Induced X-ray Emission (PIXE), and absorption (b_{abs}) measured by the Laser Integrating Plate Method (LIPM) [Eldred *et al*., 1988, Cahill *et al*., 1986]. Assuming an absorption efficiency of 10 m^2/gm, b_{abs} is expressed as a mass in ng/m^3.

The IMPROVE sites that can be paired with antecedent SFU sites have an almost unbroken record of sulfur and fine mass (and other elements measured by PIXE) from as early as 1979 and b_{abs} from 1983. Table 6.1 lists the sites and time periods that IMPROVE or SFU samplers were operated. These data provide an excellent opportunity to look for evidence of long-term trends in aerosol concentrations.

Two distinct temporal trends are considered here: seasonal, and long-term trends of statistical measures such as maxima, minima, percentiles, and standard deviations. For the sake of completeness, Appendix 1 has time lines of FM, sulfur, and b_{abs} for every IMPROVE/SFU site. Presented here for discussion are data that demonstrate identifiable trends and differences between sites.

6.1 Protocol Induced Trends of Sulfur Concentrations and b_{abs}

Two significant changes in sampling protocol have occurred since sampling began in 1979. In June 1986, the SFU sampling schedule was changed from two 72-hour duration samples per week, with start times alternating between midnight and noon, to two 24-hour samples per week, with both start times at midnight. The IMPROVE network has maintained the new schedule. In March 1988, the IMPROVE network succeeded the SFU network. There was a three month hiatus from December 1987 through February 1988 when almost no samples were obtained while equipment was changed.

Table 6.1 Sites and time periods for IMPROVE and SFU.

Acronym	Full Name	SFU Start	SFU End	IMPROVE Start	IMPROVE End
ACAD	Acadia NP	9/21/85	11/28/87	3/01/88	Present
ARCH	Arches NP	9/28/79	11/28/87	3/01/88	5/92
BAND	Bandelier NM	10/02/82	2/09/85	3/01/88	Present
BIBE	Big Bend NP	7/27/82	11/28/87	3/01/88	Present
BRCA	Bryce Canyon NP	9/21/79	12/02/87	3/01/88	Present
BRLA	Brooklyn Lake	3/01/91	7/31/93	7/31/93	Present
CANY	Canyonlands NP	9/21/79	11/28/87	3/01/88	Present
CHIR	Chiricahua NM	6/8/82	5/31/86	3/01/88	Present
CRLA	Crater Lake NP	10/12/82	11/28/87	3/01/88	Present
CRMO	Craters of the Moon	7/17/82	3/29/86	5/12/92	Present
DENA	Denali NP &	9/10/86	11/25/87	3/01/88	Present
DEVA	Death Valley NP	6/01/82	3/29/86	10/18/93	Present
GLAC	Glacier NP	9/28/82	12/5/87	3/01/88	Present
GICL	Gila NF	10/1/79	8/31/81	3/28/94	Present
GRBA	Great Basin NP	10/12/82	3/29/86	5/00/88	Present
GRCA	Grand Canyon NP	8/03/79	11/28/87	3/01/88	Present
GRSA	Great Sand Dunes	9/15/80	8/31/81	5/04/88	Present
GRSM	Great Smoky Mtns	1/31/84	11/28/87	3/01/88	Present
GUMO	Guadalupe Mtns NP	2/19/83	12/02/87	3/01/88	Present
LAVO	Lassen Volcanic NP	6/29/82	5/29/84	3/01/88	Present
MEVE	Mesa Verde NP	10/30/82	12/05/87	3/01/88	Present
MORA	Mount Rainier NP	7/23/83	12/16/87	3/01/88	Present
PEFO	Petrified Forest NP	7/30/79	11/25/87	3/01/88	Present
ROMO	Rocky Mountain NP	9/21/79	12/02/87	9/15/90	Present
SAGU	Saguaro NM	7/2/85	8/31/88	3/1/88	Present
SALM	Salmon NF	9/01/90	11/13/93	11/09/93	Present
SHEN	Shenandoah NP	7/13/82	11/28/87	3/01/88	Present
TONT	Tonto NM	8/3/79	11/29/83	3/01/88	Present
VOYA	Voyageurs NP	7/13/85	Present	3/01/88	Present
YELL	Yellowstone NP	9/29/79	12/05/87	3/01/88	Present
YOSE	Yosemite NP	9/25/82	10/28/87	3/01/88	Present

NP = National Park
NM = National Monument
NF = National Forest

Both changes in protocol are relatively close to each other in time. Therefore, it is difficult to separate the effects of one change from the other using the data. Since there are no monitoring sites where SFU samplers and IMPROVE samplers were operated side by side, any changes due to protocol must be hunted for in the data. The purpose of this chapter is not to put this issue to rest by exhaustive statistical analysis but rather to alert the reader to the possibility. However, since the

changes in protocol affect all sampling sites, the affects should be systematic across the network.

Two changes in the data that are most probable are a smoothing effect due to the change in the sampling duration and a bias in elemental concentrations, absorption and fine mass due to the change from SFU samplers to IMPROVE samplers. One would expect a smoothing effect for data collected over 72 hours compared to data collected over 24 hours. Smoothing of the data would show a tighter distribution about the mean resulting in a smaller standard deviation and less extreme maximum and minimum values. Bias in the data, resulting from switching the equipment from SFU samplers to IMPROVE samplers, comes from the actual sampling methodology. For example, the SFU fine mass ($PM_{2.5}$) is a sequential filter that sites behind a filter that collects coarse material, while the IMPROVE module A filter has a cyclone inlet that is calibrated to 2.5 microns. Any discrepancy in cutpoint efficiency and derivative, as a function of aerodynamic radius between the two samplers, could generate a bias in seasonal mean values. If there is a long-term trend in the data, this bias could either enhance the trend or mask it.

It appears, based on a cursory inspection of the data as presented here, that a systematic effect associated with changes in protocols is not evident for fine mass and sulfur concentrations. Most clearly identifiable changes in the data can be explained by other physical causes. One such notable change occurred at Mount Rainier where the sampling site was moved from a high altitude to a low altitude location. Other explanations are related to changes in emissions. In general, the expected changes due to smoothing did not materialize, instead the changes in data behavior appear random and slight at best. No systematic bias in the data between SFU samplers and IMPROVE samplers was noted, suggesting that any bias at one particular site must be due to circumstances unique to that site such as equipment calibration, or characteristics of the ambient aerosol and meteorology that would affect sampler performance, or actual location/orientation of the equipment.

In the case of absorption, Figure 6.1 shows time lines for b_{abs} for five sites that demonstrate a clear change before and after the IMPROVE network was initialized. The sites included are Acadia, Glacier, Great Smoky Mountains, Mount Rainier, and Shenandoah National Parks. It is clear by inspection of Figure 6.1 that a significant change occurred after March 1988. Almost all sites for all seasons show significant increases in b_{abs} between sampling regimes with the IMPROVE values being larger than the SFU. As with sulfur, it should be noted that increases of b_{abs} at Mount Rainier are likely related to changing of the sampler location. Reasons for the changes at the other sites are not known and it should be noted that these five sites are exceptions as most sites show little if any change by inspection.

6.2 Seasonal Trends of Sulfur

Sulfur concentrations often have a readily identifiable seasonal trend [Day *et al*., 1996, Malm *et al*., 1994; Sisler *et al*., 1993; Sisler and Malm, 1989; Trijonis and Yuan 1987; Flocchini *et al*., 1981]. These trends have been related to a number of factors including meteorology, photochemistry, and long-range transport with sulfur concentrations being the highest during the summer and lowest during the winter.

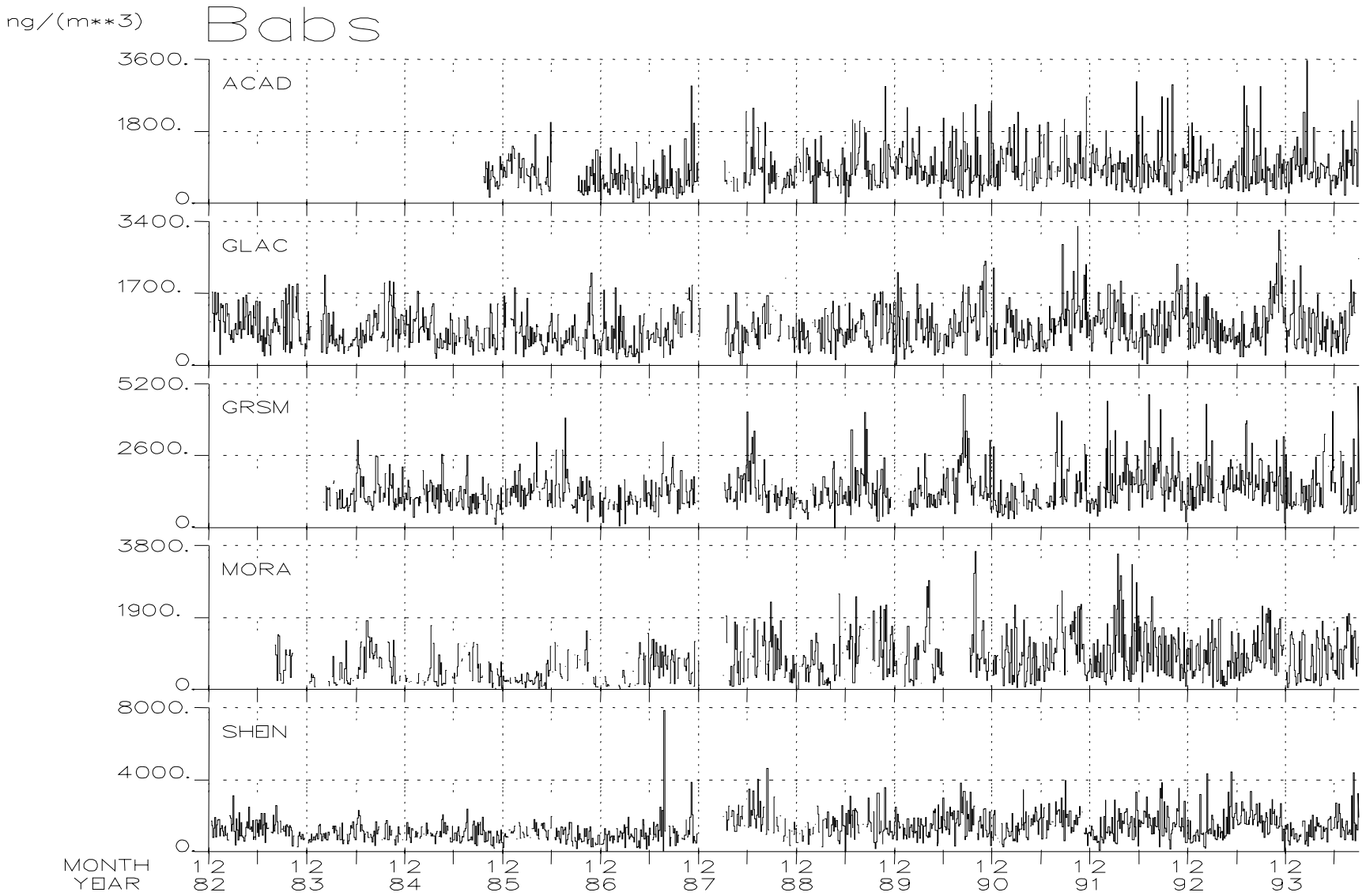

Figure 6.1 Time line of absorption (b_{abs}) at five sites that demonstrate a clear change before and after the IMPROVE network was initiated.

Figure 6.2 shows the time lines of sulfur at seven sites: Shenandoah, Great Smoky Mountains, Yosemite, Rocky Mountain, Canyonlands, Yellowstone, and Glacier National Parks. Table 6.2 has seasonal statistics for these sites. At two sites, Yellowstone and Glacier, one extreme value was discarded from the time lines presented in Figure 6.2. This value, 1364 ng/m^3 at Yellowstone on May 31, 1989 is a factor of 10 higher than the mean and 200% higher than the next highest value. Similarly, one value of 1326 ng/m^3 at Glacier on June 2, 1993, was discarded.

These sites demonstrate a range in amplitude of seasonal variation. The two sites with the highest sulfur concentrations, Great Smoky Mountains and Shenandoah, are in the East. The maximum sulfur concentrations for these sites, 8700 and 6900 ng/m^3 at Shenandoah and Great Smoky Mountains, respectively, occurred during the summer.

At Shenandoah, Great Smoky Mountains, Yosemite, and Rocky Mountain National Parks, sulfur concentrations have clear seasonal patterns. The pattern is less clear at Canyonlands, while at Yellowstone and Glacier a seasonal pattern is not apparent. These seven sites represent the range of seasonal variability of sulfur in the data set.

It is notable that even at sites with strong seasonal trends there are some sampling periods that have zero or near zero concentrations in any season.

Yosemite is interesting as the maximum sulfur is only about 1400 ng/m^3, yet a seasonal pattern is clearly evident from the minimums, which are much greater during the summer months. At Rocky Mountain, the seasonality is much weaker than at Yosemite as evidenced by the variability in time that yearly maximum values occur. However, it is clear from the minimum values that a seasonal trend exists with higher minimums occurring during the summer.

The three remaining sites shown in Figure 6.2, Canyonlands, Yellowstone, and Glacier have much lower sulfur concentrations. None of these sites exhibit obvious seasonal trends as displayed by the other sites. Their maximum values are quite a bit less than the other sites and about equal to each other.

6.3 Seasonal Trends of Absorption (b_{abs})

Absorption, like sulfur, has a strong seasonal trend at many sites with highest concentrations usually occurring during the summer and early autumn months. Figure 6.3 shows time lines of b_{abs} at six sites across the United States: Acadia, Glacier, Great Smoky Mountains, Rocky Mountain, and Yosemite National Parks, and Saguaro National Monument. This ensemble demonstrates the range of the strength of the seasonal signature that varies from none at Acadia and Saguaro, to moderate at Glacier and Great Smoky Mountains, to strong at Rocky Mountain and Yosemite.

Table 6.3 has seasonal statistics for absorption at these six sites. Acadia, a site with minimal seasonality, has a mean value that varies from 750 ng/m^3 in the spring to 950 ng/m^3 in the winter. Acadia's maximum concentrations are similar between seasons at about 3000 ng/m^3, except during the winter when the maximum value of 3562 ng/m^3 was obtained.

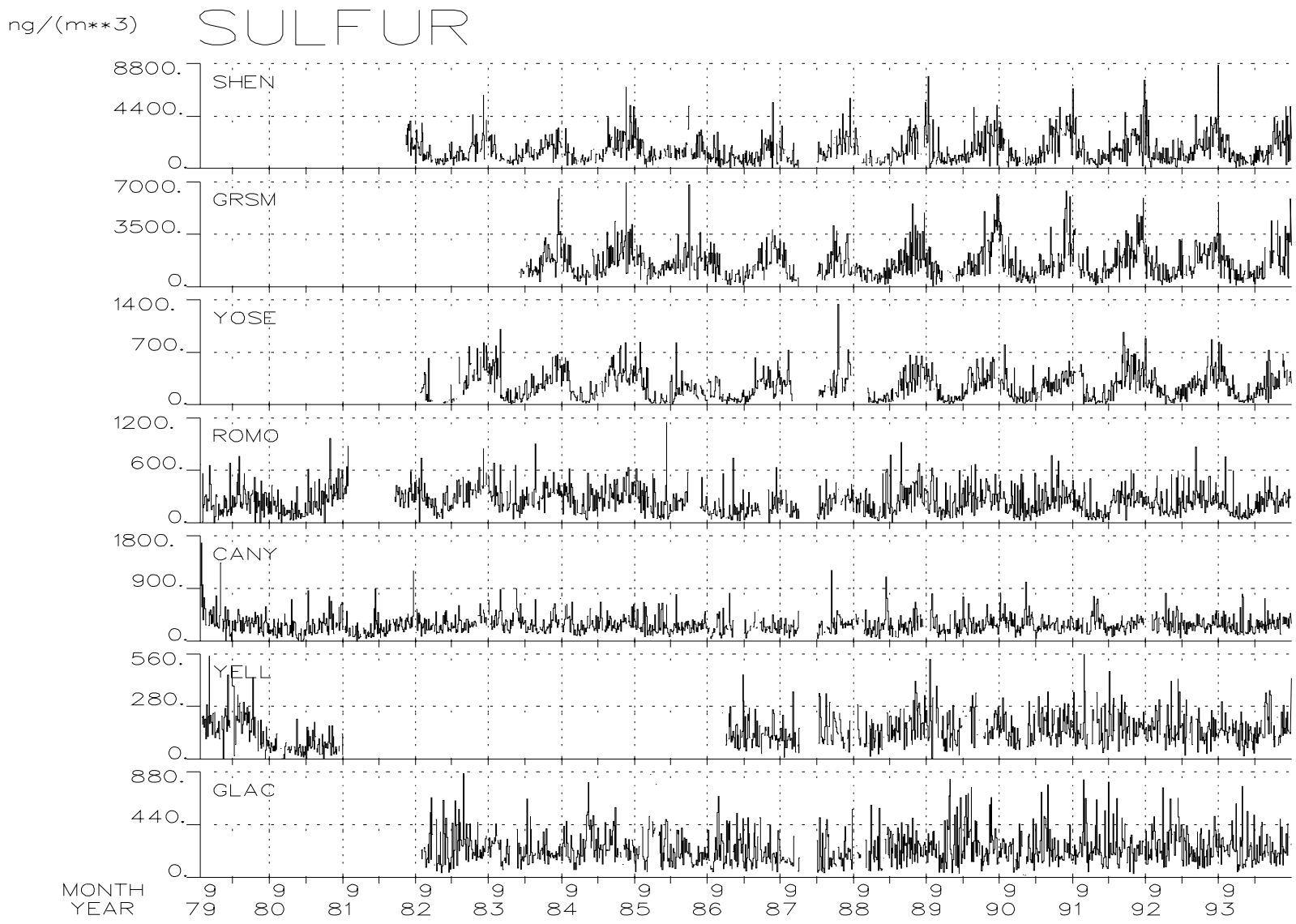

Figure 6.2 Time lines of sulfur concentration at seven sites that demonstrate a range of seasonal behavior with the strongest seasonality at the top and the weakest at the bottom.

Table 6.2. Seasonal statistics (in ng/m^3) for particulate sulfate at seven sites.

Site	N	Mean	Std Dev	Minimum	Maximum
SPRING					
SHEN	299	1415	809	131	5199
GRSM	267	1508	838	175	6789
YOSE	284	261	156	11	964
ROMO	354	270	140	0	921
CANY	374	257	127	36	1202
YELL	220	177	120	0	1365
GLAC	308	257	146	36	866
SUMMER					
SHEN	304	2495	1286	11	8665
GRSM	267	2407	1250	393	6928
YOSE	283	374	178	55	1339
ROMO	354	319	130	0	963
CANY	374	306	130	66	1206
YELL	237	148	73	0	432
GLAC	301	216	96	26	669
AUTUMN					
SHEN	283	1413	1059	15	7722
GRSM	237	1374	892	27	5610
YOSE	259	260	182	16	1008
ROMO	348	236	148	0	877
CANY	343	282	175	0	1679
YELL	192	149	92	0	558
GLAC	274	231	132	39	862
WINTER					
SHEN	255	827	441	62	2588
GRSM	214	831	462	110	3152
YOSE	256	86	69	12	525
ROMO	327	168	143	14	1146
CANY	329	280	194	0	1339
YELL	205	135	89	0	488
GLAC	261	259	181	13	1326

Saguaro shows even less variability in the mean with a low of 826 ng/m^3 in the spring to a high of 927 ng/m^3 in the winter.

Glacier and Great Smoky Mountains have relatively stable means with Glacier obtaining its low of 743 ng/m^3 during spring and its high of 1085 ng/m^3 in the autumn. Great Smoky Mountains obtains its lowest during the winter at 1156 ng/m^3 and highest in the summer with 1585 ng/m^3. The seasonality at Great Smoky Mountains and Glacier is more readily observed

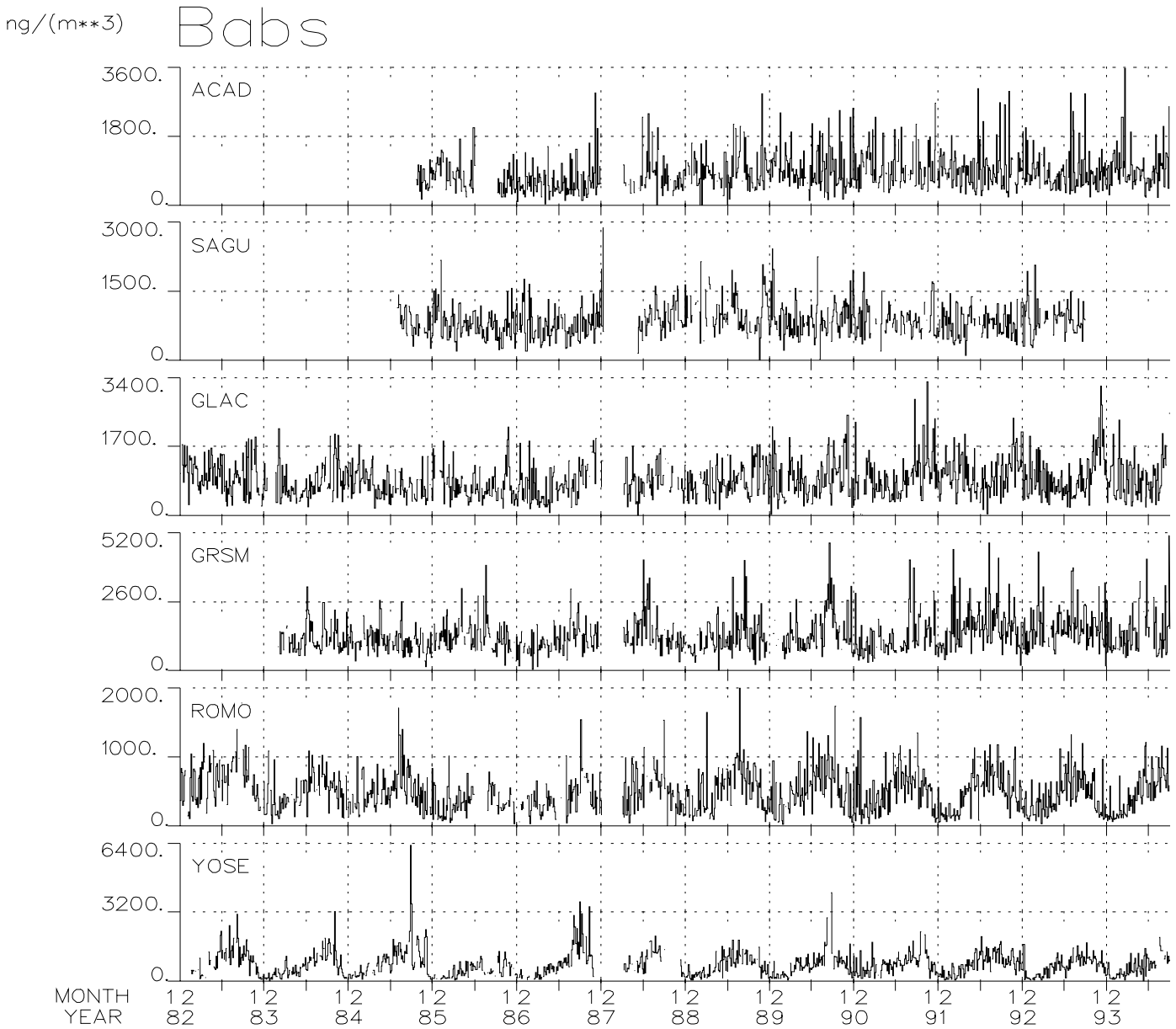

Figure 6.3 Time lines of absorption at six sites that demonstrate a range of seasonal behavior with the weakest seasonality at the top and the strongest at the bottom.

Table 6.3 Seasonal statistics for absorption (in ng/m^3) at six sites.

Site	N	Mean	Std Dev	Minimum	Maximum
SPRING					
ACAD	211	750	418	0	3041
SAGU	167	826	295	98	1799
GLAC	305	743	361	0	1994
GRSM	265	1332	567	0	4195
ROMO	290	480	255	36	1633
YOSE	282	661	357	0	2305
SUMMER					
ACAD	196	942	589	0	2932
SAGU	210	843	299	21	2239
GLAC	297	812	371	38	2852
GRSM	266	1585	887	391	5104
ROMO	272	713	281	37	1990
YOSE	278	1155	617	148	6295
AUTUMN					
ACAD	218	779	509	116	2963
SAGU	186	868	369	0	2087
GLAC	255	1085	571	152	3284
GRSM	235	1275	599	132	3292
ROMO	263	449	256	0	1729
YOSE	239	867	588	56	3655
WINTER					
ACAD	195	950	455	0	3563
SAGU	161	927	468	198	2883
GLAC	259	911	461	20	2347
GRSM	209	1156	627	51	4564
ROMO	262	308	245	23	1566
YOSE	242	300	264	0	1773

by the extreme values. The minimum for Great Smoky Mountains varies from 0 (below detection) to 381 ng/m^3 in the summer when the maximum of 5104 ng/m^3 is obtained as well. Glacier exhibits similar though not as extreme behavior where the largest minimum of 152 ng/m^3 and largest maximum of 3284 ng/m^3 are in the winter.

Yosemite and Rocky Mountain, which have the strongest seasonal variation, have means of 300 ng/m^3 and 308 ng/m^3 in the winter, and 1155 ng/m^3 and 713 ng/m^3 in the summer.

6.4 Long-Term Variability

Because of seasonal variability, long-term trends can more easily be explored by examining

trends in seasonally-averaged data over a number of years. Seasonal statistics by year are graphically portrayed at each site for both fine mass concentrations, sulfur concentrations, and absorption. Appendix 2 has plots for every site and season. The box icon used for each season portrays the minimum, the mean minus one standard deviation, the 25th percentile, 50th percentile (median), mean, 75th percentile, mean plus one standard deviation, and maximum. The percentiles are connected by a solid line. Presented here are representative examples for sites that demonstrate trends and the lack of trends.

6.4.1 Bryce Canyon National Park

Bryce Canyon in the autumn (Figures 6.4a, 6.4b, 6.4c) is an example showing an apparent change in fine mass concentrations (Figure 6.4a). Excluding the fall of 1979, there appears to be a step increase in fine mass concentrations beginning in 1987. All percentiles, means, maxima and standard deviations increase noticeably after 1987. It is tempting to associate this with a bias caused by changing the equipment from an SFU sampler to an IMPROVE module A; however, the changeover did not occur until after the autumn of 1987 when the 75th percentile and mean are greater than all succeeding years.

Sulfur concentrations (Figure 6.4b) at Bryce Canyon show no apparent trend. The sulfur concentrations from year to year are variable with the median hovering around 250 ng/m^3. However, the highest median value occurs at the start of the data record in the winter of 1979 at about 400 ng/m^3, which exceeds the 75th percentile for all other years. This season has been analyzed by a number of researchers and has been associated with transport from the smelters in Arizona.

Absorption is somewhat greater than sulfur at around 400 ng/m^3 and displays a variable pattern between years. The first year of the absorption record is notable in that the 75th percentile is greater than the maxima for all subsequent years except 1993; similarly, the mean for 1983 at about 600 ng/m^3 is on par with the 75th percentile for all years after and including 1988.

6.4.2 Rocky Mountain National Park

Fine mass concentrations at Rocky Mountain National Park (Figure 6.5a) during winter, the season of best visibility, shows no trend for the 25th and 50th percentile, which vary around 900 ng/m^3 and 1500 ng/m^3, respectively. There is a most interesting block of years beginning in 1986
running through 1991 that demonstrate inflated variability marked by increased standard deviations caused by high maximum values and 75th percentiles driving the mean values up. Association of this behavior with the decrease in sampling time from 72 hours to 24 hours is at first tempting. This explanation seems doubtful noting the dramatic quieting that occurs after 1991 when the standard deviations, maximums, and 75th percentiles dropped sharply. Also, it is worth noting that the change in protocol did not occur until the summer of 1986 after the start of the period of inflation in the winter of 1986.

Sulfur concentrations (Figure 6.5b) have a fairly constant median level of sulfur during the winters of about 150 ng/m^3. The pattern of variability is mixed and the median sulfur concentration never moves in the same direction for more than two seasons.

A clear downward trend in absorption (Figure 6.5c) is readily seen. The median absorption in the winter of 1982-1983 is about 400 ng/m^3 then drops to about 125 ng/m^3 by the winter of

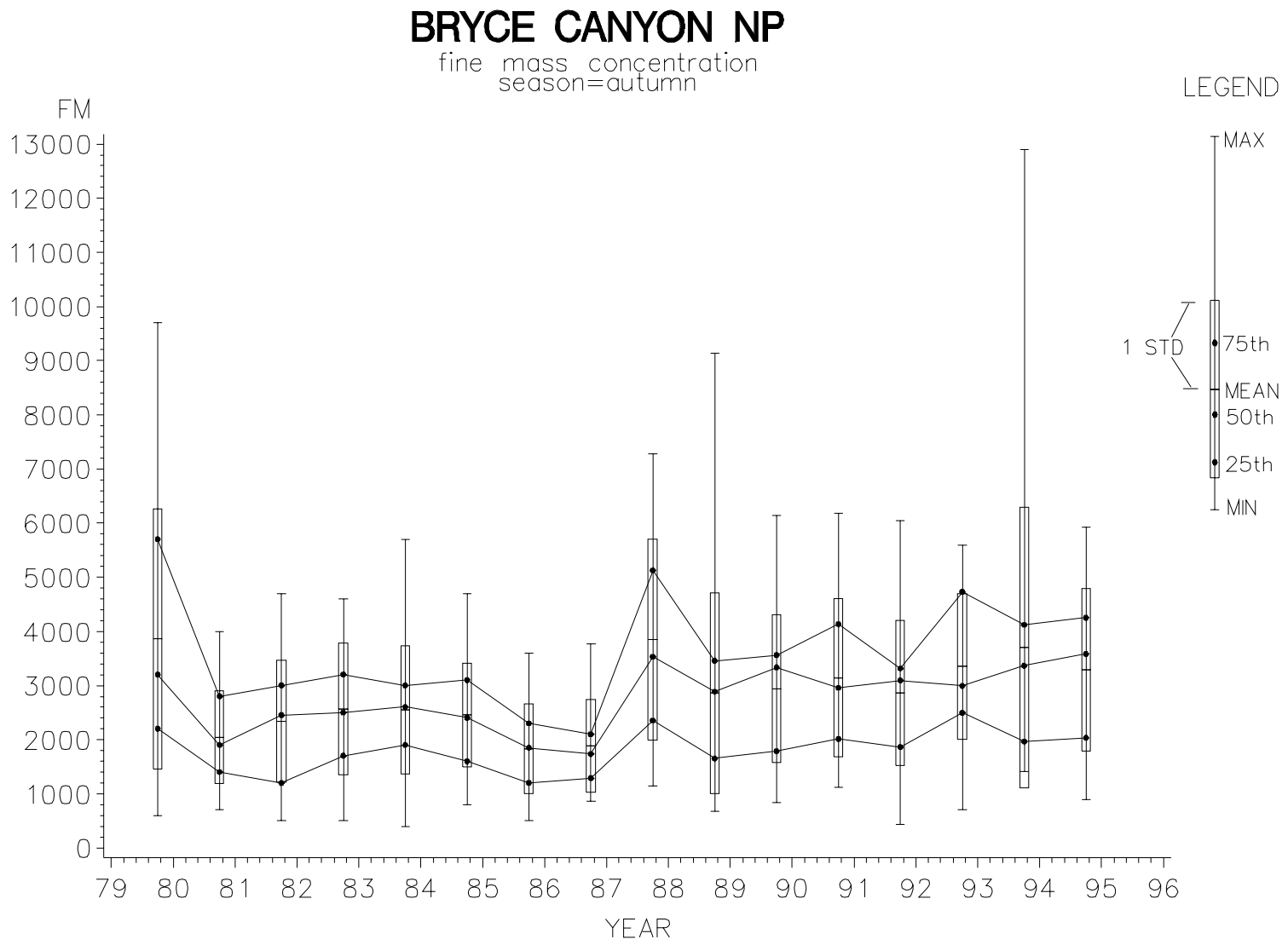

Figure 6.4a Monthly statistics for fine mass concentration (ng/m^3) at Bryce Canyon National Park in the autumn.

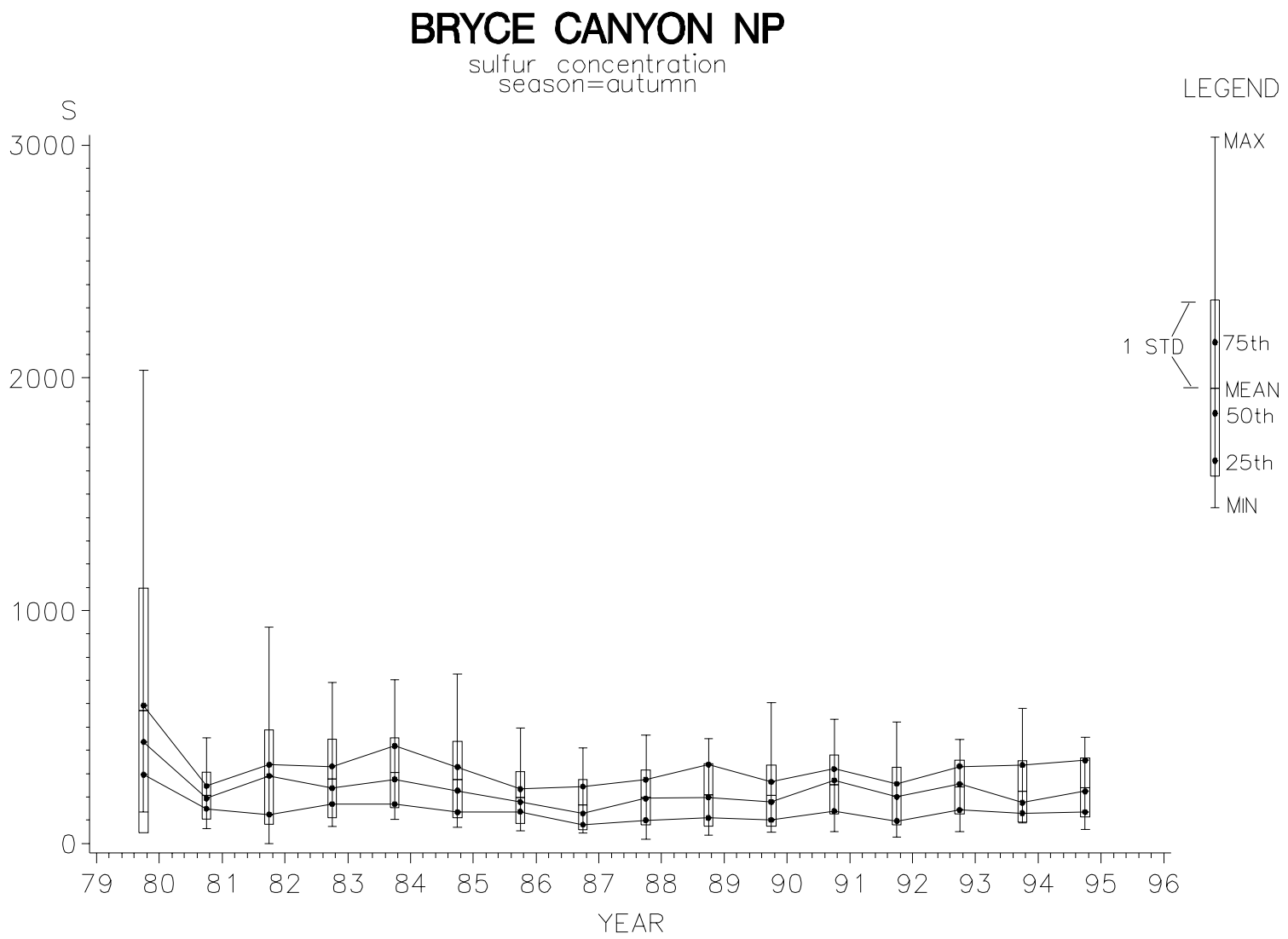

Figure 6.4b Monthly statistics for sulfur concentration (ng/m^3) at Bryce Canyon National Park in the autumn.

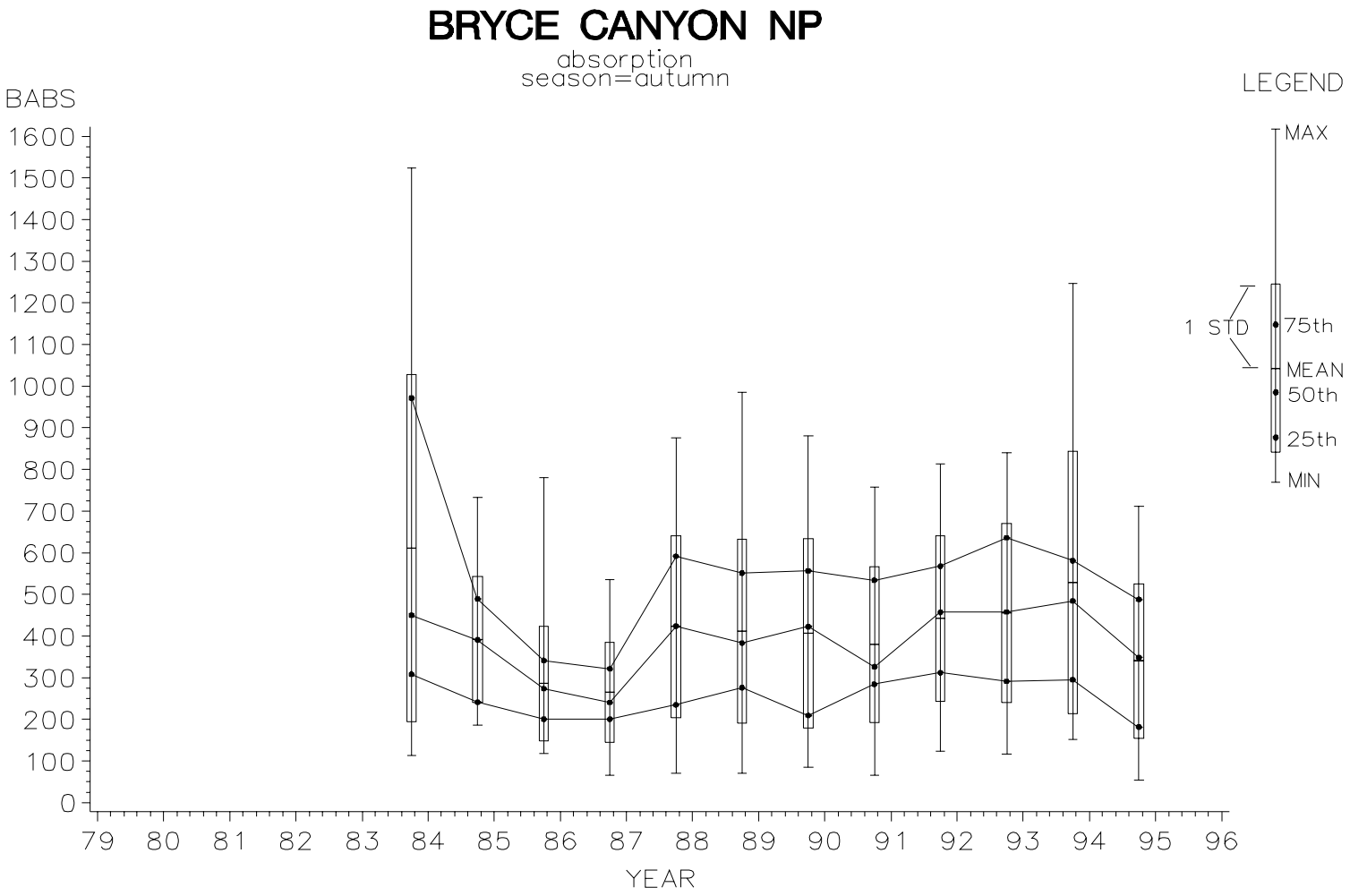

Figure 6.4c Monthly statistics for absorption (ng/m^3) at Bryce Canyon National Park in the autumn.

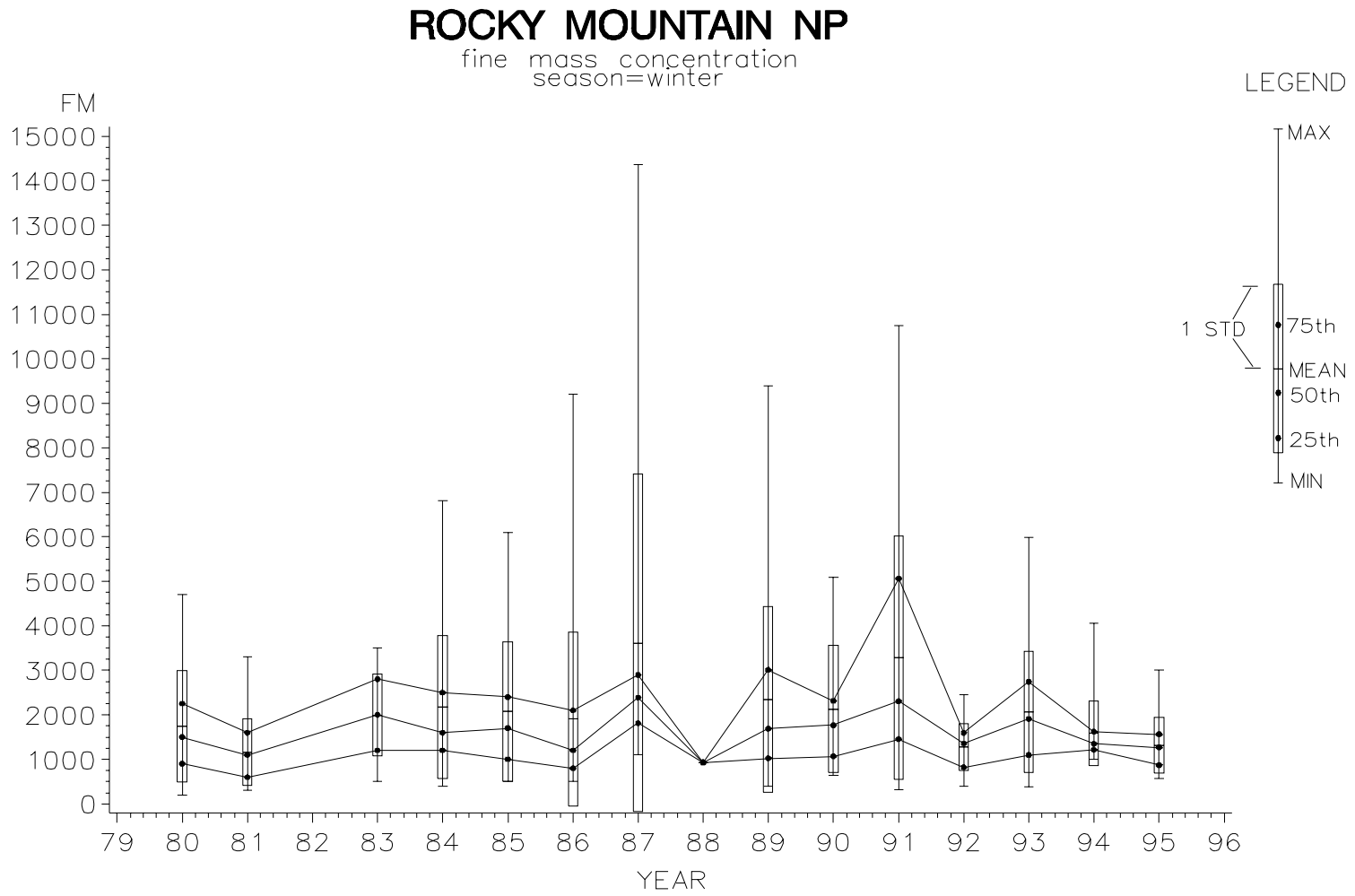

Figure 6.5a Monthly statistics for fine mass concentration (ng/m^3) at Rocky Mountain National Park in the winter.

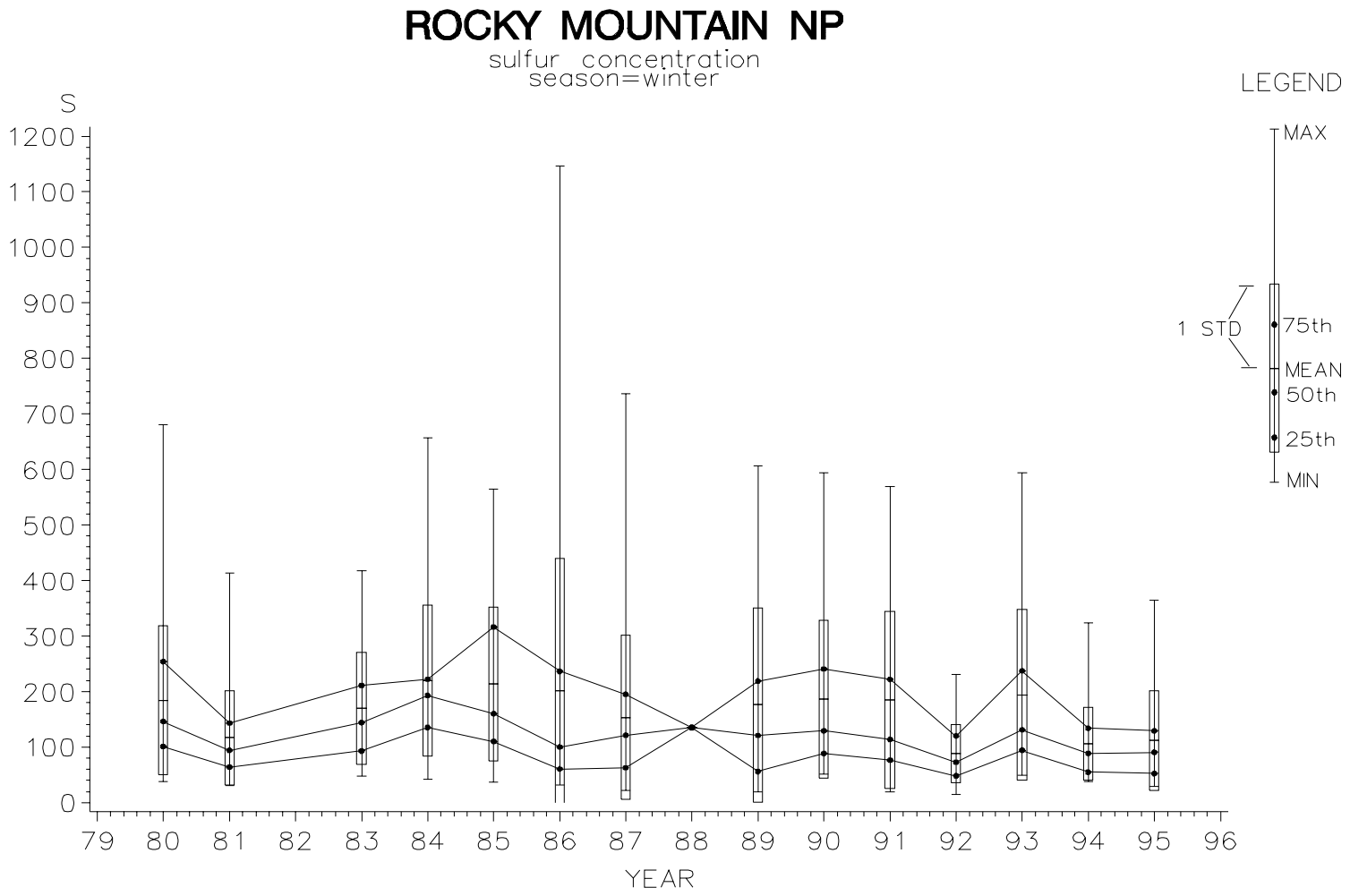

Figure 6.5b Monthly statistics for sulfur concentration (ng/m^3) at Rocky Mountain National Park in the winter.

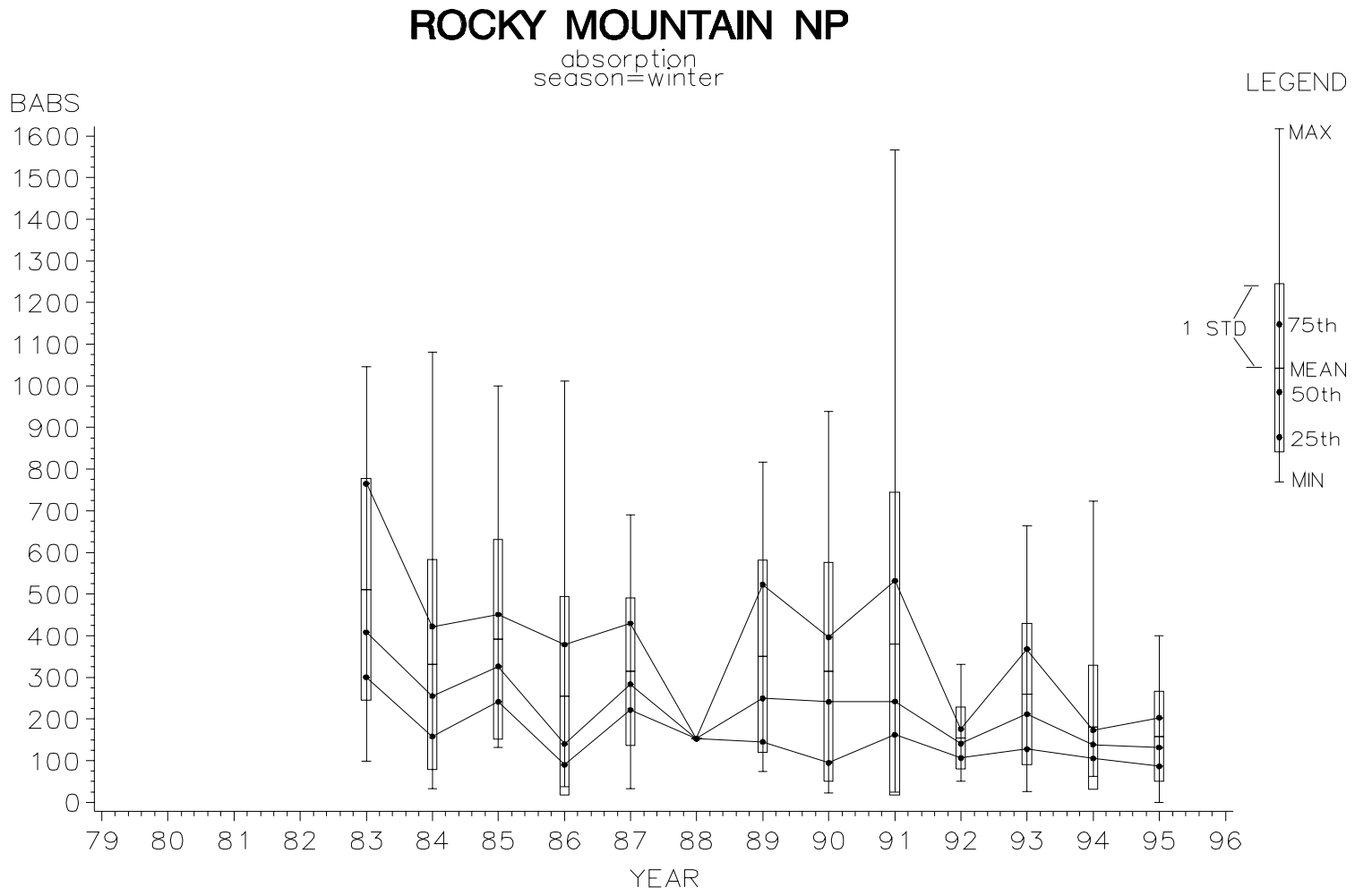

Figure 6.5c Monthly statistics for absorption (ng/m^3) at Rocky Mountain National Park in the winter.

1994-1995. Since 1991-1992 the median absorption has never exceeded 200 ng/m^3. The trend of the 75th percentile is even more impressive, the maximum occurs in the winter 1982-1983 at about 800 ng/m^3 then drops to less then 200 ng/m^3 in recent years.

6.4.3 Guadalupe Mountains National Park

Fine mass concentrations at Guadalupe Mountains (Figure 6.6a) in the autumn have been quite variable. Concentrations decreased steadily the first four years. The 75th percentile and 50th percentile decrease every year from 6500 ng/m^3 and 5200 ng/m^3, respectively in 1982 to 4200 ng/m^3 and 3500 ng/m^3, respectively, in 1986. The 25th percentile obtains its minimum as well in 1986 of 2000 ng/m^3. After 1986 there is a precipitous rise in the 50th and 75th percentile in 1990 to almost 6000 ng/m^3 and 9000 ng/m^3, respectively. Then a quick recovery to almost 1986 levels occurs by 1993 followed by an upturn in 1994.

Sulfur at Guadalupe Mountains in the autumn (Figure 6.b) does not display the gyrations of fine mass and appears to be trending downward. The median concentration is highest (650 ng/m^3) during autumn 1984, then drops to about 400 ng/m^3 the next year. After a slight increase in 1986 to 500 ng/m^3 the median sulfur never exceeds that level again and trends downward. The last four years show a steady decline of the median to 350 ng/m^3 in 1994.

Absorption, on the other hand (Figure 6.6c), while trending down at first, increases to a high of 700 ng/m^3 for the median in autumn 1990, then steadily declines. Similarly, the 75th percentile trends up to its maximum in 1988 at almost 1000 ng/m^3 then steadily declines to about 600 ng/m^3 in the autumn of 1994. The large increase in b_{abs}, coincident with the change from SFU to IMPROVE between 1987 and 1988, is suspicious and should be further investigated to confirm that the apparent trend is not a measurement artifact.

6.4.4 Crater Lake National Park

Fine mass concentrations at Crater Lake during the winters (Figure 6.7a) appear to have trended down slightly. During the first five winters the 75th percentile has trended down from 3400 ng/m^3 to 2500 ng/m^3. With the exception of the winter of 1990-1991, which shows a significant up tick in all measures (except the minimum), all winters after 1989 the 75th percentile is below 2000 ng/m^3 for five out of six winters.

On the other hand, during the winter, sulfur appears to be holding steady at around 60 ng/m^3 for the median (Figure 6.7b). The winters of 1984-85, 1985-86, and 1986-87 are interesting due the very large maximums with concentrations as much as a factor of 10 larger than the medians.

Crater Lake in the winter displays a strong absorption trend (Figure 6.7c). In the winter of 1982-83, the 75th percentile value was about 900 ng/m^3. During the next five out of six winters of record all percentiles decline with the 75th percentile obtaining a minimum of less than 400 ng/m^3 during the winter of 1989-90. The remaining winters, until the last, have a very steady 25th percentile at about 150 ng/m^3. The other percentiles are variable and obtain their global minimum during the winter of 1993-94. The last winter of 1994-95 shows a dramatic increase in all measures, with the 75th percentile exceeding 1400 ng/m^3.

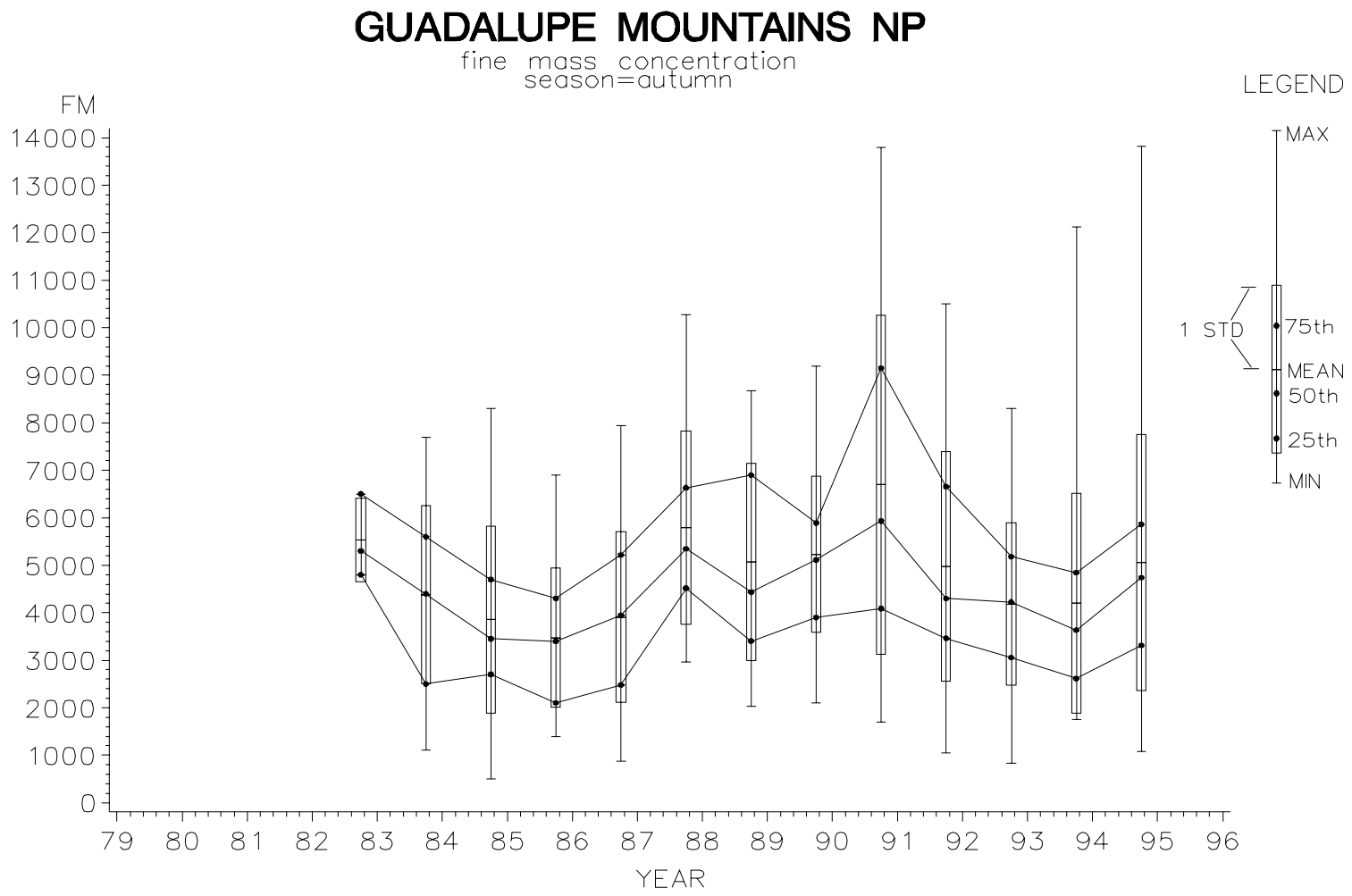

Figure 6.6a Monthly statistics for fine mass concentration (ng/m^3) at Guadalupe Mountains National Park in the autumn.

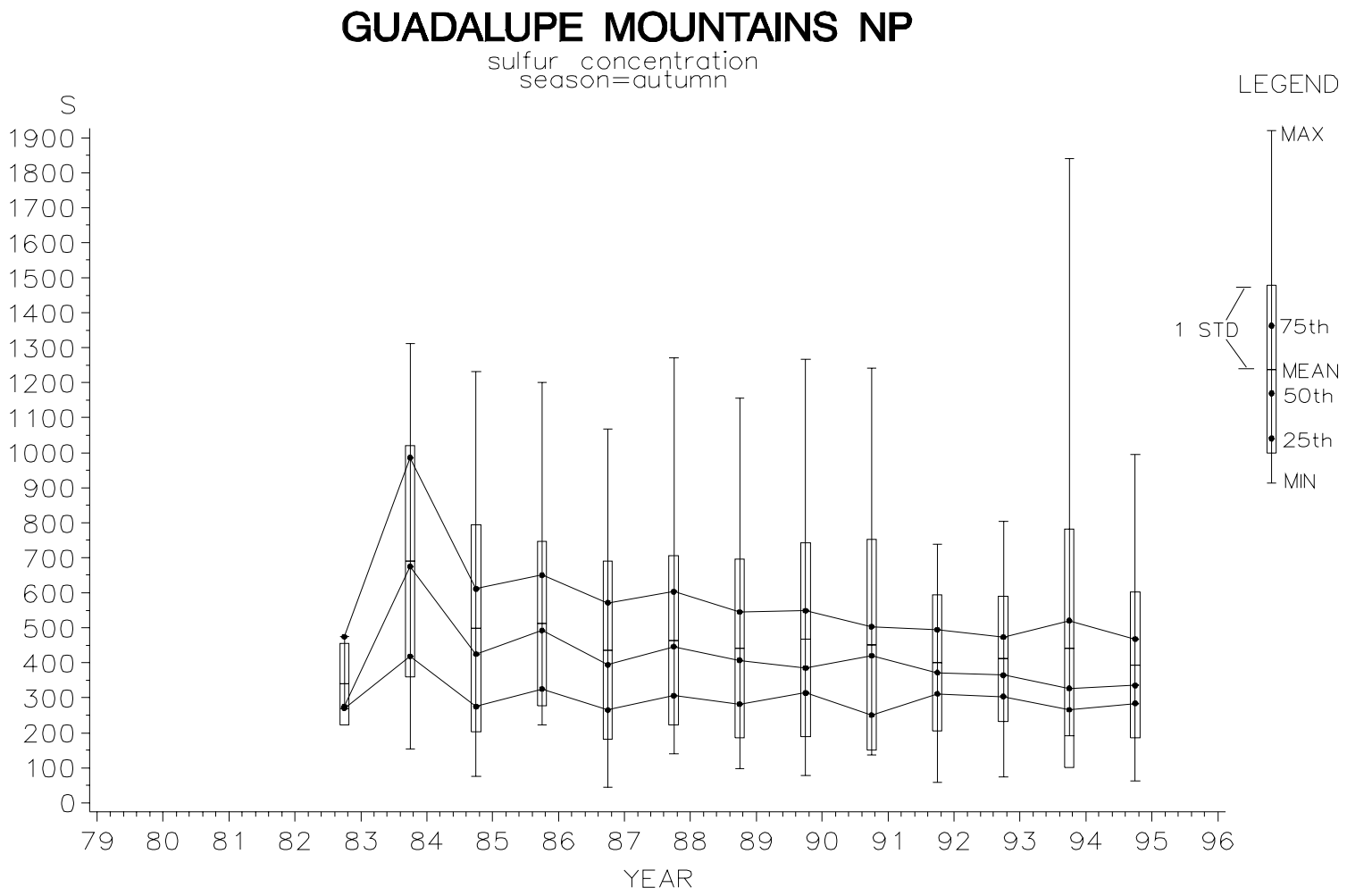

Figure 6.6b Monthly statistics for sulfur concentration (ng/m^3) at Guadalupe Mountains National Park in the autumn.

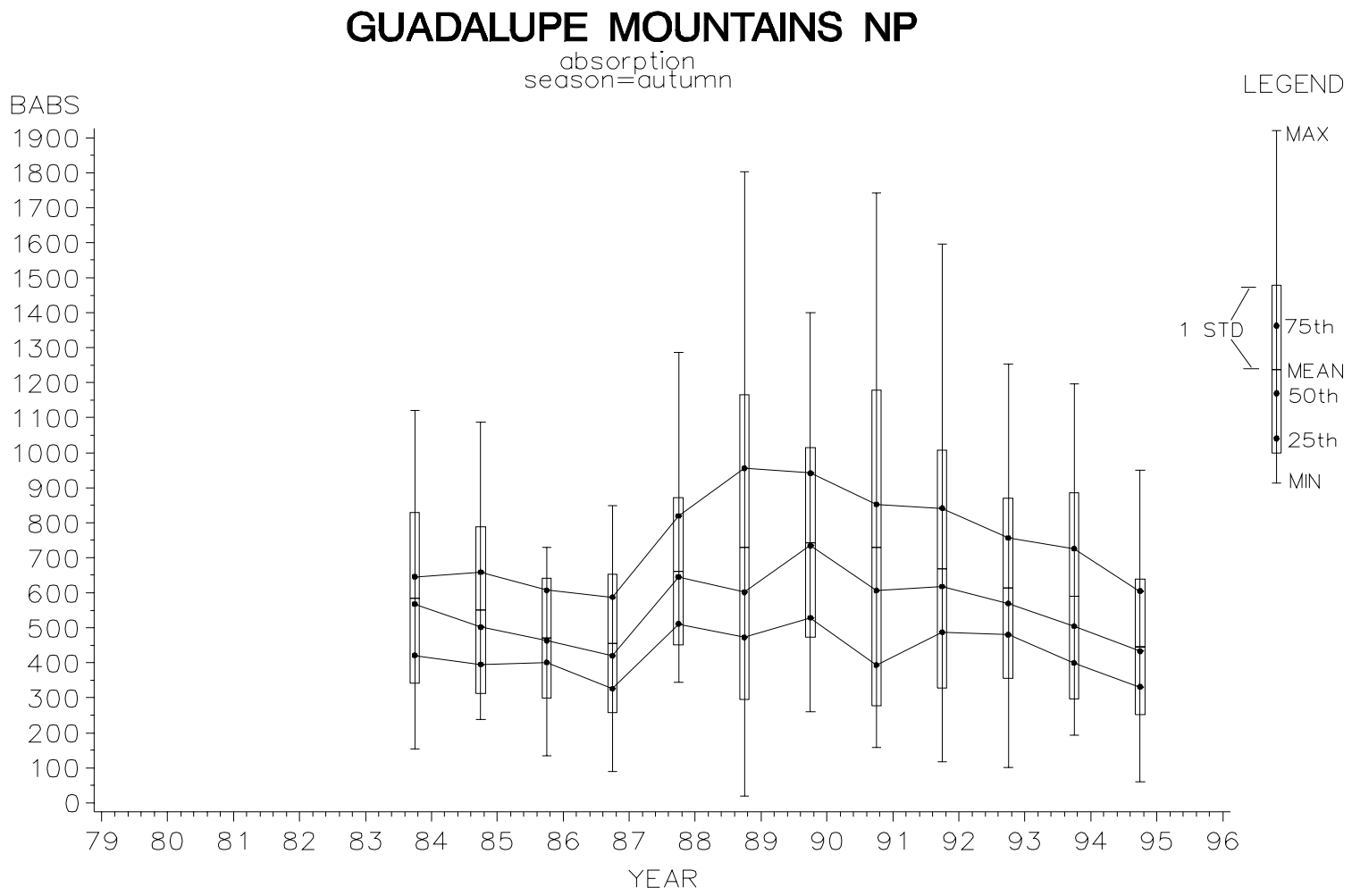

Figure 6.6c Monthly statistics for absorption (ng/m^3) at Guadalupe Mountains National Park in the autumn.

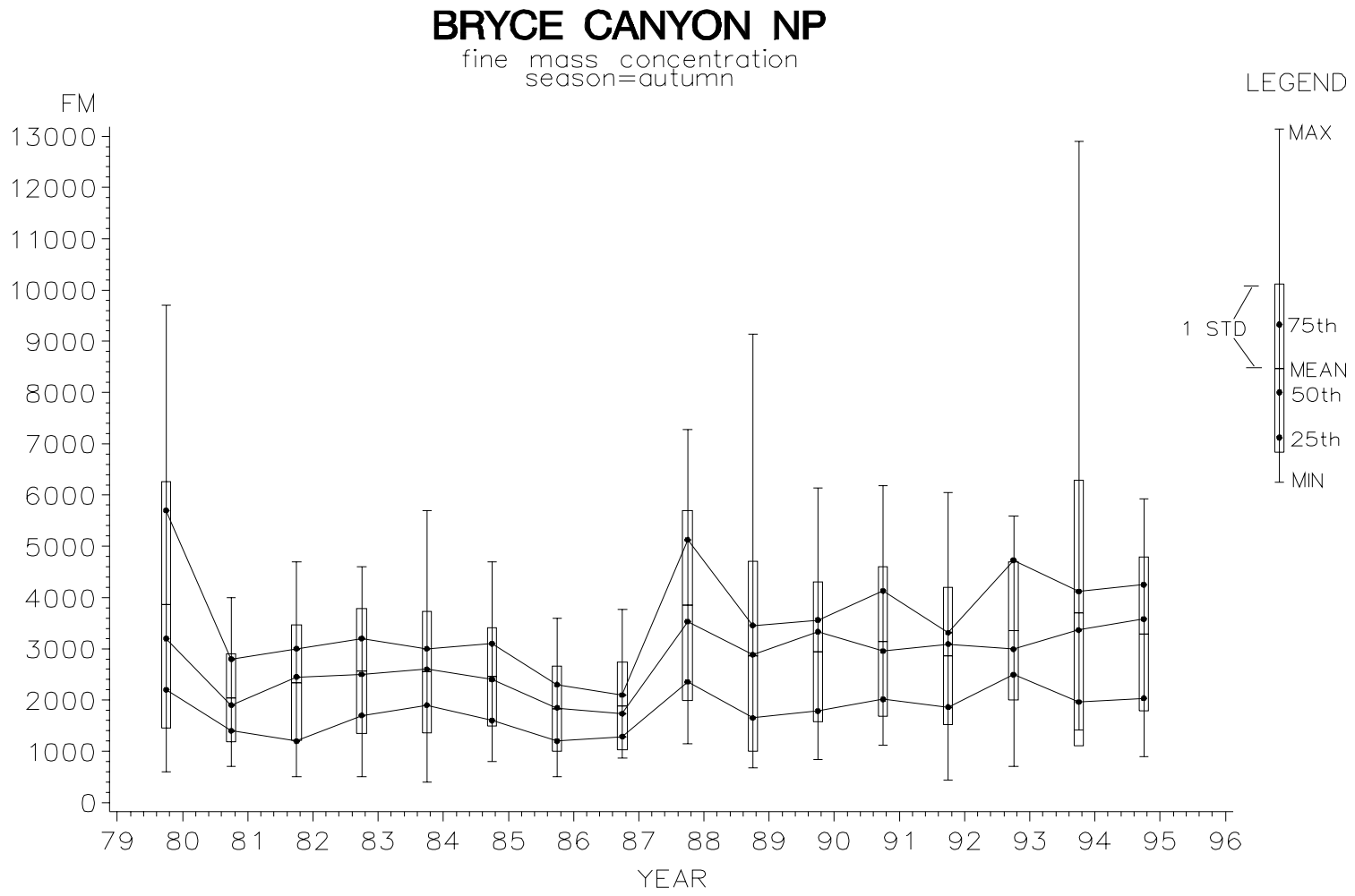

Figure 6.7a Monthly statistics for fine mass concentration (ng/m^3) at Crater Lake National Park in the winter.

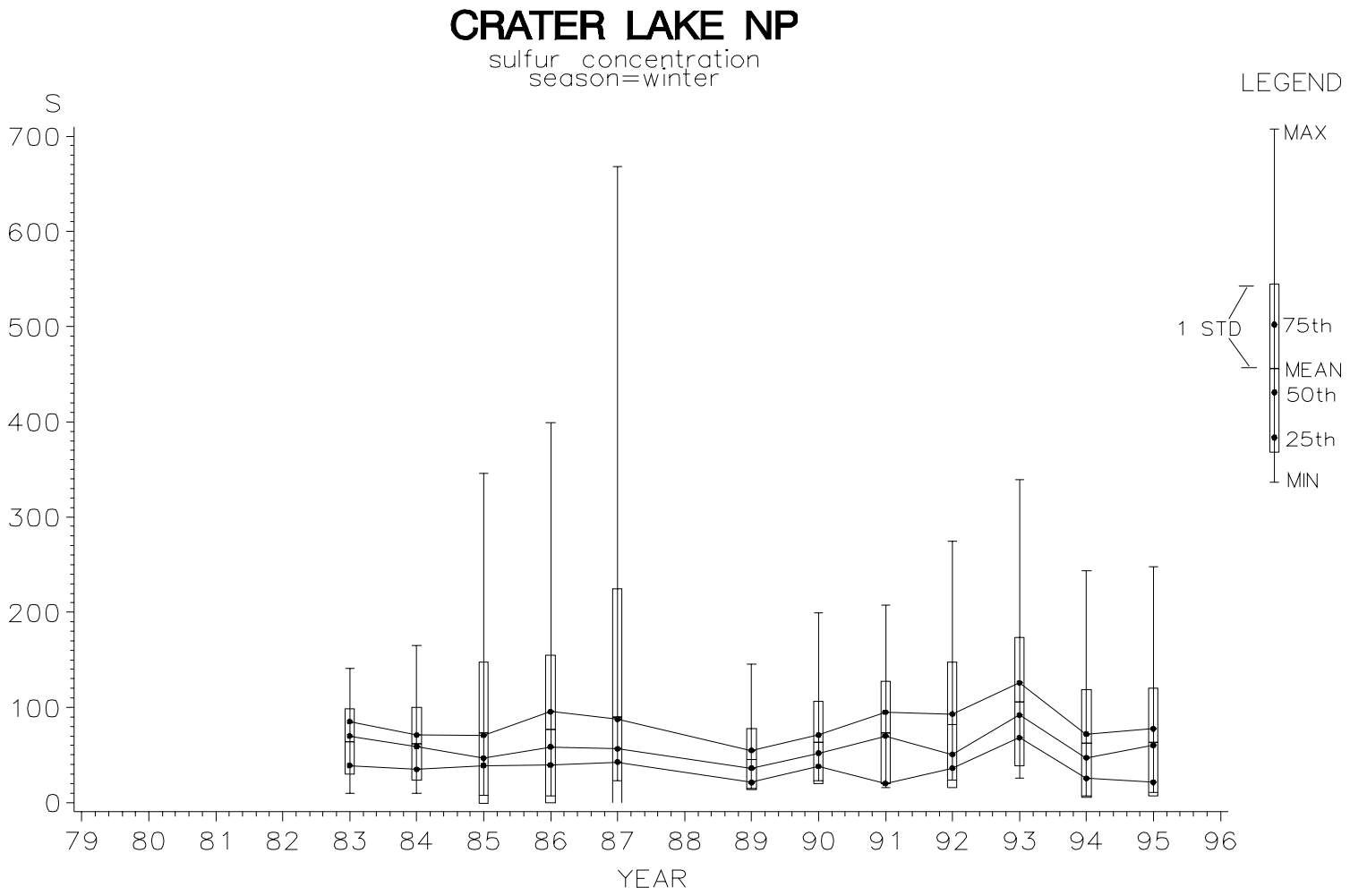

Figure 6.7b Monthly statistics for sulfur concentration (ng/m^3) at Crater Lake National Park in the winter.

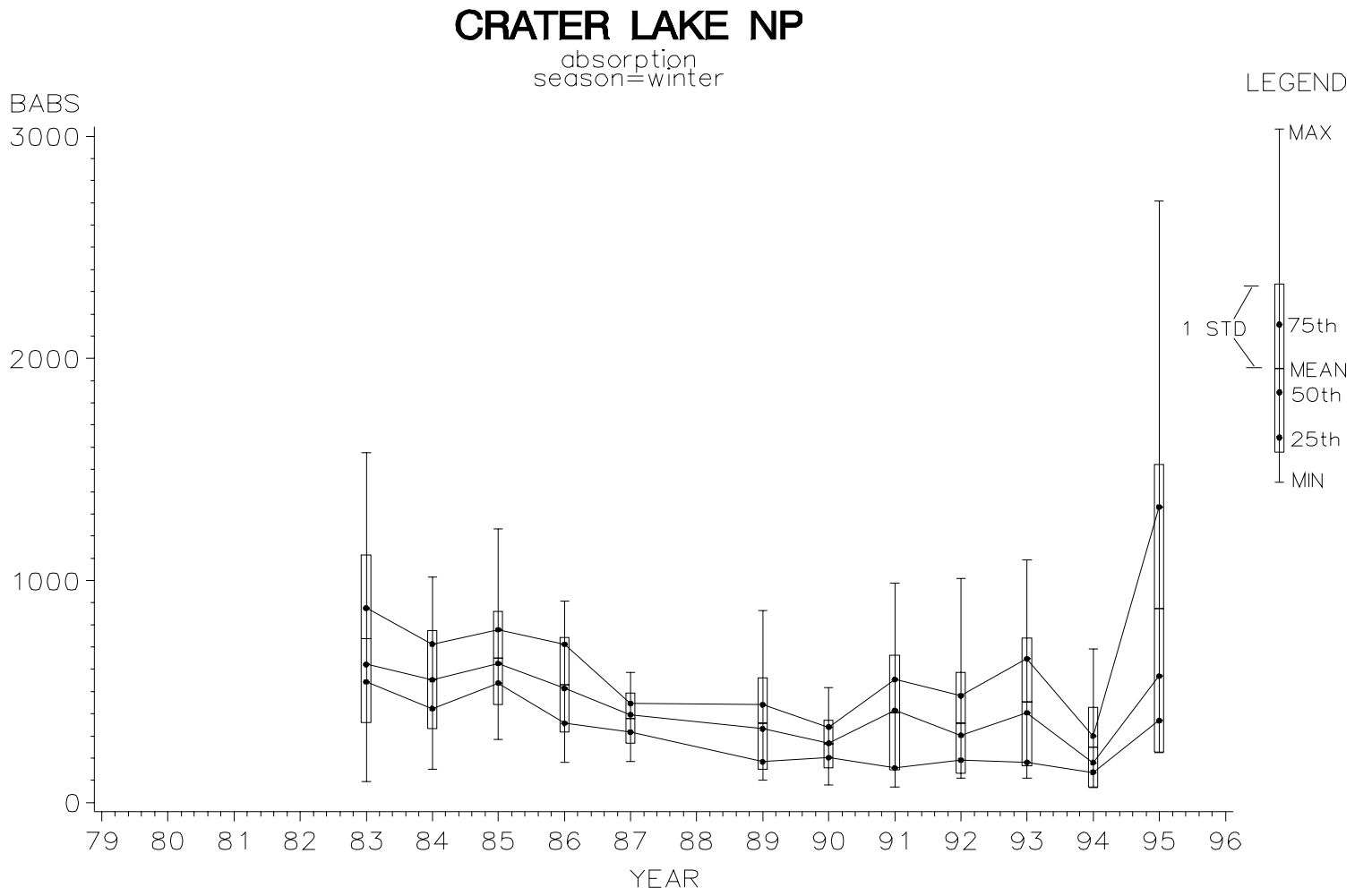

Figure 6.7c Monthly statistics for absorption (ng/m^3) at Crater Lake National Park in the winter.

6.4.5 Great Smoky Mountains National Park

Great Smoky Mountains in the autumn (Figure 6.8a) displays constant levels of fine mass concentrations for the 50th percentile at about 9000 ng/m^3. The 75th percentile obtains its maximum in 1990 at about 21000 ng/m^3 then drops steadily to 13000 ng/m^3 by 1995. There is a large decline in medium concentration coincident with the SFU to IMPROVE change in 1987-1988. However, because this type of change is not seen at other sites or at this site in other seasons, it is believed to be coincidental.

The median sulfur concentration (Figure 6.8b) is high in 1986 at about 1500 ng/m^3 then drops to a low of about 800 ng/m^3 in 1988. After 1988, with the exception of a sharp decrease in 1992, the median sulfur concentration increases to its maximum of about 1700 ng/m^3 in 1993 then pulls back to about 1100 ng/m^3 by 1994.

Absorption (Figure 6.8c) demonstrates an increasing trend. The median value, with slight variability, increased from about 900 ng/m^3 in the autumn of 1985 to greater than 1500 ng/m^3 in 1994. The 75th percentile shows a similar rise from about 1200 ng/m^3 in 1985 to almost 2000 ng/m^3 in 1991 and 1993. A similar trend is displayed by the 25th percentile, rising from about 600 ng/m^3 to almost 1000 ng/m^3. In 1994, the 75th and 50th percentiles decrease sharply from the high in 1993 to about 1600 ng/m^3 and 1200 ng/m^3, respectively, but only a slight decrease is seen for the 25th percentile.

6.4.6 Mesa Verde National Park

Fine mass concentrations during the summer at Mesa Verde (Figure 6.9a) demonstrates an interesting trend. The 25th percentile, beginning in 1986, increased dramatically from around 2200 ng/m^3 to 5000 ng/m^3 in 1990, then dropped off sharply to 3000 ng/m^3 by 1992. The same trend is closely mirrored by the 50th percentile and to a lesser extent by the 75th percentile, which rose from about 4000 ng/m^3 in 1985 to almost 8500 ng/m^3 in 1990 and then drops back to 4000 ng/m^3 in 1992. Since 1992 all percentiles have increased significantly; the 75th from 4000 ng/m^3 to 5000 ng/m^3; the 50th from about 3300 ng/m^3 to almost 4000 ng/m^3; and the 25th rose from about 3000 ng/m^3 to almost 3400 ng/m^3.

Median concentrations of sulfur at Mesa Verde (Figure 6.9b) are highest during the first two measurement summers of 1983 and 1984 at about 400 ng/m^3, then decrease to their minimum in 1987 at less than 200 ng/m^3. This same pattern is shown by the 25th percentiles and 75th percentiles, with the 25th percentile decreasing from 340 ng/m^3 to about 120 ng/m^3. After 1987 the 25th percentile increased every year except two, obtaining a level of about 280 ng/m^3 in 1994. The 50th percentile and 75th percentile rise to about 320 ng/m^3 and 440 ng/m^3 by 1990, respectively. After 1990 the 50th percentile essentially hovers about 320 ng/m^3 and the 75th percentile drops by to around 380 ng/m^3.

Absorption (Figure 6.9c) shows a similar trend as sulfur with its maximum median of about 650 ng/m^3 in 1983 and minimum median of 400 ng/m^3 in 1987. Median absorption then increases with sulfur to another high in 1990 of about 550 ng/m^3 then generally decreases to 450 ng/m^3. The 25th percentile decreased from 480 ng/m^3 in 1983 to 280 ng/m^3 in 1986 increased to

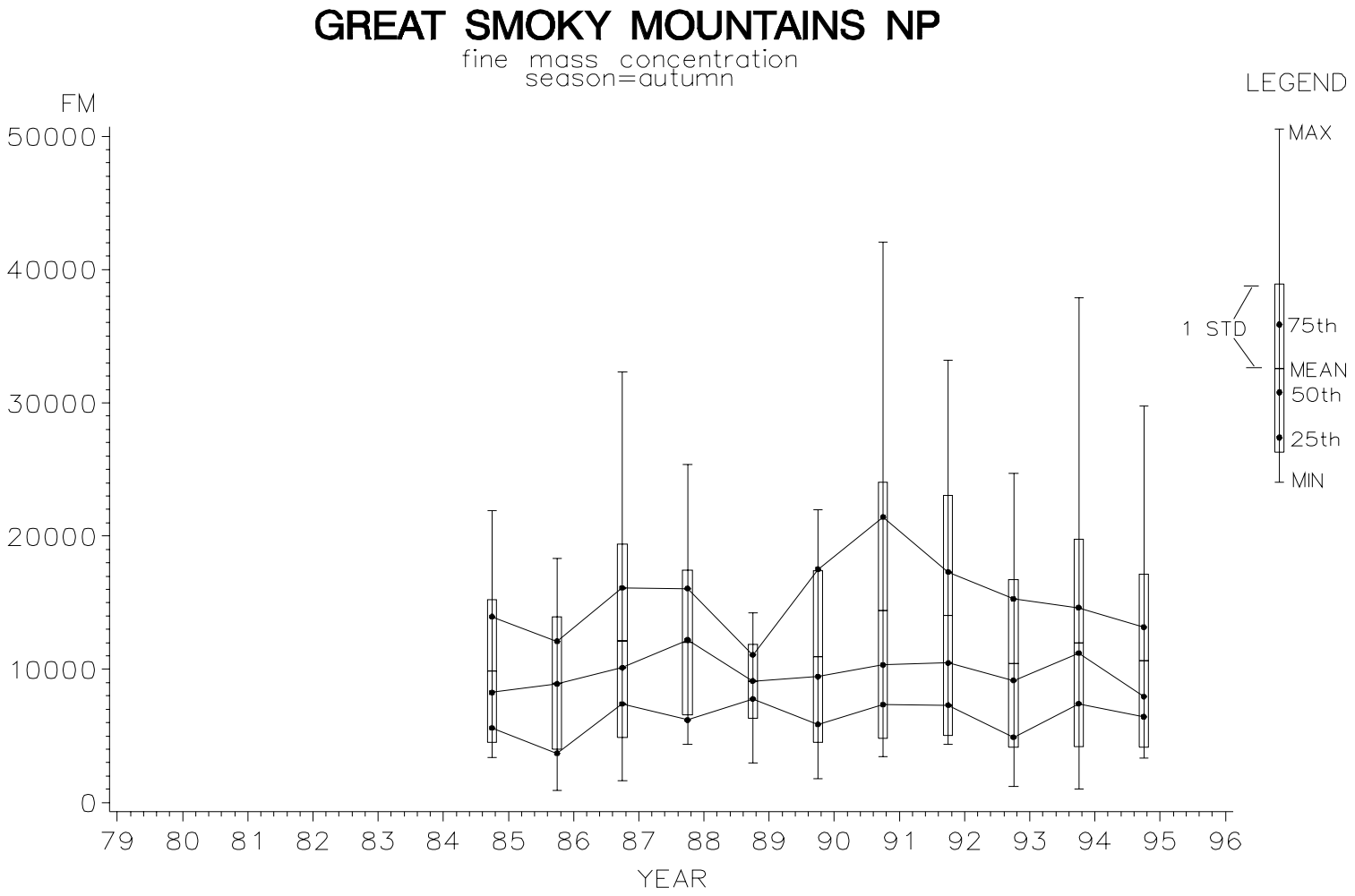

Figure 6.8a Monthly statistics for fine mass concentration (ng/m^3) at Great Smoky Mountains National Park in the autumn.

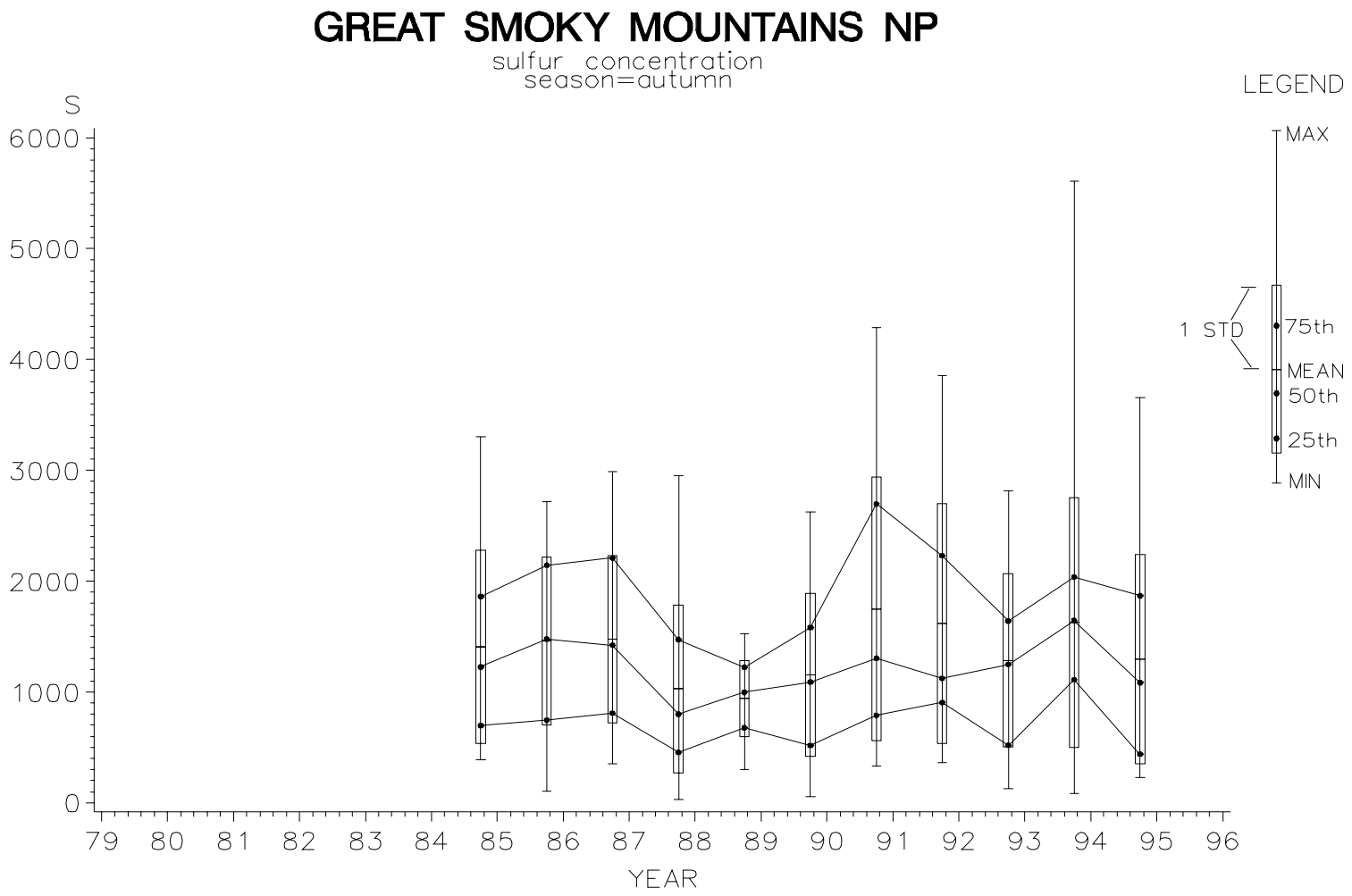

Figure 6.8b Monthly statistics for sulfur concentration (ng/m^3) at Great Smoky Mountains National Park in the autumn.

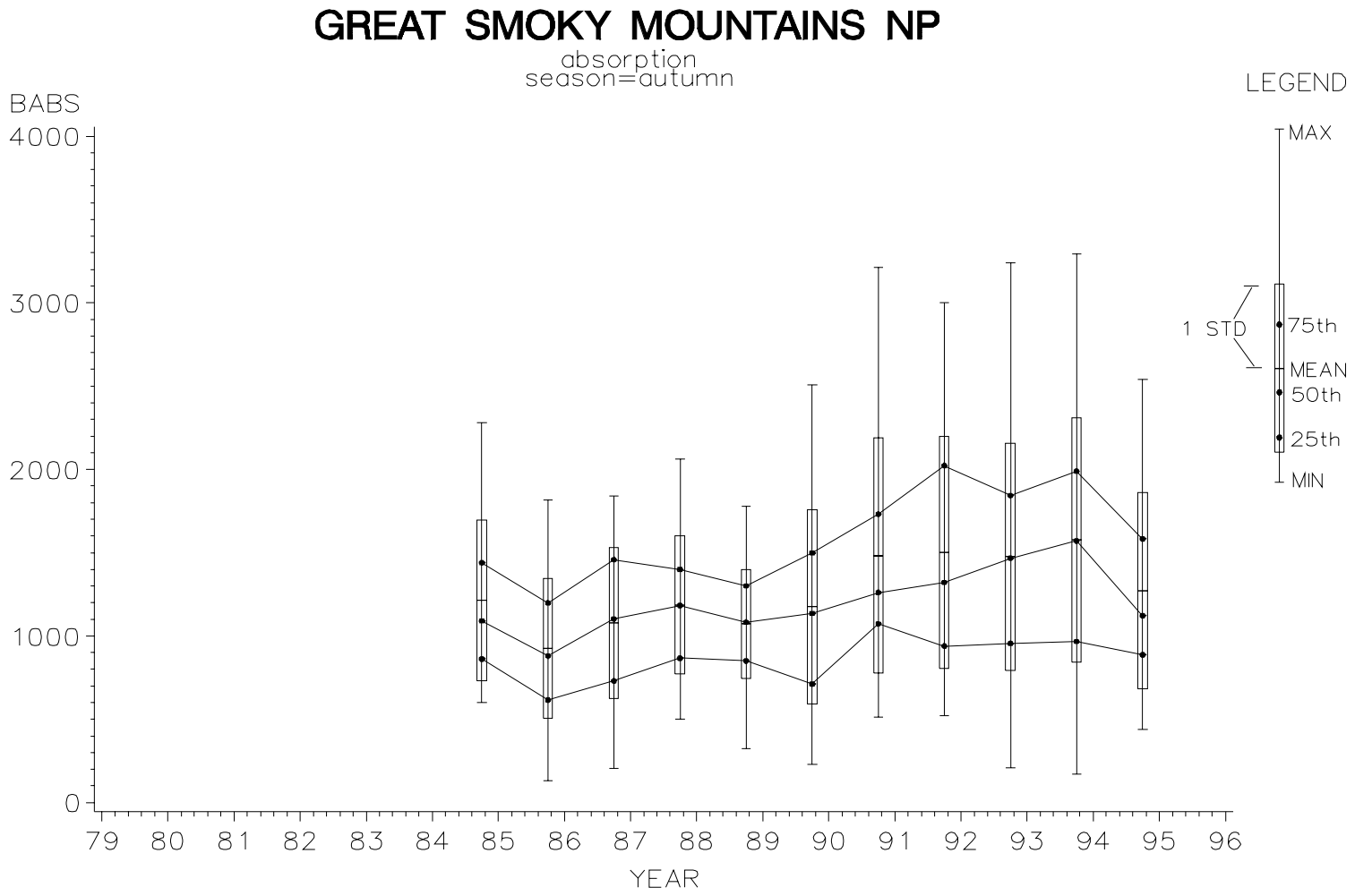

Figure 6.8c Monthly statistics for absorption (ng/m^3) at Great Smoky Mountains National Park in the autumn.

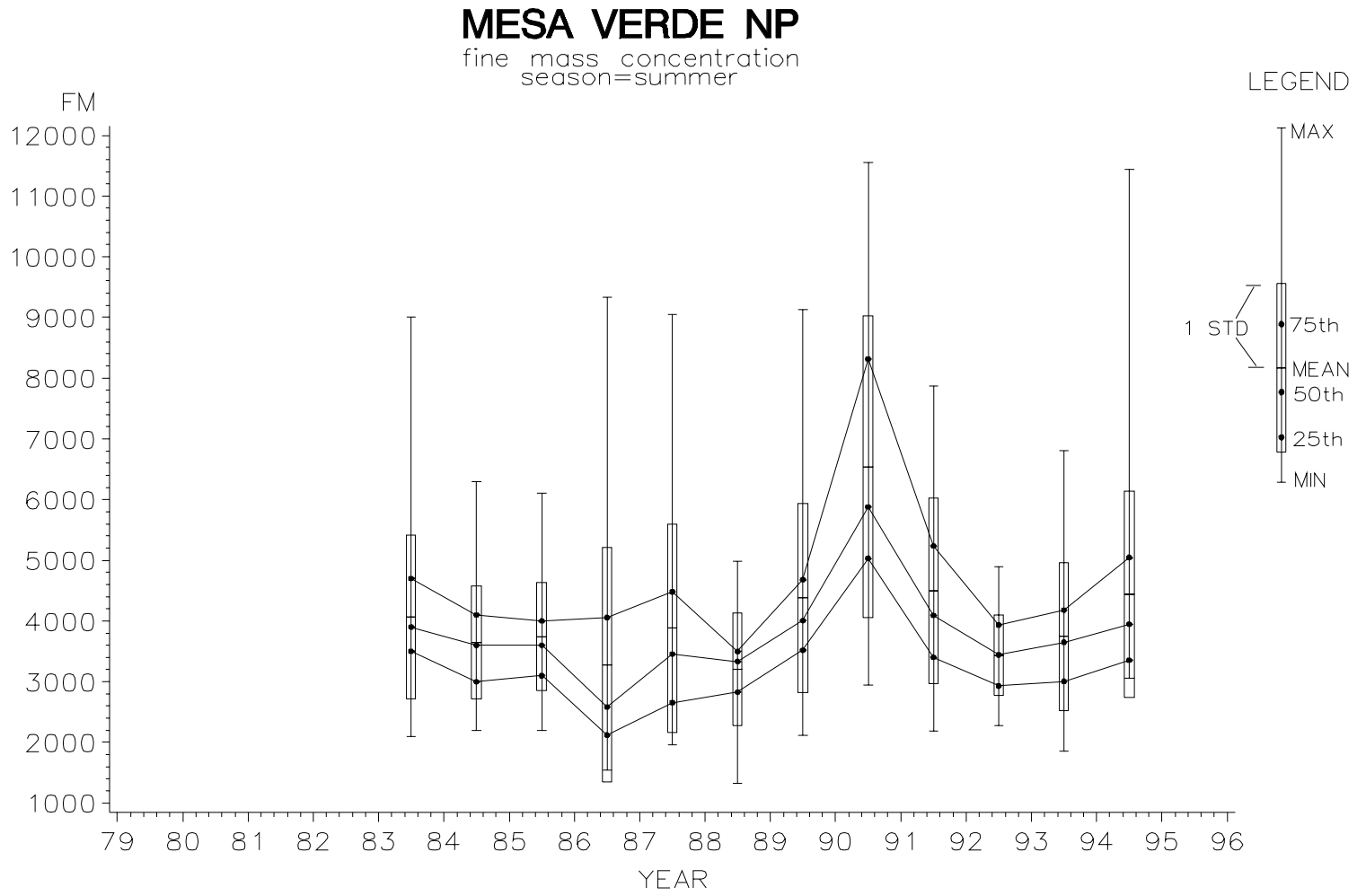

Figure 6.9a Monthly statistics for fine mass concentration (ng/m^3) at Mesa Verde National Park in the summer.

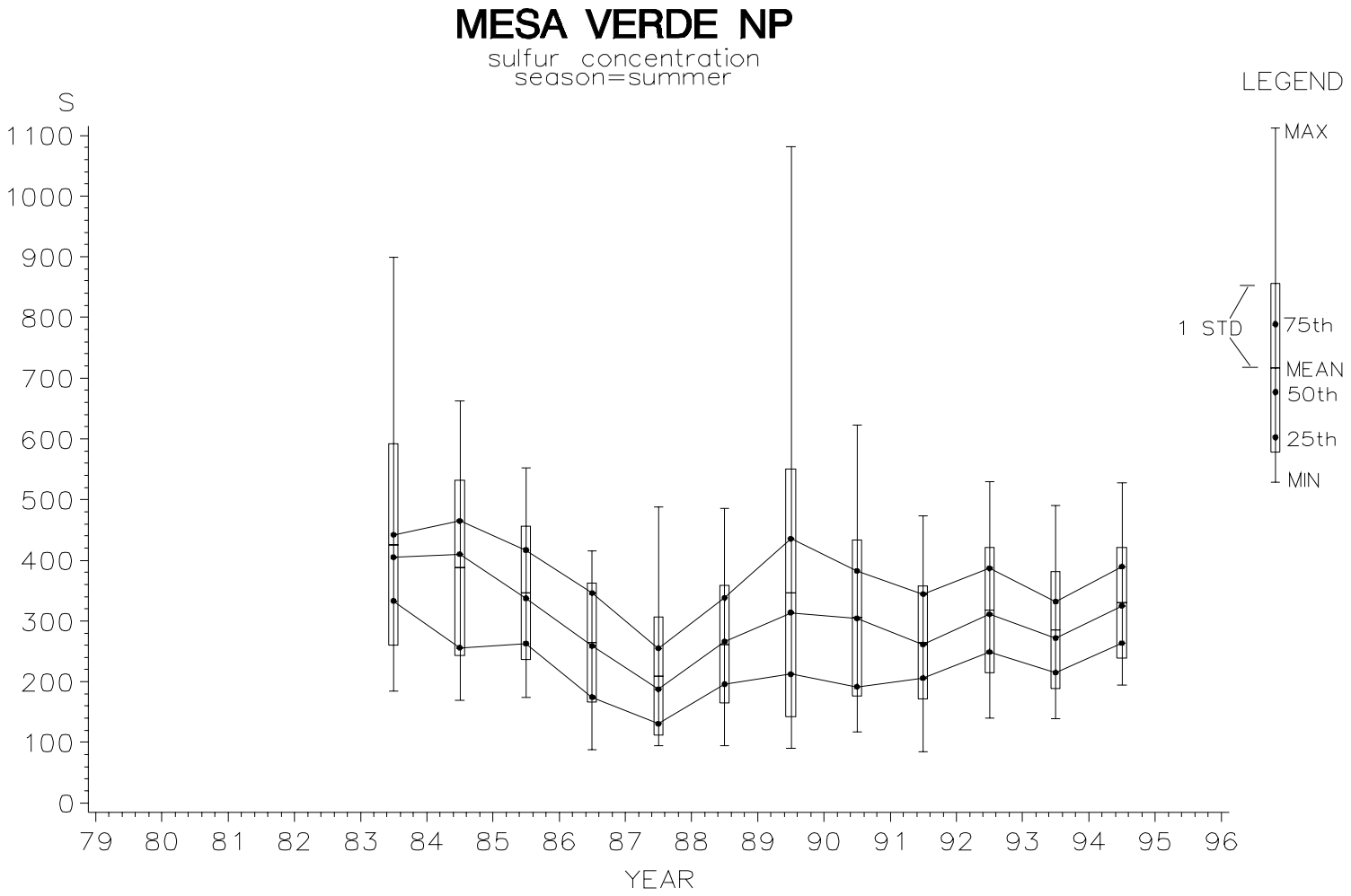

Figure 6.9b Monthly statistics for sulfur concentration (ng/m^3) at Mesa Verde National Park in the summer.

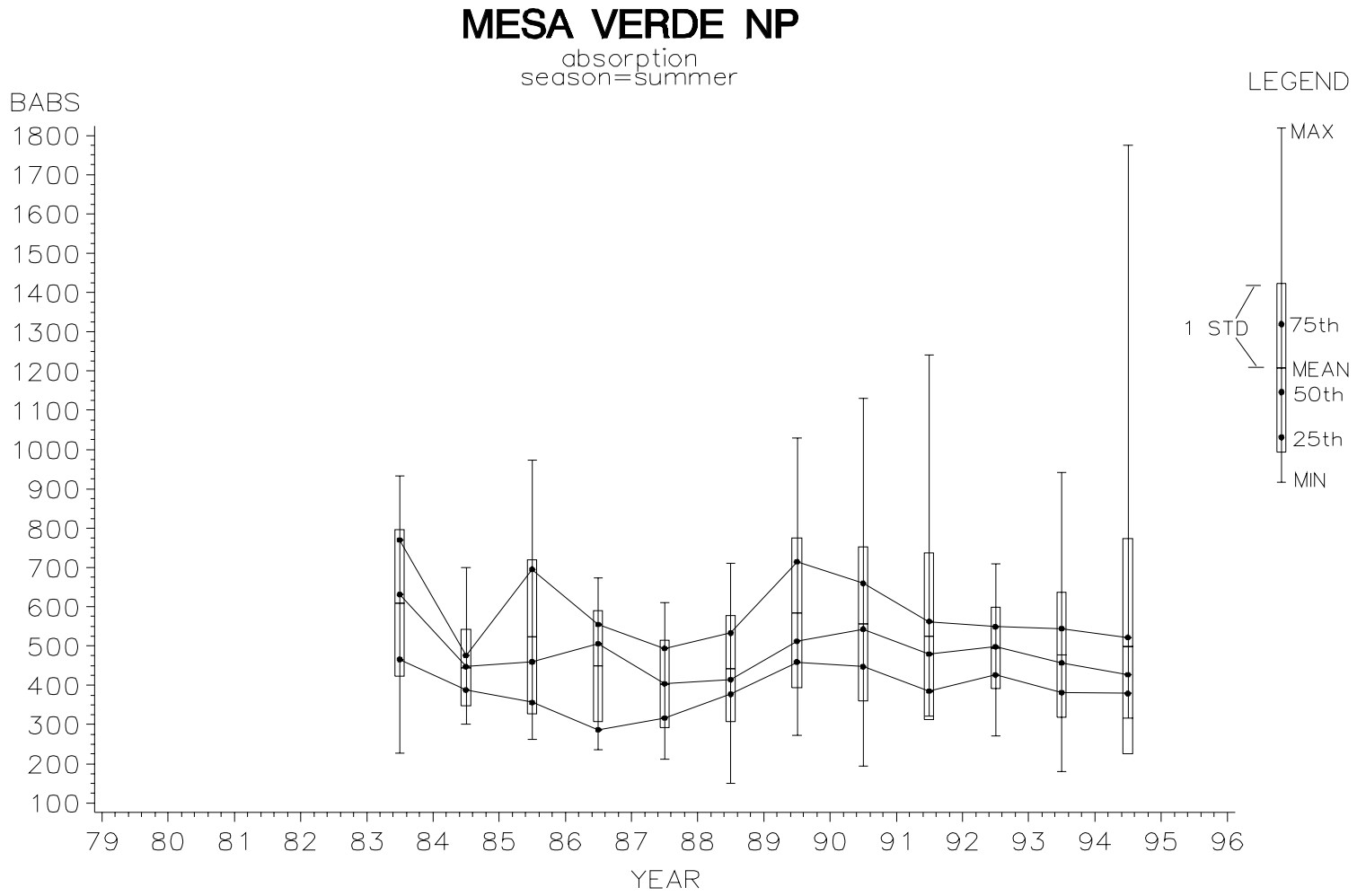

Figure 6.9c Monthly statistics for absorption (ng/m^3) at Mesa Verde National Park in the summer.

almost 460 ng/m^3 by 1989. The 75th percentile has a similar pattern with a high value of about 800 ng/m^3, then decreasing to 480 ng/m^3 in 1987 before rising again to almost 700 ng/m^3 in 1990. After 1990 the 75th percentile drops steadily to about 460 ng/m^3, the 50th and 25th percentile are trending down as well but not as dramatically.

6.4.7 Chiricahua National Monument

Fine mass concentrations at Chiricahua (Figure 6.10a) during the summer show little change. The only notable feature is the spike in 1990 for the 75th percentile at over 11000 ng/m^3, which then drops sharply to little more than 5000 ng/m^3 by 1992, followed by an increase to about 7500 ng/m^3 in 1994. The 25th and 50th percentiles do not demonstrate any trends. The 75th percentile varies between its high of almost 7000 ng/m^3 in the summer of 1981 and its low of about 4500 ng/m^3, while the 25th percentile varies between 5500 ng/m^3 in 1981 and 3000 ng/m^3 in 1987.

A particular point of interest is to what extent are changes in emissions reflected by changes in sulfur concentrations. Large fluctuations in smelter emissions have occurred in the desert southwest during the 1980s, providing an opportunity to study the relationship between emissions and aerosol sulfur concentrations. In the intermountain region between the continental divide and the Sierra Nevada, 90% of United States emissions were from 15 power plants and 12 smelters. Seven of the smelters were located in southern Arizona. Since the late 1980s, four of the seven Arizona smelters were shut down and the rest were controlled [Sisler and Malm, 1989; Oppenheimer, 1987; Epstein and Oppenheimer, 1986]. The reduction in smelter emissions is evident from the change in sulfur distributions at Chiricahua during the summer as shown in Figure 6.10b. Beginning in 1987 the variance drops considerably. There is no appreciable change in the minima and 25th percentile values, so the reduction in variance is attributed to reduced medians, means, 75th percentiles, and maxima. From 1988 through 1990 median concentrations increase from 350 ng/m^3 to about 650 ng/m^3 then drop to 400 ng/m^3 in 1991. Since 1991 there has been a steady increase to about 650 ng/m^3 by the median.

Absorption shows no consistent trend (Figure 6.10c). The median, from its high in 1983 of about 700 ng/m^3, decreases for the next three out of four years to its low in 1987 of 400 ng/m^3, then rises again to a high value of 700 ng/m^3 in 1989. Since 1989, there appears to have been a slight decline in median absorption.

6.4.8 Grand Canyon National Park - Winter

Figure 6.11a shows the winter distributions at Hopi Point in Grand Canyon for fine mass concentrations. Winter distributions are notable for the very high maxima in 1980 and 1987 at almost 25000 ng/m^3 and 18000 ng/m^3, respectively. There has been a significant increase in the 25th percentile, which starts out less than 1000 ng/m^3 then rising to almost 2000 ng/m^3 by 1989. After falling back slightly to 1500 ng/m^3, the 25th percentile essentially stays flat until 1994 when it drops back to about 1000 ng/m^3. The same behavior, although somewhat more variable, is displayed by the 50th percentile and 75th percentile, a maximum of about 4000 ng/m^3 and 2500 ng/m^3 are obtained in 1989, respectively. After 1989 the 75th and 50th percentiles drop to about 2000 ng/m^3 and 1500 ng/m^3, respectively.

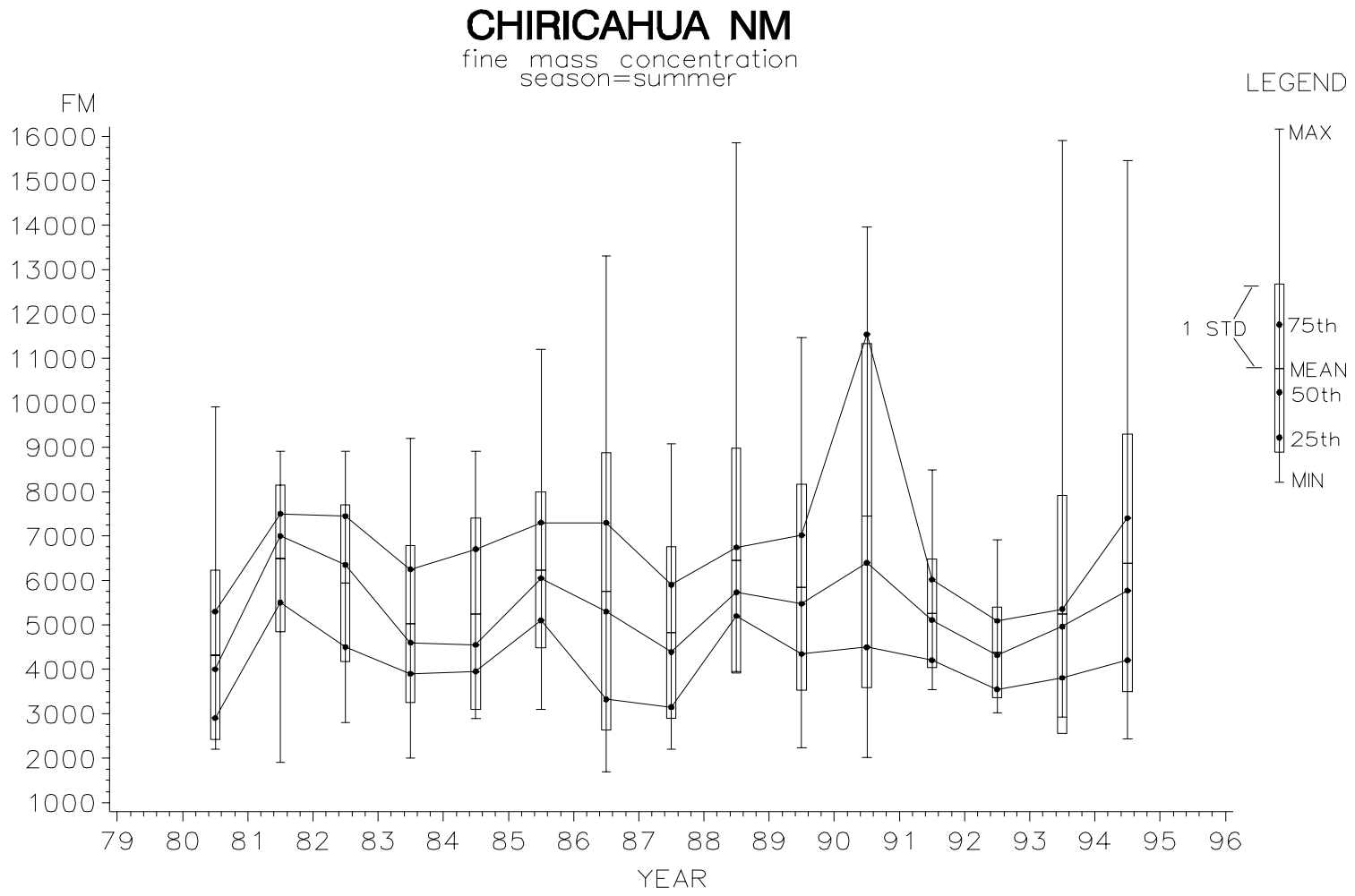

Figure 6.10a Monthly statistics for fine mass concentration (ng/m^3) at Chiricahua National Monument in the summer.

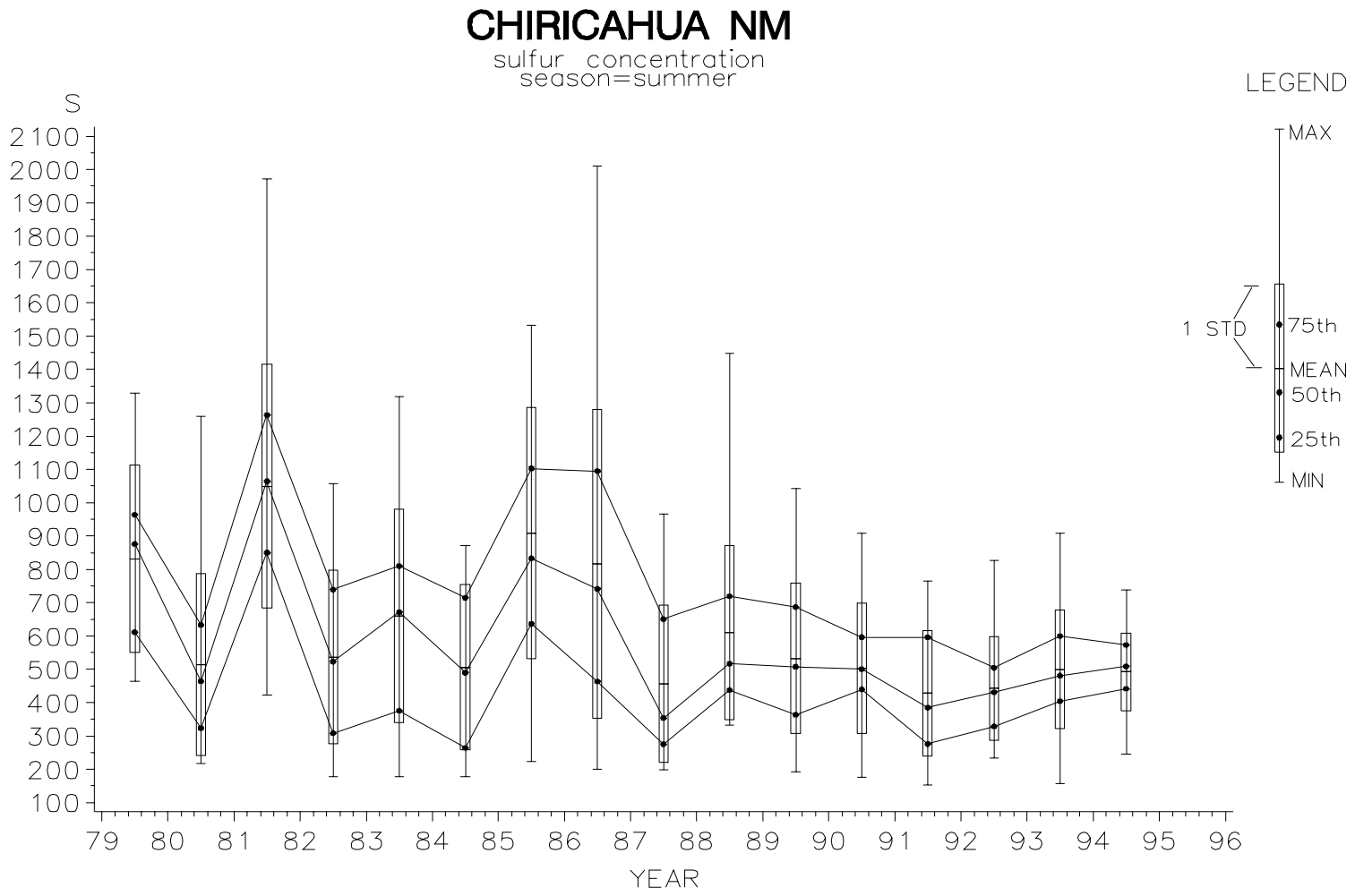

Figure 6.10b Monthly statistics for sulfur concentration (ng/m^3) at Chiricahua National Monument in the summer.

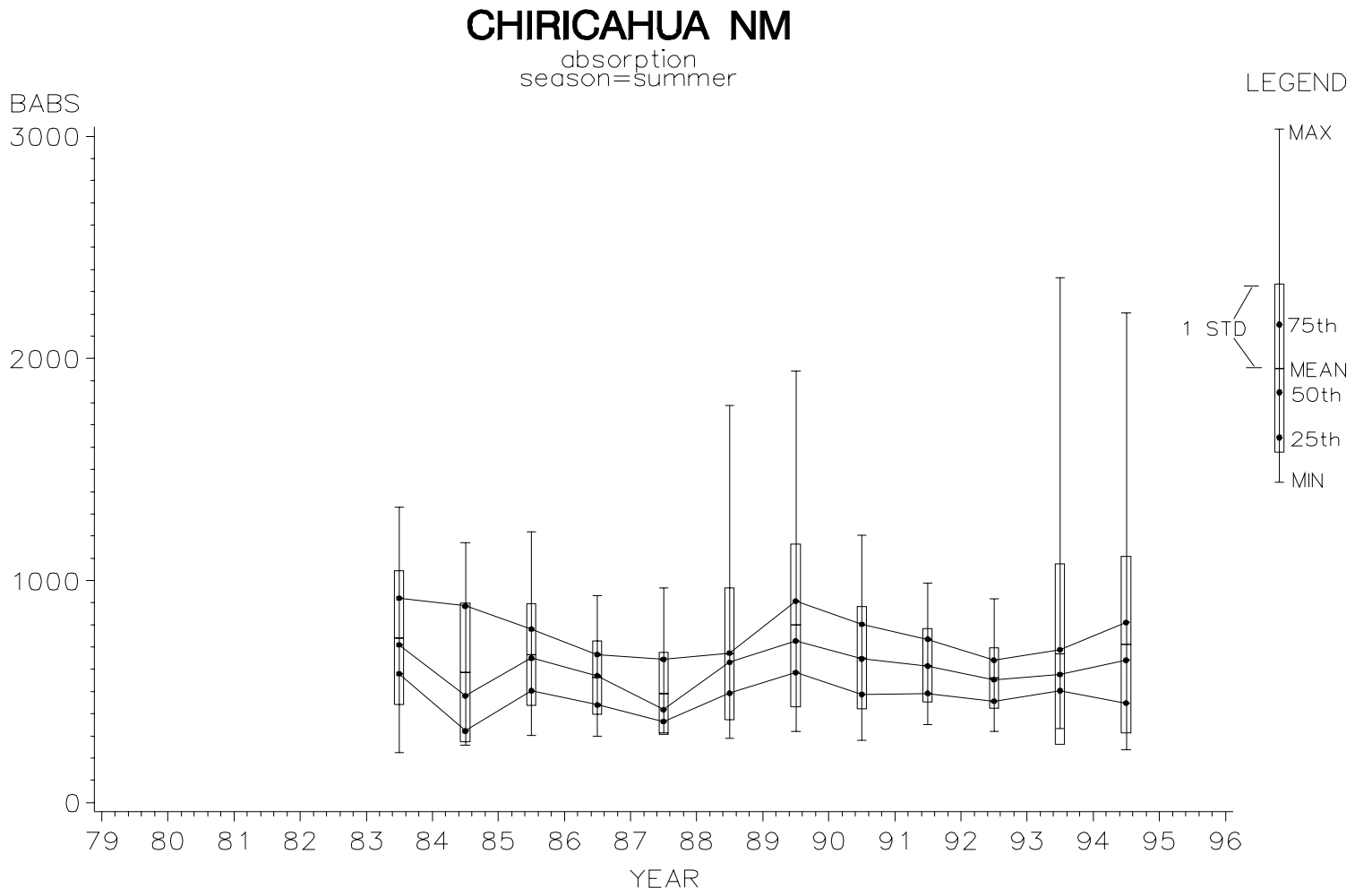

Figure 6.10c Monthly statistics for absorption (ng/m^3) at Chiricahua National Monument in the summer.

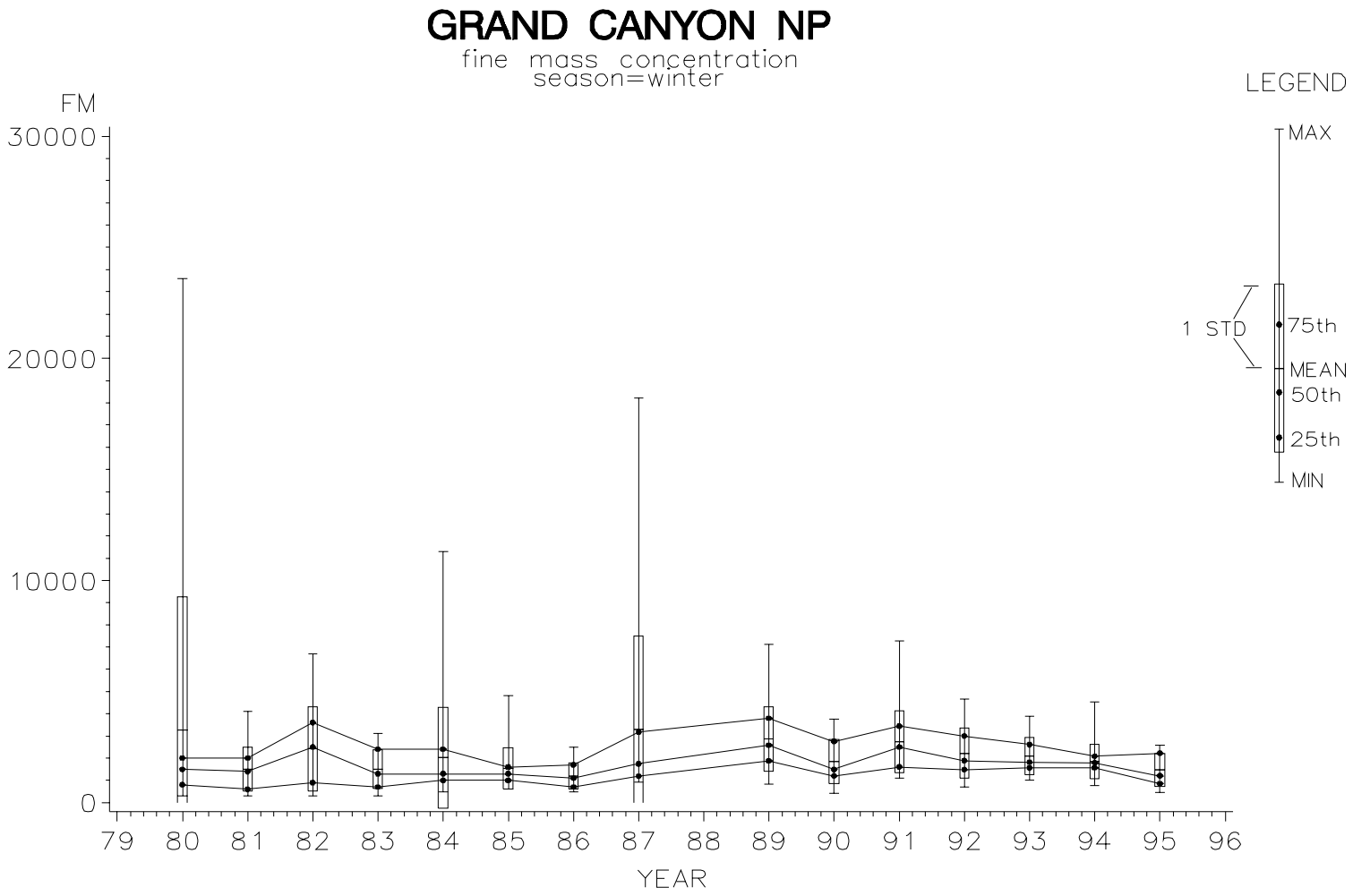

Figure 6.11a Monthly statistics for fine mass concentration (ng/m^3) at Grand Canyon National Park in the winter.

Sulfur concentrations show two distinct trends for the 25th percentile (Figure 6.11b). For the first four years the 25th percentile concentration is essentially flat at about 50 ng/m^3 then rises to over 120 ng/m^3 for 1991, 1992 and 1993. By 1995 it has dropped back to about 50 ng/m^3. This same pattern is displayed with more variance by the 50th percentile rising from its lowest value of about 60 ng/m^3 in 1982 to almost 200 ng/m^3 by 1992, then dropping off to 100 ng/m^3 by 1995. No trend is apparent for the 75th percentile.

Absorption (Figure 6.11c) shows a similar trend as sulfate. Levels start out low in 1983 and 1984 with concentrations about 100 ng/m^3, 200 ng/m^3, and 300 ng/m^3 for the 25th, 50th and 75th percentiles, respectively. By 1989 the 25th and 75th percentiles reach their maxima of 250 ng/m^3 and 550 ng/m^3, respectively, the 50th percentile obtains its maximum of about 400 ng/m^3 in 1991. After 1991 concentration levels drop significantly and steadily until 1995 to about 75 ng/m^3, 125 ng/m^3, and 200 ng/m^3 for the 25th, 50th and 75th percentile, respectively.

6.4.9 Grand Canyon National Park - Summer

Fine mass concentrations have significantly increased during the summers since 1980 (Figure 6.12a). It is particularly obvious by the rise in the 25th percentile almost doubling from about 1500 ng/m^3 in 1981 to almost 3000 ng/m^3 in 1994. A similar trend is seen for the 50th percentile, which has increased from about 2500 ng/m^3 in 1981 to about 4500 ng/m^3 in 1994. The 75th percentile, after some initial variance, has increased from 4000 ng/m^3 in 1984 to about 6000 ng/m^3 in 1994. This trend is also played out by the minima. In 1980 and 1981 the minima were about 500 ng/m^3, however during the last three years (1993-1995) the minima concentrations are about 3000 ng/m^3.

Figure 6.12b shows the summer distributions of sulfur at Hopi Point. Beginning in 1980, sulfur has median values that trend up from about 210 ng/m^3 to about 400 ng/m^3 in 1985, then fall to 200 ng/m^3 in 1987. From 1988 through 1993 the median for sulfur is quite stable and ranges between 250 ng/m^3 to about 325 ng/m^3. In 1994, the median increases to about 375 ng/m^3. The 25th percentile shows two clear trends; from a low of about 100 ng/m^3 in 1980 it increased to around 350 ng/m^3 in 1985, then drops sharply to 150 ng/m^3 in 1987. After 1987 the concentrations of the 25th percentile increase five years out of seven to more than 300 ng/m^3. A slight trend towards decreasing variability is evidenced by a decrease in standard deviations attributed to a decrease of maxima and an increase of minima.

The median value of absorption (Figure 6.12c) is lowest in 1984 at about 300 ng/m^3 then doubles to 600 ng/m^3 in 1985. From 1985 through 1994 the median remains relatively stable, ranging from a high of 700 ng/m^3 in 1989 to a low of 500 ng/m^3 in 1990, then dropping in 1995 to about 400 ng/m^3. The 25th and 75th percentiles essentially track the median rising and falling almost in lockstep. The 25th and 75th percentiles reach their maxima in 1989 of about 600 ng/m^3 and 900 ng/m^3, respectively then fall off by 1995 to about 500 ng/m^3 and 300 ng/m^3.

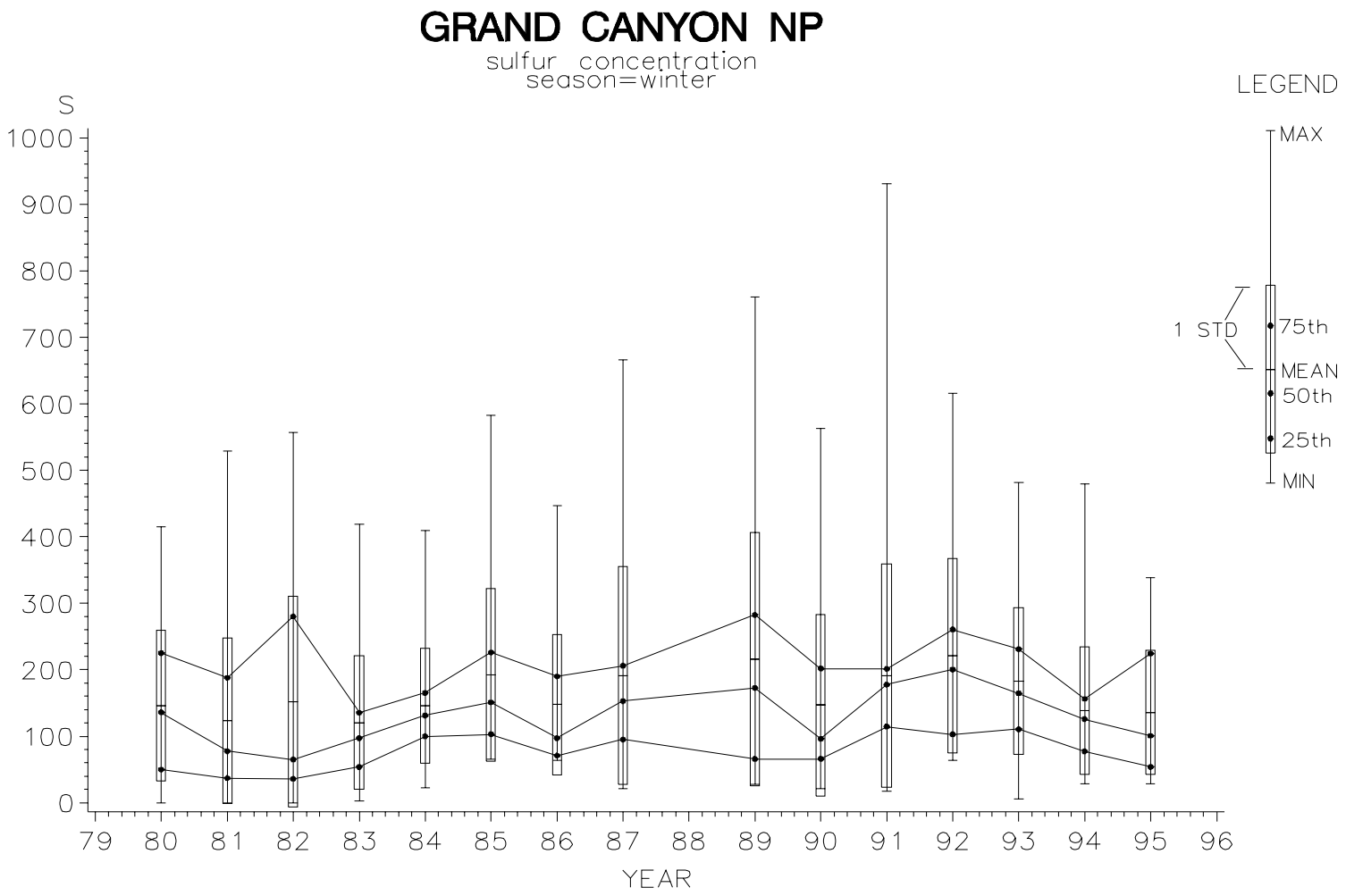

Figure 6.11b Monthly statistics for sulfur concentration (ng/m^3) at Grand Canyon National Park in the winter.

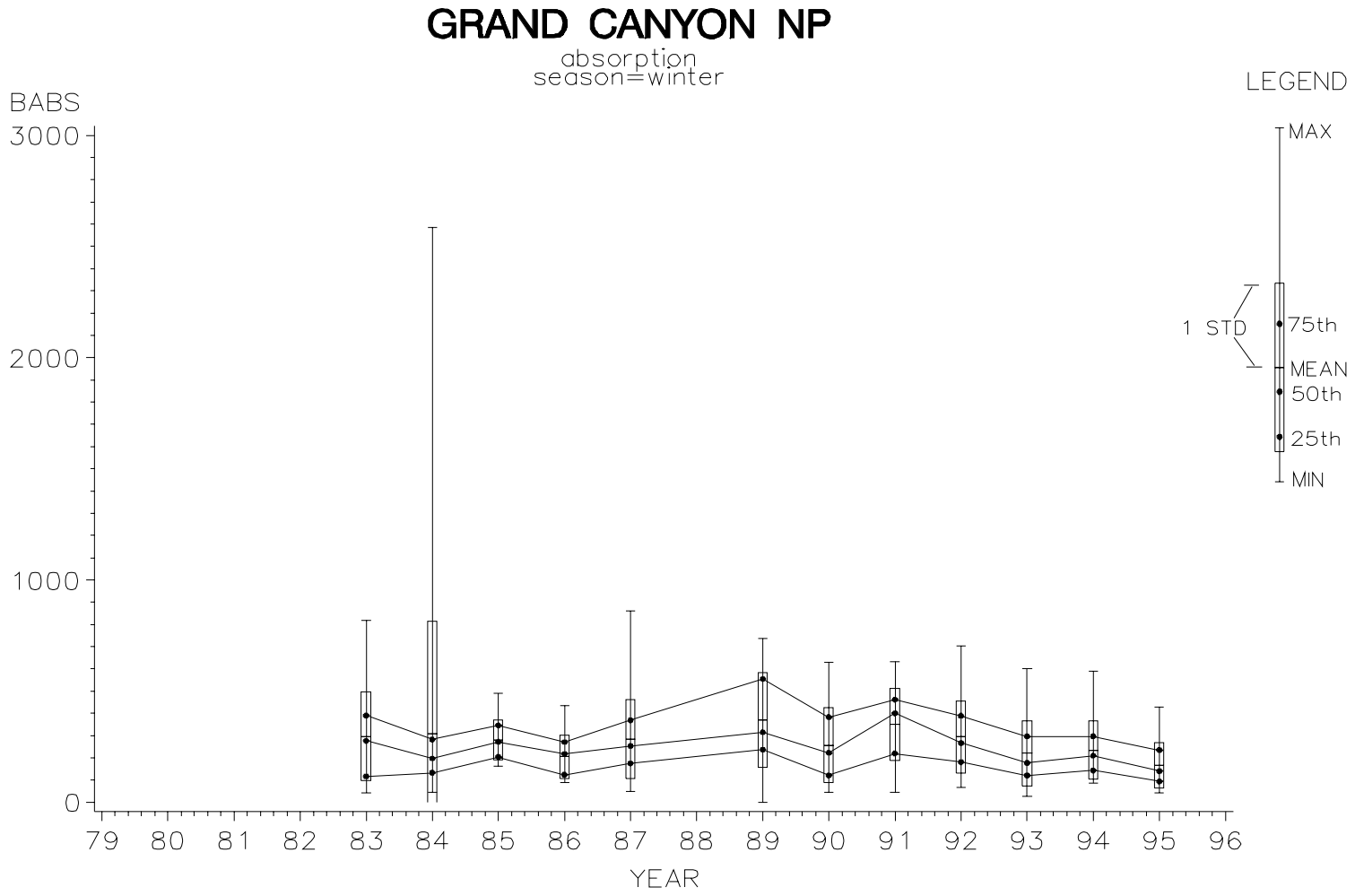

Figure 6.11c Monthly statistics for absorption (ng/m^3) at Grand Canyon National Park in the winter.

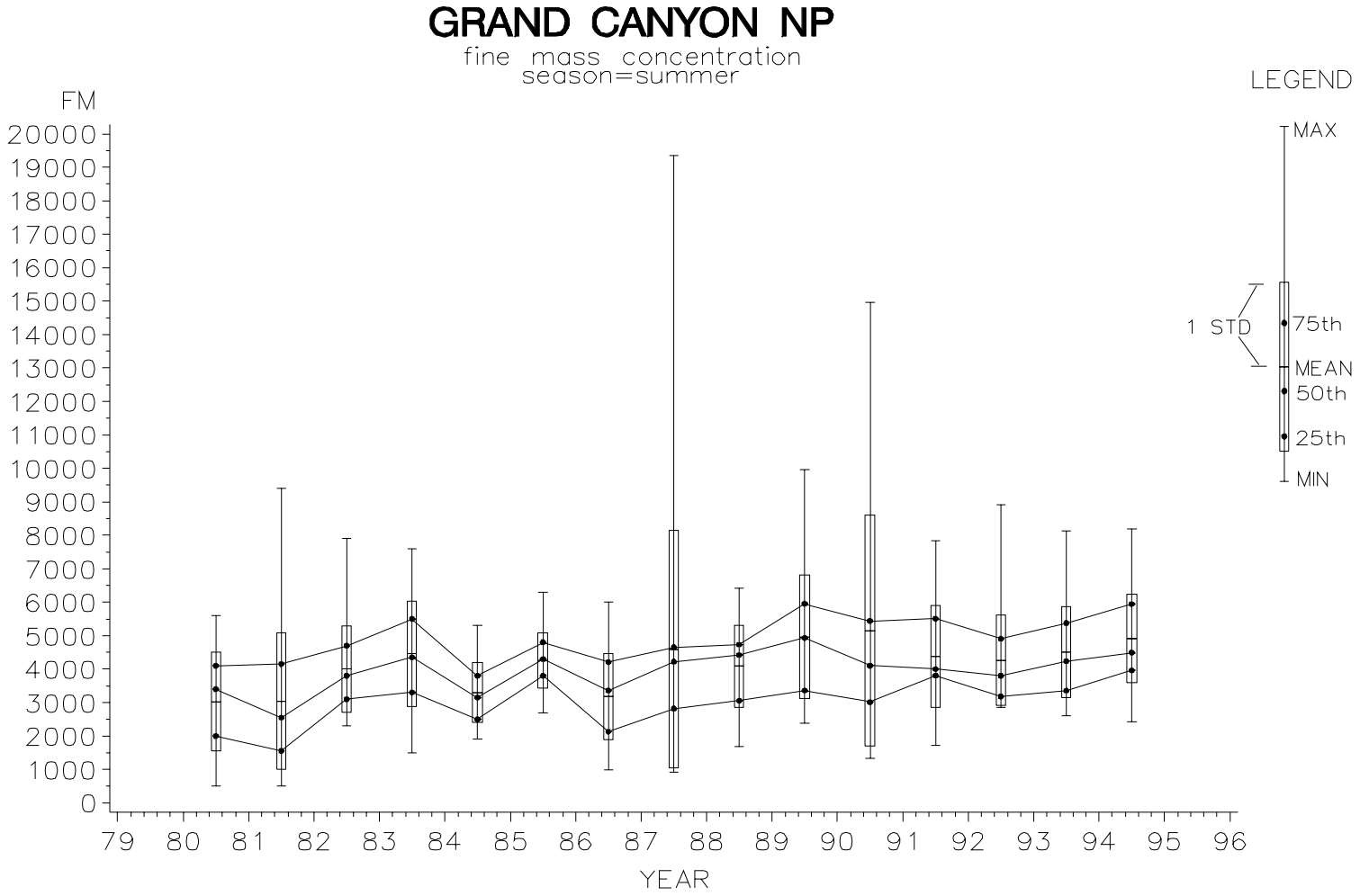

Figure 6.12a Monthly statistics for fine mass concentration (ng/m^3) at Grand Canyon National Park in the summer.

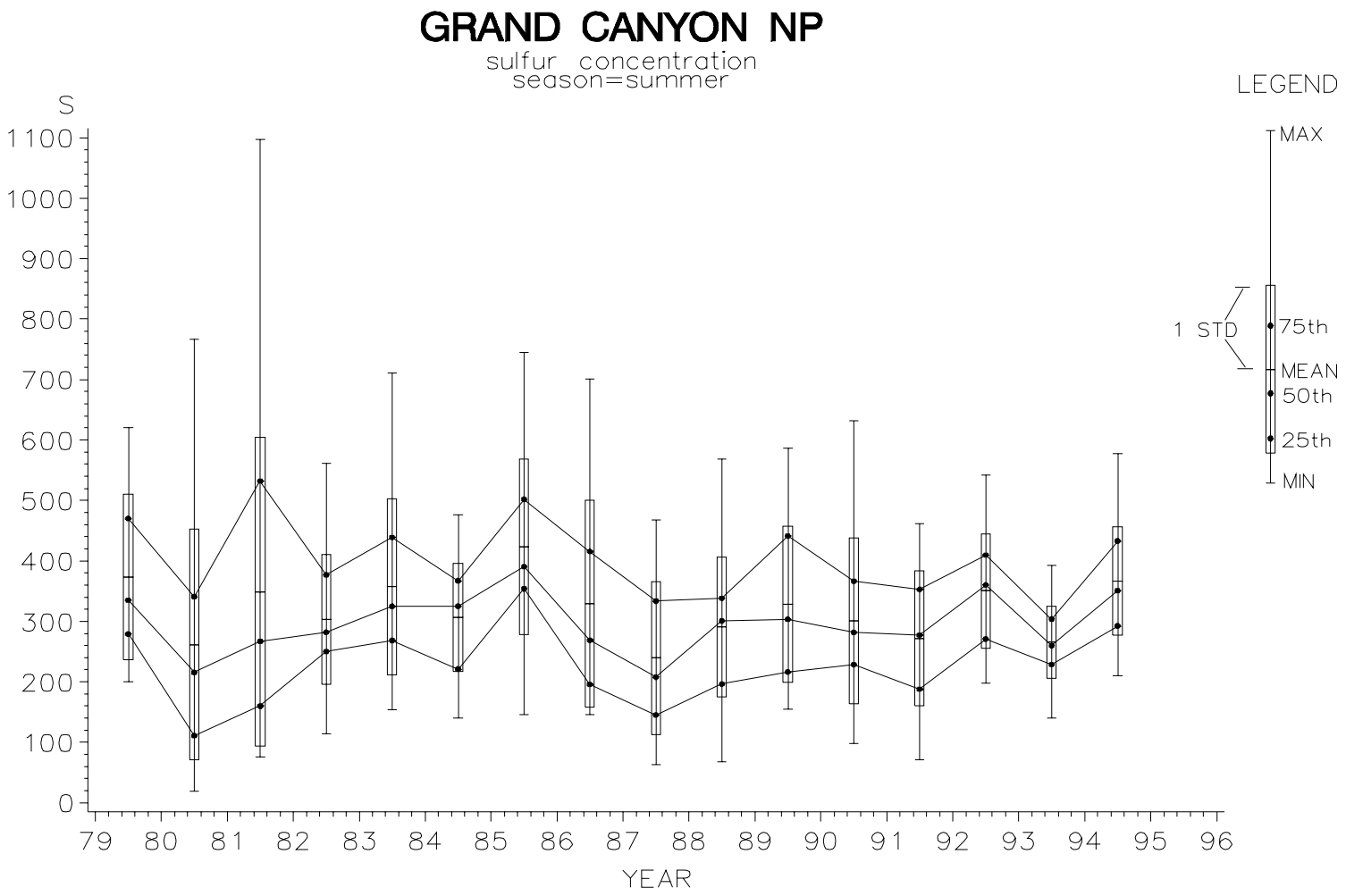

Figure 6.12b Monthly statistics for sulfur concentration (ng/m^3) at Grand Canyon National Park in the summer.

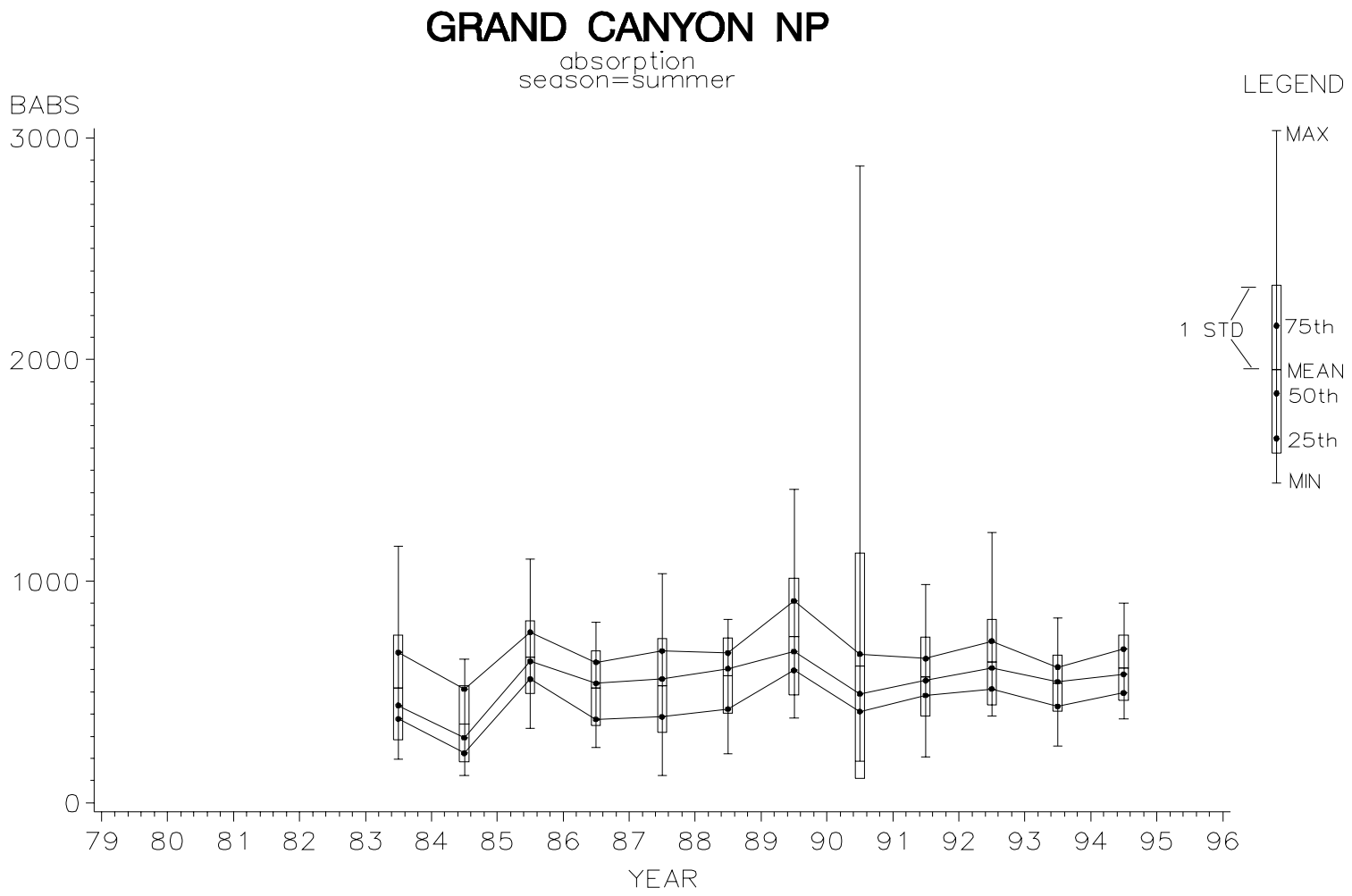

Figure 6.12c Monthly statistics for absorption (ng/m^3) at Grand Canyon National Park in the summer.

6.4.10 Grand Canyon National Park - Autumn

Fine mass concentrations (Figure 6.13a) have been trending upwards in the autumn at Hopi Point since obtaining their minimum in 1980. This is particularly evidenced by the 25th percentile and minima. In 1980, the minimum concentration was 200 ng/m^3, by 1993 it had increased to its maximum in excess of 1600 ng/m^3 before falling back to about 1000 ng/m^3 in 1994. The 25th percentile in 1980 was about 700 ng/m^3 and increased to almost 3000 ng/m^3 in 1992, then falls back to about 2000 ng/m^3 in 1994. Similar behavior by the 50th percentile is present with its minimum of 1200 ng/m^3 occurring in 1980; however, the 50th percentile obtains its maximum of about 4200 ng/m^3 in 1987 then remains relatively steady.

As with fine mass, sulfur has increased since 1980 when the 25th percentile obtained its minimum of about 60 ng/m^3 as shown by Figure 6.13b. By 1983 sulfur concentrations for the 25th percentile increase sharply to about 240 ng/m^3 then fall off to about 125 ng/m^3 in 1985. By 1990 the 25th percentile increases to almost 200 ng/m^3 and remains at this level with some variability through 1994. There is a trend towards decreased variability as evidenced by the standard deviation and is attributed to decreased maxima and increased minima.

Absorption displays little or no long-term trend (Figure 6.13c). Beginning in 1983 all three percentiles drop sharply by 1984; the 75th percentile moves from over 600 ng/m^3 to about 350 ng/m^3; the 50th percentile decreases from about 550 ng/m^3 to less than 250; and the 25th percentile drops from about 300 ng/m^3 to 200 ng/m^3. After 1984 all percentiles show steady increases by 1987 to their 1983 levels. From 1987 until 1993 the three percentiles are essentially steady with some variability at about 650 ng/m^3, 550 ng/m^3, and 350 ng/m^3 for the 75th, 50th, and 25th percentiles, respectively.

6.5 Interrelationships of Fine Mass, Sulfur and Absorption

Matrix scatter plots provide a useful tool for understanding the correlation of daily fine mass, b_{abs}, and sulfur, as well as for distinguishing differences between sites and seasons. Some correlation between fine mass and its constituents is expected, particularly in the case of sulfur where ammonium sulfate aerosol comprises a large fraction of the mass at many sites. By the same argument a limited amount of correlation between b_{abs}, sulfur, nitrate, organic carbon, and fine soil by virtue of their association with fine mass would not be unexpected. Sulfur and b_{abs} demonstrate the greatest amount of correlation between the constituent species. The strength of the correlation is variable and relatively strong at certain sites. Strong correlations suggest several possibilities including common anthropogenic sources or transport pathways and internally mixed aerosol. On the other hand, lack of correlation is indicative of different sources and externally mixed aerosols.

In the determination of b_{abs} a correction for "shadowing" is made. This is because as the filter becomes loaded with particles, the observed proportion of absorption to fine mass decreases. This is believed to be the case because some of the particles shadow others from the light source. Thus, a correction must be applied. If it is correct, then any correlation of b_{abs} with fine mass would be due to physical reasons. On the other hand, an over correction for fine mass would artificially increase absorption and the correlation of b_{abs} with fine mass [Campbell *et al.*, 1995].

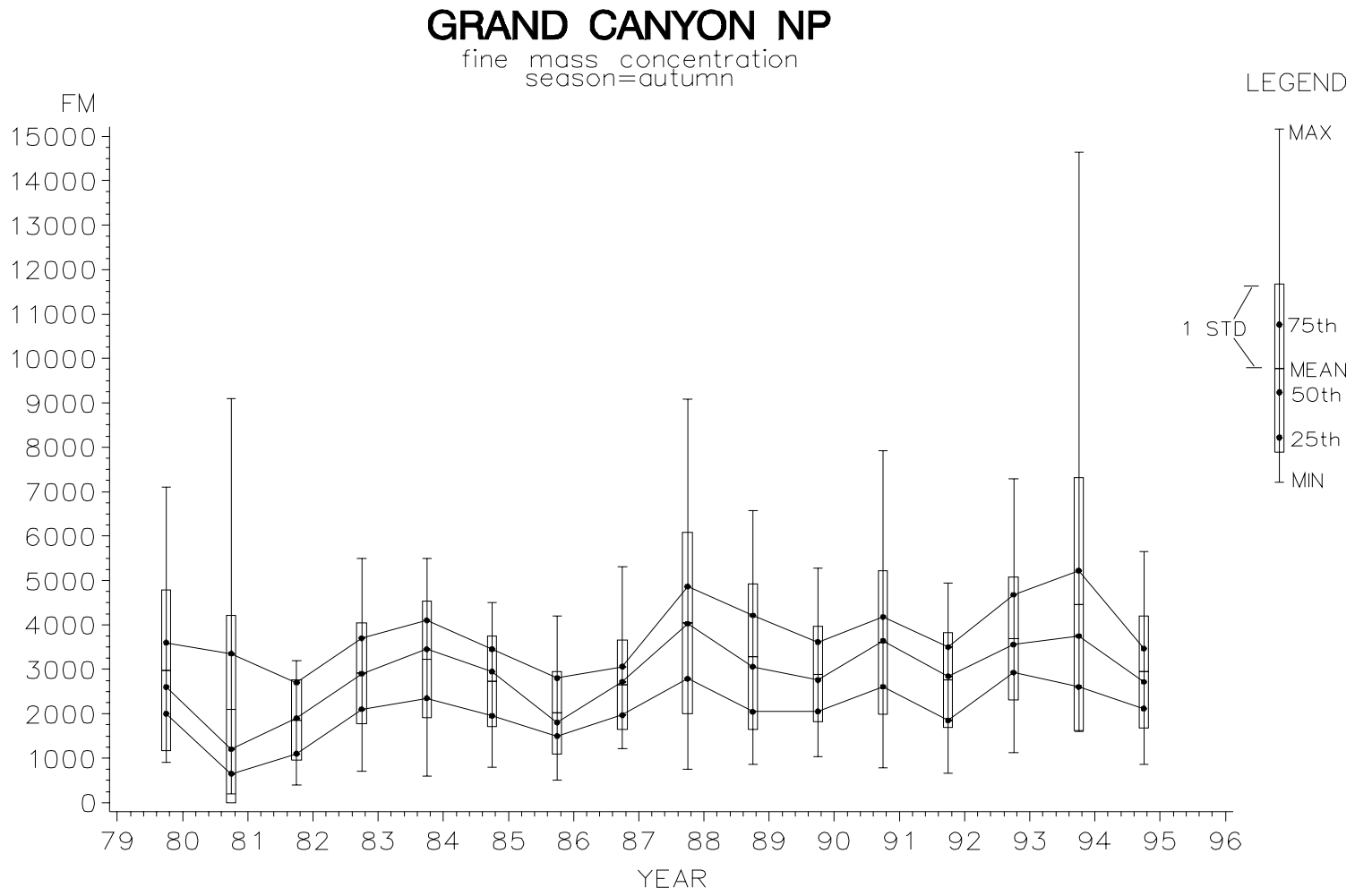

Figure 6.13a Monthly statistics for fine mass concentration (ng/m^3) at Grand Canyon National Park in the autumn.

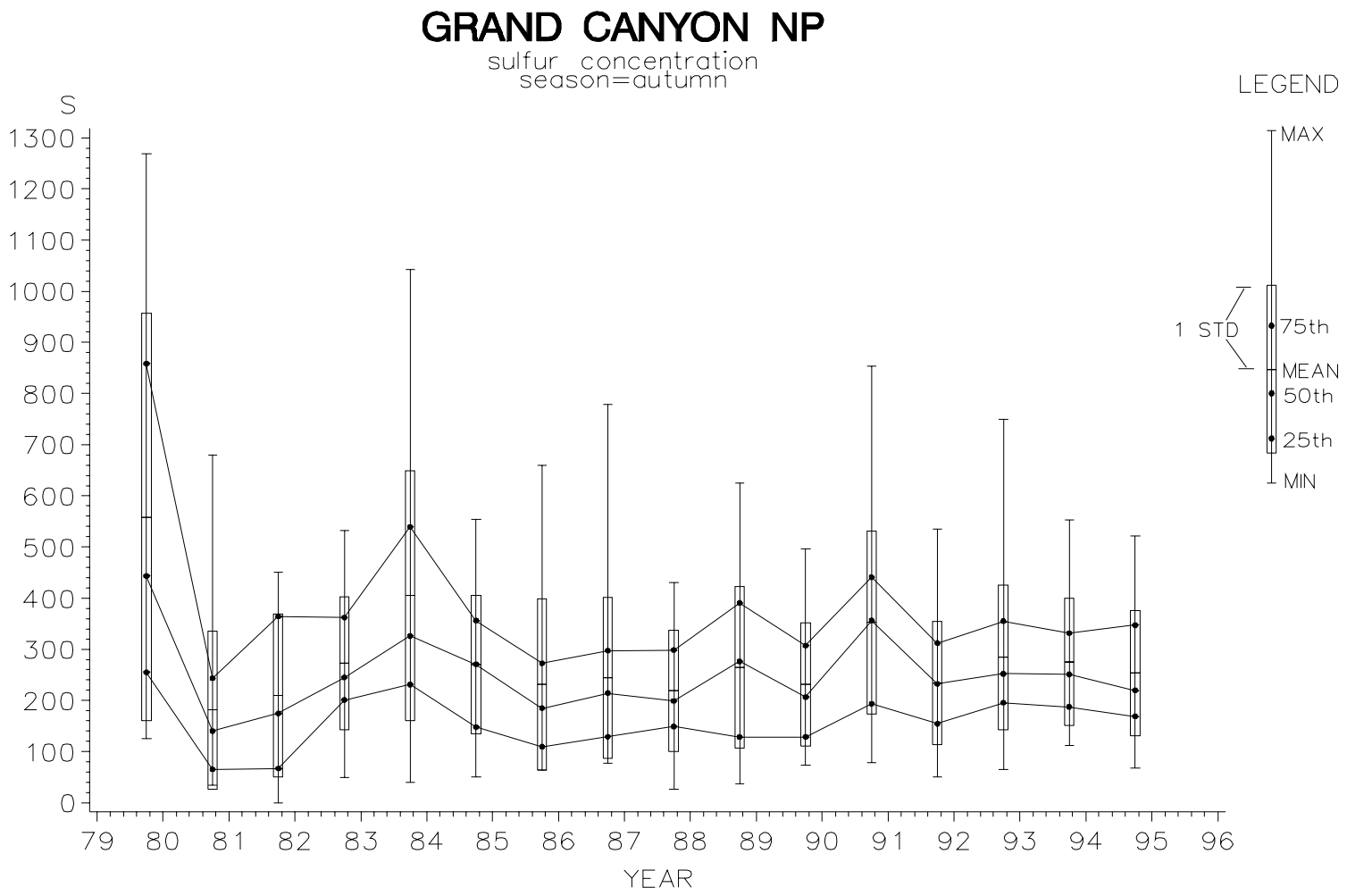

Figure 6.13b Monthly statistics for sulfur concentration (ng/m^3) at Grand Canyon National Park in the autumn.

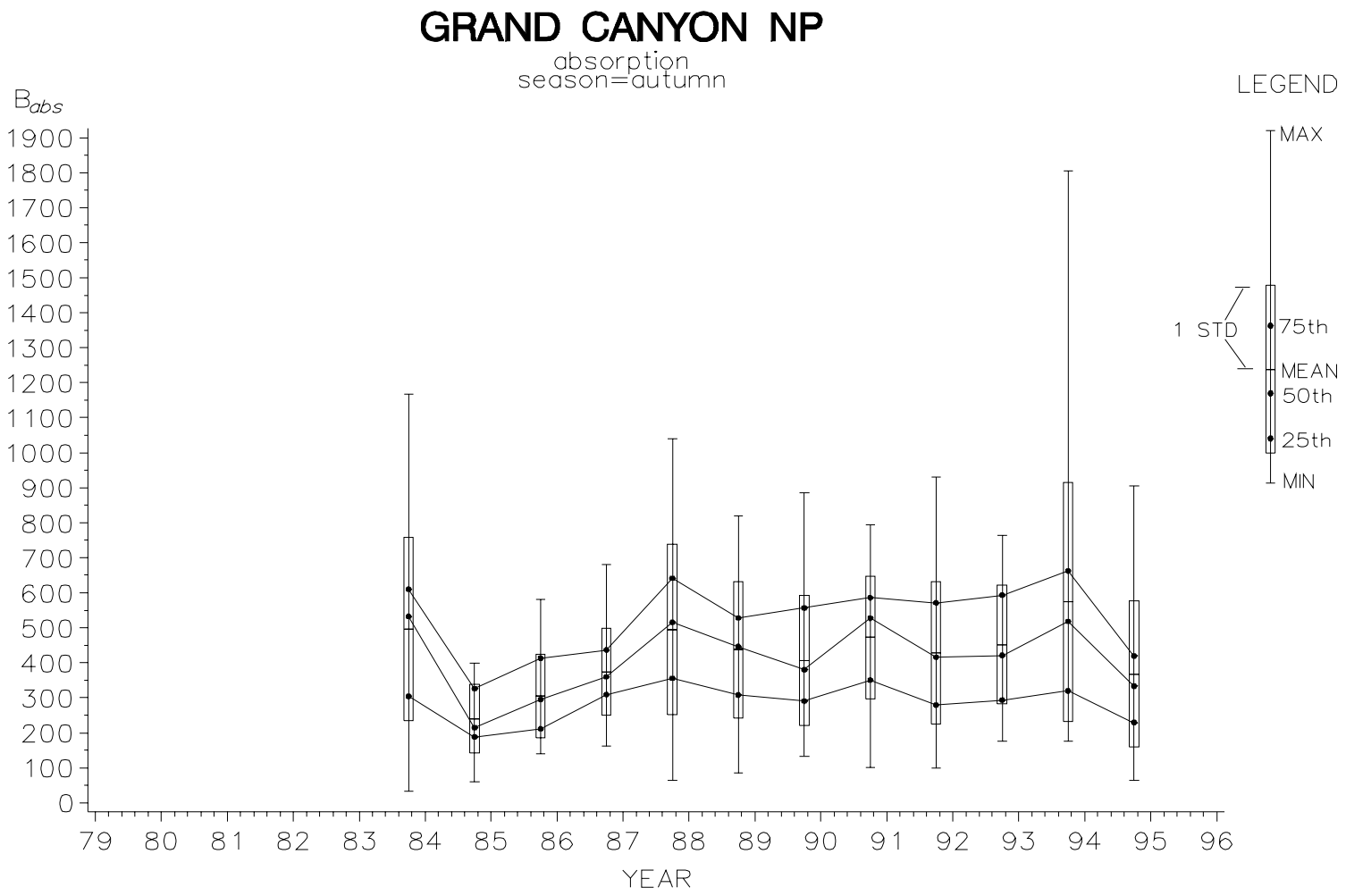

Figure 6.13c Monthly statistics for absorption (ng/m^3) at Grand Canyon National Park in the autumn.

6.6.1 Daily Scatter Plots

Appendix 3 has matrix scatter plots of fine mass, sulfur, and b_{abs} by season for all IMPROVE monitoring sites. Presented here are a representative subset of sites that demonstrate the variability, range, and character of the correlations with emphasis on differences between sites. Overlaid on each scatter plot are two sets of concentric ellipses. The major axis lies on the first principal component and the ellipse center lies on the mean value of both species. The ellipses define contours that enclose points that fall within the 50% and 90% of a bivariate normal distribution. A perfectly round ellipse indicates no correlation, and the oblateness indicates the degree of correlation. Perfect correlation would result in the ellipse collapsing into a straight line.

6.6.1 Shenandoah National Park

The scatter plots for Shenandoah (Figure 6.14) display many of the qualities expected for a site impacted by numerous anthropogenic sources. Sulfate constitutes a major fraction of the fine mass and accordingly the correlation of sulfur to fine mass is high, particularly in the autumn followed by the spring. Absorption is surprisingly correlated with fine mass even though b_{abs} composes a much smaller fraction of the mass. The correlation of b_{abs} with sulfur, although significant, especially in the winter, appears to be the weakest of the three relationships. Autumn is interesting because of the similarity of the scatter of b_{abs} against sulfur and fine mass. There is a readily identifiable subpopulation at lower concentrations and the appearance of a hard edge applies to both scatters. A hard edge is indicative of a strong influence from one source type or source area as evidenced by one ratio of b_{abs} to sulfur. The scatter away from the hard edge indicates occasional influx additional sulfur with proportionately less b_{abs} from other sources.

6.6.2 Glacier National Park

Glacier (Figure 6.15) is an interesting contrast to Shenandoah. The strongest correlations with fine mass are with b_{abs} rather than sulfur. The correlation of sulfur to b_{abs} is quite weak as evidenced by the roundness of the ellipse. This is especially evident during the spring and autumn with the strongest b_{abs} sulfur correlation occurring in the winter. The scatter plots of b_{abs} vs sulfur and sulfur vs fine mass suggest two types of days are being observed. One group of days has high b_{abs} and low sulfur. The other group has low b_{abs} and high sulfur.

6.6.3 Denali National Park

At Denali (Figure 6.16), many interesting features are evident. During the winter and spring correlations of b_{abs} with sulfur are the strongest of any site in the IMPROVE network. During the summer and autumn, when the correlations are lowest, the hard edges indicate two groups of days or "populations" dominated either by sulfur or by b_{abs} (similar to those discussed above for Glacier). Each population would most likely be associated with a distinct source type and/or region. The possibility of two populations during autumn and summer are also suggested by the scatter of sulfur against b_{abs}. The strongest correlation between b_{abs} and fine mass occurs during the summer. During the winter all three aerosol measures are relatively well correlated with each other.

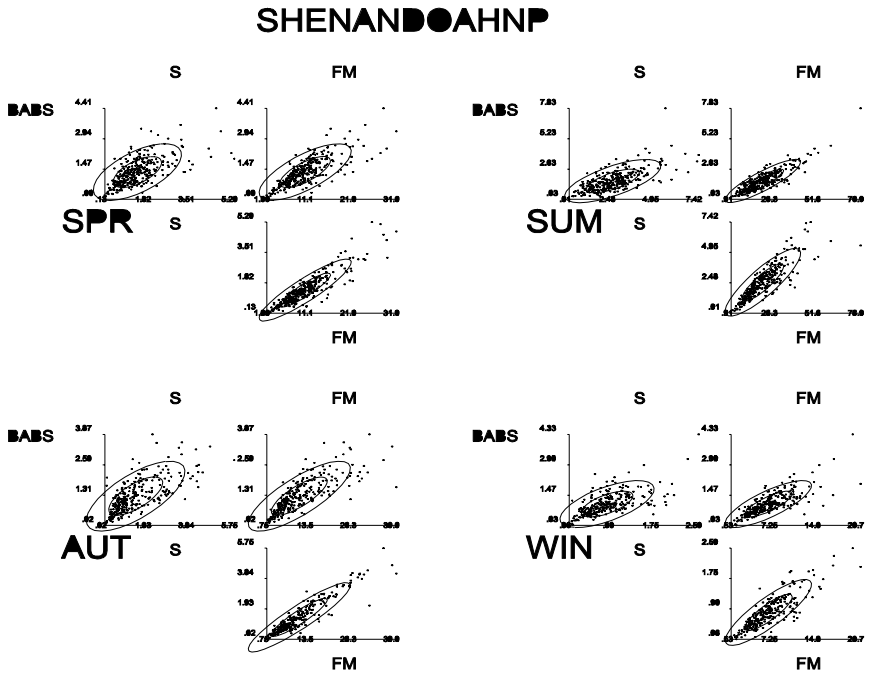

Figure 6.14 Matrix scatter plots of absorption (b_{abs}) sulfur (S) and gravimetric fine mass (FM) for the four seasons at Shenandoah National Park. Assuming an absorption efficiency of 10 m^2/gm all units are $\mu g/m^3$.

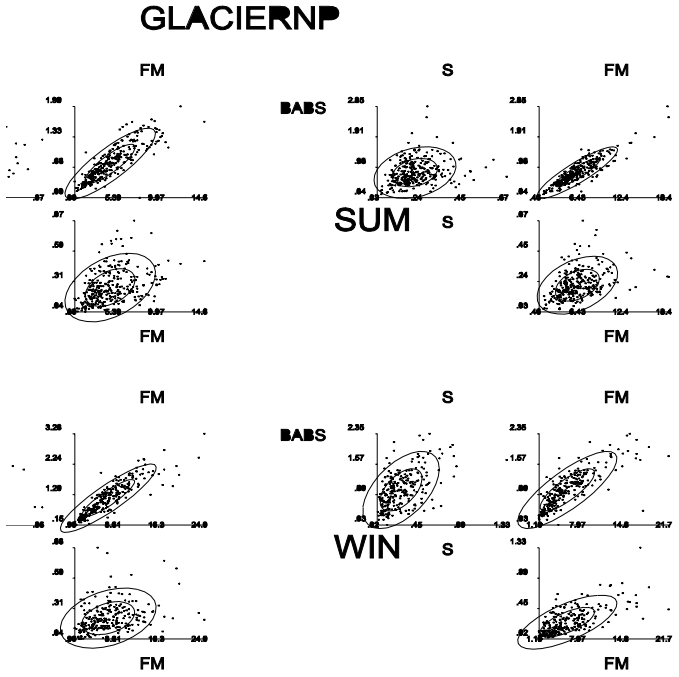

Figure 6.15 Matrix scatter plots of absorption (b_{abs}) sulfur (S) and gravimetric fine mass (FM) for the four seasons at Glacier National Park. Assuming an absorption efficiency of 10 m^2/gm all units are $\mu g/m^3$.

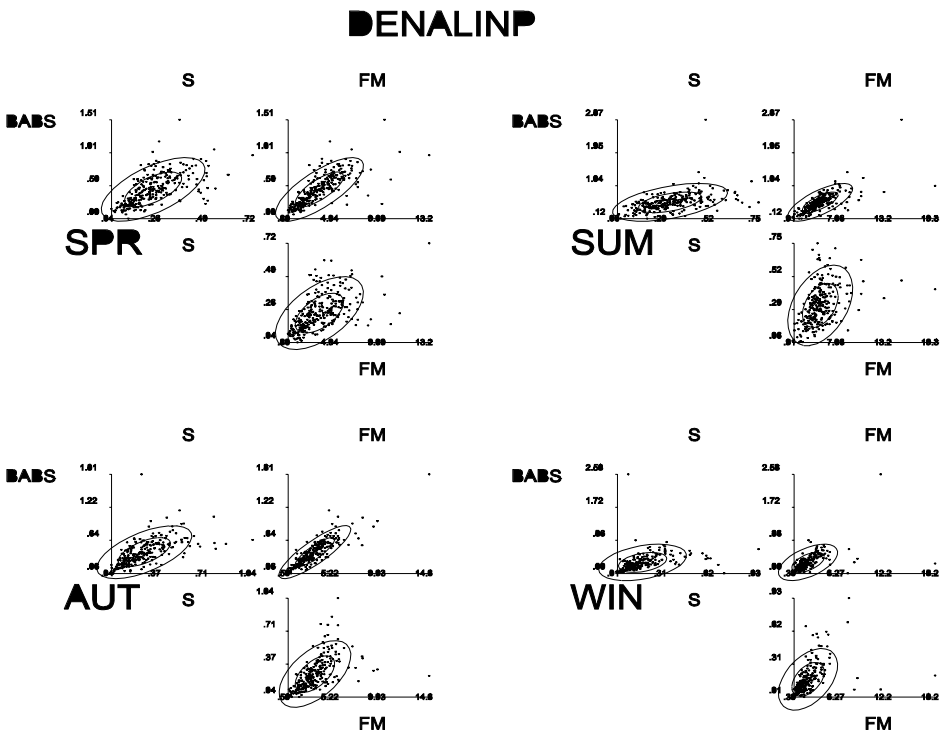

Figure 6.16 Matrix scatter plots of absorption (b_{abs}) sulfur (S) and gravimetric fine mass (FM) for the four seasons at Denali National Park. Assuming an absorption efficiency of 10 m^2/gm all units are $\mu g/m^3$.

6.6.4 Bridger Wilderness Area

At Bridger (Figure 6.17), there are relatively moderate to strong correlations of all three aerosol measures with each other. The correlation of b_{abs} with sulfur is especially strong during the winter followed by the summer. The strongest correlations of b_{abs} with fine mass are during the spring and autumn. In the scatter of b_{abs} vs fine mass during the summer, two populations are evident. There is a population that appears very tight and then another group of days with elevated fine mass. This pattern is also seen to a lesser extent in the scatter between sulfur and fine mass.

6.7 Conclusions

Changes in sampling protocol, whether by sample duration (24-hour vs 72-hour) or sampler type (SFU vs IMPROVE) appear to have a minimal affect on observed concentrations of fine mass, sulfur or absorption. This is especially the case for sulfur where the noted changes were slight and variable between sites. The only site with a clear change between protocols was at Mount Rainier, which is coincident with a change in sampler location and altitude. For the case

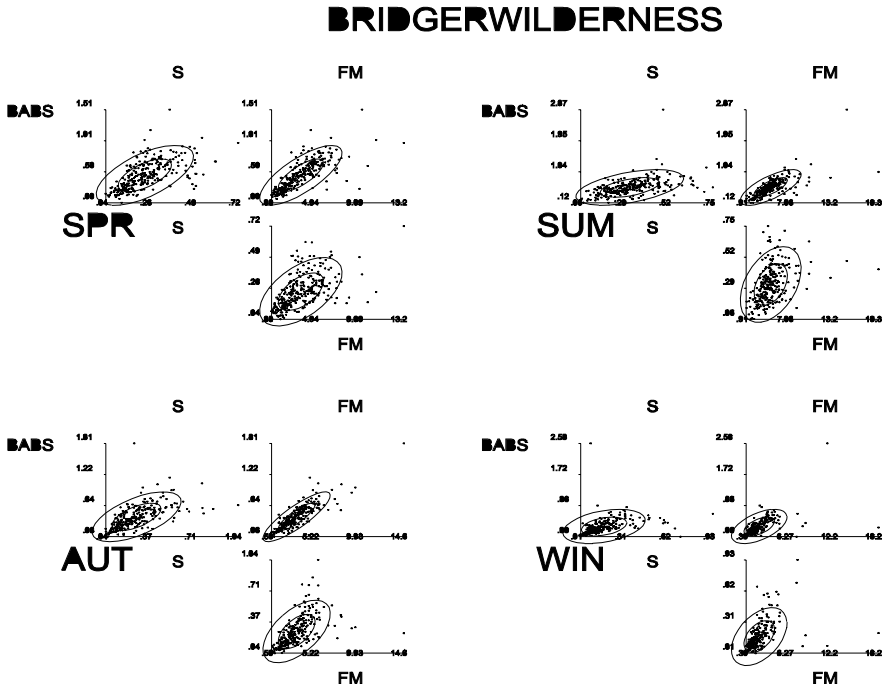

Figure 6.17 Matrix scatter plots of absorption (b_{abs}) sulfur (S) and gravimetric fine mass (FM) for the four seasons at Bridger Wilderness. Assuming an absorption efficiency of 10 m^2/gm all units are $\mu g/m^3$.

of absorption, five sites demonstrate clear changes between sampler type, one of those sites is again at Mount Rainier, while the other sites show notable increases in absorption during most seasons.

Demonstrated long-term trends fall into three categories: increases, decreases, and variable. Sites that demonstrated decreases are at Crater Lake and Rocky Mountain National Parks where absorption dropped dramatically, and at Guadalupe Mountains National Park where sulfur is decreasing in the autumn. A clear demonstration of decreased sulfur concentrations as a result of emission reductions is in the desert southwest at Chiricahua. Two sites where increases have been observed are at the Grand Canyon in the autumn where the 25th percentile of sulfur concentrations have increased steadily since 1980, and at Great Smoky Mountains National Park where autumn concentrations of sulfur and absorption have increased. Other sites that demonstrate little or variable changes in sulfur concentrations are at Bryce Canyon, Rocky Mountain, and Crater Lake National Parks. Variable or little change in absorption was noted at the Grand Canyon National Park in the winter, and Chiricahua National Monument in the summer.

The most notable observation from a national perspective is the lack of a clear uniform trend of sulfur concentration or absorption. There are local success stories related to emission controls, and

there are failures most likely associated with increased local emissions or long-range transport. The bulk of the sites show little or variable trends in the long run.

The matrix scatter plots demonstrate correlations ranging between slight to strong between gravimetric fine mass, b_{abs}, and sulfur. Some of the strongest correlations are between fine mass and b_{abs} even though light-absorbing material is a small fraction of fine mass suggesting an internal mixture of carbon with the primary constituents of the fine mass. The exceptions to this are sites in the eastern United States where sulfur is a large fraction of the fine mass; here sulfur shows strong correlations with fine mass indicative of strong sources. Weak correlations are usually manifested by 'fan shaped' scatters, some with hard edges, which suggest multiple sources with variable ratios of b_{abs} or sulfur.

6.8 References

Cahill, T.A., R.A. Eldred, and P.J. Feeney, Particulate monitoring and data analysis for the National Park Service 1982-1985, University of California, Davis, 1986.

Campbell, D., S. Copeland, and T. Cahill, Measurement of aerosol absorption coefficient from Teflon Filters Using Integrating Plate and Integrating Sphere Techniques, *Aerosol Sci. and Tech.,* **22**, 287-292, 1995.

Day, D., W.C. Malm, S.M. Kreidenweis, Seasonal variations in aerosol acidity estimated from IMPROVE data, *Proc. International Specialty Conference Aerosols and Atmospheric Optics: Radiative Balance and Visual Air Quality, Air & Waste Management Association (AWMA),* Pittsburgh, PA, 1994.

Eldred, R.A., T.A. Cahill, M. Pitchford, and W.C. Malm, IMPROVE-a new remote area particulate monitoring system for visibility studies, *Proc. Air Pollution Control Association (APCA) 81st Annual Meeting*, Pittsburgh, PA, Paper No. 88-54.3:1-16, 1988.

Epstein, C., and M. Oppenheimer, Empirical relation between sulfur dioxide emissions and acid deposition derived from monthly data, *Nature*, **323**, 1986.

Flocchini, R.G., T.A. Cahill, L. Ashbaugh, R.A. Eldred, and M. Pitchford, Seasonal behavior of particulate matter at three rural Utah sites, *Atmos. Environ.,* **35**, 315-320, 1981.

Malm, W.C., J.F. Sisler, D. Huffman, R.A. Eldred, and T.A. Cahill, Spatial and seasonal trends in particle concentration and optical extinction in the United States, *J. Geophys. Res.,* **99(D1)**, 1347-1370, 1994.

Oppenheimer, M., Empirical source receptor relations for sulfate in the western U. S., *Proc. 80th Annual Meeting of the Air Pollution Control Association (APCA),* Pittsburgh, PA, 1987.

Sisler, J.F., and W.C. Malm, Relationship of trends in regional sulfur dioxide emissions to particulate sulfate concentrations in the southwestern U. S., *Transactions of the International Specialty Conference on Visibility and Fine Particles, Air & Waste Management Association*

(AWMA), Pittsburgh, PA, 1989.

Sisler, J.F., D. Huffman, and D.A. Latimer, Spatial and temporal patterns and the chemical composition of the haze in the United States: an analysis of data from the IMPROVE network, 1988-1991, Report by Cooperative Institute for Research in the Atmosphere (CIRA), Colorado State University, Ft. Collins, CO 80523, ISSN: 0737-5352-26, 1993.

Trijonis, J.C., and K. Yuan, Empirical studies of the relationship between emission and visibility in the southwest, EPA-450/5-79-009, Research Triangle Park, NC, 1987.